Annual Report on Nuclear Physics Activities

July 1, 1982 - June 30, 1983

Editors:
H. Gemmeke, F. Käppeler, Ch. Weddigen
Institut für Kernphysik

Kernforschungszentrum Karlsruhe

KERNFORSCHUNGSZENTRUM KARLSRUHE

Institut für Kernphysik

KfK 3621

ANNUAL REPORT

on

NUCLEAR PHYSICS ACTIVITIES

July 1, 1982 - June 30, 1983

Editors:

H. Gemmeke, F. Käppeler and Ch. Weddigen

Last Annual Reports:

1981 - 1982: KfK 3427 (82)

1980 - 1981: KfK 3280 (81)

ABSTRACT

This report surveys the activities in fundamental research from July 1, 1982 to June 30, 1983 at the three institutes of the KfK which are concerned with nuclear physics. The research program comprises laser spectroscopy, nuclear reactions with light ions, neutron physics, neutrino physics and physics at medium and higher energies.

ZUSAMMENFASSUNG

Der vorliegende Bericht gibt einen Überblick über die Arbeiten an den drei Kernphysikalischen Instituten des Kernforschungszentrums Karlsruhe im Zeitraum vom 1. Juli 1982 bis zum 30. Juni 1983. Das Forschungsprogramm umfaßt die Gebiete Laserspektroskopie, Kernreaktionen mit leichten Ionen, Neutronenphysik, Neutrino-Physik, sowie Mittel- und Hochenergiephysik.

PREFACE

We have the pleasure to present the third report on nuclear physics activities at the Nuclear Research Center Karlsruhe.

In the past years, the collaboration between the three institutes active in nuclear physics, IK I, IK II and IAK II, has been intensified by joint planning, joint seminars and documented by a joint report. This tendency has now been formalized by a decision of our Supervisory Board to merge all groups active in nuclear physics into one 'Institute for Nuclear Physics' The former 'Institute for Applied Nuclear Physics II' is now called 'Institute for Nuclear Physics III'. In this way, the present report summarizes the work of the 'Institute for Nuclear Physics'.

Three groups of the Institute for Nuclear Physics I are engaged in work in various fields of nuclear physics and particle physics:

Fast Neutron Physics: Scattering experiments on very light nuclei are carried out using the polarized neutron beam of the Karlsruhe Cyclotron (POLKA). The main goal is to determine precise phase shifts from experiments with polarized neutrons on unpolarized and also on polarized protons. Moreover, the internal structure and dynamics of the nuclei up to the $A = 5$ system are to be studied. Last year, the POLKA facility was used successfully in a number of experiments.

The large-volume polarized proton target developed by the 'Experimental Methods' Group has meanwhile been put into operation successfully and has been in use for scattering experiments with the polarized neutron beam since May, 1983.

High Energy Physics: This Group runs the CELLO detector system at the e^+e^- storage ring, PETRA, in Hamburg within the framework of an international collaboration. The detector serves for experiments to study e^+e^- collisions at the highest energies at present attainable. CELLO, with its modern liquid-argon calorimeter, lends itself particularly well to studies of the electromagnetic component in these reactions. This allows, e.g., precise studies of quantum electrodynamics, detailed studies of quark and gluon jets performed and the search for new quarks. The detector has meanwhile been upgraded and moved back into the beam since the summer of 1982. All its components are working satisfactorily

and are strongly involved in the search for a new quark during the continuous energy increases in PETRA.

Neutrino Physics: The newly founded Working Group is concerned with neutrino physics in the energy range between approximately 10 and 50 MeV, at the Spallation Neutron Source under construction at the Rutherford-Appleton Laboratory (RAL) in England. This is a new field of work involving fundamental questions in the fields of elementary particle physics, nuclear physics and astrophysics.

The project was proposed by KfK. In the meantime, a bilateral agreement has been signed between KfK and RAL. Several smaller working groups of the University of Oxford (Prof.Dr.N.E.Booth), Queen Mary College of London (Prof.Dr.J.A.Edgington), University of Erlangen (Prof.Dr.E.Finckh) and University of Tübingen (Prof.Dr.A.Faessler) have meanwhile joined the project. The detector system is being developed and built at KfK. It will be installed in a massive blockhouse of iron at the Rutherford SNS by the end of 1985.

The Institute for Nuclear Physics II is mostly working on medium energy physics at CERN and SIN.

One Group, continuing a long tradition in the field of exotic atoms at CERN, has concentrated its activities on the LEAR Project (Low-Energy Antiproton Ring). The project, the realization of which was backed very strongly by Karlsruhe, promises to offer unique possibilities for work with slow antiprotons. Spectra were obtained in a test run of 20 minutes which formerly took several months of measuring time. This also proved the successful conversion of the equipment to high counting rate capabilities. A Karlsruhe proposal makes use of the idea of the cyclotron trap proposed by Mr.Simons. This unit was tested with pions and myons at SIN, and the computed predictions were confirmed. It will now be brought to LEAR. Karlsruhe is involved personally and financially also in a technical upgrading of LEAR, namely the use of electron cooling.

The experiments at SIN focus on problems of pion interaction (scattering and absorption) with simple systems consisting of few nucleons. Theoretical assumptions, especially those about the existence of dibaryon states, are verified on the basis of additional information that can be obtained by using polarized targets.

Also the low-energy spectrometer designed by Karlsruhe will mainly be used in studies of very simple systems at energies close to the pion threshold. The Coulomb nuclear interferences have been studied in preliminary experiments on carbon. The results of these experiments demonstrate that the proposed measuring technique allows to study pion-hydrogen scattering in the region of Coulomb interference. This reaction is of great theoretical significance.

Research of the Institute for Nuclear Physics III takes place in the following fields:

Nuclear astrophysics: Capture cross sections of fast neutrons in the keV to MeV range are measured in order to understand in detail the build-up of heavy elements in stars. These measurements are supplemented by studies of nuclear spectroscopy on nuclei of specific importance to stellar neutron capture reactions.

Nuclear reactions: Alpha particle and ^{6}Li beams from the Karlsruhe Isochronous Cyclotron are used for studying nuclear reactions at 26 MeV/nucleon. The emphasis is at present on the break-up of ^{6}Li in nuclear collision with the aim to study the momentum distribution of its constituents. A medium size magnetic spectrometer which will allow measurements down to very small reaction angles is being put into operation.

Laser spectroscopy: This technique is applied to sub-ng amounts of radioactive atoms in order to determine hyperfine structure and isotopic shifts of atomic transitions. The results yield information on nuclear moments and on the change of nuclear charge radii due to varying neutron number. Previous measurements on a long series of lead isotopes have been extended, and studies of tin isotopes have started.

Applied gamma-ray spectroscopy: Here instruments are developed to determine concentration and isotopic composition of fissile material. The instruments make use either of the intrinsic radioactivity or of X-ray absorption and fluorescence. Their main applications are in the safeguards of nuclear fuel and in process control during fabrication and reprocessing.

The Institute for Nuclear Physics III is also responsible for the operation
of the Karlsruhe Isochronous Cyclotron. The cyclotron laboratory has
been considerably extended during the last three years by the in-
stallation of a second cyclotron in an annex to the cyclotron building.
This accelerator will go into operation in late 1983 (after a consi-
derable delay caused by economic difficulties of the manufacturer)
and will be operated on a commercial basis for producing isotopes for
nuclear medicine and for irradiating machine parts for wear studies
in industry.

(A. Citron)   (G. Schatz)   (B. Zeitnitz)

CONTENTS

1. NUCLEAR PHYSICS

1.1 NUCLEAR ASTROPHYSICS

1.1.1 NEUTRON CAPTURE IN s-WAVE RESONANCES OF ^{56}Fe, ^{58}Ni, and ^{60}Ni

K. Wisshak, F. Käppeler, G. Reffo[+], F. Fabbri[+],
KfK-report 3516 (1983) and Nucl. Sci. Eng. (submitted)

The exact determination of the capture widths of broad s-wave resonances in structural materials is an important problem because of two reasons: (i) By their large capture area, these resonances contribute significantly to the average capture cross section. (ii) In previous measurements their large ratio $\Gamma_n/\Gamma_\gamma \sim 10^3$ caused severe systematic uncertainties due to capture of resonance scattered neutrons. The sensitivity of the capture detectors to scattered neutrons limits the accuracy of present experiments at LINAC accelerators to 20 - 30 %. These uncertainties do not meet the requirements formulated for capture cross sections of structural materials (1).

In this work the neutron capture widths of s-wave resonances in ^{56}Fe (27.7 keV), ^{58}Ni (15.4 keV) and ^{60}Ni (12.5 keV) have been determined using a setup completely different from previous experiments. A pulsed 3-MV Van de Graaff accelerator and a kinematically collimated neutron beam, produced via the ^{7}Li(p,n) reaction, was used in the experiments. Capture gamma-rays were observed by three Moxon-Rae detectors with graphite-, bismuth-graphite-, and bismuth-converter, respectively. The samples were positioned at a neutron flight path of only 9 cm and the distance from sample to detector is $\sim$ 16 cm. Thus events due to capture of resonance scattered neutrons in the detectors or in surrounding materials are completely discriminated by their additional time of flight. The high neutron flux at the sample position allowed the use of very thin samples (0.15 mm - 0.45 mm), avoiding large multiple scattering corrections. The data obtained with the individual detectors were corrected for the efficiency of the respective converter materials. For that purpose, detailed theoretical calculations of the capture gamma-ray spectra of the measured isotopes and of gold, which was used as a standard, were performed. The final results are: Γ_γ(27.7 keV, ^{56}Fe) = 1.06 $\pm$ 0.05 eV, Γ_γ(15.4 keV, ^{58}Ni) = 1.53 $\pm$ 0.10 eV and Γ_γ(12.5 keV, ^{60}Ni) = 2.92 $\pm$ 0.19 eV. The accuracy obtained with the present

experimental method represents an improvement of a factor 3-6 compared to previous experiments.

With these results Maxwellian average cross section were calculated for kT = 30 keV. The following values were obtained for $<\sigma v>/v_T$: (39.0 $\pm$ 2.5 mb, ^{58}Ni), (31.4 $\pm$ 1.6 mb, ^{60}Ni) and (13.9 $\pm$ 1.1 mb, ^{56}Fe). The investigated s-wave resonances contribute up to 40 % to these average cross sections.

In a typical fast reactor spectrum these resonances cause about 10 % of the total capture rate in structural materials and are therefore- together with the 1.15 keV resonance in ^{56}Fe- most important for reactor calculations.

(1)   N. Dayday, Ed., "World Request List for Nuclear Data", INDC(SEC)-78/URSF, International Atomic Energy Agency, Vienna (1981)

+   E.N.E.A. Bologna, Italy

1.1.2   NEUTRON CAPTURE IN s-WAVE RESONANCES OF ^{64}Ni

K. Wisshak, F. Käppeler, R.L. Macklin[+], G. Reffo[++], F. Fabbri[++], KfK-report 3582 (1983) and Nucl. Sci. Eng. (submitted)

The experimental method to determine the capture widths of s-wave resonances in structural materials with high accuracy as described in contribution 1.1.1 has also been applied to ^{64}Ni. This isotope has two s-wave resonances at 13.9 keV and 33.8 keV with very large ratios Γ_n/Γ_γ (2900 and 7700, respectively). These high values do not allow for an exact determination of the respective capture widths in LINAC experiments, and therefore this investigation was started in collaboration with the Oak Ridge National Laboratory. The results will serve to normalize the neutron sensitivity correction of LINAC measurements. In this way the accuracy of these experiments for resonances with large Γ_n/Γ_γ ratios can be significantly improved in those energy regions which are not accessible to our method.

The final results (Γ_γ(13.9 keV) = 1.01 $\pm$ 0.07 eV and Γ_γ(33.8 keV) = 1.16 $\pm$ 0.08 eV) are considerably smaller than the rough estimates obtained in previous work. The Maxwellian average neutron capture cross section for kT = 30 keV is $<\sigma v>/v_T$ = 10.7 $\pm$ 0.9 mb; it is determined to 63 % by the two investigated resonances.

+   Oak Ridge National Laboratory, Oak Ridge, Tennessee, USA

++   E.N.E.A. Bologna, Italy.

1.1.3 THE CHEMICAL FIXATION OF Kr ISOTOPES IN ZEOLITE 5A-PREREQUISITE FOR THE DETERMINATION OF 25 keV NEUTRON CAPTURE CROSS SECTIONS WITH THE ACTIVATION METHOD

R.-D. Penzhorn[+], G. Walter, H. Beer,

Zeitschrift für Naturforschung 38a (1983) 712

By chemical fixation of Kr in zeolite 5A adequate samples can be obtained to determine the cross section of reactions such as $^{84}Kr(n,\gamma)$ $^{85}Kr^m$ and $^{86}Kr(n,\gamma)$ ^{87}Kr. The employed zeolite loading was of the order 52-66 (cm³ STP Kr / g zeolite). The capture cross section of the reaction $^{84}Kr(n,\gamma)$ $^{85}Kr^m$ was determined at thermal and 25 keV neutron energy. The value obtained at 25 keV is of relevance to the stellar nucleosynthesis of heavy elements by the s-process.

[+]   KfK, Institut für Radiochemie

1.1.4 NEUTRON CAPTURE CROSS SECTIONS AT 25 keV MEASURED BY ACTIVATION

G. Walter, H. Beer

The Maxwellian averaged neutron capture cross sections of ^{71}Ga, ^{75}As, $^{79,81}Br$, ^{86}Kr and $^{85,87}Rb$ have been measured at kT = 25 keV by activation relative to the standard ^{197}Au.

Neutrons were produced by the reaction $^7Li(p,n)^7Be$ 27 keV above the reaction threshold, the energy spectrum being almost Maxwellian (deviation ∿3 %) for the chosen experimental setup.

After activation the induced activities were counted in subsequent time intervals via a strong characteristic gamma-ray line with a γx-Germanium detector (45 cm³, energy resolution 1.6 keV at 1.33 MeV).

These cross sections form part of the data basis for a correct analysis of the s-process synthesis path through the elments between Germanium and Strontium. This mass region is important because there are two major s-process branchings at ^{79}Se and ^{85}Kr which are expected to yield information on the s-process neutron density and temperature.

1.1.5 THE ABUNDANCE OF TECHNETIUM IN STARS

G. Schatz, Astron. Astrophys. 122 (1983) 327

It is known since more than 30 years that the unstable element technetium occurs in the atmosphere of some stars (1,2). All these are cool stars in a late stage of their evolution. Of the three processes responsible for the production of heavy elements in stars, the r-, s-, and p-process, the latter is ruled out because it would lead to a large overabundance of molybdenum and, to a lesser extent, of samarium which is not observed. The r-process is associated with supernova explosions, and it is obvious from astronomical evidence that the technetium containing stars cannot be supernova remnants. It is therefore generally accepted that technetium in these stars is produced by the s-process somewhere in the stellar interior and mixed to the surface.

The only long-lived s-process isotope of Tc is ^{99}Tc with a laboratory half-life of 2.1 x 10^5a. Its fast neutron capture cross section has recently been measured (3). Using this result and the latest s-process systematics (4) it is then possible to calculate the abundance of ^{99}Tc or its ratio to the abundance of other elements. The result is

$$N_s(^{99}\text{Tc})/N_s(\text{Ba}) = 0.0162 \pm 0.0025$$

The abundance ratio actually observed should be smaller than this figure for two reasons:

(i)   Part of the barium now seen in the stellar atmosphere was incorporated into the star during formation whereas any technetium present at that time has since decayed.

(ii)   The half-life of ^{99}Tc is considerably reduced at the high temperature of the stellar interior (5). This is due to possible allowed ß-decays of low-lying exciting states whereas the ground-state ß-decay is second forbidden. It can be estimated that the stellar half-life is 1 to 10 a at the most probable s-process temperature of 3.5 x 10^8K.

A quantitative determination of the stellar technetium abundance can therefore give clues to the time of mixing from the s-process zone to the stellar surface.

(1)   P. Merril, Astrophys. J. 116 (1952) 21
(2)   I.R. Little-Marenin, S.J. Little, Astron. J. 84 (1979) 1374
(3)   R.L. Macklin, Nucl. Sci. Eng. 81 (1982) 520
(4)   F. Käppeler, H. Beer, K. Wisshak, D.D. Clayton, R.L. Macklin,
        R. Ward, Astrophys. J. 257 (1982) 821
(5)   A.G.W. Cameron, Astrophys. J. 130 (1959) 452

1.1.6 NEUTRON CAPTURE CROSS SECTIONS OF THE STABLE XENON ISOTOPES AND
       THEIR APPLICATION IN STELLAR NUCLEOSYNTHESIS

H. Beer, F. Käppeler, G. Reffo[+], G. Venturini[+], Astrophysics and
Space Science (in press)

The neutron capture cross sections of ^{124,132,134}Xe have been mea-
sured by the activation technique at 25 keV neutron energy. These data were
supplemented by calculated capture cross sections for ^{128,129,130,131}Xe via
the statistical model based on carefully evaluated local parameter system-
atics. The complete set of capture cross sections obtained in this way is
shown in Table I together with previous, more global calculations. The un-
certainty of our theoretical results is estimated to 20 %.

Table I Comparison of the Xenon Cross Sections obtained in this work with
         Various Calculations at kT = 30 keV.

Xe - Isotopes	$\sigma_{n\gamma}$ (mb)					
	Harris (1)	Holmes et al.(2)	ENDF/B-V (3)	Benzi et al.(4)	present work calc.	exp.
128	510	232	206	239	249	
129	1454	666	560	572	470	
130	207	143	156	189	153	
131	570	587	310	491	348	
132	74.9	91	85	116	65	61+4
134	37.5	47.5	41	60	33	29+2
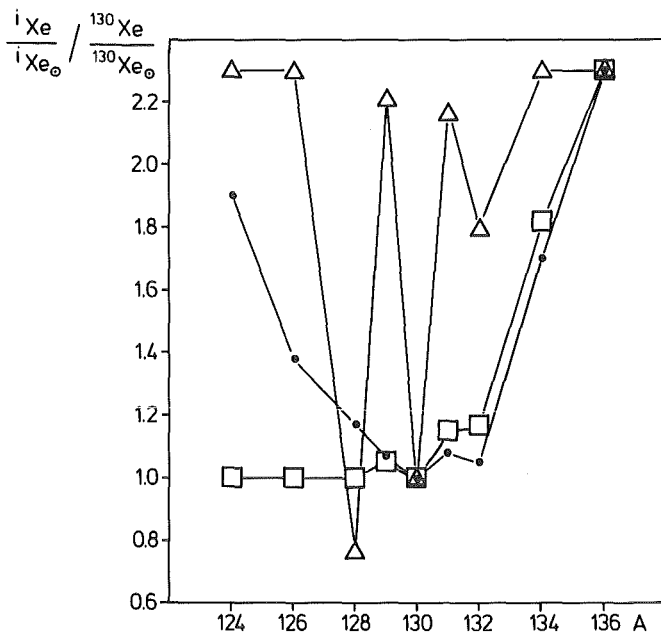
Fig. 1
Isotopic anomaly in chemi-
cally prepared residues of
the Allende meteorite (5)
as shown by the black dots.
Open squares result from
an interpretation in terms
of an exotic component
added to the solar system
material. Open triangles
indicate the effect of de-
pleting solar system xenon
in its s-process component.

With these cross sections we determined the solar xenon abundance through s-process systematics and decomposed the abundances of ^{129,131,132}Xe into their s- and r-process contributions. Furtheron, various isotopic anomalies in the xenon isotopes which were detected in several meteorites are discussed in detail. As an example, Fig. 1 shows that the anomaly found in the Allende meteorite (5) can be explained rather by an intermediate type r-process (or nß-process) than by the original interpretation by Clayton and Ward (6) as being due to a depletion of solar system xenon in its s-process component.

(1)   M.J. Harris, Astrophys. Space, Sci. 77 (1981) 357
(2)   J.A. Holmes, S.E. Woosley, W.A. Fowler, B.A. Zimmerman,
        At. Data and Nucl. Data Tables 18 (1978)
(3)   Kinsey, ENDF/B Summary Documentation, BNL-NCS-17541 (1979)
(4)   V. Benzi, R. D'Orazi, G. Reffo, M. Vaccari, CNEN-report RT/FI6 (1972)
(5)   R.S. Lewis, B. Srinivasan, E. Anders, Science 190 (1975) 1251
(6)   D.D. Clayton, R.A. Ward, Ap. J. 224 (1978) 1000

+   E.N.E.A., Bologna, Italy

1.1.7   NEUTRON CAPTURE CROSS SECTIONS OF ^{142,143,144}Nd

G.J. Mathews[+], F. Käppeler, K. Wisshak

The Nd isotopes are important for the s-process because of two reasons:

(i) ^{142}Nd is an s-only nucleus with the magic neutron number 82; that means, it represents an important normalization point for the s-process abundances.

(ii)   The only significant isotopic anomalies in heavy elements (besides the noble gases) were found for Nd. Any interpretation has to check whether this anomaly might have to do with an enrichment or a depletion in s-process material (1).

To improve the data basis for such an analysis, we have remeasured the capture cross sections of ^{142,143,144}Nd between 6 and 250 keV neutron energy. The experimental setup consisted of two C_6D_6 detectors with off-line pulse height weighting. Neutrons were produced at the Karlsruhe Van de Graaff accelerator via the ^{7}Li(p,n)-reaction. A flight path of 0.60 m and an overall time resolution of $\sim$ 1.2 ns allowed for a resolution of $\Delta E/E$ = 30 keV. Our results for the 30 keV Maxwellian averaged cross sections are shown in Table I together with previous data.

Table I   30-keV Maxwellian Averaged Cross Sections (mb)

Isotope	Ko 78 (2)	Mu 78 (3)	Na 79 (4)	this work
^{142}Nd	48 + 8	57 + 7		51 + 4
^{143}Nd		265 + 50	319 + 26	258 + 11
^{144}Nd	65 + 10			123 + 6

We find good agreement with existing measurements for all isotopes but for ^{144}Nd where a severe discrepancy of more than a factor 2 shows up. The s-process analysis is in progress.

(1)   D.D. Clayton, Ap. J. (in press) and priv. communication
(2)   V.N. Kononov, B.D. Yurlov, E.D. Poletaev, V.M. Timokhov, Sov. J. Nucl. Phys. 27 (1978) 5
(3)   A.R. de L. Musgrove, B.J. Allen, B.W. Boldeman. , Proc. Int. Conf. on Neutron Physics and Nuclear Data, Harwell, September 1978, OECD Nuclear Energy Agency (1979) p. 449
(4)   Y. Nakajima, A. Asami, Y. Kawarasaki, Y. Furuta, T. Yamamoto, Y. Kanda, Proc. Int. Conf. on Neutron Physics and Nuclear Data, Harwell, September 1978, OECD Nuclear Energy Agency (1979) p.438

+   Univ. of California, Lawrence Livermore Laboratory, Livermore, Calif. USA

1.1.8 ^{148,150}Sm: A TEST FOR s-PROCESS NUCLEOSYNTHESIS

R. R. Winters[+], F. Käppeler, K. Wisshak, G. Reffo[++], A. Mengoni[++]

The s-only isotopes ^{148,150}Sm allow to check the prediction of s-process nucleosynthesis, namely that the product $\sigma_{n\gamma} \cdot N_s$ (N_s being the resulting abundance) should be about equal for the isotopes involved in this process.

Similar tests using isotopes of Te and Ba verified the σN-equality within the respective cross section uncertainties of 10 - 15 %. However, for the example of Sm the situation was confused by a big discrepancy between previous measurements (see Table I).

We have remeasured the capture cross sections of ^{148,149,150}Sm in the energy range from 4 to 250 keV giving careful attention to reducing systematic uncertainties.

The absolute cross sections were determined with an uncertainty of 4.5 % as is quoted in Table I, whereas for the cross section ratios for

which part of the uncertainties cancel out, a 3.3 % uncertainty was found. This seems to be kind of a limit for present day techniques.

Table I   Experimental values for the 30 keV Maxwellian Averaged Cross Section (mb)

Isotope	Ma 67 (1)	Ko 78 (2)	Mi 79 (3)	this work
^{148}Sm	257 ± 50	281 ± 23		269 ± 12
^{149}Sm	1620 ± 280		2490 ± 200	1489 ± 65
^{150}Sm	370 ± 72	690 ± 51		458 ± 18

Comparison of the results in Table I shows that good agreement is found only for ^{148}Sm. For the other two isotopes severe descrepancies could be resolved by the present measurement.

For the astrophysically important cross section ratio $\sigma^{148}Sm/\sigma^{150}Sm$ we obtained

$$\frac{(\sigma N)^{148}Sm}{(\sigma N)^{150}Sm} = 0.90 \pm 0.03.$$

This value being significantly different from unity implies a branching of the s-process capture path at ^{147}Nd and $^{147,148}Pm$. In order to analyse these branchings, the capture cross sections of the unstable branching isotopes were calculated according to the Hauser-Feshbach formalism using a consistent set of carefully evaluated parameters.

With all these informations constraints for the shape and the normalization of the $\sigma N(A)$-curve as well as for the neutron density during the s-process were derived. The respective results are most affected by the uncertainty in the cross section ratio of ^{148}Sm and ^{150}Sm. Further improvements in the measurement technique would therefore be important for this problem.

(1)   R.L. Macklin, J.H. Gibbons, Phys. Rev. 159 (1967) 1007
(2)   V.N. Kononov, B.D. Yurlov, E.D. Poletaev, V.M. Timokhov, Sov. J. Nucl. Phys., 27 (1978) 5
(3)   M. Mizumoto et al., Proc. Int. Conf. on Nucl. Cross Sections for Technology, Knoxville, Tennessee, October 22-26, 1979, NBS Special Publication 594, U.S. National Bureau of Standards (1980) p. 328
+   Denison University, Granville, Ohio, USA
++   E.N.E.A., Bologna, Italy.

1.1.9 ^{178,179,180}Hf AND ^{180}Ta(n,γ) CROSS SECTIONS AND THEIR CONTRIBUTION TO STELLAR NUCLEOSYNTHESIS

H. Beer, R.L. Macklin[+], Phys. Rev. C **26** (1982) 1404

The neutron capture cross sections of ^{178,179,180}Hf were measured in the energy range 2.6 keV to 2 MeV. The average capture cross sections were calculated and fitted in terms of strength functions. Resonance parameters for the observed resonances below 10 keV were determined by a shape analysis. Maxwellian averaged capture cross sections were computed for thermal energies kT between 5 and 100 keV. The cross sections for kT = 30 keV were used to determine the population probability of the 8$^-$ isomeric level in ^{180}Hf by neutron capture as (1.24 ± 0.06) % and the r-process abundance of ^{180}Hf as 0.0290 (Si ≡ 10^6).

These quantities served to investigate the origin of ^{180}Ta^m by neutron capture nucleosynthesis. The detailed analysis showed that the s-process contributes only ∿ 10 % to the buildup of the ^{180}Ta^m solar abundance provided our estimated logft value of 6.4 for the ^{180}Hf^m → ^{180}Ta^m beta decay transition is correct. A final clarification must await a measurement of this fractional beta decay f_β^m. If it should turn out that f_β^m is substantially greater than the present estimate one has to investigate the question of how the ^{180}Ta^m isomer could survive in the hot stellar photon bath under s-process temperature conditions because any excited level which could equilibrate the isomer with the 8.1 h ground state would rapidly destroy the result of the s-process synthesis. This would mean that ^{180}Ta^m can be used as a stellar thermometer of the s-process.

There is still the possibiliby that post-r-process nucleosynthesis can produce a sizable amount of ^{180}Ta^m. To confirm this would mainly require a careful search for a branch in the ^{180}Lu decay feeding the ^{180}Hf^m isomeric state. The study of these extended questions in the frame of s- and r-process nucleosynthesis requires, however, a detailed knowledge of the ^{180}Ta level scheme below 500 keV.

+ Oak Ridge National Laboratory, Oak Ridge, Tennessee, USA

1.1.10 THE SOLAR MERCURY ABUNDANCE

G. Walter, H. Beer, Astronomy and Astrophysics 123 (1983) 279

For the determination of elemental solar abundances C1 type carbon-aceous meteorites represent the primary source of information. This is true for at least the bulk of elements. Exceptions are the highly volatile noble gases but also mercury which shows an enormous variability in meteoritic samples (1).

In this situation it appears to be justified to refer to the con-cepts of nucleosynthesis and to try an interpolation via neighbouring nuclei.

In the present investigation the solar mercury abundance is estimated through s-process systematics. The analysis is based on the measurement of the neutron capture cross section of ^{202}Hg which is dominantly of s-process origin. The r-process contribution to this isotope was approximated by r-only ^{204}Hg. With the measured cross section of 72 ± 5 mb we derived a solar mer-cury abundance of 0.24 ± 0.04 / 10^6Si using the σN-systematics of Käppeler et al. (2).

A comparison of published solar abundances for mercury and the result of this work is given in Table I:

Table I Comparison of solar abundances for mercury

Ref.		Solar mercury abundance
Suess and Urey	(3)	0.284
Cameron	(4)	0.75
Suess and Zeh	(5)	0.44
Cameron	(6)	0.4
Cameron	(7)	0.21
Palme et al.	(8)	0.4
Anders and Ebihara	(9)	0.52 ± 0.26
this work		0.24 ± 0.04

(1)   B. Mason, Cosmochemistry. Part 1. Meteorites, in Data of Geochemistry, 6th edn., ed. M. Fleischer (Geol. Survey Prof. Paper 440-B-1, U.S. Govt. Print. Off., 1979)
(2)   F. Käppeler, H. Beer, K. Wisshak, D.D. Clayton, R.L. Macklin, R.A. Ward, Ap. J. 257 (1982) 821
(3)   H.E. Suess, H.C. Urey, Rev. Mod. Phys. 28 (1956) 53
(4)   A.G.W. Cameron, in Origin and Distribution of the Elements, ed. L.H. Ahrens (Pergamon Press, Oxford, 1968)
(5)   H.E. Suess, H.D. Zeh, Astrophys. Space Sci. 23 (1973)173
(6)   A.G.W. Cameron, Space Sci. Rev. 15 (1973)121
(7)   A.G.W. Cameron, in Essays in Nuclear Astrophysics, eds. C.A. Barnes, D.N. Schramm (Cambridge University Press, Cambridge Mass., 1982)
(8)   H. Palme, H.E. Suess, H.D. Zeh, in Landolt-Börnstein, New Series VI/2, Chapt. 3,4 (Springer, Heidelberg 1981)
(9)   E. Anders, M. Ebihara, Geochim. Cosmochim. Acta 46 (1982) 2363

1.1.11 DIRECT RADIATIVE CAPTURE: TEST OF THE LANE-LYNN MODEL AND DEVELOPMENT
OF A METHODOLOGY FOR CALCULATIONS

A. Mengoni, KfK-report 3452 (1982)

The Lane-Lynn model for direct radiative capture (DRC) is extended to isotopes where no experimental information on the low-lying levels (spectroscopic factors etc.) is available. To this end we assumed that all the partial transitions to the final levels are lumped in the $s_{1/2} \rightarrow p_{3/2}$, $s_{1/2} \rightarrow p_{1/2}$ transitions only (where the p-wave final states are single particle states with complete strength). Within these assumptions the direct capture cross sections for calcium isotopes between A = 40 and A = 48 (Fig. 1) as well as for ^{136}Xe were calculated. We showed that the uncertainties of these calculations are $\lesssim$ 20 % if we compare the results to the calculations with the Lane-Lynn model for ^{42,48}Ca and ^{136}Xe where the respective experimental informations are available. An additional uncertainty of $\sim$ 10 % has to be admitted in the calculations due to the uncertainty of the scattering radius which accounts for the effect of distant levels in the DRC model.
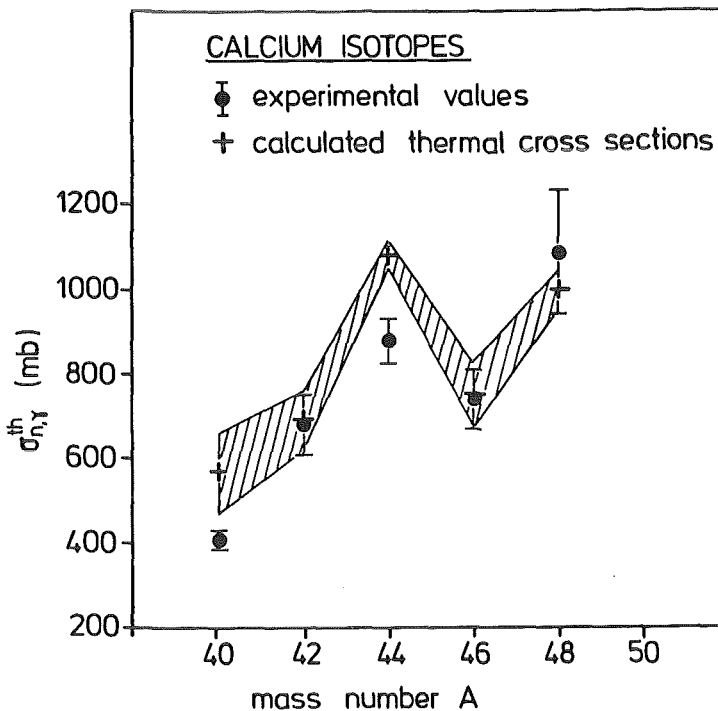
Fig. 1
Comparison of calculated DRC cross sections with experimental values from Ref.(1) for even-mass calcium isotopes at thermal energy. The calculated values $\sigma_{n,\gamma}^{DRC}$ are derived under the assumptions given in the text. The hatched error band of the calculated values corresponds to the uncertainties of the scattering radius R'^{exp}.

The new approach allows for an evaluation of thermal cross sections and, more important, for the calculation of DRC cross sections of extremely neutron rich nuclei which are significant for nucleosynthesis of the heavy elements in the rapid neutron capture process (r-process).

(1)   S.F. Mughabghab, M.Divadeenam and N.E. Holden, Neutron Cross-Sections (Academic Press, New York) 1981, Vol. 1, part A.

1.1.12 NEUTRON CAPTURE RATES IN THE r-PROCESS: THE ROLE OF DIRECT RADIATIVE CAPTURE

G.J. Mathews[+], A. Mengoni, F.-K. Thielemann[++], W.A. Fowler[+++],

Ap. J. (in press)

The nuclear physics associated with neutron capture along the r-process path is reviewed, and it is noted that the usual statistical assumptions for the capture rates may not be valid. We have shown that direct radiative capture can introduce a significant, and perhaps more appropriate, contribution to the neutron capture rate for nuclei in the vicinity of the r-process path and should be included in r-process reaction networks.

As an example, the Cd isotopes with $120 \leq A \leq 140$ have been investigated. The DRC calculations are shown in Fig. 1 in comparison with the statistical compound nucleus model. Once the neutron shell closure at $N = 82$ is
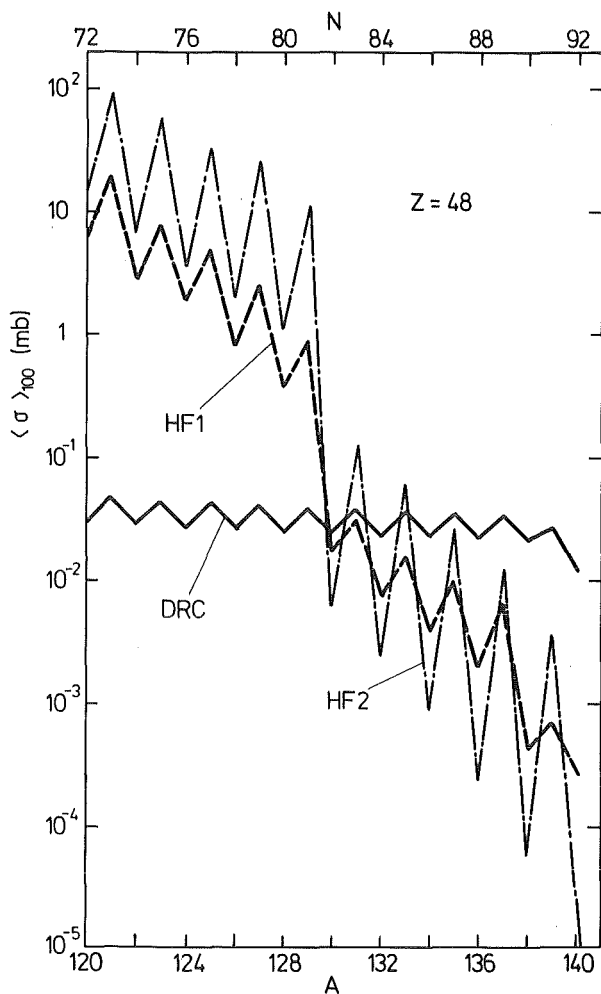
Fig. 1
A comparison of Maxwellian averaged neutron capture cross sections at kT = 100 keV for Cd isotopes through the r-process path at A = 130. DRC indicates the direct radiative capture component. HF1 and HF2 show two different approaches to the statistical Hauser-Feshbach model. It can be seen that beyond the closed neutron shell at N = 82 the direct radiative capture component dominates the neutron capture rate.

reached, the level density decreases drastically, and therefore the compound nucleus capture cross section falls well below the DRC contribution which in turn remains practically constant. This holds at least for energies around 100 keV corresponding to typical r-process temperatures.

Since the DRC estimates presented here can be taken as realistic lower limits to the actual neutron capture rates, these cross sections can be utilized to infer an upper limit to the critical neutron density above which (n,γ) equilibrium can probably be assumed in any r-process production calculation. This limit we determine to be $n_{crit} < 1.5 \times 10^{20}$ cm^{-3}. In a future paper detailed systematics of the DRC reaction rates (including other multipolarities and angular momenta) will be summarized for application to r-process network calculations.

+   Lawrence Livermore National Laboratory, Livermore, California, USA
++   Max-Planck-Institute für Physik und Astrophysik,München
+++   W.K. Kellogg Radiation Laboratory, California Institute of Technology, Pasadena, California, USA

1.2 NEUTRON PHYSICS

1.2.1 THE NEUTRON CAPTURE CROSS SECTION OF ^{243}Am IN THE ENERGY RANGE FROM 5 TO 250 keV

K. Wisshak, F. Käppeler, G. Rupp, KfK-report 3503 (1983) and Nucl. Sci. Eng. (in press)

Neutron capture in ^{243}Am contributes significantly to the production of ^{244}Cm, which is of importance in fast reactor studies as a strong neutron emitter, and hence affects the total neutron production rate (1). Several requests for capture cross section measurements have been formulated (1, 2, 3, 4) asking for an accuracy of $\sim$ 10 % in the keV range. The quoted applications are burn-up studies, the build-up of transplutonium elements, neutron shielding of transport casks for spent fuel elements, fuel reprocessing and storage as well as the long term radioactivity hazard.

Due to the very high radioactivity of the sample material no experimental data for the capture and subthreshold fission cross section of ^{243}Am are available from literature up to now. In the present experiment these cross sections were measured in the energy range from 5 to 250 keV using ^{197}Au and ^{235}U as the respective standards. Neutrons were produced via the ^{7}Li(p,n) and the T(p,n) reaction with the Karlsruhe 3-MV pulsed Van de Graaff accelerator. Capture events were detected by two Moxon-Rae detectors with graphite and bismuth-graphite converters, respectively. Fission events were registered by a NE-213 liquid scintillator with pulse-shape discriminator equipment. Flight paths as short as 50-70 mm were used to obtain an optimum signal-to-background ratio. After correction for the different efficiency of the individual converter materials the capture cross section could be determined with a total uncertainty of 3 - 6 %. The respective values for the fission cross section are 8 - 12 %. The final results for the capture cross section of ^{243}Am are shown in Fig. 1 together with predictions from model calculations.
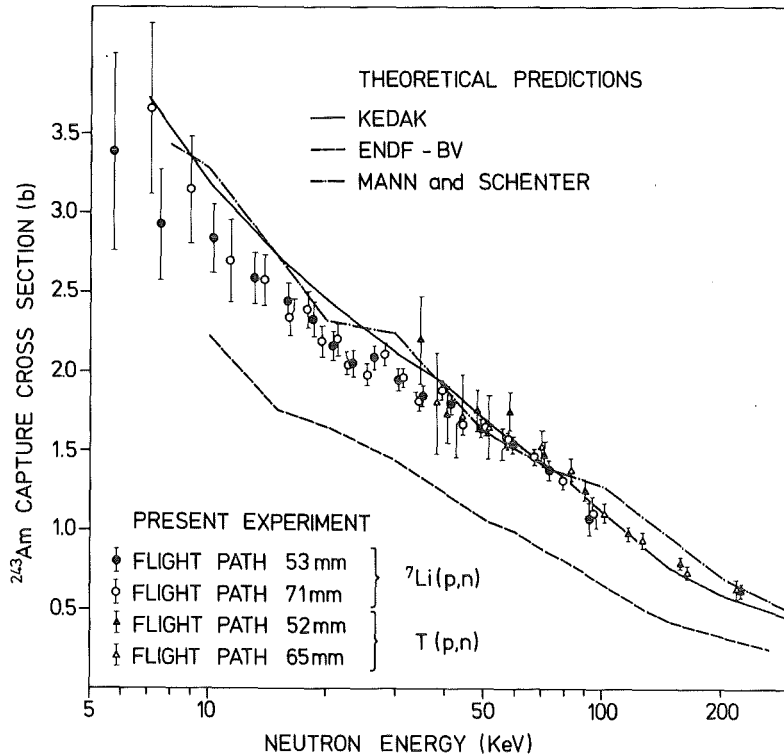
Fig. 1 The neutron capture cross section of ^{243}Am

(1)   B.H. Patrick and M.G. Sowerby, "U.K. Nuclear Data Progress Report
       1979", UKNDC (80) P 96
       NEANDC (E) 212 Vol. 8, INDC (UK-32)/LN
       United Kingdom Atomic Energy Authority, Harwell (1980)
(2)   N. Dayday, Ed., "World Request List for Nuclear Data", INDC (SEC)-78/
       URSF, International Atomic Energy Agency, Vienna (1981)
(3)   J. Bouchard, Proc. of the Second Advisory Group Meeting
       in Transactinium Isotope Nuclear Data, Cadarache 2-5 May, 1979,
       IAEA-TECDOC-232, International Atomic Energy Agency (1980) p.1
(4)   H. Kouts, Proc. of the Second Advisory Group Meeting on Transactinium
       Isotope Nuclear Data, Cadarache 2-5 May, 1979,
       IAEA-TECDOC-232, International Atomic Energy Agency (1980) p.23
(5)   F.H. Fröhner, B. Goel, U. Fischer, and H. Jahn, Proc. Int. Conf. on
       Nuclear Data for Science and Technology, Antwerp 5-10 Sept., 1982,
       D. Reidel Publishing Company (1983) p. 211
(6)   F.M. Mann and R.E. Schenter
       Nucl. Sci. Eng., 63, (1977) 242.

1.2.2 BACKWARD ANGLE A_y MEASUREMENT FOR $\vec{n}$ p SCATTERING UP TO 50 MeV

F.P. Brady[*], P. Doll, W. Heeringa, K. Hofmann, H.O. Klages,
J. Wilczynski

First measurements of A_y were carried out at POLKA (1) by having the collimated neutron beam impinge on a target consisting of a vertical cylinder (76.2 mm high x 76.2 mm diameter) of NE 213 liquid scintillator at 6 m from the $\vec{n}$ source. Scattered neutrons were detected at 2 m in 14 NE 213 liquid scintillators (vertical cylinder 200 mm high x 140 mm diameter) at 7 angles covering the range from $16°$ to $71°$ lab.. Each event (a target-detector coinci- dence) was characterized by the source-target (or incident) time-of-flight (TOF), the target-detector TOF, the pulse heights in the target and detector scintillators, the pulse shape in the detector scintillator, the detector number, and the $\vec{n}$ spin direction. The first parameter, which was measured re- lative to the cyclotron RF, gave the incident neutron energy which was divi- ded into 10 energy bins whose average energies were 17, 19, 22, 25, 27.5, 30, 33, 36, 40 and 50 MeV.

Here we report on new measurements of A_y for two backward $\vec{n}$ p CM angles. Using the set-up described elsewhere in this report, A_y was measured by de- tecting and identifying recoil protons from a CH_2 polyethylene target in ΔE-E telescopes at $\pm~14°$ and $\pm~20°$ lab.. In this case the incident TOF was derived from the ΔE-E coincidence. The other parameters measured were the ΔE and E pulse heights, telescope number, and $\vec{n}$ spin direction. In each experiment all parameters were written on magnetic tape. After off-line analysis the data were corrected for finite geometry and multiple scattering effects. Then from events for each energy bin and each pair of left (L) and right (R) detectors and for neutron spin up $\uparrow$ and down $\downarrow$, the usual asymmetry $\varepsilon = (\sqrt{L\uparrow\cdot R\downarrow} -\sqrt{L\downarrow\cdot R\uparrow})/(\sqrt{L\uparrow\cdot R\downarrow} + \sqrt{L\downarrow\cdot R\uparrow})$ and hence $A_y = \varepsilon/P_n$ is calculated. The resulting values of A_y (as %) for two incident neutron energies are shown in Fig.1. For compari- son other data from earlier work are also shown. In general the POLKA results have much smaller uncertainties particularly at 30 MeV where the $\vec{n}$ beam in- tensity is larger. The data at 22, 25, 27.5 and 33 MeV also have small $\Delta A_y \lesssim 0.5$ (%). The largest ΔA_y, $\lesssim 1.5$ (%), are at 50 MeV. The uncertainties in the $151°$ data from p detection are about the size of the data points. (Similar data for $140°$ are not yet analyzed.) This method gives high statisti- cal accuracy and is free of the multiple scattering corrections required for neutron detection data at similar CM angles.

At 17 MeV our results confirm the very precise data from Duke (2).

For energies above 20 MeV the existing data base was considerably improved. At 50 MeV the results agree well with the data from UC Davis (3,4). In Fig.1 the curve through the data is from a phase shift analysis (5) which did not include the 151° data from p detection. A more recent analysis including the 151° data has also been made (6), and the results show clearly the improved determination of some of the phase shifts, particularly the $^{3}D_{3}$ phase.
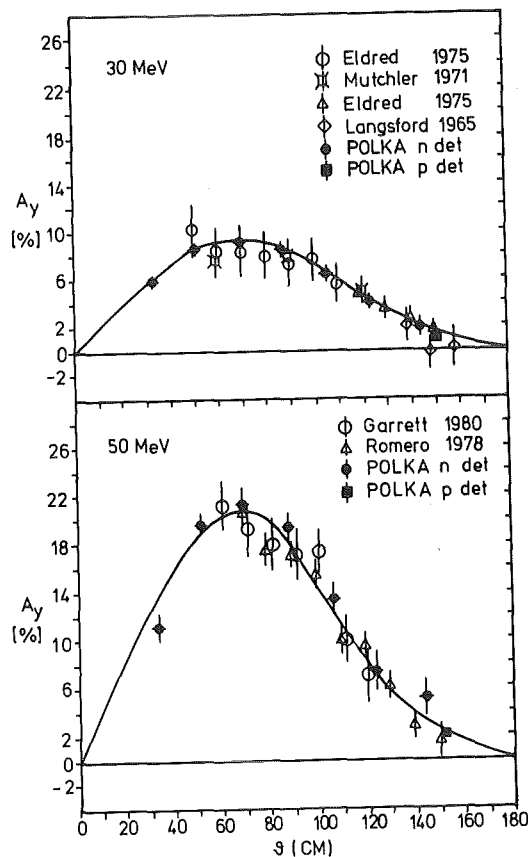
Fig.1: A_{y} data at 30 and 50 MeV. Eldred, Mutchler, Langsford, Garrett and Romero refer to refs. 7,8,9,3, and 4 respectively.

(1)   J. Hansmeyer, Diplomarbeit, Universität Karlsruhe, 1983
(2)   W. Tornow et al., Phys. Rev. Lett. 39 (1977), 915
(3)   R. Garrett et al., Phys. Rev. C21 (1980), 1149
(4)   J.L. Romero et al., Phys. Rev. C17 (1978), 468
(5)   J. Wilczynski et al., Verhandlungen DPG (VI) 18 (1983), p.976
(6)   J. Wilczynski et al., to be published
(7)   R.A. Eldred, B.E. Bonner, and T.A. Cahill, Phys. Rev. C12 (1975), 1717
(8)   G.S. Mutchler, and J.E. Simmons, Phys. Rev. C4 (1971)
(9)   A. Langsford et al., Nucl. Phys. A61 (1965), 457

*   Dept. of Physics, U.C. Davis, CA 95616

1.2.3 A PRELIMINARY PHASE SHIFT ANALYSIS FOR THE n-p SYSTEM UP TO 50 MeV

H.O. Klages, J. Wilczynski

Although the two-nucleon-system has been studied extensively for many years, there remain severe problems in a unique description of the system. In phase shift analyses (1-3) of the experimental data below 100 MeV several parameters deviate from phase shifts predicted by theoretical models. For some phase shifts even different models come to inconsistent answers. Although there are new cross section measurements available (4) the parameters $^1P_1$ and ε_1 remain still not well determined because of the insufficiency of the neutron-proton data base. Analysis shows that $^1P_1$ and ε_1 are strongly correlated on the base of the existing neutron-proton data. Sensitivity calculations indicate that this correlation can be reduced by an accurate measurement of the angular distribution of the analyzing power A_{yy} and a very precise determination of the differential cross section at backward angles.

Recently, at the Karlsruhe polarized neutron facility POLKA a measurement of the angular distribution of the analyzing power A_{yy} in the energy range from 20 MeV to 50 MeV was conducted (5). The data of this experiment are still being analyzed. A measurement of the differential cross section of the neutron-proton scattering at backward angles in the energy range of interest is also in preparation at POLKA. So the experimental situation will soon be calling for a new analysis which should be able to determine the isospin-singletparameters $^1P_1$ and ε_1 in a more stringent way.

The phase shift analysis reported here was intialized by a new precise measurement of the neutron-proton analyzing power A_y in the energy range from 17 MeV to 50 MeV (6). Calculations show that a precise knowledge of the analyzing power A_y is sensitive to (among other phase shifts) all ^3D phase shifts. $^3D_3$ phase shift is predicted differently by several theoretical models whereas $^3D_1$ and $^3D_2$ are in good agreement with values given by all models (7,8).

This single energy phase shift analysis was carried out at 25, 30, 40 and 50 MeV by taking into account all available neutron-proton data. Phase shifts with $J \le 3$ were fitted to the experiment data. Phase shifts contributing to higher J-values were fixed at values predicted by the Bonn OBEP (7). The energy dependence of all phase shifts was taken from the same OBE-model.

As expected, the addition of the new precise analyzing power data improved the knowledge of the ^3D phase shifts. In Fig.1a-c the central-, tensor- and spin-orbit phase parameters are presented which are linear combinations of the ^3D_J phase shifts with J = 1,2,3.

The phase shift analyses reported here could not determine the $^1P_1$ phase shift and the mixing parameter ε_1 which were discussed above, but investigate the behaviour of the ^3D phase shifts. In the next step, as soon as the new analyzing power A_{yy} data are available, the uncertainties in the parameters $^1P_1$ and ε_1 will be further reduced. The inclusion of proton data in a full analysis will lead to more reliable "experimental" phase shifts for the nucleon-nucleon system in this energy range.
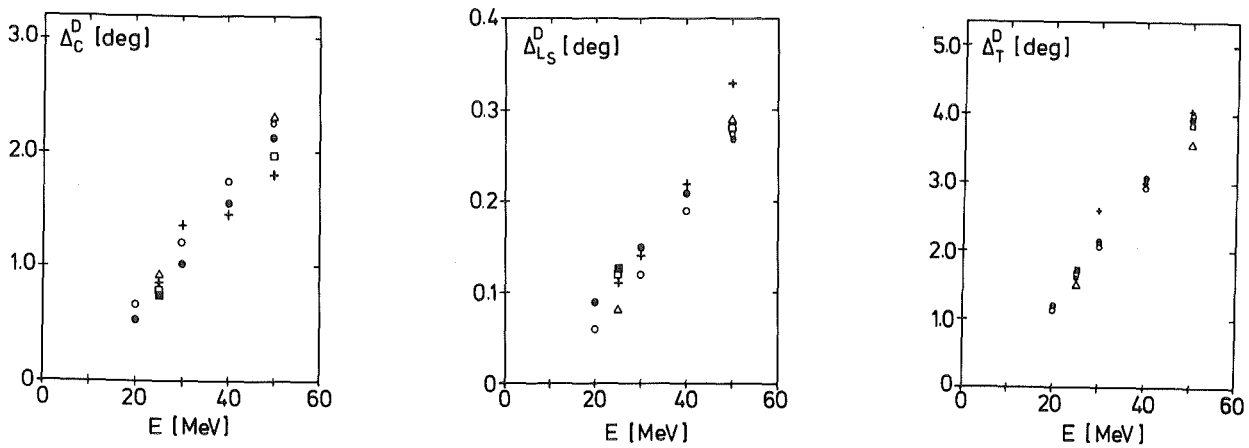
Fig.1a-c: $\Delta_C^D = + \dfrac{1}{15} (3 \cdot {}^3D_1 + 5 \cdot {}^3D_2 + 7 \cdot {}^3D_3)$

$\Delta_{LS}^D = - \dfrac{1}{60} (9 \cdot {}^3D_1 + 5 \cdot {}^3D_2 - 14 \cdot {}^3D_3)$

$\Delta_T^D = - \dfrac{7}{120} (3 \cdot {}^3D_1 - 5 \cdot {}^3D_2 + 2 \cdot {}^3D_3)$

+ this work, o MAW X (Ref.11), ● Bonn OBE (Ref.7), □ Paris Potential (Ref.8), Δ A&W (Ref.9), ▣ BBS (Ref.10).

(1)   R.A. Arndt, R.H. Hackman, and L.D. Roper, Phys. Rev. C15 (1977), 1021
(2)   P. Signell, in The (n,p) Reaction and the Nucleon-Nucleon Force, edited by C.D. Goodman, S.M. Austin, S.D. Bloom, J. Rapaport, and G.R. Satchler, Plenum Press, N.Y., 1980, page 1.
(3)   D. Bugg, J. Phys. G: Nucl. Phys. 6 (1980), 1329
(4)   J. Montgomery et al., Phys. Rev. C16 (1977) 499
(5)   Contribution 1.2.8 to this report
(6)   Contribution 1.2.1 to this report
(7)   K. Holinde and R. Machleidt, Nucl. Phys. A247 (1975) 495
(8)   M. Lacombe et al., Phys. Rev. C21 (1980) 861
(9)   R.A. Arndt and B.J. VerWest, 9th Int. Conference on the Few-Body Problem, Eugene, Oregon 1980
(10)   G.E. Bohannon, T. Burt, P. Signell, Phys. Rev. C13 (1976) 1816
(11)   M.H. MacGregor, R.A. Arndt, R.M. Wright, Phys. Rev. C182 (1969) 1714

1.2.4 SCATTERING OF POLARIZED NEUTRONS ON Ti AND TiH$_2$ SAMPLES

A. Bischoff, F.P. Brady[*], P. Doll, E. Finckh[**], W. Heeringa,
H.O. Klages, J. Wilczynski

Scattering experiments of polarized neutrons on a Ti and a TiH$_2$ sample were performed, to investigate the possibility of extracting reliable asymmetries for $\vec{n}$-p scattering. After a flight path of 5.2 m from the POLKA source the neutrons were scattered from the sample which was mounted between thick iron plates to simulate the surroundings of the polarized target. The scattered neutrons were detected by 5 pairs of symmetrically aranged detectors for which the distance to the scattering samples was optimized to achieve a kinematical separation between scattering from Ti and H. The following parameters where measured: The detector number, the total time-of-flight from the POLKA source via the sample to the detector, the proton recoil energy in the detector and the pulse shape in the detector. To subtract out carefully the amount of n-p scattering for a given incident neutron energy to the left or right detector, time-of-flight spectra for all detectors were taken at zero degrees; the neutron flux was monitored precisely by a pair of proton recoil telescopes before the scattering experiment. In addition background runs with no sample were performed. An independent check on the normalization is given by elastic scattering at 15°. Fig.1 shows recoil energy spectra from scattering on TiH$_2$ and after subtraction of scattering from Ti.
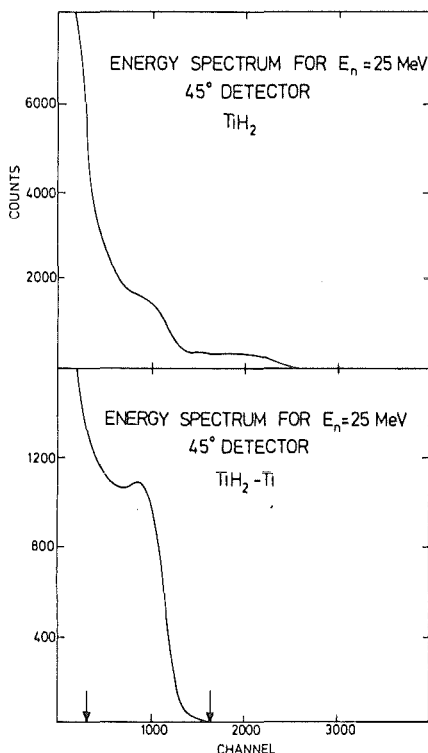
Fig.1:
a) Pulse height spectrum for neutrons of 25 MeV scattered by 45° on TiH$_2$
b) Ti background spectrum subtracted

The countrate in the subtracted spectrum was evaluated as indicated by the arrows. A lower threshold had to be set to exclude scattering events which result from lower neutron energies from previous cyclotron bursts. Fig.2 shows the asymmetries extracted for 9 energy intervalls from 19 MeV to 50 MeV incident neutron energy.
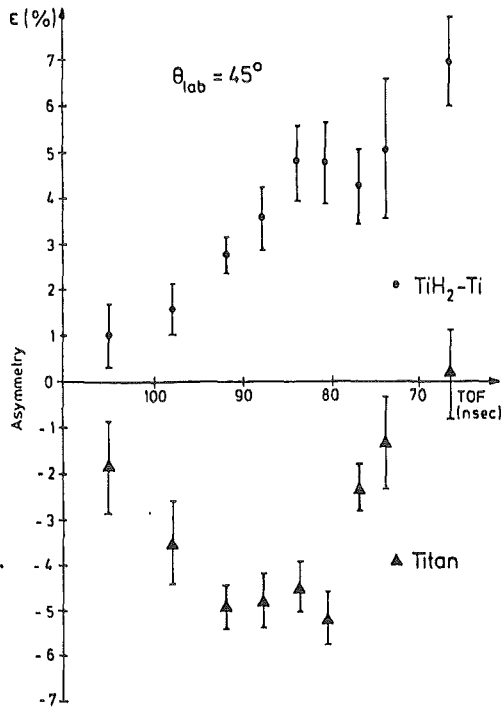
Fig.2: Count rate asymmetries in the time-of-flight spectra at 45°. Each data point corresponds to an energy bin in the range from 19 MeV to 50 MeV, calculated for the n-p scattering

The upper part shows the asymmetries ε for $\vec{n}$-p scattering, which agree fairly well with the ε from a previous $\vec{n}$-p experiment on a hydrocarbonate sample, the lower part shows ε for $\vec{n}$-Ti scattering in the same time-of-flight intervalls, which agree fairly well with optical model predictions. Similar data taken at 15°, 50°, 56° and 63° will prove the experimental methode to be reliable for measuring A_{yy} with this polarized target and our continous energy polarized neutron beam.

*   Dept. of Physics, U.C. Davis, CA 95616
**   University of Erlangen

1.2.5 DETERMINATION OF THE PROTON POLARIZATION IN TiH_2 WITH POLARIZED NEUTRONS

R. Aures, W. Heeringa, P. Jany, H.O. Klages, R. Maschuw, F.K. Schmidt

A brute-force polarized proton target has been developed for scattering experiments with fast polarized neutrons. The target material is titaniumhydride, which has the advantages of very high proton density and sufficient heat conductivity. During hydrogenation the titanium falls apart into a powder, which is pressed into copper cylinders afterwards. The sample is placed in the centre of a superconducting split pair magnet with a field strength of 8.2 T in this experiment, and it is cooled by a ^3He-^4He dilution refrigerator.

The temperature of the sample is measured with nuclear orientation thermometry using ^{60}Co in a cobalt single crystal soldered onto the copper cylinder. In principle the polarization of the protons can be calculated from the magnetic field and the temperature. However, several insufficiently known effects, e.g. warming up by the beam and spin-lattice relaxation make it desirable to measure the polarization directly.

We have done this recently in a transmission experiment using polarized neutrons of 1.2 MeV. Up to about this energy the total cross section of protons for neutrons depends strongly and in a well-known way on their relative spin orientation. A measurement of the count rate difference ε between parallel and anti-parallel spins is thus a direct and sensitive method to determine the proton polarization. The following relation holds for the quantities involved:

$$\varepsilon = \frac{N^{\uparrow\uparrow} - N^{\uparrow\downarrow}}{N^{\uparrow\uparrow} + N^{\uparrow\downarrow}} = \tanh \left(-NL \; p_p p_n \; \frac{\sigma^{\uparrow\uparrow} - \sigma^{\uparrow\downarrow}}{2}\right)$$

Here N and L are the proton density and the length of the target, p_p and p_n are the proton and neutron polarization and the sigma's are the total cross sections for both spin orientations.

Polarized neutrons were obtained by the reaction $^3H(p,n)^3He$ at a reaction angle of $\Theta_{lab} = 35°$ with protons of 2.26 MeV. The spin direction of the collimated neutron beam was reversed by the field of a superconducting solenoid about every 15 min. The obtained proton polarization data are shown in Fig.1 as crosses.
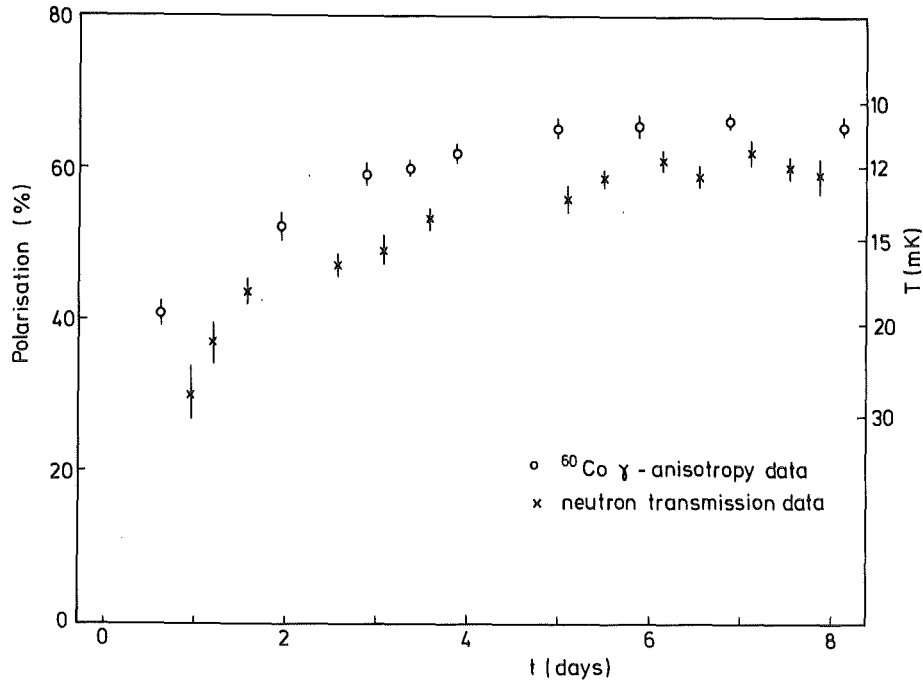
Fig.1: The proton polarization obtained by the transmission experiment and the temperature found in the γ-anisotropy measurements as function of the cooling time.

After about 6 days of cooling a stable situation was attained. The result after this time is p_p = 60.4 $\pm$ 0.7% when only the error in ε is taken into account. The error increases to 2.5% when all other errors are included.

The circles in Fig.1 are the temperatures obtained by the ^{60}Co γ-measurements. The temperature found after 6 days was 10.7 $\pm$ 0.2 mK, corresponding to a polarization of p_p = 65.4 $\pm$ 0.9%. With this target we have constructed the first brute-force polarized proton target useful for scattering experiments.

1.2.6 ANALYZING POWER OF THE ELASTIC $\vec{n}$-d SCATTERING FROM 14 MeV to 50 MeV

F.P. Brady[*], P. Doll, E. Finckh[**], W. Heeringa, K. Hofmann, H.O. Klages, W. Nitz, J. Wilczynski

The three-nucleon systems have been studied extensively both in experiments and theoretical approaches during the last years (1,2,3). Most precision data were obtained for the p-d system, whereas in the three-body calculations based on Faddeev-type equations the observables of the n-d channel were studied. The Coulomb interaction was treated perturbatively in these calculations and the question remained whether the existing discrepancies were due to these approximations or to the details of the nucleon-nucleon input (4). Recently, differential cross section data for the elastic n-d scattering in a wide range of energies were published (5) with an accuracy comparable to the p-d results. For the analyzing power only at a few energies (6,7,8) high precision data are available until now. Here we present the preliminary results of a measurement of the analyzing power A_y for the elastic $\vec{n}$-d scattering.

The experiment was performed using the continous energy polarized neutron beam at the Karlsruhe cyclotron. A deuterated liquid scintillator detector served as scattering sample. 20 neutron detectors were used in symmetric pairs at a distance of 1 m from the sample. Angular distributions were measured in the range from 39° c.m. to 153° c.m.. Multiparameter data acquisition was performed including pulse shape discrimination techniques for the neutron detectors and for the scattering sample. This enables us to distinguish clearly between signals from elastic scattering events, i.e. recoil deuterons, and from breakup protons in the scattering sample, as shown in Fig.1.
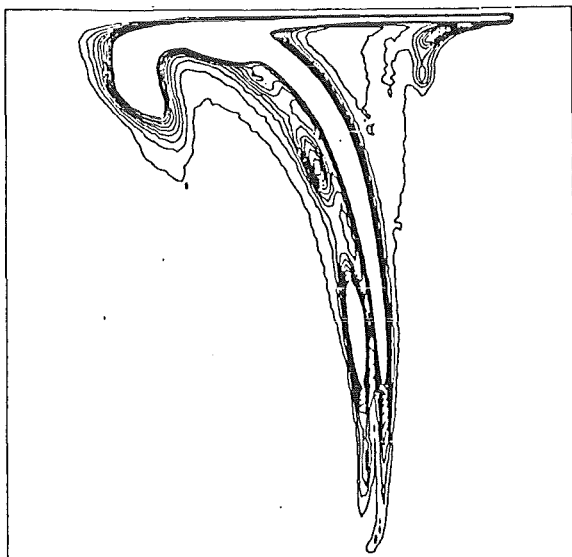
Fig.1: Two-dimensional view pulse height vs. pulse shape in the scattering sample. Shown are data for the neutron energy range from 36 to 50 MeV and for backward scattering angles.

The evaluation of analyzing power data for the FSI region of the break-up channel is described in contribution 1.2.6. The data for the elastic $\vec{\text{n}}$-d scattering were analyzed in 12 energy bins from 14 MeV to 50 MeV. In the energy range above 20 MeV the accuracy of our results is such that the existing data base is considerably improved. In the next step our raw data have to be corrected for multiple scattering and for finite geometry.

This new set of precise data together with the recent results for the differential cross section will allow conclusive comparison with p-d observables and with the predictions of three-nucleon calculations. Fig.2 shows our raw data at 30 MeV together with the $\vec{\text{p}}$-d results of Johnston et al. (9) ✵ and $\vec{\text{n}}$-d data of Dobiasch et al. (7)△ .
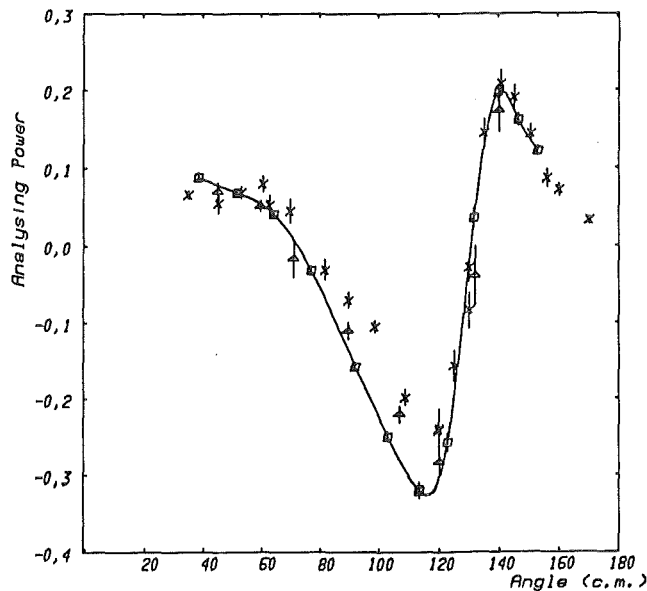
Fig.2: Comparison of $\vec{\text{n}}$-d and $\vec{\text{p}}$-d analyzing power data at 30 MeV (see text)

(1)   S. Fiarman and S.S. Hanna, Nucl. Phys. A251 (1975), 1
(2)   W. Grüebler, Nucl. Phys. A353 (1981), 31c
(3)   J.A. Tjon, Nucl. Phys. A353 (1981), 47c
(4)   H. Zankel and G.M. Hale, Phys. Rev. C24 (1981), 1384
(5)   P. Schwarz et al., Nucl. Phys. A398 (1983), 1
(6)   W. Tornow et al., Phys. Rev. Lett. 49 (1982), 312
(7)   H. Dobiasch et al., Phys. Lett. 76B (1978), 195
(8)   J.L. Romero et al., Phys. Rev. C25 (1982), 2214
        J.W. Watson et al., Phys. Rev. C25 (1982), 2219
(9)   A.R. Johnston et al., Phys. Lett. 19 (1965), 289

*   Dept. of Physics, U.C. Davis, CA 95616
**   Physikalisches Institut, Universität Erlangen

1.2.7 ANALYZING POWER DISTRIBUTIONS FOR THE ^{2}H($\vec{n}$,n)np BREAKUP IN THE FSI
RANGE

F.P. Brady[*], P. Doll, E. Finckh[**], W. Heeringa, K. Hofmann, H.O. Klages
W. Nitz, J. Wilczynski

In the study of the nucleon-nucleon potential it seems important to
get more information about the off-shell behaviour of three nucleon scat-
tering processes, because the off-shell matrix elements cannot be determined
in two-body reactions. Furtheron the polarization effects in the region of
the final-state-interaction (FSI) of the elastic nd scattering are very sen-
sitive for the test of the influence of higher partial waves in three-body
calculations (1). Theoretical considerations indicated for some phase space
regions that one can get more information on the repulsive case in the N-N
interaction. This leads to better knowledge of the short-range nuclear for-
ces (2). Experimental data for the breakup analyzing power exists only at
22.7 MeV (3), so there is still more need for precise data even at higher
energies.

The experiment reported here was performed at the Karlsruhe cyclotron
using the continuous energy neutron beam from POLKA (4). The experimental
set-up is described in contribution 1.2.5 to this report. The very good pulse
shape properties of the deuterated liquid scintillator, which served as a
scattering sample, enabled us to discriminate protons from the nd breakup
channel and recoil deuterons from elastic scattering in the data analysis.
Fig.1 shows the separation of these processes during the off-line data ana-
lysis.

This distinction allows the determination of the analyzing power of
the elastic nd scattering and the breakup channel simultaneously. The data
were analyzed in 10 energy bins from 16 MeV to 40 MeV in an angular range
from 30°_{CM} to 146.4°_{CM}. The position of the FSI region in the scattering matrix
is calculated from the kinematical situation that the particles in the np
pair have a relative kinetic energy smaller than 1 MeV. Fig.2 shows the ana-
lyzing power distribution for the FSI events at 22.5 MeV, without corrections
for background events, multiple scattering and finite geometry. The open
circles in Fig. 2 show the breakup data of the $\vec{p}$d experiment of ref. (3)
and the dashed line represents the result of a calculation by Doleschall.
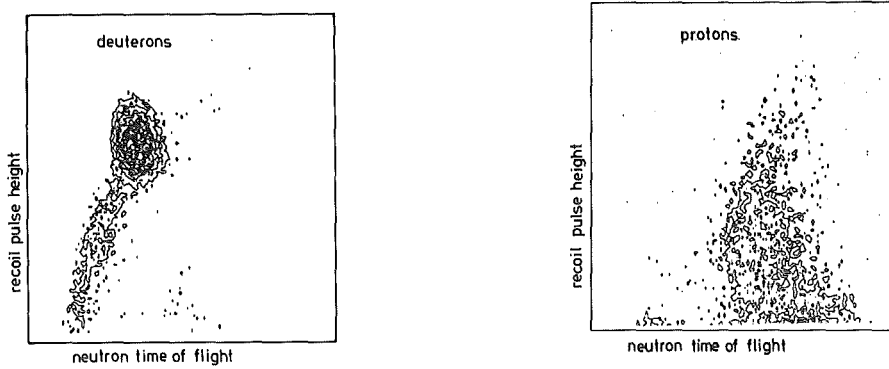
Fig.1: Two-dimensional representation of neutron scattering events (25 MeV, 102^{o}_{lab}) during the off-line data analysis. Left part: elastic nd scattering and double scattering events. Right part: n-d breakup processes and inelastic carbon scattering with a proton in the exit channel
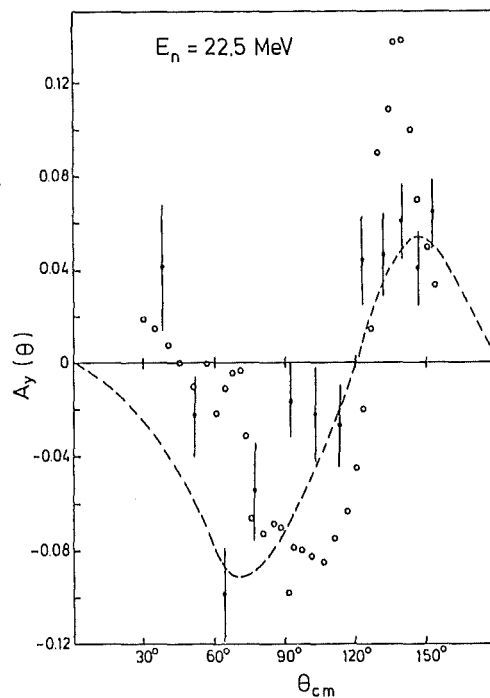
Fig. 2: Angular distribution of the analyzing power for the reaction $D(\vec{N},n)np$ (FSI) at 22.5 MeV. Open circles and dashed line see text.

(1)   J.H. Stuivenberg and R. van Wageningen, Nucl. Phys. A304 (1978), 141
(2)   W.M. Kloet and J.A. Tjon, Nucl. Phys. A210 (1973), 380
      M.I. Haftel et al., Phys. Rev. C14, 2 (1976), 419
(3)   F.N. Rad et al., Phys. Rev. Lett. 35 (1975), 1134
(4)   H.O. Klages et al., Nucl.Instr.Meth. (in print)

*   Dept. of Physics, U.C. Davis, CA 95616
**   Physikalisches Institut, Universität Erlangen

1.2.8 MEASUREMENT OF THE ANALYZING POWER OF THE ELASTIC $\vec{n}$-^{3}He SCATTERING
       UP TO 50 MeV

F.P. Brady[*], P. Doll, B. Haesner[**], W. Heeringa, K. Hofmann, P. Jany,
H.O. Klages, Chr. Maier, J. Wilczynski

In the framework of systematic investigations (1,2,3) of the four
nucleon system using the n+^{3}He entrance channel, the analyzing power of the
elastic $\vec{n}$-^{3}He scattering has been measured in the energy range from 16 to
50 MeV.

We made use of the continuous energy polarized neutron beam at the
Karlsruhe cyclotron (4). A liquid-^{3}He scintillation detector (5) served as
scattering sample. Neutrons were detected by 20 liquid scintillation detec-
tors at a distance of 1 m from the sample.

The analyzing power was measured at 14 angles from 38° CM to 158° CM.
Multiparameter data acquisition and off-line data analysis was performed.
The data were split into 11 energy bins centered at 16, 18, 20, 22, 24, 27,
30, 33, 36, 40 and 50 MeV, according to a recent measurement (3) of the
differential cross section for the elastic n-^{3}He scattering up to 30 MeV.

Angular distributions for A_y were determined with high statistical
accuracy compared to previous data in the energy range above 15 MeV (1,6,7).
Whereas the data of Lisowski et al. (6) at 17.1 MeV are in good overall agree-
ment with our results at 16 and 18 MeV, the angular distribution of Busse et
al. (7) at 22 MeV shows a different shape. By our new data at this energy
the deviating results of Dobiasch et al. (1) were confirmed.

For a final analysis in terms of phase shifts for the n-^{3}He system
our data have to be corrected for multiple scattering and finite geometry
effects. First calculations (8) show that these corrections are small due to
the careful multiparameter off-line data analysis. Preliminary results are
shown in Fig.1 and 2 for E_n = 22 MeV and E_n = 40 MeV, respectively.
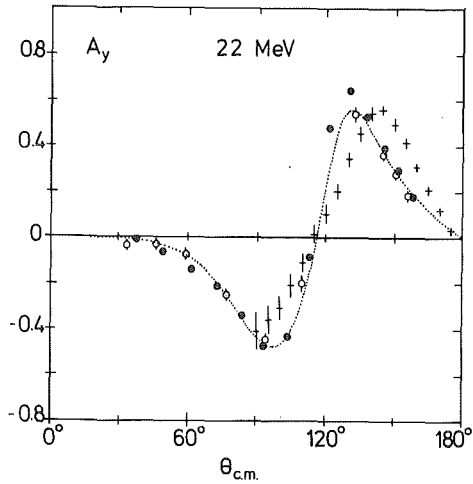
Fig.1: Our results at 22 MeV (full circles) compared to the data of Busse et al. (7) (crosses) and to the work of Dobiasch et al. (1) (open circles and dotted line).

Fig.2: The angular distribution of the $\vec{n}$-^{3}He analyzing power at 40 MeV. The statistical accuracy of the results is indicated.
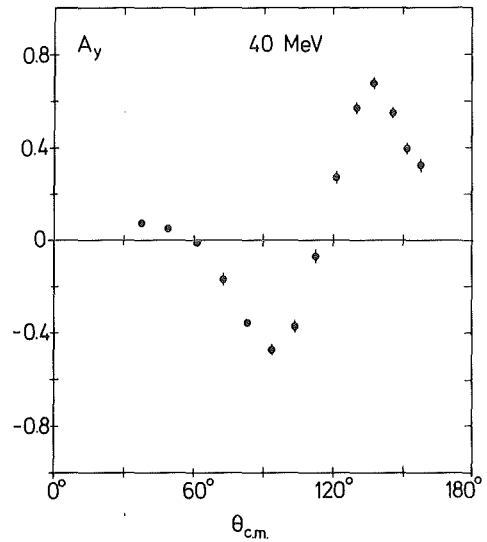
(1)   H. Dobiasch, Ph.D. thesis, Karlsruhe (1979)
        H.O. Klages et al., to be published
(2)   B. Haesner et al., Phys. Rev. C, in print
(3)   B. Haesner, Ph.D. thesis, Karlsruhe (1982)
(4)   H. Krupp, Diploma thesis, Karlsruhe (1983)
        H.O. Klages et al., submitted to Nucl. Instr. and Methods
(5)   R. van Staa et al., Nucl. Instr. Meth. 136 (1976), 241
(6)   P.W. Lisowski et al., Nucl. Phys. A259 (1976), 61
(7)   W. Busse et al., Nucl. Phys. A187 (1972), 21
(8)   Chr. Maier et al., Verhandl. DPG (VI) 18 (1983), 978

*   Dept. of Physics, U.C. Davis, CA 95616
**   TÜV Hessen, Frankfurt

1.2.9 MEASUREMENT OF THE SPIN CORRELATION PARAMETER A_{yy} FOR $\vec{n}-\vec{p}$ SCATTERING
IN THE ENERGY RANGE UP TO 50 MeV

R. Aures, A. Bischoff, F.P. Brady[*], P. Doll, E. Finckh[**], W. Heeringa,
K. Hofmann, H.O. Klages, J. Wilczynski, B. Zeitnitz

Recent nucleon-nucleon phase shift analyses (1-4) show that in the
energy range below 100 MeV several isospin-singlet parameters are not well
determined. The set of observables measured until now is by no means complete
and the accuracy of the neutron-proton data in this energy range is not suffi-
cient. Therefore, especially the $^1P_1$ phase shift and the $^3S_1-^3D_1$ mixing para-
meter ϵ_1 from the phase shift analyses do not agree with model predictions
(5,6). Sensitivity calculations reveal that certain observables depend strong-
ly on variations of these parameters. The impact of $^1P_1$ and ϵ_1 on the dif-
ferential cross section and on the spin correlation parameters A_{yy} and A_{zz}
is discussed briefly.

A variation of the $^1P_1$ phase shift at 25 MeV by two standard deviations
changes the differential cross section at far backward angles by about 2%.
The mixing parameter ϵ_1 does not effect this quantity but has a strong in-
fluence on A_{yy} as can be seen in Fig.1. The phase shift $^1P_1$ is important for
this observable at backward angles only. A_{zz} however is very sensitive to
variations of both ϵ_1 and $^1P_1$. The predicted distributions for A_{zz} depend
strongly on the starting values for the calculations (7). A measurement of
A_{yy} or of A_{zz} at forward and backward angles would fix ϵ_1 and $^1P_1$ simulta-
neously. The few existing data for A_{yy} (8,9) at backward angles are not suffi-
cient for this purpose.

At the Karlsruhe polarized neutron facility, POLKA, an experiment was
carried out to measure the analyzing power A_{yy} for $\vec{n}-\vec{p}$ scattering. Data were
taken in the energy range from 20 MeV to 50 MeV by detecting neutrons at
c.m. angles of $\pm 30^o$, $\pm 90^o$, $\pm 100^o$ and $\pm 112^o$. The polarization of the con-
tinous energy neutron beam used in this experiment varies from 0.3 at 20 MeV
to about 0.5 at 50 MeV neutron energy (10). In the scattering target a pro-
ton polarization of about 70% was achieved by "brute force polarization" of
a TiH_2 sample which was cooled to a temperature of 10 mK inside a strong
magnetic field of B = 9 T.

The scattering from hydrogen was separated by a difference measure-
ment using a pure Ti scattering sample in the cryostat. In a test experi-
ment it could be demonstrated that this method works neatly even with a con-
tinuous energy neutron beam. Using an unpolarized TiH_2 target, we were able

to reproduce the analyzing power A_y for the $\vec{n}$-p scattering.
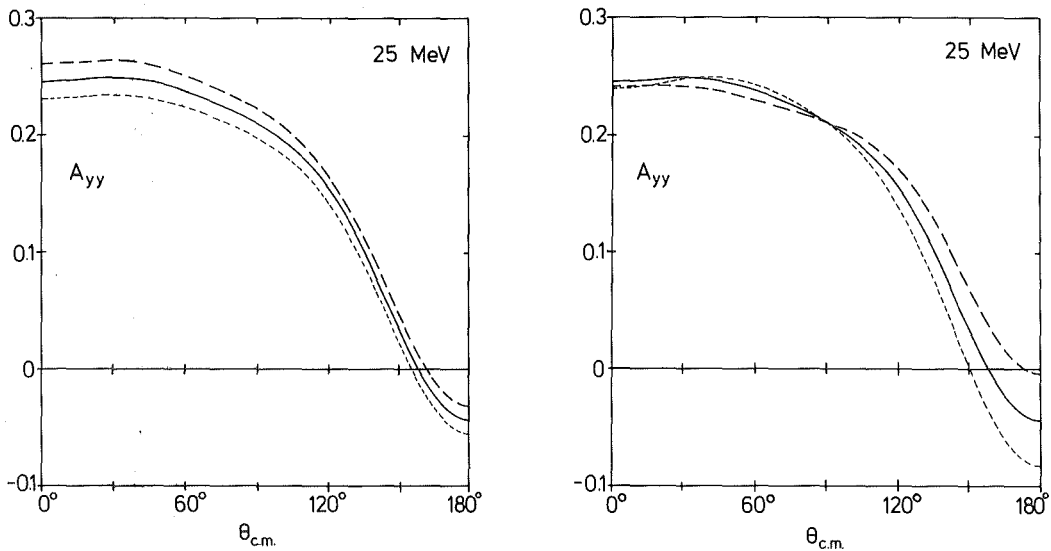
Fig.1: Sensitivity of the spin correlation parameter A_{yy} at 25 MeV to variations of the mixing parameter ε_1 and of the $^1P_1$ phase shift. Starting values are taken from the Paris potential (6).

a) $\varepsilon_1 = 1.6^{\circ}$ varied by $\pm 0.5^{\circ}$

b) $^1P_1 = -7.0^{\circ}$ varied by $\pm 2.0^{\circ}$

The data of the A_{yy} experiment are presently beeing analyzed. The estimated accuracy of the results will enable us to put sharper constraints on ε_1 (and probably $^1P_1$) in a new phase shift analysis including also the new Karlsruhe data (11) on A_y in the energy range from 17 to 50 MeV.

(1)   R.A. Arndt, J. Binstock and R. Bryan, Phys. Rev. D8 (1973), 1397
(2)   R. Bryan and J. Binstock, Phys. Rev. D19 (1974), 72
(3)   R.A. Arndt, R.H. Hackman and L.D. Roper, Phys. Rev. C15 (1977), 1021
(4)   P. Brady, in "Few Body Systems and Nuclear Forces I", Proceedings, Graz 1978, page 137
(5)   K. Holinde and R. Machleidt, Nucl. Phys. A247 (1975), 495
(6)   U. Lacombe et al., Phys. Rev. C21 (1980), 861
(7)   J. Wilczynski et al., Verhandlungen DPG (VI) 18 (1983), 976
(8)   D.H. Fitzgerald et al., Phys. Rev. C21 (1980), 1190
(9)   J.J. Malanify et al., Phys. Rev. Lett. 17 (1966) 481
(10)   H. Krupp, Diploma thesis, Karlsruhe (1983)
(11)   F.P. Brady et al., this report, and
        J. Hansmeyer, Diploma thesis, Karlsruhe (1983)

*   Department of Physics, U.C. Davis, CA 95616
**   Physikalisches Institut, Universität Erlangen

1.3   NUCLEAR REACTIONS BY CHARGED PARTICLES

1.3.1   OPTICAL POTENTIALS AND ISOSCALAR TRANSITION RATES FROM 104 MeV ALPHA-PARTICLE SCATTERING BY THE N=28 ISOTONES ^{48}Ca, ^{50}Ti and ^{52}Cr

R. Pesl, H.J. Gils, H. Rebel, E. Friedman[+], J. Buschmann,
H. Klewe-Nebenius, S. Zagromski,
KfK-report 3378 (1983) and Z. Physik A313 (1983) 111

Precisely measured differential cross sections for elastic and inelastic scattering of 104 MeV alpha-particles by ^{48}Ca, ^{50}Ti and ^{52}Cr are reported. The analyses aim primarily at the determination of strength, radial shapes and deformation of the scattering potentials, looking for isotonic differences of N=28 isotones. The mean square radii of the (real) potentials are discussed in terms of mean square radius differences of the matter distributions. The isoscalar transition rates derived by coupled channel analyses of the measured cross sections are compared with electromagnetic rates. In addition to the analyses on the basis of a slightly generalized extended optical model a semi-microscopic deformed folding model has been applied, using a density-dependent effective alpha-bound nucleon interaction. Though an excellent description of the data over the full angular range is obtained the resulting values of the deformation parameters appear to be not consistent with results from various different methods.

[+] Racah Institute of Physics, The Hebrew University, Jerusalem, Israel

1.3.2   ISOSCALAR OCTUPOLE TRANSITION RATES IN ^{50}Ti, ^{52}Cr, and ^{208}Pb FROM MODEL-INDEPENDENT ANALYSES OF 104 MeV α-PARTICLE SCATTERING

V. Corcalciuc[+], H. Rebel, R. Pesl, H.J. Gils,
J. Phys. G: Nucl. Phys. 9 (1983) 177

Applying a recently proposed method for model-independent analyses experimental differential cross sections for 104 MeV α-particle scattering have been analyzed. Reliable values of isoscalar $(0^+-3_1^-)$ octupole rates in ^{50}Ti, ^{52}Cr and ^{208}Pb are presented and compared with electromagnetic rates.

Table I   Transition rates for the $0^+ \rightarrow 3^+_1$ transition in ^{50}Ti, ^{52}Cr and ^{208}Pb resulting from the analysis of radial moments of the real transition potentials in α-particle scattering and from electromagnetic methods

Quantity	^{50}Ti	^{52}Cr	^{208}Pb	
G_3(s.p.u.	12.1 ± 0.5	11.1 ± 0.3	$43.0 \pm 1,3$	RMA of FB potentials
G_3(s.p.u.)	11.7	9.8	37.6	RMA of WS-derivative
G_3(s.p.u.)	-	6.1 ± 0.3	38.4	electrom. (1,2)
G_3(s.p.u.)	9.6	9.7	52.0	theoret. (3,4)

(1)   P.M. Endt, Atomic and Nuclear Data Tables 26/6 (1979) 547
(2)   H. Rothaas, J. Friedrich, K. Merle, B. Dreher, Phys. Lett. 51B (1974) 23
(3)   V. Gillet, B. Giraud, J. Picard, M. Rho, Phys. Lett. 27B (1968) 483
(4)   C.J. Veje, K. Danske Vidensk.Selsk., Mat.-Fys.Medd. 35 No 1 (1966) 1

[+] Central Institute of Physics, Bucharest, Romania

1.3.3   FUSION AND NONFUSION PHENOMENA IN THE ^{6}Li + ^{40}Ca REACTION AT 156 MeV

J. Brzychczyk[+], L. Freindl[+], K. Grotowski[+], Z. Majka[+], S. Micek[+], R. Planeta[+], M. Albińska[++], J. Buschmann, H. Klewe-Nebenius[+++], H. J. Gils, H. Rebel, S. Zagromski, Nucl. Phys. (in press)

Reaction products from ^{6}Li-induced reactions on ^{40}Ca at 156 MeV have been studied using the dE x E identification as well as the inclusice γ-ray method. The complete fusion cross-section has been found to be $\sigma_f = (67\pm20)$ mb. The Z distribution of fusion evaporation residues is compared with statistical model predictions. The Z spectrum of reaction products shows a maximum at $15 \lesssim Z \lesssim 20$, probably due to transfer and to incomplete fusion. It is suggested that the small value of the fusion cross-section is due to the strong competition of ^{6}Li break-up processes.

[+]   Institute of Physics, Jagellonian University and Institute of Nuclear Physics, Cracow, Poland
[++]   Institute of Physics, Technological University, Cracow, Poland
[+++]   KfK, Institut für Radiochemie

1.3.4 LOCAL DENSITY APPROXIMATION IN EFFECTIVE DENSITY-DEPENDENT αN-INTERACTIONS.

H. J. Gils

In folding models of the real optical potential for nucleon, light- and heavy-ion scattering the effective projectile-nucleon interactions used show up to be density-dependent. For finite range interactions a local density approximation (LDA) has necessarily to be introduced the form of which is not a priori given and may influence the properties of the folded optical potentials.

The effective αN-interaction $V_{\alpha N}(\vec{r}_N, \vec{r}_\alpha, \rho_m)$ used in single folding models for α-nucleus scattering is divided into a density-independent factor $f(|\vec{x}|)$ depending on the distance $|\vec{x}| = |\vec{r}_N - \vec{r}_\alpha|$ between the α particle and the interacting nucleon and a density-dependent factor $v_{DD}(\rho_m)$ (1)

$$V_{\alpha N}(\vec{r}_N, \vec{r}_\alpha, \rho_m) = f(|\vec{x}|) \cdot v_{DD}(\rho_m) \qquad (1)$$

where ρ_m is the target nuclear matter density. For the radial form factor $f(|\vec{x}|)$ a Gaussian plus Yukawa form is used for convenience with strength (V) and range (a) parameters V_G, a_G, V_Y, a_Y. The density dependence has previously been parametrized as (1)

$$v_{DD}(\rho_m) = 1 - \gamma \rho_m^{2/3} \qquad (2)$$

with the parameter $\gamma \approx 2$ fm^2 determined from fits to experimental data. Subject of the local density approximation is the question which *local* density $\rho_m(\vec{r})$ (i.e. the local density at which space coordinate $\vec{r}$) has to be used in Eq.(2). For practical purposes most frequently the forms

$$v_{DD}^N(\rho_m) = 1 - \gamma \rho^{2/3}(\vec{r}_N) \qquad (3a)$$

$$v_{DD}^{N\alpha/2}(\rho_m) = 1 - \gamma \rho^{2/3}\left(\frac{\vec{r}_N + \vec{r}_\alpha}{2}\right) \qquad (3b)$$

have previously been used (1,2) and were assumed to be equivalent due to the short range of $f(|\vec{x}|)$. If this is true, then also the form

$$v_{DD}^\alpha(\rho_m) = 1 - \gamma \rho^{2/3}(\vec{r}_\alpha) \qquad (3c)$$

should be equivalent to Eqs. (3a,b). In addition, we introduce a new form of LDA, namely

$$v_{DD}^M(\rho_m) = [1 - m\gamma \rho^{2/3}(\vec{r}_N)] [1 - (1-m)\gamma \rho_m^{2/3}(\vec{r}_\alpha)] \qquad (4)$$

which allows a continuous change between Eq.(3a) (m = 1) and Eq.(3c) (m = 0) and also approaches Eq.(3b) closely (m = 0.5).

The different forms of a LDA (Eqs. 3,4) have been compared in analyses of elastic α particle scattering cross sections of ^{40}Ca at E_α = 104 MeV in order to find out whether these approaches are equivalent in describing the data and reproducing the phenomenological potentials as previously assumed (1,2). The nuclear density ρ_m calculated by Brown et al. (3) has been used for this purpose and the parameters V_G, a_G, V_Y, γ were varied together with the imaginary part (Woods-Saxon form) of the optical potential. The results compiled in Tables I and II clearly indicate that the different forms are not equivalent.

The variation of the parameters over the "mixing" parameter m of the form (Eq. 4) is shown in Fig. 1. For m = 0.2 all parameters of $f(|\vec{x}|)$ are independent of m and γ confirming the factorization of $V_{\alpha N}$ into $f(|\vec{x}|)$ and v_{DD} (Eq.1). With the "mixed" LDA and the parameters obtained for m = 0.2 seven other 1 $f_{7/2}$ - shell nuclei could be fitted (4) yielding much better results than the previously used LDA (1).

Table Ia Parameters of the effective αN-interaction obtained from analyses of ^{40}Ca(α,α) using different forms of the LDA

LDA Eq.	χ^2/F	V_G (MeV)	a_G (fm)	V_Y (MeV)	a_Y (fm)	γ (fm^2)
3a	3.3	50.8	1.797	56.9	1.0	2.136
3b	2.9	21.4	1.926	162.	0.83	1.800
3c	2.6	19.1	2.020	102.	0.86	1.382
4	2.6	20.6	2.009	111.	0.85	1.645

Table IIb Volume integrals J and radial moments of the folded real optical potentials and of the WS imaginary potential as compared to the phenomenological FB-potential

LDA Eq.	χ^2/F	$-J_v/4A$ (MeV fm^3)	$\langle r^2\rangle_v^{1/2}$ (fm)	$\langle r^4\rangle_v^{1/4}$ (fm)	$\langle r^6\rangle_v^{1/6}$ (fm)	$-J_w/4A$ (MeV fm^3)	$\langle r^2\rangle_w^{1/2}$ (fm)
FB	2.2	325 $\pm$ 3	4.35 $\pm$ 0.02	4.83 $\pm$ 0.03	5.28+0.05	103.	4.93
3a	3.3	317.	4.35	4.86	5.34	99.	4.94
3b	2.9	318.	4.35	4.85	5.30	101.	4.92
3c	2.6	321.	4.35	4.84	5.29	102.	4.92
4	2.6	320.	4.35	4.84	5.29	102.	4.91
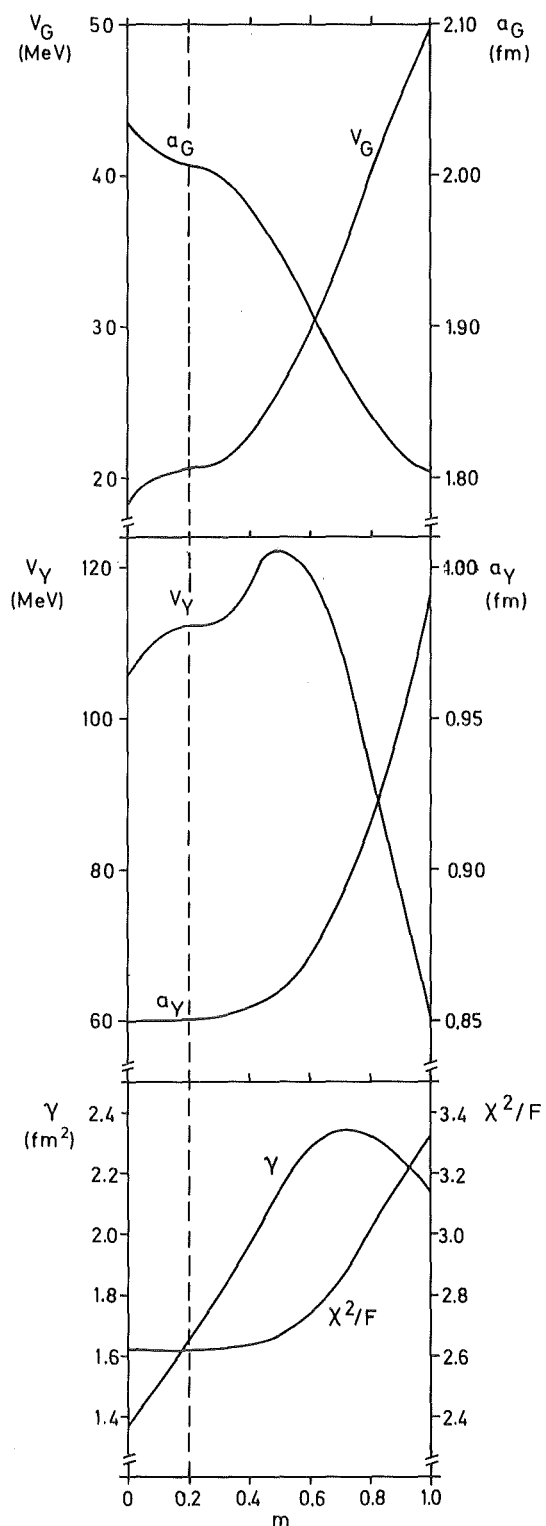
Fig. 1
Variation of the parameters
of the effective αN-interac-
tion (Eqs.3,4) over the
"mixing" parameter m and
corresponding values of χ^2/F.

(1)   E. Friedman, H. J. Gils, H. Rebel, Z. Majka, Phys. Rev. Lett. 41 (1978)
       1220

(2)   D.K. Srivastava, D. N. Basu, N. K. Ganguly, Phys. Lett. 124B (1983) 6

(3)   B.A. Brown, S.E. Massen, P.E. Hodgson, J. Phys. G 5 (1979) 1455

(4)   H.J. Gils, E. Friedman, H. Rebel, contr. 1.3.5

1.3.5 1 $f_{7/2}$ ISOTONE AND ISOTOPE DIFFERENCES OF NUCLEAR MATTER DENSITIES

H. J. Gils, H. Rebel, and E. Friedman[+]

The differences of the nuclear matter densities of 1 $f_{7/2}$ isotopes
^{40,42,43,44,48}Ca and isotones ^{50}Ti, ^{51}V, ^{52}Cr including two odd mass nuclei
have been investigated by folding model analyses of elastic α particle
scattering cross sections. The single-folding model analyses use a density-
dependent effective αN-interaction with an improved local density approxima-
tion (1). The nuclear matter densities ρ_m were parametrized as the sum of an
initial distribution function $\rho_o(r)$ (two parameter Fermi form) and a Fourier-
Bessel series (FB) (2)

$$\rho_m(r) = \rho_o(r) + \sum_{i=1}^{N} \beta_n j_o \left(\frac{n\pi r}{R_c}\right) \qquad (1)$$

The parameters β_n were varied together with the imaginary part of the opti-
cal potential in order to fit the experimental cross sections. The values of
χ^2 per degree of freedom obtained in the fits were as small as in potential
analyses using a "model-independent" FB potential. The resulting folded op-
tical potentials were in excellent agreement with the FB potentials (3) con-
firming the validity of the procedures used. As an example, Fig. 1 shows the
nuclei matter density of ^{50}Ti extracted from the analyses including the
error band (shaded area) obtained from the error correlation matrix (4).

ρ_m (fm^{-3})

^{50}Ti

r[fm]
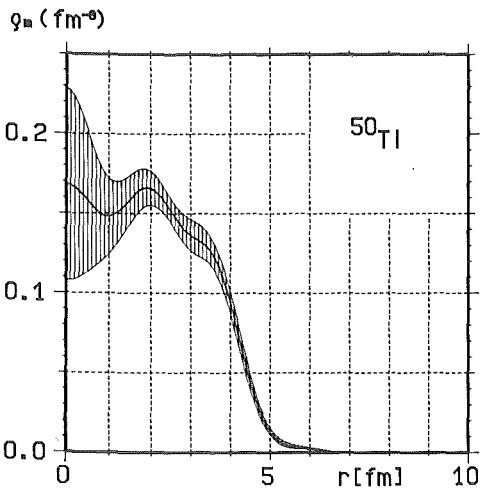
Fig.1 Nuclear matter density of
^{50}Ti with error band (shaded area)
from FB-folding model analysis.

Differences of the nuclear matter densities as compared to the closed shell
nuclei ^{40,48}Ca are shown in Fig. 2 for the isotope chain (upper row) and the
isotone chain (lower row). The differences show a systematic behaviour of
the even nuclei which is similar for isotopes and isotones. The additional
nucleons seem not only to be built into the 1 $f_{7/2}$ shell but also into ra-

dial regions corresponding to neighbouring shells. The odd nuclei ^{43}Ca, ^{51}V were found to have rms radii larger than those of their even neighbours (c.f. Table I), a fact which is also obvious from the shape differences (Fig.2) (which peak at larger radii).
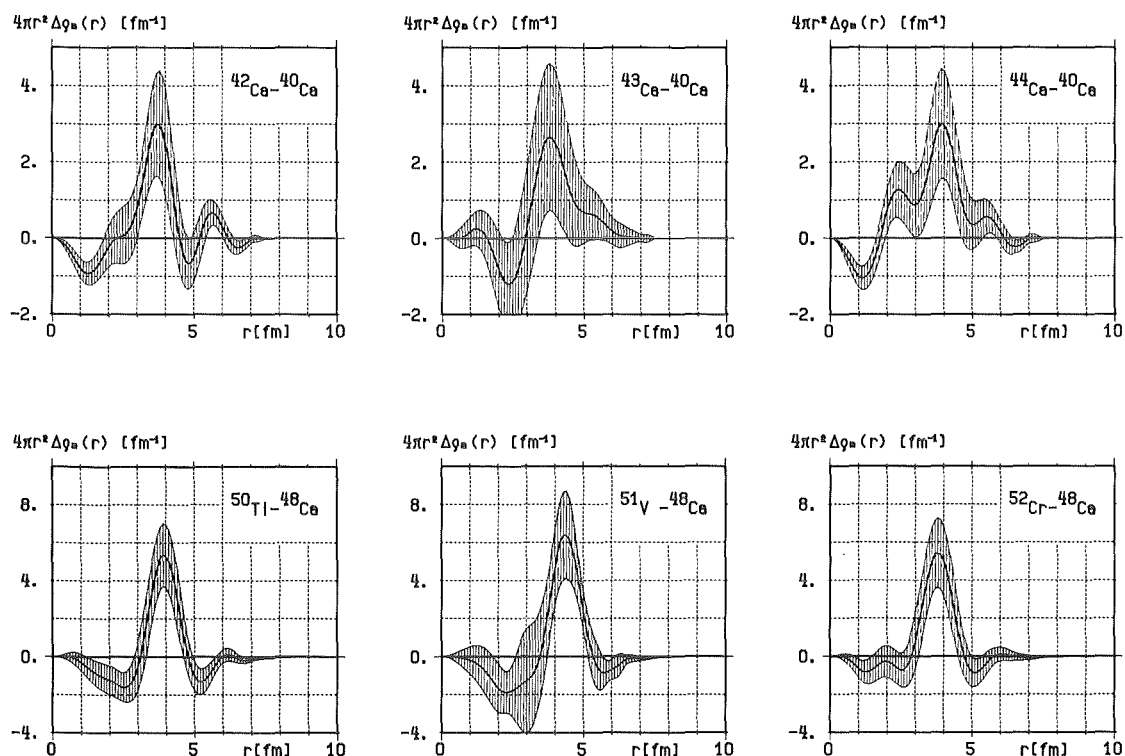
Fig.2 Differences of nuclear matter densities of Calcium isotopes and (N=28) isotones with error band (shaded area)

Table I   Root-mean-square radii of nuclear matter densities as obtained from elastic α particle scattering

Target	^{40}Ca	^{42}Ca	^{44}Ca	^{48}Ca	^{50}Ti	^{52}Cr
$<r^2>_m^{1/2}$ (fm)	3.38+.02	3.43+.02	3.45+.02	3.51+.03	3.55+.02	3.54+.02

(1)   H. J. Gils, contr. 1.3.4
(2)   E. Friedman, H.J. Gils, H. Rebel, Z. Majka, Phys. Rev. Lett. 41 (1978) 1220
(3)   H. J. Gils, E. Friedman, H. Rebel, KfK 3556 (1983)
(4)   E. Friedman, C.J. Batty, Phys. Rev. C17 (1978) 34
       H. J. Gils, E. Friedman, H. Rebel, J. Buschmann, S. Zagromski, H. Klewe-Nebenius, B. Neumann, R. Pesl, G. Bechtold, KfK 2838 (1980)

+   Racah Institute of Physics, The Hebrew University, Jerusalem, Israel

1.3.6 ISOSCALAR TRANSITION RATES AND SINGLE FOLDING MODEL WITH DENSITY-DEPENDENT FORCES

D.K. Srivastava[+], H. Rebel

Isoscalar transition rates in nuclei are most interesting nuclear structure quantities as they are rather directly related to the nuclear transition densities. However, a great deal of confusion has prevailed over the last years about the comparability of these values obtained by electromagnetic procedures and the result derived from inelastic scattering of hadrons, in particular of α-particles thus clouding the immense value of such studies. Having recognized the unsuitability of the Bernstein procedure (1) implicit folding model analyses (2,3) on the basis of Satchler's theorem have been applied in a number of studies to account for the disparity between the values obtained by electromagnetic methods and α-particle scattering. Though the implicit folding model analysis proves to be by far more successful than the crude Bernstein procedure, a strong l-dependent disparity remained largely unaccounted for. We have found that a proper accounting of the density-dependence of the α-particle-bound nucleon interaction removes this difficulty and establishes the unique value of medium energy α-particle scattering for the study of isoscalar transition rates.

In this semimicroscopic method the real part of the deformed optical potential is given by

$$U_R(\vec{r}_\alpha) = \int \rho(\vec{r})(1-\gamma \, \rho^{2/3}(\frac{\vec{r}_\alpha+\vec{r}}{2})) \, v_o \, e^{-|\vec{r}-\vec{r}_\alpha|/b^2} \, dr^3 \qquad (1)$$

where the values of α, v_o and b are standardized by the fit to elastic α-particle - ^{40}Ca scattering data. The target density ρ is deformed by any reasonable procedure. Concentrating on its multipole moments q_1^ρ, defined by

$$q_1^f = \int f(\vec{r}) \, r^1 \, Y_{1o}(\hat{r}) \, d\vec{r} \qquad (2)$$

the dependence on the deformation prescription is largely eliminated in these integral quantities. With the assumption that $\rho(\frac{\vec{r}+\vec{r}_\alpha}{2}) \approx \rho(\vec{r})$ within the range of the force, it can be shown that

$$\frac{q_1^u}{J_u} = \frac{q_1^\rho}{A} \cdot C_1 \qquad , \qquad (3)$$

J_u being the volume integral of the real optical potential and C_1 an l- and A-dependent correction factor as shown in Fig. 1.
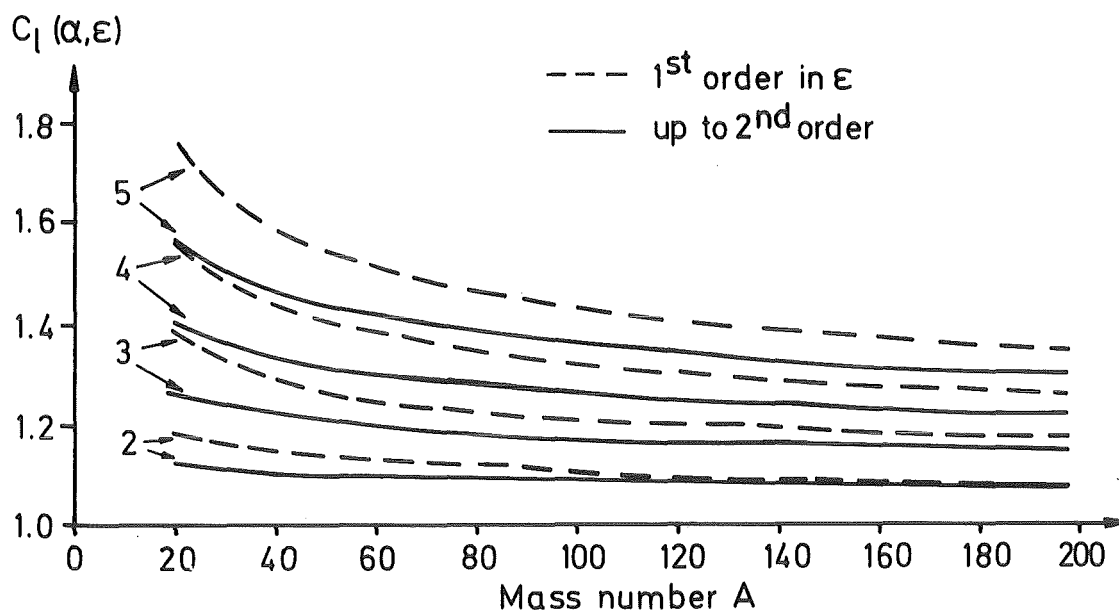
Fig.1   Correction of the normalized multipole moments of a deformed Fermi
        distribution due to the density dependence

For γ = o or for a homogeneous distribution ρ with vanishing surface
diffuseness C_1 = 1. In realistic cases (say a Fermi distribution) $C_1 \neq 1$ and,
when included, it resolves the discrepancies previously found (3).

(1)   A.M. Bernstein, in Adcances in Nucl. Physics 3 (1969) 325
(2)   H. Rebel, R. Pesl, H.J. Gils, E. Friedman, Nucl. Phys. A368
       (1981) 61
(3)   G.J. Wagner, P. Grabmayr, H.R. Schmidt, Phys. Lett.133B (1982) 447
+   BhabhaAtomic Research Centre, Calcutta (India)

1.3.7   LIMITATION OF THE α + ^{40}Ca FUSION CROSS SECTION

M. Albińska[+], H. Klewe-Nebenius[++], R. Planeta[+++],
J. Buschmann, S. Zagromski, H.J. Gils, K. Grotowski[++++], H. Rebel

In context of experimental studies of break-up-fusion reactions in-
duced by 156 MeV ^{6}Li (1), we investigated separately the fusion of α-par-
ticles with ^{40}Ca. In the interactions of the strongly clusterized ^{6}Li with
the target some kind of incomplete fusion reactions are expected to con-

tribute dominantly (2). The α+ ^{40}Ca fusion cross sections have been measured at E_α = 60,80 and 104 MeV (LAB) by observing and analysing the inclusive γ-ray spectra emitted from the reaction products (3). The α-particle beam of the Karlsruhe Isochronous Cyclotron was focused onto a 43 mg/cm² natural Ca target, and the beam current was measured by means of a well shielded Faraday cup located 6 m behind the reaction chamber (and using additional focussing after the target). Inclusive γ-ray spectra were registered by a Ge(Li) detector with 15 % detection efficiency for the 1332 keV ^{60}Co line. The γ-spectra containing about 260 lines each were analyzed with the computer code SAMPO and were used for identifying the reaction products with masses A = 9-43. As statistical model calculations support, the main part of the reaction cross section (represented by the observed mass spectra with A<41) can be attributed to fusion. The experimental results which are shown in Fig.1 together with results for lower energies (4) and with the total reaction cross section derived from optical model analysis of elastic scattering (σ_R^{OM}) (5), provide information about that region of the fusion excitation function where the fusion probability decreases, limited by the competition of other reaction channels.

Due to the very close masses of the target and the compound nucleus A = 44 it is difficult to identify the evaporation part well distinguished from target-like products originating from transfer processes followed by γ-deexcitation. However, we can present upper limits for fusion cross sections by summing up the evaporation region in the mass spectrum.

Recently Matsuse, Arima and Lee (6) introduced a new concept of a critical distance of two colliding heavy ions where they lose their identity and start fusing. Using the (ground-state) nuclear ms radii

$$<r^2>_A = \frac{3}{5} (1.12 \cdot A^{1/3})^2 \; [1+3.84 \; A^{-2/3}] \tag{1}$$

the critical distance $<d^2>^{1/2}$ between two colliding nuclei (A_1, A_2, A = A_1 + A_2) is defined by

$$A<r^2>_A = A <r^2>_{A_1} + A_2 <r^2>_{A_2} + \frac{A_1 \, A_2}{A} <d^2> \tag{2}$$

Assuming the effective potential close to $<d^2>^{1/2}$ being essentially a harmonic oscillator potential (modified by the Coulomb potential), the effective barrier height $E_{FE(J)}$ of the fused system and for the spin J at the critical distance can be calculated. Adopting the proposed value (6) of the oscillator constant, the calculated cross section (σ_{fu}^{calc}) and the fusion entry line E_{FE} are displayed in Figs.1 and 2, respectively.
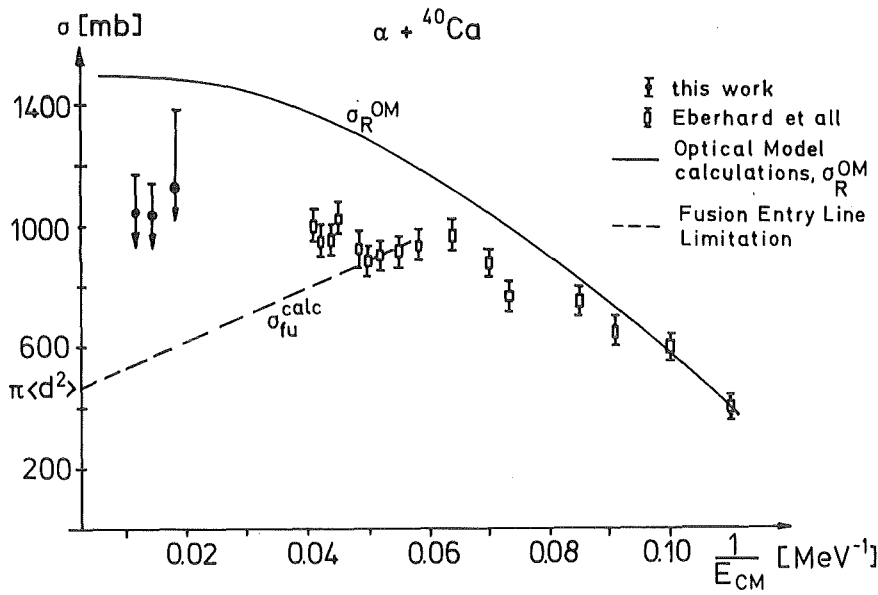
Fig.1 Fusion excitation function for the $\alpha + {}^{40}$Ca system

For lower energies (see Fig. 2) the fusion barrier line EB appears to be a limit. It is clear that for higher energies none of the yrast lines, E_y nor E_{sy} (7), of the compound nucleus ^{44}Ti*, does limit fusion cross sections. The result is in agreement with results obtained for the $\alpha + {}^{233}$U system (6). The cross sections predicted by the model of Matsuse et al. for the fusion of $\alpha + {}^{40}$Ca are much lower than our measured data. If these values are adopted as upper limits for complete fusion, the cross section difference has to be ascribed to multiparticle transfer reactions.

The critical distance calculated for the $\alpha + {}^{40}$Ca system $<d^2>^{1/2} = r_{cr} = 0.76$ fm agrees well with previously reported results for ^{44}Ti* revealing that the fusion cross section is limited in this case by compound nucleus properties (8).
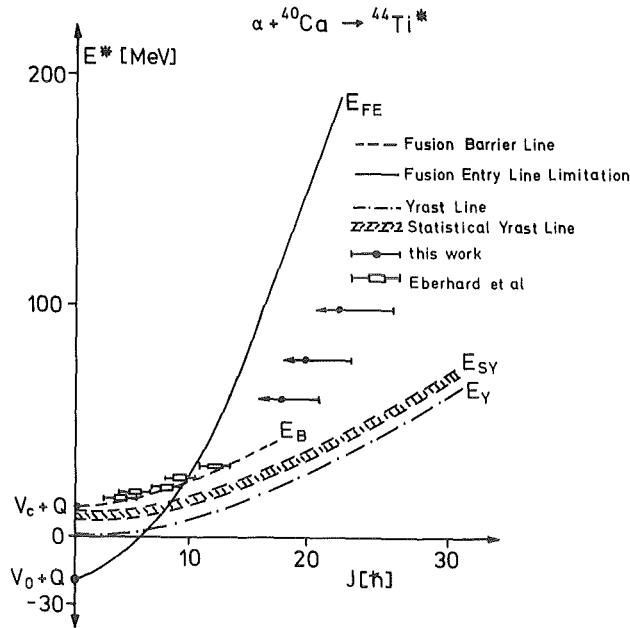
Fig.2

Fusion cut-off lines in the E*-J diagram of the compound nucleus ^{44}Ti* formed via $\alpha + ^{40}$Ca. The fusion entry line E_{FE}, and the fusion barrier E_B are calculated with parameters taken from Ref.6, V_c is the Coulomb barrier, V_o the effective potential at $r=<d2>^{1/2}$. The yrast lines are calculated with the rigid-body moment of inertia, $E_{SY} = E_Y + \Delta Q$ with $\Delta Q = (10 \pm 2.5)$ MeV

(1)   J. Brzychczyk, L. Freindl, K. Grotowski, Z. Majka, S. Micek,
        R. Planeta, M. Albińska, J. Buschmann, H. Klewe-Nebenius, H.J. Gils,
        H. Rebel, S. Zagromski, Nucl. Phys. A (in press), contr. 1.1.3
(2)   B. Neumann, J. Buschmann, H. Klewe-Nebenius, H. Rebel, H.J. Gils,
        Nucl. Phys. A329 (1979) 259
(3)   K. Grotowski, P. Belery, Th. Delbar, Y.El Masri, Gh. Grégoire,
        R. Janssens, J. Vervier, G. Paic, M. Albińska, J. Albiński, S. Kopta,
        T.Kozik, R. Planeta, Phys. Rev. C23 (1981) 2513
(4)   K.A. Eberhard, Ch. Appel, R. Baugert, L. Cleeman, J. Eberth, V. Zobel,
        Phys. Rev. Lett. 43 (1979) 107
(5)   H.J. Gils, E. Friedman, H. Rebel, J. Buschmann, S. Zagromski,
        H. Klewe-Nebenius, B. Neumann, R. Pesl, G. Bechtold, Phys. Rev. C21
        (1980) 1239
(6)   T. Matsuse, A. Arima, S.M. Lee, Phys. Rev. C26 (1982) 2338
(7)   S.M. Lee, T. Matsuse, A. Arima, Phys. Rev. Lett. 45 (1980) 165
(8)   M. Albińska, P. Belery, Th. Delbar, Y. El Masri, Gh. Grégore,
        C. Michel, J. Vervier, J. Albiński, K. Grotowski, S. Kopta, T. Kozik,
        R. Planeta, G. Paič, Phys. Rev. C27 (1983) 207.

+   Institute of Physics, Technological University, Cracow, Poland
++   KfK, Institut für Radiochemie
+++   Institute of Physics, Jagellonian University, Cracow, Poland
++++   Institute of Physics, Jagellonian University and Institute of
        Nuclear Physics, Cracow, Poland

1.3.8 INVESTIGATION OF THE ^{6}Li + ^{40}Ca INTERACTION IN A COINCIDENCE EXPERIMENT

J. Buschmann, L. Freindl[+], H.J. Gils, K. Grotowski[++], H. Klewe-Nebenius[+++], B. Neumann, R. Planeta[+], H. Rebel, S. Zagromski

It was recently found, that for the ^{6}Li + ^{40}Ca reaction at 156 MeV (LAB) the complete fusion exhausts only a rather small part of the total reaction cross section (1), while ^{6}Li break-up channels provide about 35% (2). Our present experiments study some particular contributions of incomplete fusion channels to the ^{6}Li + ^{40}Ca total reaction cross section. For that purpose the γ-ray spectra emitted from heavy residual nuclei were measured in coincidence with those fragments which moved with the beam velocity of the ^{6}Li projectiles. Detection angles were $\theta_L = 9°$ and $12°$. Applying the standard procedure similar to that of Wilczyński et al. (3) we determined the cross sections for the (^{6}Li, pγ), (^{6}Li, dγ), (^{6}Li,αγ) channels:

$$34 ^{+14}_{-9} \qquad 30 ^{+12}_{-7} \qquad 78 ^{+142}_{-41}$$

We claim that the above reaction channels belong to a class of binary reactions called incomplete fusion. This statement is based on a proper selection of the experimental situation, first of all on the coincidence condition with beam velocity fragments of the projectile. The binary character of the investigated reactions is corroborated by a reasonable agreement with predictions of the Wilczyński "sum rule" model (3).

Incomplete fusion channels together with complete fusion exhaust a relatively small part of the total reaction cross section. The balance of all known reactions initiated by the ^{6}Li + ^{40}Ca collision at 156 MeV indicates a missing cross section of the order of few hundred millibarns. The prediction of the "sum rule" model suggests that at least part of this cross section may be attributed to (deep-inelastic) pick-up reactions.

(1)   J. Brzychczyk, L. Freindl, K. Grotowski, Z. Majka, S. Micek, R. Planeta, M. Albinska, J. Buschmann, H. Klewe-Nebenius, H.J. Gils, H. Rebel, S. Zagromski, Nucl. Phys. (in press), Rap. INP No. 1200/PL (1982)
(2)   B. Neumann, H. Rebel, H.J. Gils, R. Planeta, J. Buschmann, H. Klewe-Nebenius, S. Zagromski, R. Shyam, H. Machner, Nucl. Phys. A382 (1982) 296
(3)   K. Siwek-Wilczyńska,, E.M. du Marchie van Voorthuysen, J. van Popta, R.M. Siemssen, J. Wilczyński, Nucl. Phys. A330 (1979) 150

+   Institute of Physics, Jagellonian University, Cracow, Poland
++   Institute of Physics, Jagellonian University and Institute of Nuclear Physics, Cracow, Poland
+++   KfK, Institut für Radiochemie

1.3.9 INCLUSIVE γ-RAY SPECTRA FROM ^{208}Pb BOMBARDED BY 73 - 156 MeV ^{6}Li IONS

M. Albińska[+], H. Klewe-Nebenius[++], H. Rebel, H.J. Gils, J. Buschmann, S. Zagromski, J. Albiński[+++]

Projectile break-up in the field of the target nucleus followed by a fusion process of one of the fragments has been shown (1) to be a dominant mode in ^{6}Li induced nuclear reactions in the energy range above 15 MeV/amu. In order to study these "internal break-up" processes in detail for the ^{6}Li + ^{208}Pb system, we started coincidence measurements between light charged ejectiles and γ-rays produced in the collisions. In a pre-experiment of the coincidence studies we investigated the inclusive γ-ray spectra after bombarding a 46 mg/cm² thick ^{208}Pb target by 73, 84, 93, 107, 113, 125, 130 and 156 MeV (LAB) ^{6}Li ions. The Ge(Li) detector (15 % efficiency for the 1332 keV ^{60}Co line) was placed at 90° to the beam axis in order to avoid Doppler broadening. Prompt, delayed and various background spectra were measured. The prompt spectra comprise about 250 lines each. Up to now the spectra measured at 156 MeV were analysed using the computer code SAMPO. About 85 % of the observed lines could be identified. As a by-product the γ-background arising from activation of the target chamber and detector shielding material has been carefully investigated, mainly originating from interactions of secondary neutrons with Al and Fe.

From the γ-spectra the production cross sections for target residues (resulting from neutron-evaporation-γ-deexcitation) can be determined. In
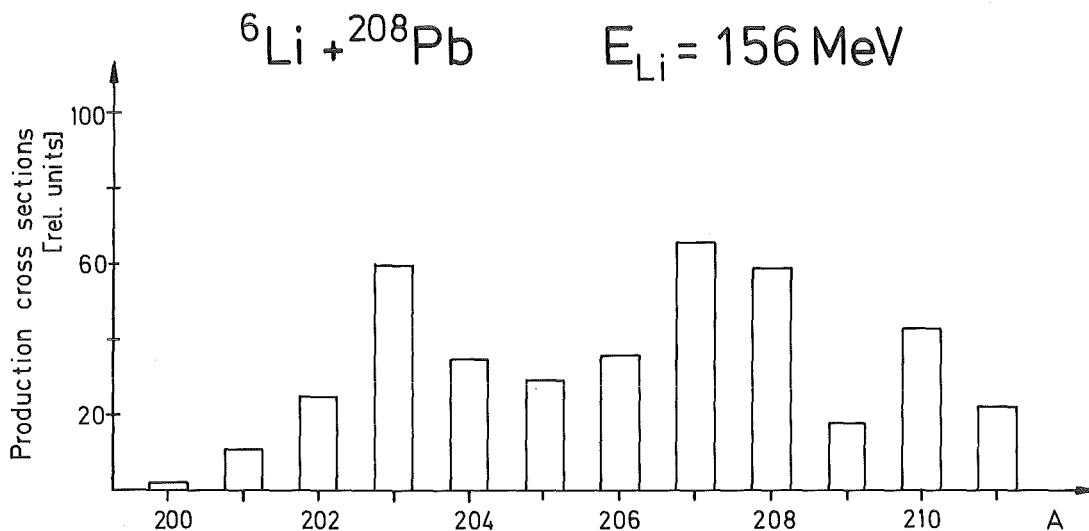
Fig.1 Mass spectrum of the reaction products when bombarding ^{208}Pb by 156 MeV ^{6}Li ions (cross section uncertainty in order of 15 %).

this way we may obtain global information about complete and incomplete fusion channels. Fission products, if existing, should be visible in the mass spectrum for A ≈ 100 - 110. Within the accuracy of about 15 %, inherent to the in-beam γ-method we may neglect the compound nucleus deexcitation way by fission.

(1)   B. Neumann, J. Buschmann, H. Klewe-Nebenius, H. Rebel and H.J. Gils
        Nucl. Phys. A329 (1979) 259
+   Institute of Physics, Technological University Cracow, Poland
++   KfK, Institut für Radiochemie
+++   Institute of Nuclear Physics, Cracow, Poland

1.3.10 INTERNAL BREAK-UP CONTRIBUTIONS IN THE ^{6}Li + ^{40}Ca INTERACTION AT
       156 MeV

M. Albińska[+], J. Albiński[++], R. Planeta[+++], H. Klewe-Nebenius[++++],
H. Rebel

Recent experimental investigations of nuclear reactions induced by 156 MeV ^{6}Li ions bombarding ^{40}Ca have demonstrated that the complete fusion comprises only 3 % of the total reaction cross section while the reaction cross section measured by observing the γ-rays from the reaction products is considerably larger (1). The missing part can be ascribed to incomplete fusion. By further measurements (2) one of the expected incomplete fusion channels, the fusion of α-particles at the beam-velocity corresponding to 156 MeV ^{6}Li projectiles has been investigated. The available experimental information is compiled in Fig.1 displaying the Z spectra of the reaction products. These were derived by observation of the γ-rays after bombarding ^{40}Ca by 156 MeV ^{6}Li and 104 MeV α-particles, respectively (^{40}Ca (^{6}Li, xγ) and ^{40}Ca (α,xγ)) or by observing the recoiling target residues with large momentum transfer (^{40}Ca (^{6}Li, recoils)). We recognize that (α + ^{40}Ca) fusion processes are a considerable contribution to that what has been observed in the ^{6}Li induced reactions. The complementary contribution from (d + ^{40}Ca) fusion has not been studied experimentally. Statistical model calculations (using the LANCELOT code) predict the corresponding evaporation region slightly shifted to larger A values as compared to the (α + ^{40}Ca) case. It can be expected that the d + ^{40}Ca reaction will complement the cross section found in the region with Z > 16. The Z spectrum for Z ≥ 12 results from different

process (not considered here) and is certainly affected by O and C contaminations of the ^{40}Ca target.
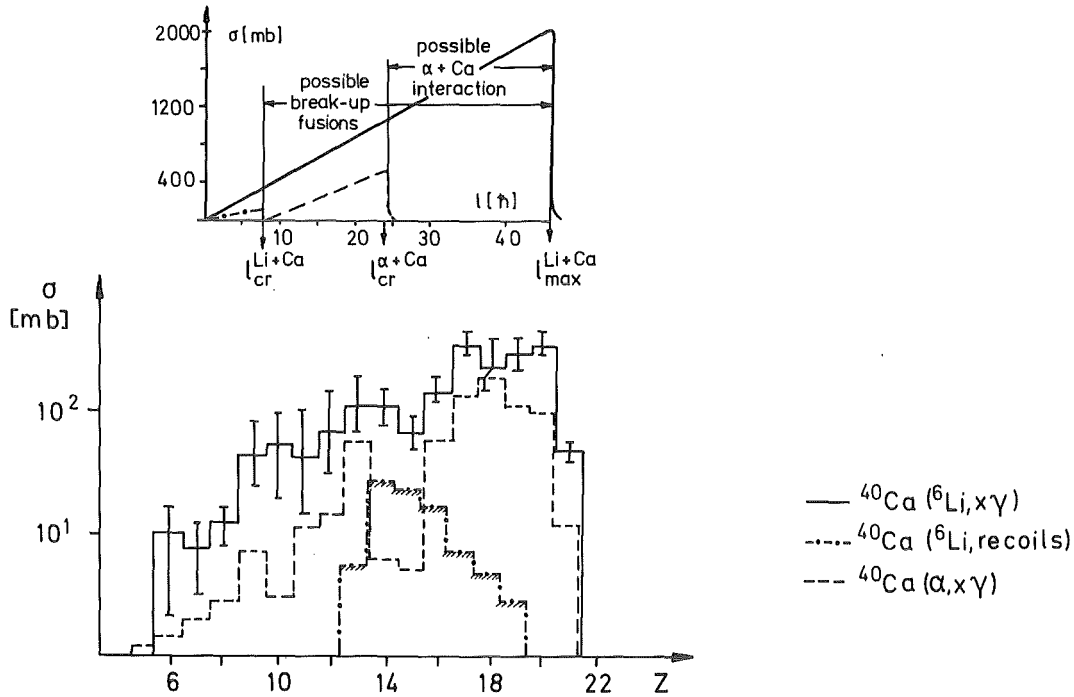
Fig.1 Experimental charge spectra for ^{6}Li + ^{40}Ca (156 MeV) and α + ^{40}Ca (104 MeV (LAB)) reactions. The inset indicates the angular momentum localization for complete and incomplete fusion processes in ^{6}Li + ^{40}Ca collisions at 156 MeV.

The critical angular momentum for the ^{6}Li + ^{40}Ca system derived from the fusion cross section within the sharp cut-off approximation is equal to $l_{cr}^{Li+Ca} = 8$ h (1). In the same way the $l_{cr}^{\alpha+Ca} = 16$ h value was calculated. Transforming $l_{cr}^{\alpha+Ca}$ to the Li + Ca channel we get the angular momentum window $\Delta l = 8 - 24$ h for the (α + Ca) incomplete fusion reaction. Assuming that the remaining cross section in the evaporation region of the ^{6}Li + ^{40}Ca interaction is due to fusion of deuterons, the corresponding angular momentum window would be $\Delta l' \equiv 18 - 27$ h, overlapping with the window for α-fusion. As the $l_{max}^{Li+Ca} = 45$ h (at 156 MeV) the angular momentum window $\Delta l'' = 27 - 45$ h is left for other reaction mechanisms. It should be noted that the incomplete fusion cross sections may be somewhat overestimated due to inclusion of the cross sections for Z = 20 and 21 which may originate also from direct reaction channels.

We note that the angular momentum window calculated within the Wilczyński-model (3) and using experimental half-way radii of the trans-

ferred light particle do not agree with the above results. This is not unex-
pected for a light projectile like ^{6}Li.

(1)   J.Brzychczyk, L. Freindl, K. Grotowski, Z. Majka, S. Micek, R. Planeta,
        J. Buschmann, H. Klewe-Nebenius, H. J. Gils, H. Rebel, S. Zagromski,
        Nucl. Phys. A (in press), contr. 1.1.3
(2)   M. Albińska, P. Belery, Th. Delbar, Y. El Masri, G. Grégáre, C. Michel,
        J. Veriver, J. Albiński, K. Grotowski, S. Kopta, T. Kozik, R. Planeta,
        G. Paùc, Phys. Rev. C27 (1983) 207
(3)   J. Wilczyński, K. Siwek-Wilczyriske, J. van Driel, S. Gongrijp,
        D.C.J.M. Hageman, R.V.F. Janssens, J. Inkasiak, R.M. Siemssen,
        Phys. Rev. Lett. 45 (1980) 606

+   Institute of Physics, Technological University, Cracow, Poland
++   Institute of Nuclear Physics, Cracow, Poland
+++   Institute of Physics, Jagellonian University, Cracow, Poland
++++   KfK, Institut für Radiochemie

1.3.11 DETERMINATION OF THE MULTIPOLARITY OF PROMPT ELECTROMAGNETIC
       TRANSITIONS FROM ANGULAR DISTRIBUTION OF CONVERSION ELECTRONS

H.R. Faust[+], H. Klewe-Nebenius[++], H. Rebel, K. Wisshak,
Nucl. Instr. Meth. 213 (1983) 277

A spectrometer to measure the angular distribution of conversion ele-
trons in charged particle induced reactions is described. The spectrometer
consists of a magnetic filter built with small permanent magnets and a Si(Li)
detector. The parameters of the instrument are discussed and attenuation
factors due to the finite solid angles are evaluated. Spectra of conversion
electrons following the reaction ^{169}Tm(d,xn) and ^{182}Os(d,xn) at an incident
deuteron energy of E_d = 52 MeV taken at different angles are shown.

The measured angular distributions of the conversion electrons is used
to assign multipolarities E1, M1, E2 and (M1 + E2) to prompt α-transitions.

+   Institut Laue-Langevin, Grenoble, France
++   KfK, Institut für Radiochemie

1.3.12 NEUTRON DECAY OF THE GIANT QUADRUPOLE RESONANCE IN ^{90}Zr

W. Eyrich[+], K. Fuchs[+], A. Hofmann[+], B. Mühldorfer[+], H. Rebel,
U. Scheib[+]

The study of isoscalar giant resonances in heavy nuclei has been con-
tinued. In the meantime we completed the measurements and analyses of our
$(\alpha,\alpha'n)$ experiment on ^{90}Zr investigating excitation and decay of resonant
strength in the region of the giant quadrupole resonance (GQR). One aim of
the experiment is to extract model-independent branching ratios of the n-de-
cay into the individual low lying states of ^{89}Zr. Similar to ^{207}Pb (1) the
spins of these states act as a "filter" which allows a separation of
strengths with multipolarities 1 $\geq$4 from E2 and E0 strengths. This can be
seen more quantitatively from statistical model calculations which are shown
in Fig.1.
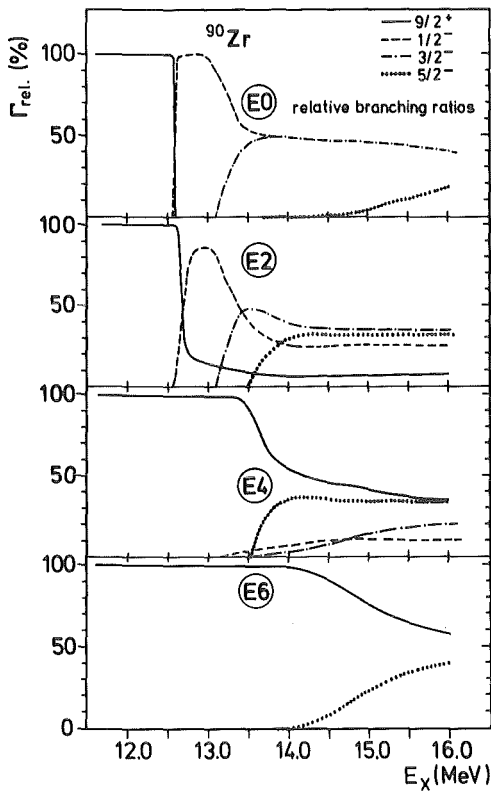
Fig.1
Relative branching ratios for the
decay of E0, E2, E4, and E6 strenghts
from the GQR region in ^{90}Zr into the
5 lowest states in ^{89}Zr (cal-
culated from the statistical model).

Above excitation energies of $E_x \approx 13.5$ MeV E0 and E2 strengths predominantly
decay into the $1/2^-$ and $3/2^-$ "low spin" states whereas E4 and E6 strength
mainly feed the $9/2^+$ " high spin" state. A representative experimental decay
spectrum of the GQR region of ^{90}Zr is displayed in Fig.2a. The strong popu-
lation of the $9/2^+$ ground state indicates the existence of strengths with
multipolarities 1 $\geq$ 4 in the observed energy region. In Fig. 2b the strength
distribution in ^{90}Zr decaying into the $9/2^+$ and the $1/2^-$ states is shown,
respectively. The strength decaying into the $1/2^-$ and $3/2^-$ state with a

predominant multipolarity l=2 is concentrated strongly around the known maximum ($E_x \approx 14.5$ MeV) of the GQR in ^{90}Zr whereas the strength decaying in-to the 9/2$^+$ state shows a relatively unstructured distribution. Fine struc-tures as seen in the case of ^{208}Pb (1) do not appear in these spectra.
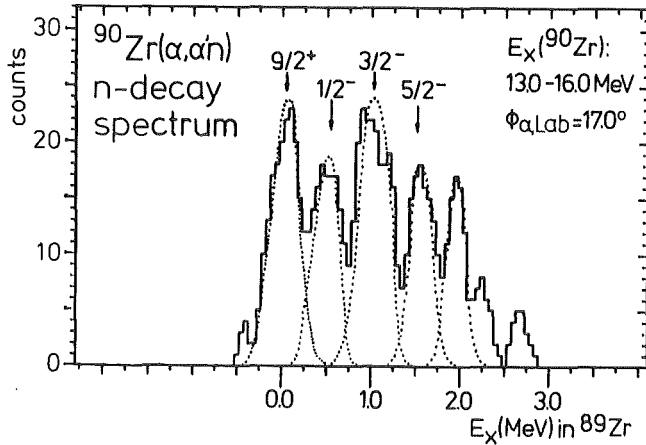
Fig. 2a

Spectrum of the n-decay of the GQR region in ^{90}Zr into the individual states of ^{89}Zr.
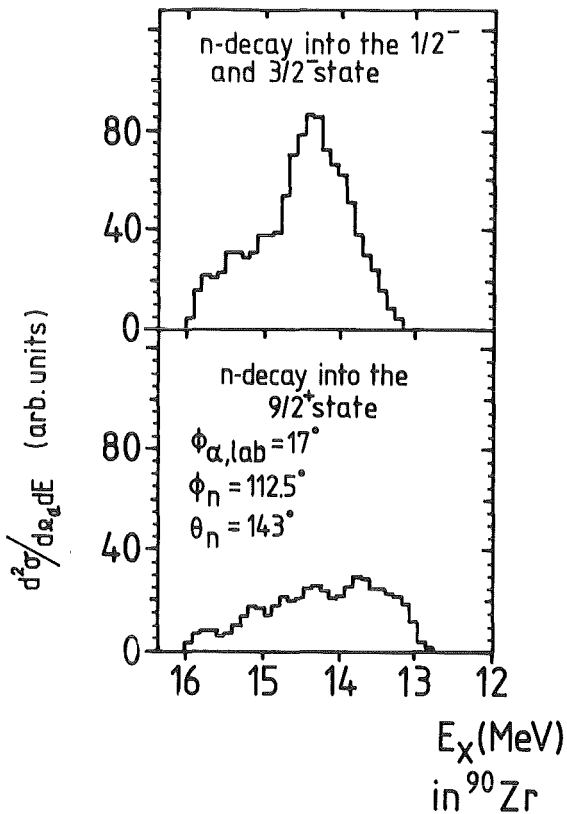
Fig. 2b

Strength distribution in the giant quadrupole resonance region of ^{90}Zr from the neutron decay into the 1/2$^-$ and 3/2$^-$ states (upper part) and into the 9/2$^+$ state (lower part) of ^{89}Zr.

(1)   H. Steuer et al., Phys. Lett. 47 (1981) 1702.
+   Physikalisches Institut der Universität Erlangen-Nürnberg

1.3.13 DIRECT DECAY COMPONENT OF THE ISOSCALAR GIANT MONOPOLE RESONANCE IN ^{90}Zr

W. Eyrich[+], K. Fuchs[+], A. Hofmann[+], B. Mühldorfer[+], H. Rebel, U. Scheib[+]

A powerful tool to get detailed information about decay properties of isoscalar giant resonances is the coincident observation of the decay particles after excitation through inelastic hadron scattering. In the preceding annual report we reported first results of an α'n coincidence experiment to study the neutron decay of the isoscalar giant monopole resonance (GMR) in ^{90}Zr. In the meantime this experiment and its analysis have been completed.

In order to obtain a model independent determination of a possible direct decay component we measured the neutron decay spectra of the GMR region for a maximum and a minimum of the excited resonant strength at 8 positions. In the case of a pure statistical decay this spectra should exhibit an evaporation shape. An experimental excess of fast neutrons corresponding to the decay into the low lying hole states of the residual nucleus gives an estimate of the direct decay component.

In Fig.1 the spectra of the decay neutrons from the center of the GMR in ^{90}Zr are shown for a maximum (lower part) and a minimum (upper part)
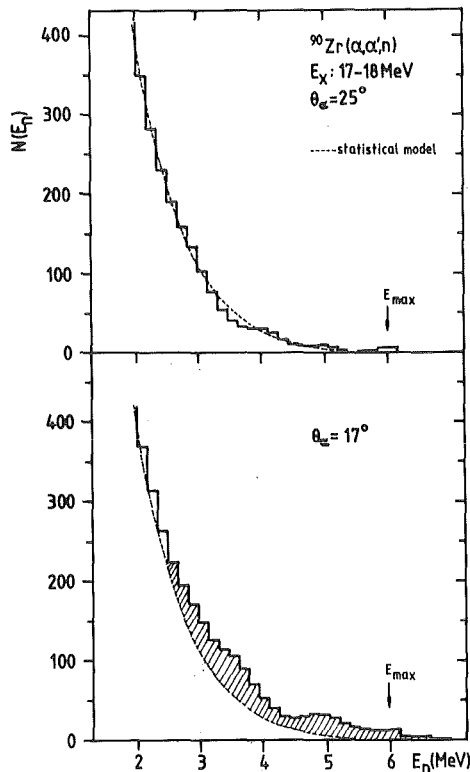
Fig.1 Neutron decay spectra of the reaction ^{90}Zr (α, α') for an excitation maximum (lower part and minimum (upper part) of the GMR

of the excited resonant strength summed over the eight measured positions of the n-detectors together with the prediction for a pure statistical decay. The spectrum corresponding to the maximum of the GMR shows a significant deviation from the statistical curve at the high energy tail whereas the spectrum of the minimum is in good agreement with the evaporation curve. The quantitative analysis leads to a direct decay component of the resonant strength in the GMR region of 15 $\pm$ 3 %. This value is very similar to our results on ^{208}Pb and seems to be typical for the GMR in heavy nuclei.

+   Physikalisches Institut der Universität Erlangen-Nürnberg

1.3.14 STUDY OF THE LOW ENERGY OCTUPOLE GIANT RESONANCE IN ^{90}Zr VIA ($\alpha,\alpha'\gamma$) COINCIDENCE EXPERIMENTS

W. Eyrich[+], K. Fuchs[+], A. Hofmann[+], H. Rebel, U. Scheib[+], B.Mühldorfer[+]

Within the last 10 years the existence of various new giant multipole resonances has been successively confirmed by electron and hadron scattering experiments. One of these excitation modes is the low energy octupole resonance (LEOR) which up to now has been studied in only few experiments. Due to its relatively low excitation energy ($E_x \approx 30 \cdot A^{-1/3}$ MeV in medium nuclei) the LEOR decays predominatnly by gamma emission.

Using the 104 MeV α-beam of the Karlsruhe cyclotron we started an ($\alpha,\alpha'\gamma$) coincidence experiment to study the LEOR in ^{90}Zr. In Fig.1 a single α-scattering spectrum is shown for an excitation maximum of the resonant strength in the LEOR region. From the measured angular distribution a predominant multipolarity of $1 = 3$ could be confirmed for the excitation region between 6 and 9 MeV. To get information about the microscopic structure of this strength branching ratios of the decay have to be deduced. In the present measurement gamma-rays with energies up to 3 MeV are detected in coincidence with the scattered α-particles for 8 positions of the γ-detectors. In the γ-spectrum coincident to the LEOR region which is shown for one position of the γ-detectors in Fig.2 the photo-peaks of various subsequent γ-transitions between low lying states in ^{90}Zr can be seen. An enhanced transition to these states, especially to the 2^+ state at $E_x = 2.18$ MeV has to be associated with a coupling of the LEOR to nuclear surface oscillations. To investigate these structure aspects more quantitatively the spectra of all measured γ-positions have to be taken into account and side feeding cor-

rections have to be considered. This work is still in progress.
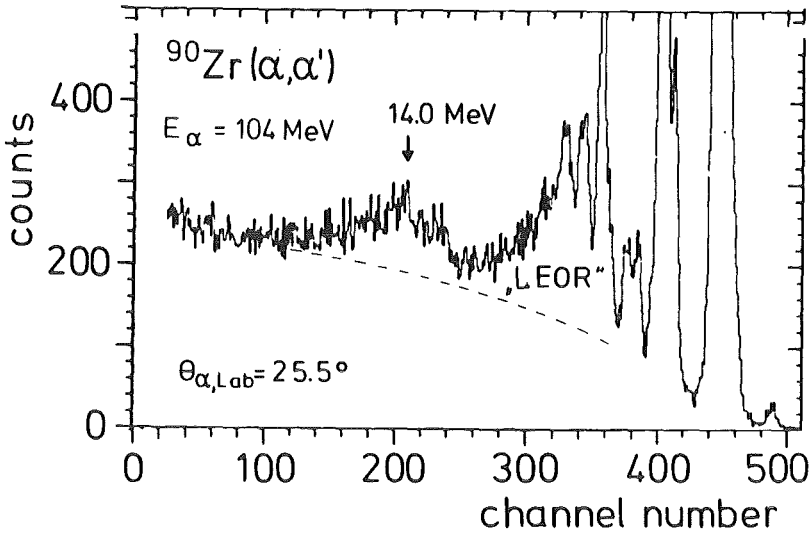
Fig. 1
^{90}Zr (α,α') singles
spectrum at an excita-
tion maximum of the
low energy octupole
resonance (LEOR)
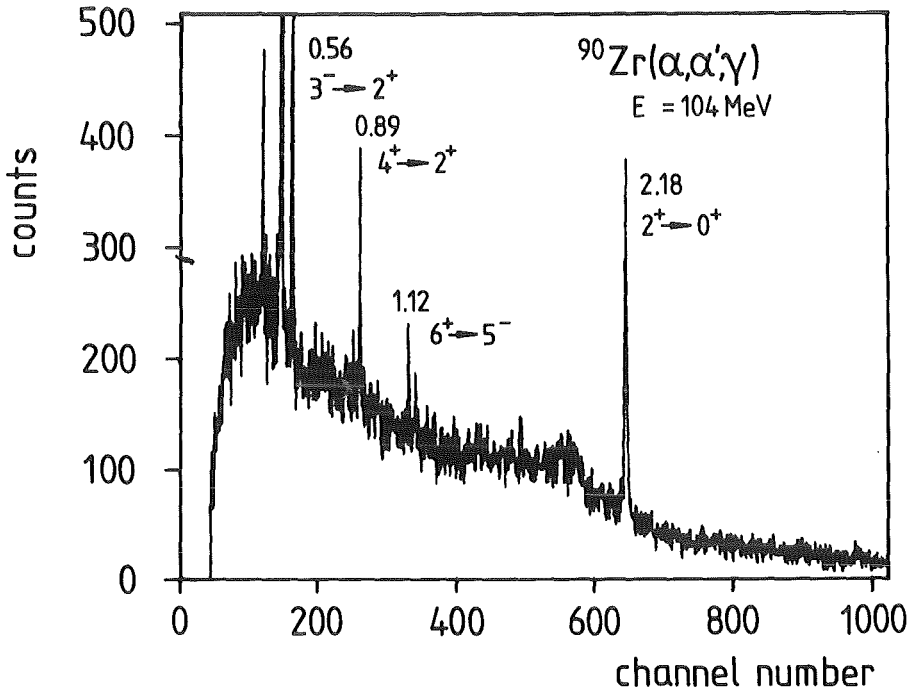
Fig. 2
γ-spectrum coincident
to the region of the
LEOR in ^{90}Zr from an
$(\alpha,\alpha'\gamma)$ measurement

+   Physikalisches Institut der Universität Erlangen-Nürnberg

1.3.15 STUDY OF ISOSCALAR ELECTRIC GIANT RESONANCES BY 156 MeV ^{6}Li-
SCATTERING AND $(^6$Li, ^{6}Li'n)-COINCIDENCE EXPERIMENTS

W. Eyrich[+], K. Fuchs[+], A. Hofmann[+], H. Rebel, U. Scheib[+], M. Tresp[+],
B. Mühldorfer, H. Schlösser

In our $(\alpha,\alpha'n)$ coincidence experiments (1) investigating excitation
and decay of the isoscalar electric giant resonances (GR) in ^{208}Pb and ^{90}Zr
it turned out that the values of the extracted percentages of the sum rules

and the deduced direct decay components of the different GR's depend to some extent on the ratio of the resonant strength to the underlying background and on the decay mode of the background. To get more information about these dependencies we started (^{6}Li, ^{6}Li')-scattering experiments and (^{6}Li,^{6}Li'n)-coincidence experiments on ^{90}Zr using the 156 MeV ^{6}Li beam of the Karlsruhe cyclotron. We measured (^{6}Li,^{6}Li')-angular distributions on ^{208}Pb, ^{90}Zr and ^{24}Mg using two telescopes consisting of surface barrier detectors. In Fig.1 (upper part) an α and a ^{6}Li scattering spectrum on ^{90}Zr are shown for an excitation maximum of the E2 and E0 giant resonances. Both spectra obviously differ essentially in their background. The small background at higher excitation energies in the ^{6}Li spectrum is mainly due to the low-lying break-up threshold of ^{6}Li. The different background structure facilitates the study of the influence of the background on the extracted properties of the giant resonances. In the lower part of the figure a coincidence spectrum between a ^{6}Li detector and a n-detector from the (^{6}Li,^{6}Li'n) experiment is displayed. Besides the peak of the prompt γ-quanta one can recognize the neutron peak of interest on a low background of accidental coincidences. The set-up of
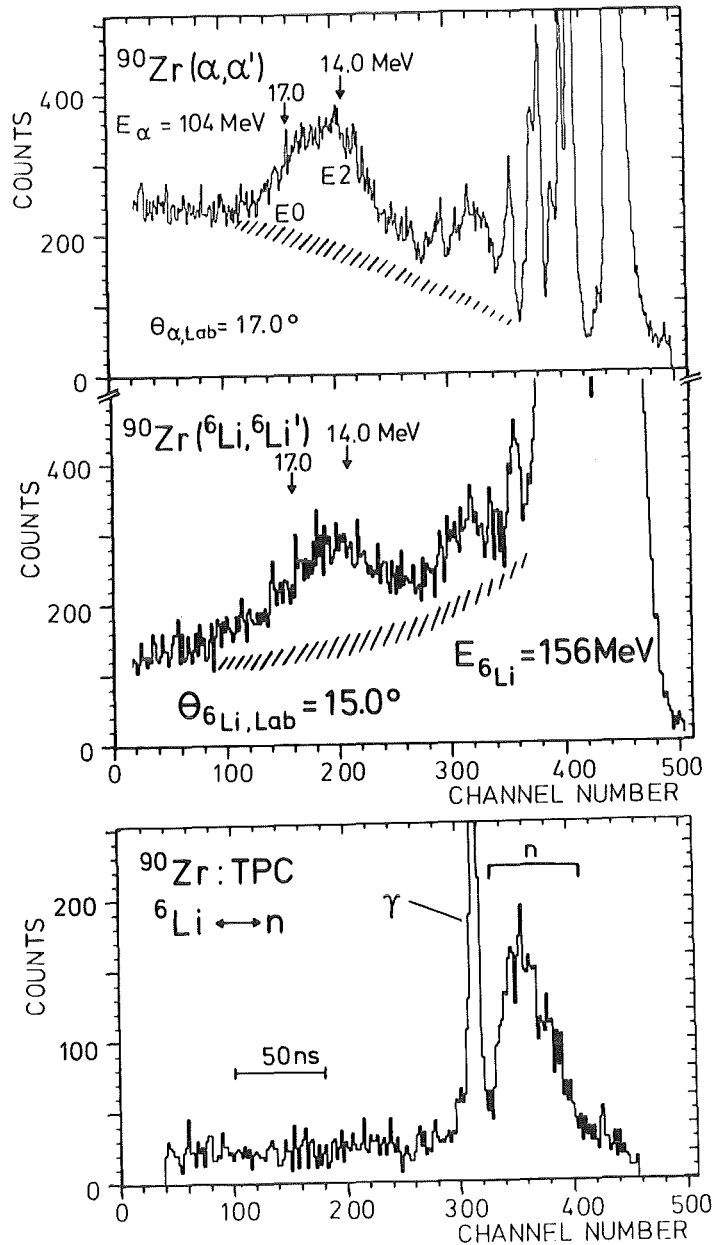
Fig.1 (top): α- and ^{6}Li-scattering spectra from ^{90}Zr for scattering angles corresponding to a maximum excitation of the GQR. (bottom): Coincidence spectrum between a ^{6}Li-detector and a n-detector.

this experiment is similar to that of the previous ($\alpha,\alpha'n$) measurements (1).
It proved to be suitable also for (^{6}Li, ^{6}Li'n)-coincidence experiments, which
seem to be feasible without further difficulties.

(1)   H. Steuer, W. Eyrich, A. Hofmann, M. Ortner, U. Scheib, R. Stamminger,
        D. Steuer, H. Rebel, Phys. Rev. Lett. 47 (1981) 1702

+   Physikalisches Institut der Universität Erlangen-Nürnberg

1.3.16 ß-γ ANGULAR CORRELATIONS IN THE DECAY OF ^{28}P

U. Scheib[+], W. Eyrich[+], H. Forkel[+], A. Hofmann[+], D. Steuer[+]

One way to look for the possible existence of second class currents
in nuclear ß-decay is the measurement of the asymmetry coefficient ε in
ß-γ angular correlations of a ß-decay followed by γ - radiation. For allow-
ed transitions the correlation function W is of the form:

$$W(E_ß,\Theta) = 1 + \varepsilon(E_ß)(3/2\cos^2\Theta - 1/2)$$

For statements about the existence of second class currents, the
measurements should be performed in isospin triplets. If for both ß-transi-
tions in those triplets the energy dependence of ε is measured and the re-
sults are combined, the contributions of first class currents cancel and
those from second class current are summed up. This is only true, however,
if isospin impurity effects caused by the Coulomb interaction can be neg-
lected. In reality, isospin impurity effects enter to some extent into the
theoretical calculations for the different transitions. Therefore, only small
A isospin triplet systems (where the theoretical wavefunctions are fairly
well known and the impurity effects are small) are suited for those investi-
gations. Promising candidates are the A = 20, A = 24 and A = 28 systems.
Since in the A = 20 system the asymmetry coefficients of the ß-γ angular cor-
relation have already been measured (1), we started to investigate the A = 24
and A = 28 systems. The measurement of a new system can be expected to be
more successful than remeasurements of the same system even with smaller
error bars, because the model dependence of the theoretical calculations
yields uncertainties which are of the same order of magnitude as the ex-
perimental ones.

The measurements of the ß$^-$ decay of the nuclei ^{24}Na and ^{28}Al have been
done at the Erlangen tandem accelerator (2). The investigation of the cor-

responding β^+-decays of ^{24}Al and ^{28}P are in progress at the Karlsruhe iso-
chronous cyclotron. For experimental reasons we began with ^{28}P.

^{28}P is produced via the ^{28}Si (p,n) reaction with an incident proton
energy of 18 MeV. Because of the short half-life of ^{28}P of only 268 ms we con-
structed a fast target handling system. In Fig.1 the schematic detector-
target arrangement is shown. The target is moved pneumatically every second
between the beam and the measuring position. During the measuring time the
the beam is stopped inside the cyclotron in order to reduce background radia-
tion. The detectors, two 3"x3" NaI(Tl)-crystals for the γ-rays and two plastic
scintillator telescopes for the positrons, are situated symmetrically around
the "beam off" position of the target.

Fig.1   Schematic view of the
experimental setup.
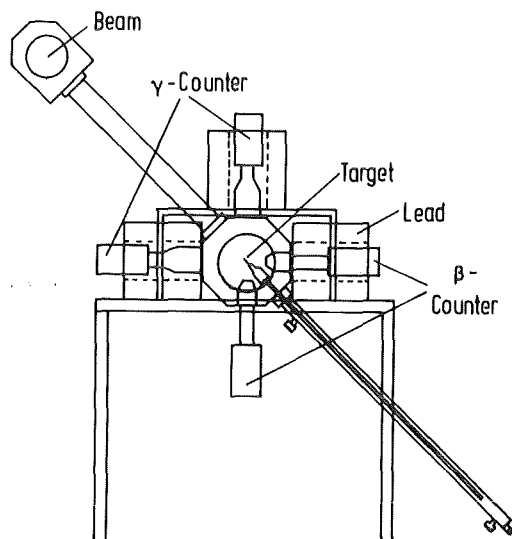
With this setup we measured simultaneously two counting rates for an
angle of 90 degrees between the positron and the coincident γ-ray and two
counting rates for an angle of 180 degrees. The coincident events were
stored event by event on magnetic tape (an event is defined by the energy
of the positron and the number of the respective counter, the energy and
detector number of the coincident γ-ray and the time difference between the
detection of these two events (TPC-spectrum)). This enabled us to set energy
and time windows afterwards thus avoiding possible systematic errors caused
e.g. by gain shifts of the detectors.

The experiments and the data evaluation are not yet finished but from
the results obtained so far from our experiments in Karlsruhe and Erlangen

we expect that we will be able to give new limits for the contribution of second class currents to the charged hadron current of the weak interaction.

(1)   N. Dupuis-Rolin, J.P. Deutsch, D. Favart, R. Prieels
        Physics Letters 79B (1978) 359
(2)   D. Steuer, Dissertation Erlangen 1982
        H. Forkel, Diplomarbeit Erlangen 1983
+   Physikalisches Institut der Universität Erlangen-Nürnberg

1.4 NUCLEAR THEORY

1.4.1 CALCULATION OF THE MOMENTUM DISTRIBUTION OF THE ALPHA-DEUTERON MOTION IN ^{6}Li

R. Beck, F. Dickmann

Experimental data (1,2) on the momentum distriubtion of the α-d motion in the nucleus ^{6}Li provide a valuable testing ground for theories (3) which aim at a study of clustering effects in this nucleus. In this contribution we report on a calculation of the α-d motion in the ground and first excited state of ^{6}Li in the framework of the Generator Coordinate Method (GCM) using as trial function a superposition of antisymmetrized (A) (α-d) and (^{5}He-p) two-cluster wave functions (4)

$$\psi_{^6Li}(JM) = P(JM)[\int d\underset{\sim}{s}_1 f_1(\underset{\sim}{s}_1)\, \Phi_{\alpha-d}(\underset{\sim}{s}_1) + \int d\underset{\sim}{s}_2 f_2(\underset{\sim}{s}_2)\, \Phi_{^5He-p}(\underset{\sim}{s}_2)] \qquad (1)$$

where

$$\Phi_{\alpha-d}(\underset{\sim}{s}_1) = A\, \Phi_\alpha(\underset{\sim}{s}_\alpha)\, \Phi_d(\underset{\sim}{s}_d),\quad \Phi_{^5He-p}(\underset{\sim}{s}_2) = A\Phi_{^5He}(\underset{\sim}{s}_{^5He})\, \Phi_p(\underset{\sim}{s}_p)$$

The functions Φ_α, Φ_d, $\Phi_{^5He}$ and Φ_p are Slater determinants of harmonic oscillator single particle functions centered at $\underset{\sim}{s}_\alpha$, $\underset{\sim}{s}_d$, $\underset{\sim}{s}_{^5He}$ and $\underset{\sim}{s}_p$. The nucleons are distributed in the lowest orbits. The operator P(JM) projects onto the eigenspace of angular momentum (5). The generator coordinates $\underset{\sim}{s}_1$ and $\underset{\sim}{s}_2$ are defined by $\underset{\sim}{s}_1 = \underset{\sim}{s}_\alpha - \underset{\sim}{s}_d$, $\underset{\sim}{s}_2 = \underset{\sim}{s}_{^5He} - \underset{\sim}{s}_p$. The GC-amplitudes f_1 and f_2, corresponding to the clusterizations (α-d) and (^{5}He-p), are determined by solving the Schrödinger equation with a phenomenological central two-body interaction (4) in the space of the functions of Eq.(1).

If we expand the overlap amplitude of the ^{6}Li ground and first excited state with a state where the α particle and the deuteron are moving relative to each other with momentum $\underset{\sim}{k}$ in partial waves,

$$\langle\psi_{\alpha-d}(\underset{\sim}{k},1\nu)|\psi_{^6Li}(LM)\rangle = \underset{LM_L}{\Sigma}\, \phi_{LL}(k)(LM_L;LM|1\nu)\,\sqrt{4\pi}\, Y^*_{LM_L}(\hat{k})i^L \qquad (2)$$

we obtain the momentum distribution

$$\rho_L(k) = \underset{L}{\Sigma}\, \phi^2_{LL}(k)$$

The wave function $\Phi_{\alpha-d}(\underset{\sim}{k}, 1\nu)$ where (1ν) stand for the spin quantum numbers of the deuteron is written in the GC-representation

$$\psi_{\alpha-d}(\underset{\sim}{k}) = \int d\underset{\sim}{s}\, f(\underset{\sim}{s},\underset{\sim}{k})\, \Phi_{\alpha-d}(\underset{\sim}{s}),\quad f(\underset{\sim}{s},\underset{\sim}{k}) = const \cdot \exp(i\underset{\sim}{s}\cdot\underset{\sim}{k} + 3K^2/(8\beta))$$

- 59 -

where ß is the common width parameter of the single particle functions. The matrix elements in Eq.(2) as well as those of the Hamiltonian are evaluated employing the algebraic programming system REDUCE 2 (6).

The result for the ground state is shown in Fig.1. The calculated momentum distribution seems to have a somewhat smaller width than that of the data . A reanalysis (7) of these data, however, shows that the experimental width should be reduced by ∿ 60 %.

The momentum distribution for the first excited state is shown in Fig.2. The value k = 0.5 fm^{-1} for its maximum corresponds to an excitation energy of 3.9 MeV. This is in reasonable agreement with the caluclated excitation energy of 3.3 MeV.
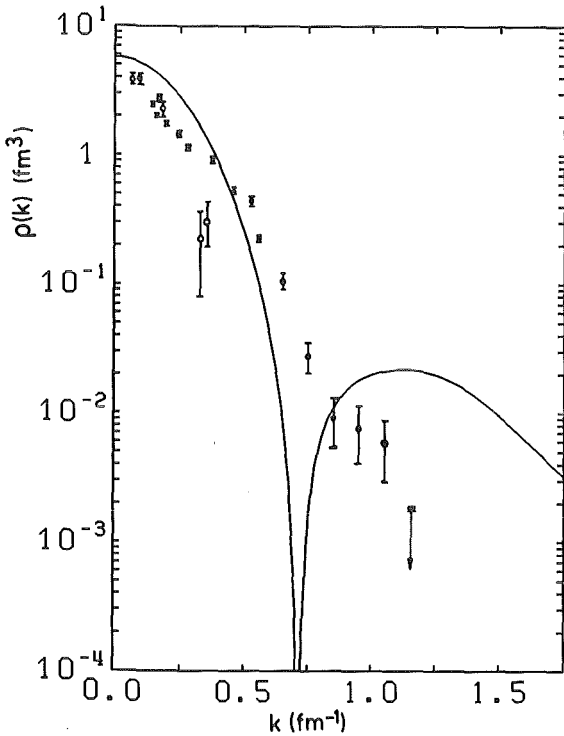
Fig.1 ^{6}Li → α+d momentum distribution for the ground state. The data are deduced from ^{6}Li(p,pd)α experiments at 590 MeV (solid circles, Ref.1) and 155 MeV (open circles, Ref.2). The theoretical curve shows a diffraction minimum at k=0.71 (fm^{-1}).
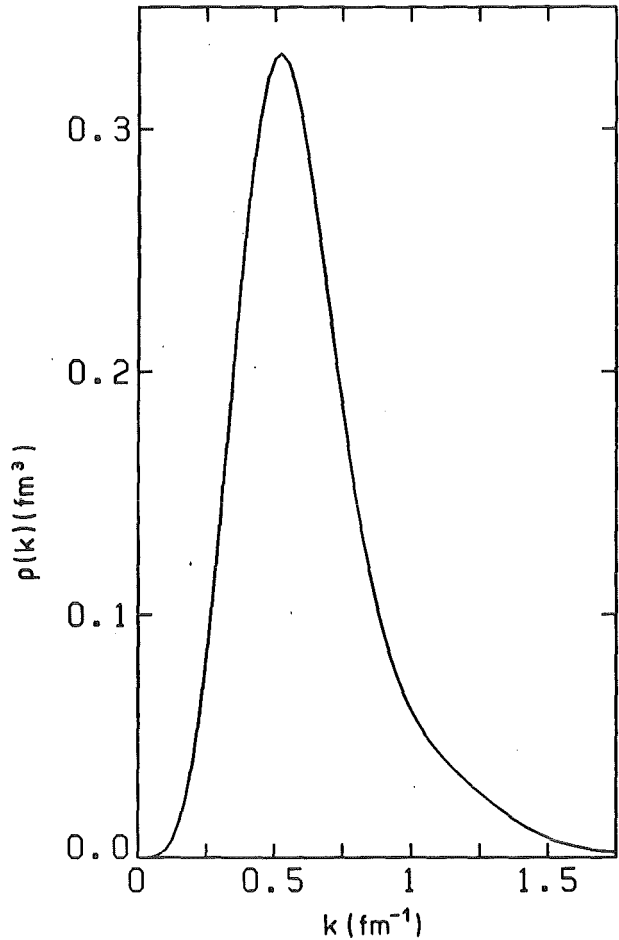
Fig.2 Same as Fig. 1 for the first excited state.

(1)   P. Kitching, W.C. Olsen, H.S. Sherif, W. Dollhopf, C. Lunke,
        C.F. Perdrisat, J.R. Priest, W.K. Roberts, Phys. Rev. C 11
        (1975) 420
        W. Dollhopf, C.F. Perdrisat, P. Kitching, W.C. Olsen, Phys.
        Lett. 58 B (1975) 425
(2)   D. Bachelier, Ph.D. thesis, Faculté des Sciences, Orsay, University
        of Paris, 1971 (unpubl.)
(3)   E.W. Schmid, Y.C. Tang, K. Wildermuth, Phys. Lett. 7 (1963) 263
(4)   R. Krivec, M.V. Mihailović, J. Phys. G: Nucl. Phys. 8 (1982) 821
(5)   R. Beck, F. Dickmann, KfK-Report 3402 (1982)
(6)   R. Beck, F. Dickmann, J. Oehlschläger, KfK-Report 3539 (1983)
(7)   S. Barbarino, M. Lattuada, F. Riggi, C. Spitaleri, D. Vinciquerra,
        Phys. Rev. C 21 (1980) 1104.

1.4.2 ELASTIC AND INELASTIC CHARGE FORM FACTORS OF ^{6}Li: APPLICATION OF
       ALGEBRAIC PROGRAMMING TO CALCULATIONS IN THE GENERATOR COORDINATE
       METHOD (GCM)

R. Beck, F. Dickmann

Applications of the GCM in the framework of the nuclear cluster model
are often hampered by the fact that the calculation of the many-body matrix
elements gets complicated due to the requirements of the Pauli principle and
of angular momentum projection. In this study (1), we show that both problems
can be handled conveniently using the algebraic programming system REDUCE 2
(2).

As an example, we choose the model of ^{6}Li introduced by Krivec and
Mihailović (3). The model space is described in contribution 1.4.1 to this
report. REDUCE 2 is applied for one- and two-body matrix elements as well
as for many-body matrix elements using various cofactor expansions.

During these algebraic calculations we want to keep track of the ana-
lytic dependence of the matrix elements on certain quantum numbers of indi-
vidual nucleons, e.g. the magnetic quantum number of a particle in a p-orbit.
This information is needed when the many-body functions are projected onto
the eigenspace of the operators of angular momentum and parity (4). This re-
quirement is met by REDUCE 2 through the possibility of introducing certain
operators depending on symbolic variables.

The interface between algebraic and numerical processing of expressions
is a rather critical part of the whole calculation which needs some careful
analytical work prior to the application of REDUCE 2. It is shown that the
algebraic expressions obtained by REDUCE 2 may be recast into a form suitable
as input to a FORTRAN program.

Results for the elastic and inelastic charge form factor of ^{6}Li are shown in Figs.1 and 2 using two different effective two-body interactions. The rms radius and B(E2) deduced from the limit values of the form factors as q tends to zero are listed in Table I.

Table I   rms radius and B(E2) for ^{6}Li. V2 stands for force 2 of Ref.5, while B stands for the Brink force of Ref.6

		V2	B	experimental
$\sqrt{<r^2>}$	(fm)	2.65	2.78	2.54
B(E2)	(fm^4)	12.9	19.5	25.1
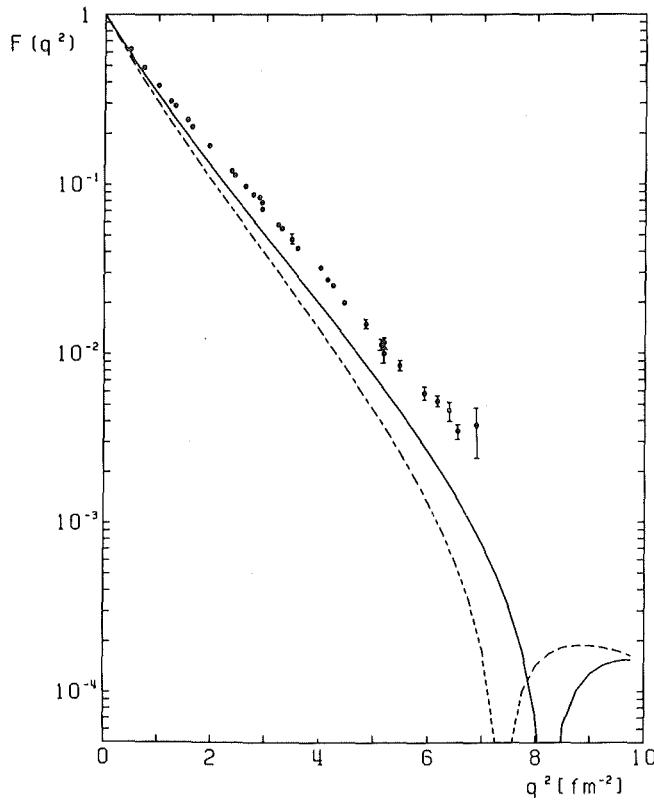
Fig.1   The elastic charge form factor of ^{6}Li. The full line corresponds to the force V2, the broken line to the force B. References for the experimental data may be found in Ref.6.
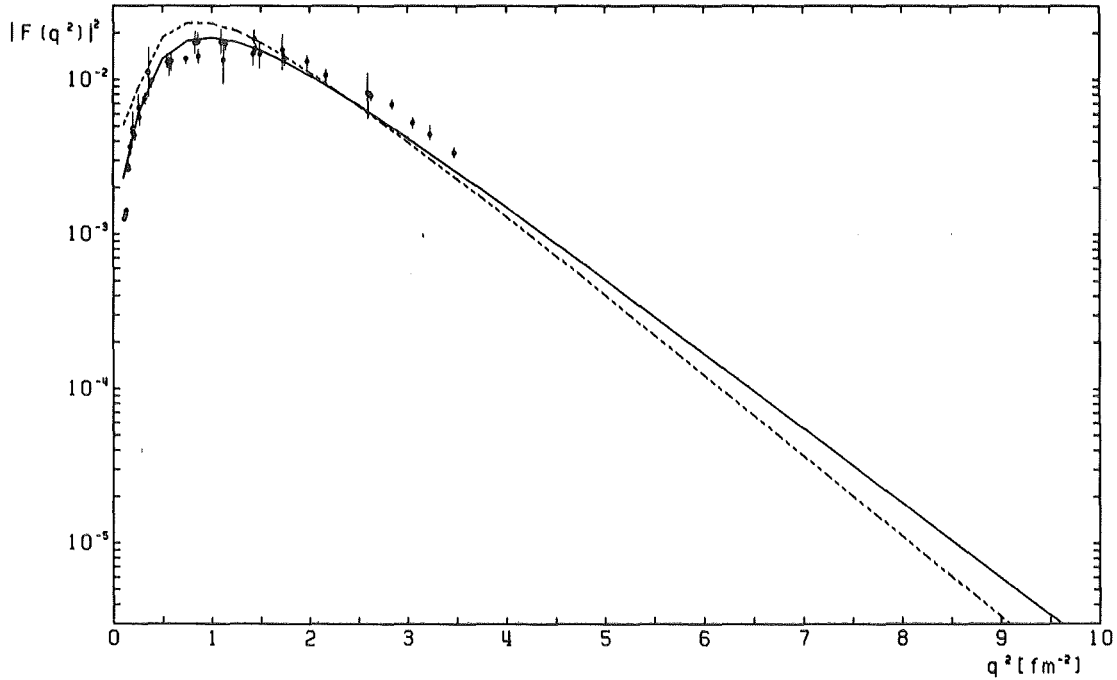
Fig.2   Square of the inelastic charge form factor of ^{6}Li. The various
         symbols are the same as in Fig. 1

(1)   R. Beck, F. Dickmann, J. Oehlschläger, KfK-report 3539 (1983)
(2)   A.C. Hearn, REDUCE User's Manual, Second Edition, University of Utah
         (March 1973)
(3)   R. Krivec, M.V. Mihailović, J. Phys. G: Nucl. Phys. 8 (1982) 821
(4)   R. Beck, F. Dickmann, KfK-Report 3402 (1982)
(5)   A.B. Volkov, Nucl. Phys. 74 (1965) 33
(6)   Y. Suzuki, K. Kubodera, Prog. Theor. Phys. 44 (1970) 617

2.   LASER SPECTROSCOPY

2.1   HIGH RESOLUTION MEASUREMENTS OF ISOTOPE SHIFTS AND HYPERFINE
      STRUCTURE IN STABLE AND RADIOACTIVE LEAD ISOTOPES

R.C. Thompson, M. Anselment, K. Bekk, S. Göring, A. Hanser,
G. Meisel, H. Rebel, G. Schatz, B.A. Brown[+],
J. Phys.G: Nucl. Phys. 9 (1983) 443

We present measurements of isotope shifts and hyperfine structure in
the lead resonance line for a total of 15 isotopes. The experimental accur-
acy is of order 4 MHz. Using independent measurements of the nuclear para-
meter λ for the stable isotopes we have derived λ for all measured iso-
topes. The derived λ values are compared with various theoretical predic-
tions for the lead nuclei. We also give values for the nuclear magnetic di-
pole and electric quadrupole moments deduced from our measurements.

+   Michigan State University, East Lansing, Michigan 48824, USA

2.2   ISOTOPE SHIFTS AND HYPERFINE STRUCTURE SPLITTINGS OF THE
      $(6p^2\ ^3P_o - 6p7s\ ^3P_1^o)$ PbI RESONANCE LINE IN ^{196,197,197m,214}Pb

M. Anselment, S. Göring, A. Hanser, J. Hoeffgen, G. Meisel, H. Rebel,
G. Schatz, W. Faubel[+]

The high-resolution measurements of isotope shifts and hyperfine
structure in radioactive lead isotopes (1) have been extended using essen-
tially the same laserspectroscopic methods and the experimental arrangement
as described in Ref.1. The ^{196,197,197m}Pb nuclides were produced by α-par-
ticle irradiation of enriched Hg and the samples were prepared with the aid
of an electromagnetic mass separator. ^{214}Pb(Ra B) was collected as daughter
product of a readily emanating ^{226}Ra sample. The isotope shifts relative to
^{208}Pb and other quantities are given in Table I.

With the calibration used in Ref.1 we have extracted the values of
the nuclear parameter λ and the variation $\delta\langle r^2\rangle_{A-208}$ of the nuclear charge
radii. All information on $\delta\langle r^2\rangle_{A-208}$ presently available, is displayed in
Fig.1 and compared with theoretical results. We note the conspicuous trend
of the odd-even staggering of the charge radii.

Table I Results of the laserspectroscopic measurements

A	Isotope shift (MHz)	Nuclear parameter λ (fm^2)	A-factor (MHz)	B-factor (MHz)
196	- 11 441 (30)	- 0.572 (16)	-	-
197	- 11 402 (19)	- 0.566 (9)	- 5324 (11)	9 (20)
197m	- 10 827 (17)	- 0.516 (2)	- 1262.7(3.0)	-54 (39)
214	+ 11 500 (99)	+ 0.545 (36)	-	-
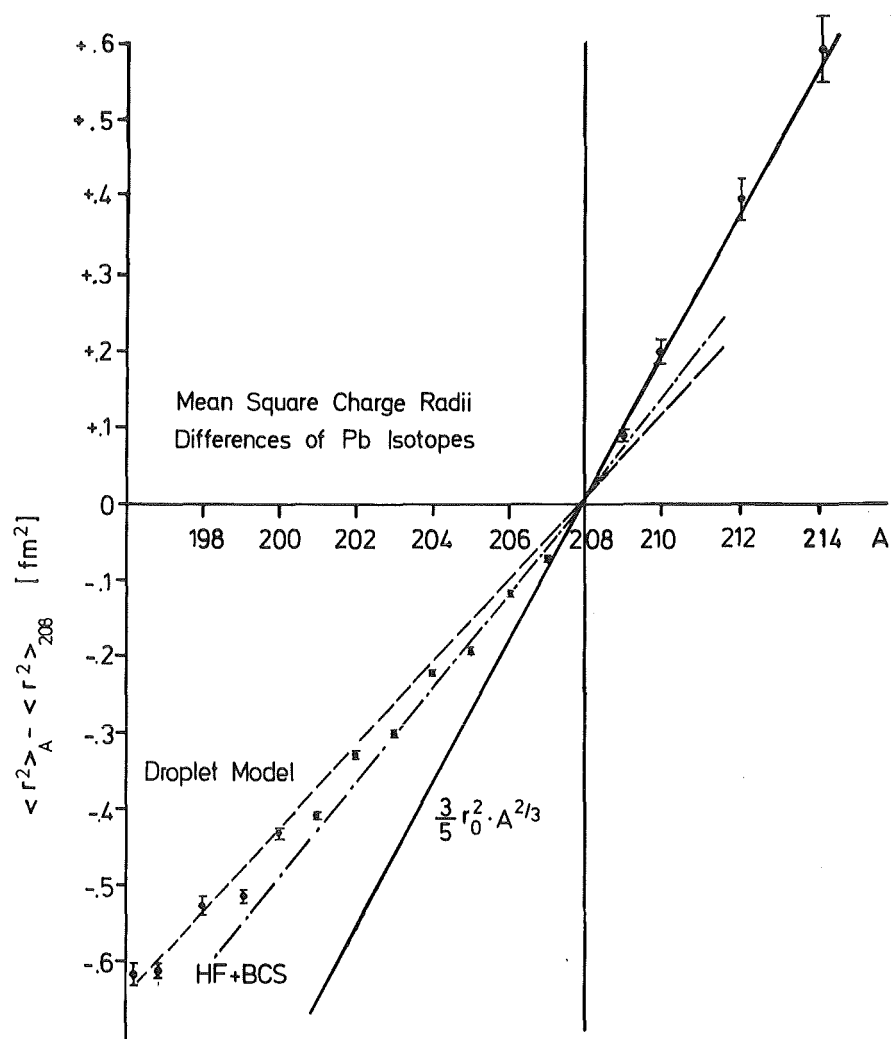
Fig.1 Mean square charge radii of Pb isotopes as compared with theoretical predictions from the droplet model and Hartree-Fock calculations.

(1)   R.C. Thompson, M. Anselment, K. Bekk, S. Göring, A. Hanser, G. Meisel, H. Rebel, G. Schatz, B.A. Brown, J. Phys. G: Nucl. Phys. 9 (1983) 493

+   KfK, Institut für Radiochemie

2.3 PRECISE rf TUNING FOR cw DYE LASERS USING OPTICAL SIDEBANDS

M. Anselment, S. Chongkum, H. Hoeffgen, G. Meisel,

The current measurements of hyperfine structure and isotope shifts of Sn and Pb (1) require to determine optical frequency differences of order 10^7 to 10^9 Hz at a level of 5×10^{14} Hz to a high precision. Therefore the laser frequency must be stabilized to reduce frequency jitter. This is achieved by locking it to a stabilized optical reference resonator, resulting in a fixed frequency laser system. Among the techniques to restore tunability, only rf methods are considered here since only these are precise enough for our purposes. One of them is the heterodyne method (2). Since this approach requires two complete dye lasers and allows only for limited accuracy the heterodyne setup was replaced by a sideband system (3). It has higher precision at increased dependability, and, since it requires only one dye laser, costs are reduced.

The sideband method uses an amplitude modulation of the laser beam with some radio frequency ν_{rf}. The spectrum of the modulated light contains the unmodulated ("carrier") frequency ν_{dye} as well as sideband frequencies ($\nu_{dye} + \nu_{rf}$) and ($\nu_{dye} - \nu_{rf}$) (Fig.1). The side frequencies can be used in a variety of ways to achieve error free laser tuning (3).
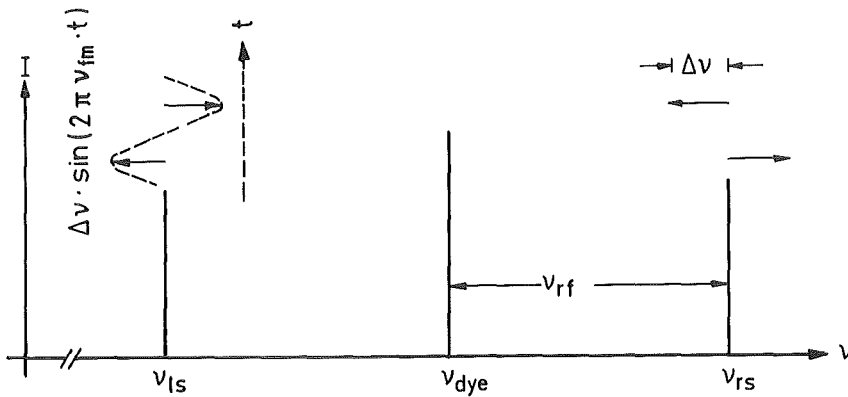
Fig.1 Frequency spectrum of the amplitude modulated laser light. The left sideband frequency (ν_{ls}) and the right sideband frequency (ν_{rs}) are displaced by ν_{rf} off the carrier (ν_{dye}). The dashed sinusoidal curve shows the time dependence of the left sideband if an additional frequency modulation (fm) $\Delta\nu$ on ν_{rf} is applied. The small horizontal arrows at ν_{ls} and ν_{rs} indicate that the fm induced displacement variations are opposite in phase for the two sidebands.

In the present setup one of the sidebands is locked to the reference resonator in the same way as in the fixed frequency system (Fig.2). If the modulating frequency is altered, the laser frequency stabilization influences the laser frequency in such a way that the selected sideband frequency remains constant since it is locked to the fixed reference etalon; in other words, a fixed side frequency with changing modulation frequency ν_{rf} leads to a laser frequency change by exactly the same amount. Thus error free rf-tuning of the dye laser frequency is achieved. The radio frequency ν_{rf} is generated under program control by a frequency synthesizer; to speed up laser lock, the processor simultaneously generates a feed-forward voltage which anticipates most of the expected feedback control signal.

In our system a continuous scan width of 1 GHz is possible which is limited by the rf synthesizer and the driving rf power amplifier available. This range can be doubled by using both sidebands in turn.

Since altogether three optical frequencies are present in the modulated beam, it is necessary to ensure that the proper sideband is brought in
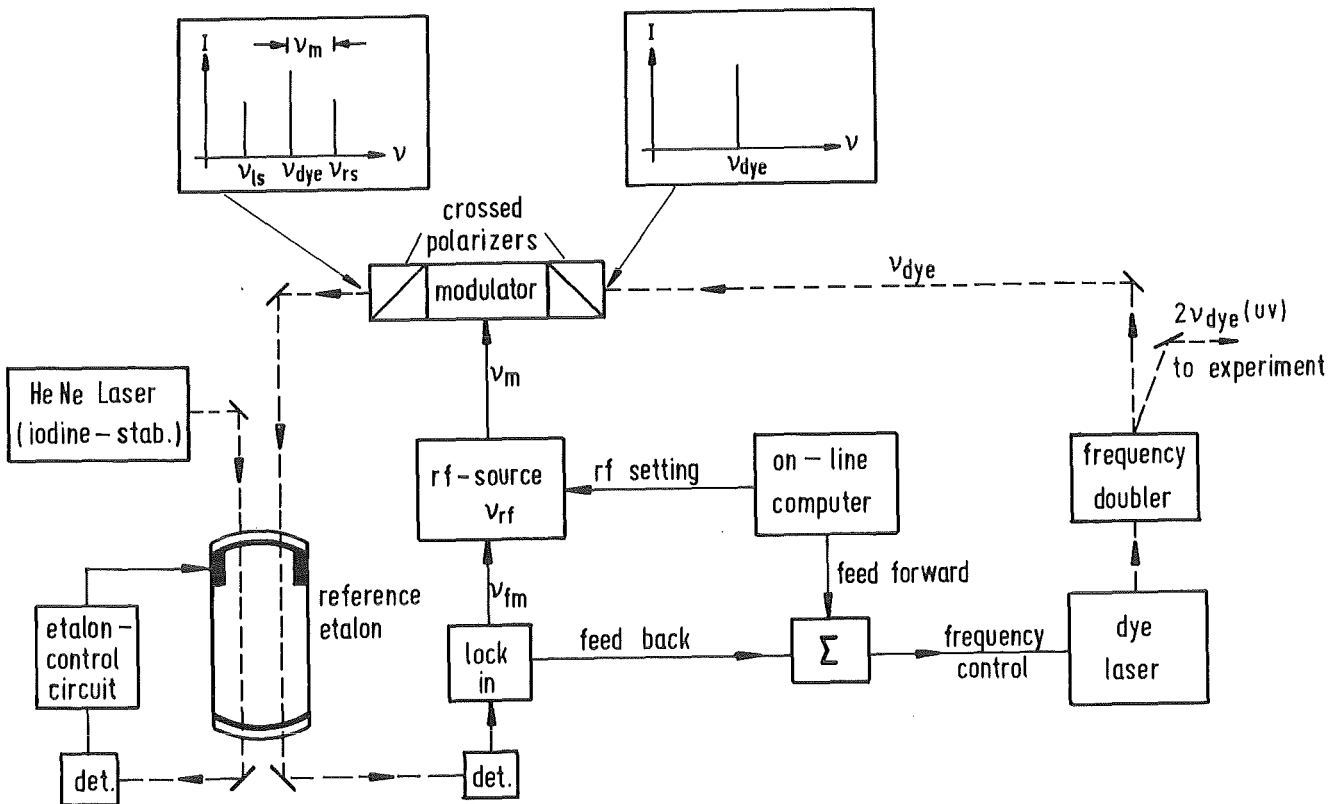
Fig. 2 Experimental setup of the laser sideband tuning system. The small graphs at the top show the frequency spectrum of the laser light before (right) and after (left) passing through the amplitude modulating unit.

coincidence with a transmission peak of the reference etalon and is then selected to lock the laser. For this purpose a new feature was introduced, namely a frequency modulation of ν_{rf} with speed ν_{fm} and width $\Delta\nu$. Thus only the sidebands but not the carrier are frequency modulated. Locking a sideband frequency to a peak of the reference etalon is accomplished by phase sensitive detection at ν_{fm} with a lock-in amplifier. Both sidebands can be distinguished from each other by their relative modulation phase which is 180° (Fig.1). Thus one sideband is identified by the choice of lock-in-phase. Switching from one sideband to the other is then simply performed by inverting the phase-sensitive detector response.

Since frequency doubled laser light (UV) is used in the present experiments the rf controlled tuning width is effectively doubled, resulting in a total tuning range of 4 GHz.

(1)   Preceding contributions 2.1 and 2.2 of this report.
(2)   R.C. Thompson, M. Anselment, K. Bekk, S. Göring, A. Hanser, G. Meisel, H. Rebel, G. Schatz, B.A. Brown, J. Phys. G: Nucl. Phys. 9 (1983) 443
(3)   B. Burghard, W. Jitschin, G. Meisel, Appl. Phys. 20 (1979) 141

2.4   LASERSPECTROSCOPY OF Sn ATOMS

M. Anselment, A. Hanser, J. Hoeffgen, S. Göring, G. Meisel, H. Rebel, G. Schatz

From the point of view of nuclear structure models currently under discussion there is a considerable interest in precise information about charge and matter distributions in nuclei around the magic proton number $Z = 50$. We started laserspectroscopic measurements of isotope shifts and the hyperfine structure of the $(5s^2 5p^2 {}^3P_o - 5s^2 5p6s^3P_1$, $\lambda=286$ nm) transition in stable and radioactive Sn atoms. The results presently available are measured with an experimental method somewhat simplified as compared to the previously used heterodyning procedure (1). The frequency doubled light of a ring dye laser excited the resonance fluorescence in an atomic beam of Sn isotopes. The frequency of the dye laser is swept over the whole frequency range of interest by its internal scan mode. Synchronously with the laser a multichannel analyzer (in multiscaling mode) is scanned, recording the photon count rate (measured by a photomultiplier looking perpendicular to the atomic beam) versus laser frequency. Fig.1 displays a spectrum obtained by this procedure which allows for a quick survey over the horizons of the
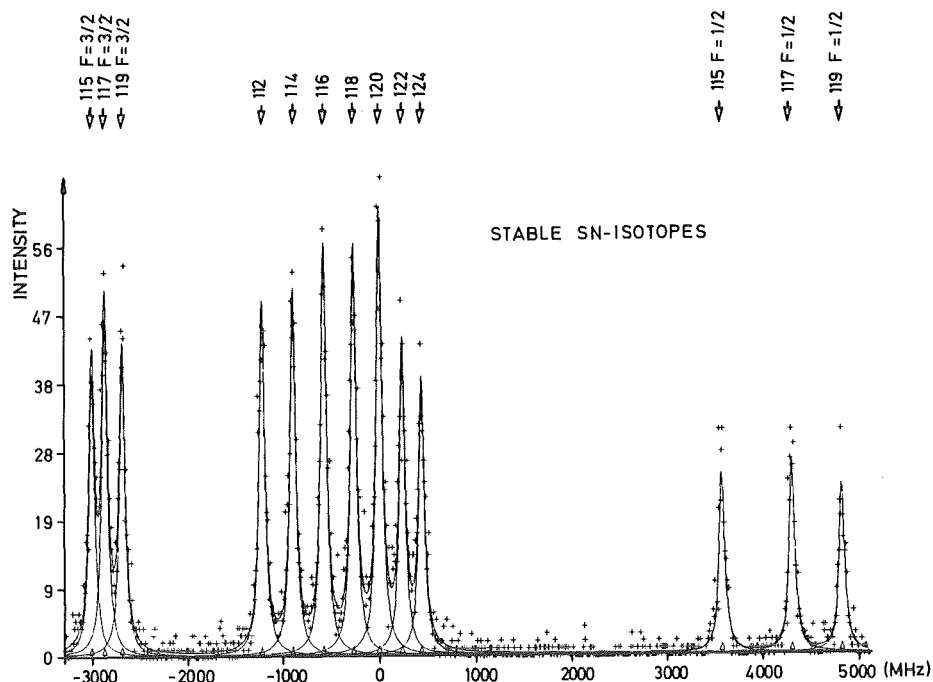
Fig.1 Isotope shifts and hyperfine splittings of the stable Sn isotopes

resonance lines. However, it is limited in accuracy due to a slight non-
linearity of the internal laser scan. The linearity of the measured spectra
can be improved by linearisation via the transmission maxima (equally spaced
in the frequency scale) of a high finesse cavity (spectral range ca.300 MHz).
Table I gives the presently available results improved in this way. It in-
cludes the radioactive nuclide ^{113}Sn and compares with results from the
Oxford group (2).

Table I Measured isotope shifts and values for the A and B factors of the
odd isotopes

Sn-Isotope		Positions [MHz] this work	Isotope shift [MHz] this work	Oxford	A-Factor [MHz] this work	Oxford
112		-1219.3(50)	-1219.3(50)	-1214.4(5)		
113	F=1/2	3122.2(70)	-1085.9(52)	-	-4208.1(66)	-
	F=3/2	-3189.9(70)				
114		- 897.4(50)	- 897.4(50)	- 894.9(13)		
115	F=1/2	3594.2(50)	- 803.5(37)	- 801.7(11)	-4397.8(47)	-4395.4(21)
	F=3/2	-3003.2(50)				
116		- 576.7(50)	- 576.7(50)	- 574.4(6)		
117	F=1/2	4315.9(70)	- 471.5(41)	- 467.6(7)	-4787.4(57)	-4790.7(17)
	F=3/2	-2865.3(50)				
118		- 266-9(50)	- 266.9(50)	- 269.2(7)		
119	F=1/2	4835.6(50)	- 176.8(37)	- 175.3(11)	-5012.5(47)	-5014.8(19)
	F=3/2	-2683.1(50)				
120		0.0	0.0	0.0(10)		
122		238.4(50)	238.4(50)	234.1(7)		
124		439.7(50)	439.7(50)	441.6(7)		

Future measurements will use the much more precise "sideband" method, including further radioactive Sn nuclides.

(1)   R.C. Thompson, M. Anselment, K. Bekk, S. Göring, A. Hanser, G. Meisel, H. Rebel, G. Schatz, B.A. Brown, J. Phys. G: Nucl. Phys. 9 (1983) 443
(2)   D. Stacey, private communication

2.5   A WAVEMETER FOR RAPID AND PRECISE WAVELENGTH MEASUREMENTS OF VISIBLE LASER LIGHT

A. Steiger, G. Meisel

To measure isotope shifts and hyperfine splittings in atoms the energy differences of interest have been determined as small changes of optical laser frequencies (1). In some projected experiments, however, the differences are so wide that the methods used so far are not applicable. A solution of the problem is to measure the full optical frequencies of each transition and to obtain the splittings as small differences of them. Such biased measurements require a high level of accuracy, namely 10^{-7} or better. The appropriate method is optical interferometry. Among the various interferometric instruments ("wavemeters") a modified version of the Fabry-Perot wavemeter of Fischer et al. (2) was chosen. Its concept, first described by Byer et al. (3), is to use a set of Fabry-Perot etalons and a grating monochromator to determine the wavelength. A fast periodic readout of the wavemeter is achieved by monitoring the interferometer patterns by linear photodiode arrays; their signals are digitized and fed into an online computer which calculates the actual wavelength value within less than a second.

The optical setup is shown in Fig.1. The incoming cw laser light of about 1 mW power is split into several beams. A small part is imaged onto the entrance slit of the grating monochromator (GCA McPherson Instr. EU 700). The image of the entrance slit is monitored by the linear photodiode array DO (Fig.1); the array of type RL1024 G by Reticon contains 1024 photodiodes which cover over their length of 25 mm a spectral range of about 50 nm at a fixed grating position. The diode-to-diode spacing of 25 μm allows one to determine the wavelength to within about 100 GHz. Etalons No.1 and 2 are solid fused silica etalons of 0.3 mm and 5 mm thickness; No.3 has 100 mm airgap with a Zerodur spacer. All etalon surfaces are coated with a broadband dielectric coating of 95 % reflectivity from 400 to 700 nm. A

INCOMING
LASER BEAM

FABRY-PEROT
ETALONS

No 3

$\delta\nu_3 = 1.5$ GHz

D3

f = 2500 mm

No 2

$\delta\nu_2 = 20$ GHz

f = 500 mm

D2

No 1

$\delta\nu_1 = 330$ GHz

f = 125 mm

D1

DO

IMAGING OPTICS AND
IMAGE DETECTION

BEAM ADAPTING
OPTICS FOR CORRECT
ILLUMINATION

GRATING MONOCROMATOR
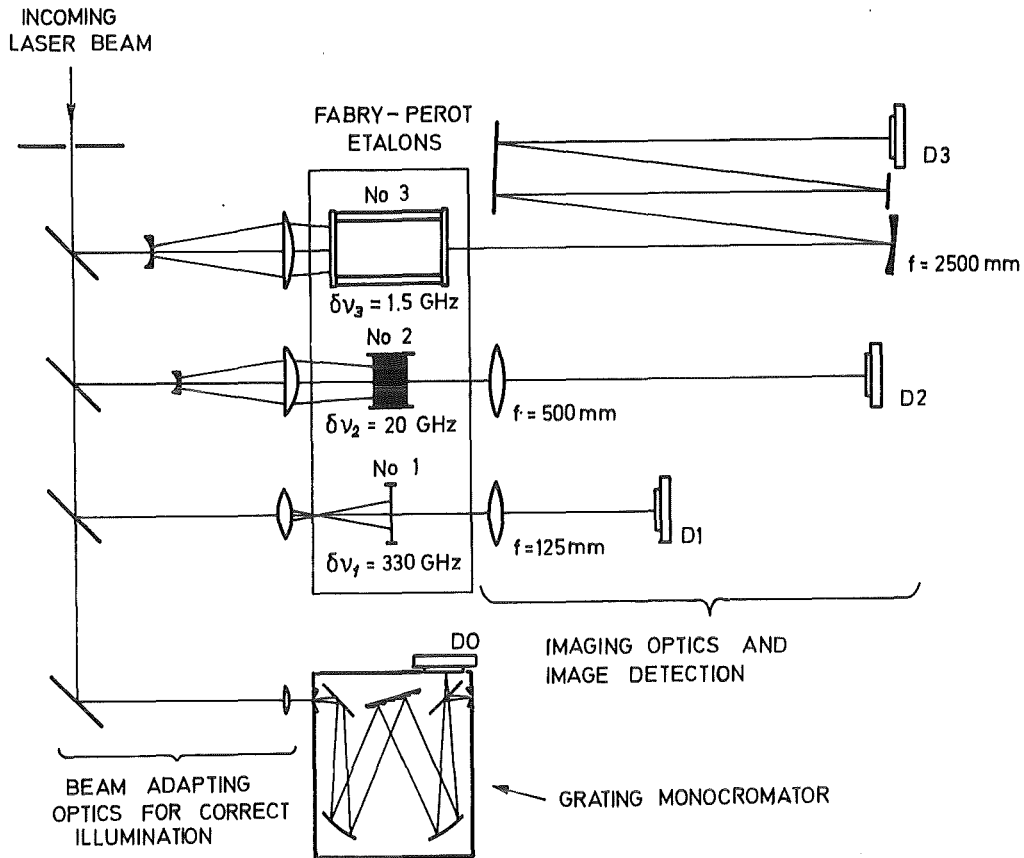
Fig.1   Schematic diagram of the wavemeter. DO to D3 are photodiode arrays.

system of cylindrical lenses in front of each etalon is designed to illuminate 3 to 5 interference rings. The interference patterns are projected onto the diode arrays D1 to D3. Fig.2 shows a sample fringe pattern as recorded with an oscilloscope. These patterns are periodic with the laser frequency, the period is the free spectral range (FSR) $\delta\nu$ of the etalon. Therefore, an etalon pattern can fix the frequency only within its FSR. The monochromator result, however, allows one to select the correct period for etalon No.1. In the same way, each etalon result serves to eliminate the ambiguity for the next thicker one. Thus, the precision to which the FSR of the third etalon is known essentially limits the accuracy of the final wavelength/frequency value.

The status of the instrument is as follows:

1.   The interface electronics for reading the diode arrays and digitizing their output has been built and successfully tested.

2.   The monochromator has been modified so that data taking by a diode array is possible.

3.   Etalons No.1 and 2 have been tested with their respective optics and diode arrays.

4. Special etalon No. 3 is being assembled.

5. The online computer (Nova 2) will be ready in its final configuration in the near future.

6. The optical setup is being constructed.
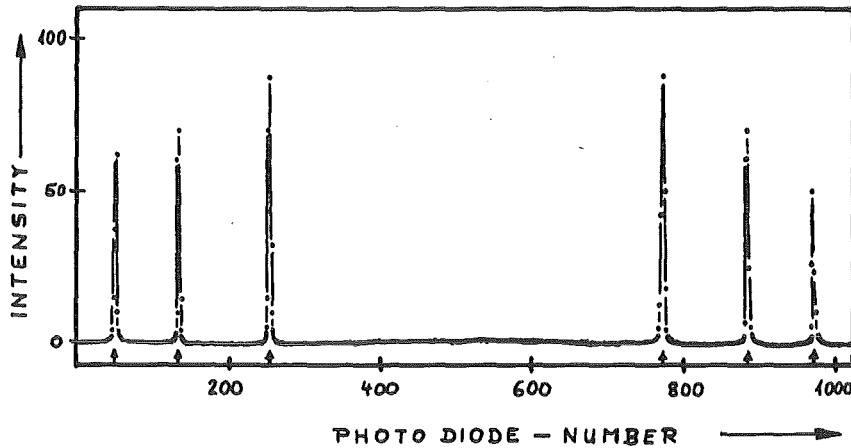
Fig.2 Signals as recorded by a diode array when etalon No.1 is illuminated with a He-Ne laser at 632.8 nm. The experimental line width is about three diodes.

(1) H. Rebel, G. Schatz, Laser Induced Fluorescence Spectroscopy in Atomic Beams of Radioactive Nuclides, in Lasers in Nuclear Physics, ed. C.E. Bemis and H.K. Carter (Harward Acad. Publ., Harward 1982)

(2) A. Fischer, R. Kullmer, W. Demptöder, Optic Communications, $\underline{39}$ (1981) 277

(3) R.L. Byer, J. Paul, M.D. Duncan, A Wavelength Meter, Laser Spectroscopy III (Springer, Heidelberg 1977)

2.6 QUADRUPOLE MOMENTS OF ODD Pb ISOTOPES FROM HYPERFINE STRUCTURE OF THE $(6p^2 \ ^3P_0 - 6p7s \ ^3P_1^o)$ ATOMIC TRANSITION IN PbI

J. Dembczynski, H. Rebel

Recently (1), the hyperfine structure (hfs) of the $(6p^2 \ ^2P_o - 6p7s \ ^3P_1^o)$ transition in PbI has been precisely measured for a series of stable and radioactive Pb isotopes. While the A factor can be calibrated in terms of the nuclear magnetic dipole moments by use of the value known for ^{207}Pb from an independent measurement, the interpretation of the B factors in terms of nuclear quadrupole moments requires a detailed consideration of the atomic structure involved. In the framework of an analysis (2) of fine- and hyperfine structure splittings and g-factors of the relevant atomic con-

figurations, the quantities necessary for a determination of the quadrupole moment from the B-factor could be semi-empirically deduced. The theoretical intermediate coupling expression of the B-factor of a 6p7s $^3P_1$ level is given by

$$B(6p7s\ ^3P_1) = 0.021311\ b_{6p}^{02} + 0.004175\ b_{6p}^{11} \qquad (1)$$

where the negligibly small contribution from the 6d electron due to mixing with the 6p6d configuration is omitted. The effective hfs one-electron parameters $b_{6p}^{\kappa k}$ (MHz) are related (3) to the quadrupole moment Q(b) and to $<r^{-3}>$ [a.u.] by

$$b_{nl}^{\kappa k} = 234.974\ <r^{-3}>_{nl}^{\kappa k} \cdot Q \qquad (2)$$

(κk = 02,11 for the p-electron).

Additionally, we know from relativistic atomic structure calculations (3)

$$b_{6p}^{11}/b_{6p}^{02} = <r^{-3}>_{6p}^{11} /<r^{-3}>_{6p}^{02} = 0.680 \qquad (3a)$$

and

$$<r^{-3}>_{6p}^{02} / <r^{-3}>_{6p}^{01} = 0.8262 \qquad (3b)$$

Using the semi-empirical result

$$<r^{-3}>_{6p}^{01} = 20.3\ (1.2) \qquad [a.u.] \qquad (3c)$$

derived from the observed magnetic-dipole hfs (2) we find

$$Q(^APb)\ [b] = -0.00868(52)\ B(^APb);\ 6p7s\ ^3P_1) \qquad (4)$$

With the B-factors given in Ref.1, we have the values in Table I which are about 40 % larger than those quoted in Ref. (1).

Table I Nuclear quadrupole moments of Pb nuclei

A	199	201	202m	203	205	209
Q [b]	+ 0.8(8)	-0.09(90)	+.58(15)	+.10(10)	+.23(6)	-.27(16)

(1)   R.C. Thompson, M. Anselment, K. Bekk, S. Göring, A. Hanser, G. Meisel, H. Rebel, G. Schatz, B.A. Brown: J. Phys. G: Nucl. Phys. 9, (1983) 443
(2)   J. Dembczynski, H. Rebel, to be published
(3)   J. Lindgren, A. Rosén, Case Stud. Atom. Phys. 4 (1974) 250

2.7 PRELIMINARY FINE- AND HYPERFINE STRUCTURE ANALYSIS OF THE ^{8}S(7p7s) CONFIGURATION IN AmI

J. Dembczynski

There is a number of experimental data (1) on the $(5f^7)^8$S(7p7s) configuration in the Am atom which provide a basis for constructing a level scheme (Fig.1).
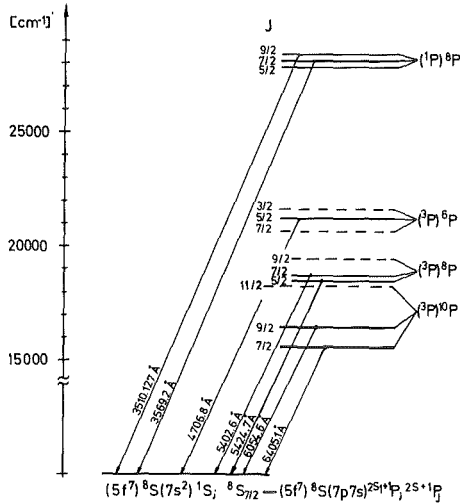
Fig.1

Preliminary energy scheme for AmI

In the space of the (7p7s) configuration the eigenvectors have been calculated (Table I) and some observed transitions could be identified as

Table I Energy levels and eigenvector composition of the $(5f^7)^8$S(7p7s)$^{2S}1^{+1}$P; $^{2S+1}$P$_J$ configuration in AmI (preliminary)

Term	J	Energy (cm^{-1})	Composition in %
$(5f^7)^8$S(7p7s)^{3}P;^{10}P	7/2	15608.15	$91(^3P)^{10}P + 8 (^3P) ^8P$
	9/2	16511.69	$83(^3P)^{10}P +15 (^3P) ^8P$
	11/2	18300.^{t}	$100(^3P)^{10}P$
$(7p7s)^3$P; ^{8}P	5/2	18429.09	$84(^3P) ^8P +39 (^3P) ^6P$
	9/2	19625.^{t}	$82(^3P) ^8P +16 (^3P)^{10}P$
$(7p7s)^1$P; ^{8}P	5/2	28056.^{t}	$99(^1P) ^8P + 1 (^3P) ^6P$
	7/2	28009.78	$97(^1P) ^8P + 2 (^3P) ^6P$
	9/2	28480.35	$96(^1P) ^8P + 3 (^3P) ^8P$
$(7p7s)^3$P; ^{6}P	3/2	21644.^{t}	$100(^3P) ^6P$
	5/2	21239.91	$84(^3P) ^6P +15 (^3P) ^8P$
	7/2	20654.^{t}	$59(^3P) ^6P +37 (^3P)$

t: theoretically predicted.

ground state transitions. Comparing the experimental levels with the calcu-
lated ones, some perturbation, most likely from the 7p6d configuration, is
observed, which will influence the hyperfine structure splitting and isotope
shifts in these transitions. This result requires a more complex study of
the $(5f^7)^8S(7p7s + 7p6d)$ configuration, if correct values for nuclear
quadrupole moments will be extracted from hyperfine structure splitting
measurements. In order to enable such studies highly precise hfs data of at
least six ground state transitions in one isotope are necessary.

(1)   M. Fred, F.S. Tomkins, J. Opt. Soc. Am. 47 (1957) 1076

2.8   A NEW PULSED AND TUNEABLE VACUUM-ULTRA VIOLET AND X-RAY
LINE SOURCE

H. Poth and A. Wolf, Phys. Lett. 94A (1983) 135

It is proposed to use the radiation emitted in electron capture by
ions occuring in electron cooling of stored stable particle beams as a
tunable photon source for vacuum-ultraviolet (VUV) and X-ray spectroscopy.
By choosing a suitable ion beam and storage energy, photon energies from
VUV to the X-ray region can be obtained. The photon line width can be made
smaller than 0.2 eV and its energy can be tuned in steps smaller than
10^{-4}. The photon source can be continuous or pulsed with a pulse duration
of 100 ns and less and repetition rates of 1 MHz and more. With present
electron cooling systems and storage-ring configurations, about $10^8 - 10^{12}$
photons can be produced into a 4π solid angle. The corresponding
intensities for observation in a solid angle of 1 msr range from 10^4 in
the VUV to more than 10^8 in the X-ray region.

3.   NEUTRINO PHYSICS

3.1   NEUTRINO PHYSICS AT THE RUTHERFORD SNS

G. Drexlin, H. Gemmeke, G. Giorginis, A. Grimm, R. Gumbsheimer,

H. Hucker, L. Husson, S. Kiontke, R. Maschuw, M. Momayezi,

K.H. Ottmann, P. Plischke, F. Raupp, E. Remane, M. Reuscher,

F.K. Schmidt, R. Schulz, G. Spohrer, J. Wochele, B. Zeitnitz

Kernforschungszentrum Karlsruhe, IK I and University of Karlsruhe

E. Finckh, W. Kretschmer, K. Stauber
University of Erlangen

N.E. Booth
Oxford University

J.A. Edgington
Queen Mary College, London

T.A. Gabriel, R.A. Lillie
Oak Ridge National Laboratory

The Karlsruhe neutrino project at the Rutherford SNS has now offici-
ally been approved by a signed agreement between the Kernforschungszentrum
Karlsruhe and the Science and Engineering Research Council (SERC) represented
by the Rutherford Appleton Laboratories (RAL).

A collaboration has been established between KfK and University of
Karlsruhe, University of Erlangen, Oxford University, Queen Mary College
London, Oak Ridge National Laboratory, and University of Tübingen.

The physics programme, properties of the ν-source etc. have been des-
cribed in detail in ref.1.

3.1.1   THE NEUTRINO FACILITY AT THE RUTHERFORD SNS

Instead of using an underground cave below the SNS target station for
the experimental neutrino area as described in the original proposal the neu-
trino detectors will now be installed in a neutrino block house at one side
of the target station (see Fig.1). The distance to the ν-source as well as the
dimensions of the shieldings were matched approximately to the same conditions
as for the cave solution. The design work on the block house plinth, an extra
neutrino crane and an extension of the existing experimtal hall has been fi-
nished and construction work will start during October 1983.

NEUTRINO BLOCKHOUSE

Scale
0 1 2 3 4 5 6 7 8 9 10m

Kernforschungszentrum
Karlsruhe m.b.H

Fig. 1: Neutrino facility at the
Rutherford SNS
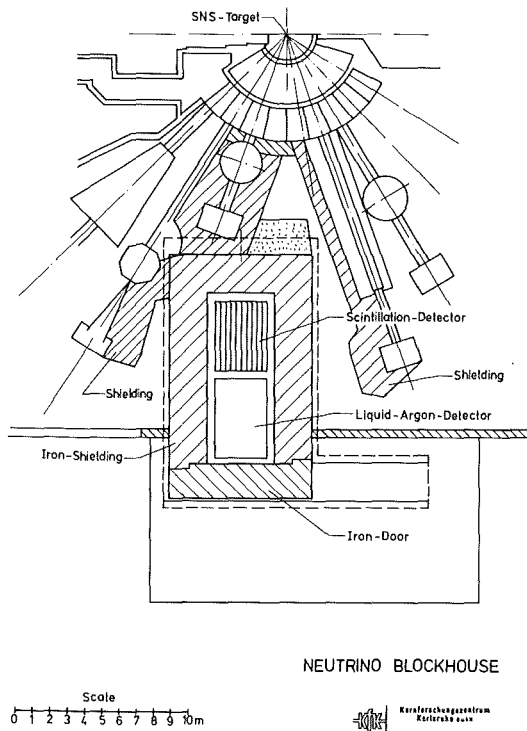
The order for about 6000 tonnes of iron for shielding purposes will be given in october 1983 too. The ν-block house will consist of continuously cast iron slabs vertically installed into a mounting frame and staggered to minimize the free path for background radiation. A movable door of about 600 tonnes will allow access to the block house. Moving of the detector will be provided by an air pad support structure. The erection of the ν-block house will take place during the second half of 1984 with support from RAL.

3.1.2 THE NEUTRINO SCINTILLATION DETECTOR

DETECTOR CONCEPTION

In a first step of the neutrino project it is planned to install a 50 ton organic scintillation detector which is expected to be fully operational until fall of 1985. The purpose of this detector is to observe semileptonic interactions of neutrinos with the ^{12}C and ^{1}H nuclei of the organic material as well as inelastic neutrino scattering on ^{12}C. With those reactions one is able to look for neutrino oscillations as well as to study the properties of weak interaction itself. For the inverse β-decay reactions on ^{12}C and ^{1}H a delayed coincidence between an electron from the charged current (ν_e, e)-process and another electron from the subsequent $\beta^{(\pm)}$-decay of the daughter nucleus has to be observed. For inelastic ν-scattering one has to look for a specific γ-radiation in an appropriate time window.

The detector is supposed to provide an energy resolution in the order of $\sigma \approx 10\%/\sqrt{E(MeV)}$, a time resolution of about 1 nsec and a spatial resolution of about 15 cm. This together with the time structure of the neutrinos from the pulsed spallation source should provide an unambiguous signature for the various events of interest.

Detailed considerations on various scintillator materials as well as experimental investigations have been carried out to find the most appropriate scintillator. Although more difficult to handle price/performance considerations finally led to the decision to use a mineral oil based liquid scintillator with a light output of about 50% anthrazene. To achieve a maximum fiducial volume the detector will consist of one large tank with 60,000 ℓ of liquid scintillator. It will be segmented into 512 optically isolated bars of 18×18 cm^2 cross section and 350 cm length, viewed by phototubes at each end (Fig. 2a). The optical segmentation consists of thin walls of tightly sealed double lucite sheets. The thin air gap in between provides totally internal reflection which guides the scintillation light to phototubes at the end of each bar (Fig. 2b). Gd-painted paper between the lucite double layer allows to detect neutrons which after thermalization produce 8 MeV γ-rays via the Gd (n,γ) reaction. The time difference between the two
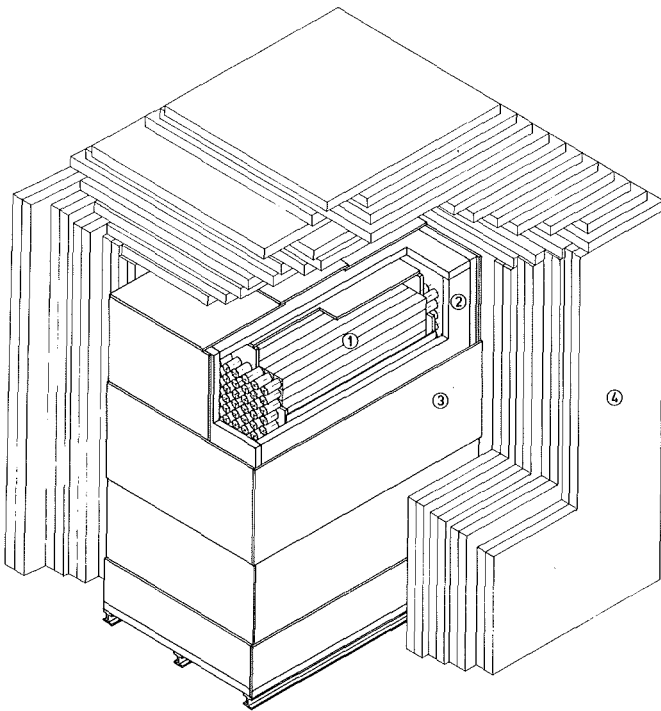
Fig.2a: 50 ton liquid scintillation detector
1. 512 liquid scintillator modules
2. passive detector shield
3. active antishield
4. neutrino blockhouse
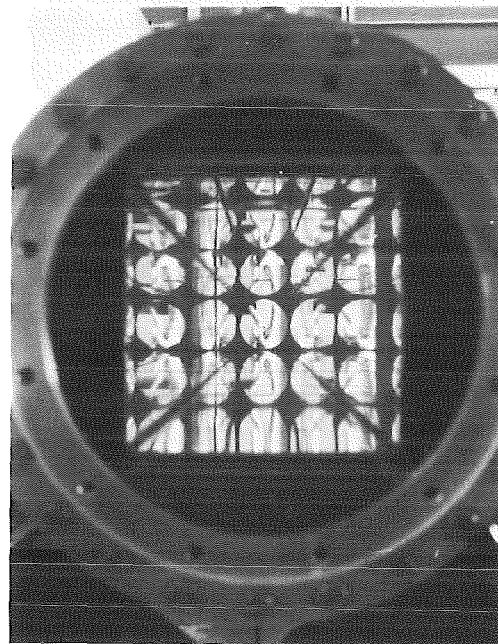
Fig.2b: View into one scintillator module with totally internal reflective boundaries

phototubes provides a spatial resolution of about 15 cm along the bar axis.

The whole detector is surrounded by an 18 cm layer of iron and an active antishield consisting of scintillator slabs. This arrangement not only detects cosmic particles entering the detector but also promises effective suppression of neutral background radiation from outside which otherwise cannot be identified unambiguously. As this background mainly originates from cosmic bremsstrahlung in the last 20 cm layer of the shielding around the detector this may be identified by a detected charged particle entering this layer through the active anticounter.

SCINTILLATOR INVESTIGATIONS

Different liquid and solid scintillators have been investigated concerning light output and light attenuation. The light output was measured by the compton edge of a γ-spectrum of ^{60}Co taking NE110 (Nuclear Enterprise) for reference and is listed in Table 1.

TABLE 1

Light output for various solid and liquid scintillators in % Anthrazene with reference to NE 110

Scintillator	L.O. exp.	L.O. th.	Scintillator	L.O. exp.	L.O. th.
Solid					
NE 110 [a]		60	GS 2003 [d]	50	50
KSTI 430 [b]	61	60	GS 2037 [d]	44	44
SCSN 20 [c]	47	52			
Liquid					
NE235H [a]	55	47.5	NE 235C [a]	61	60

a) Nuclear Enterprises, Edingburgh, Scottland
b) KSH Plastics, Geel, Belgium
c) Kyowa Gas, Tokyo, Japan
d) Röhm, Darmstadt

The light attenuation normally given by the attenuation length (1/e fall off) is strongly dependent on geometry as the number of reflections and thus the reflectivity enters into the light output of long scintillator rods. Fig. 3 shows the attenuation curves for two acrylic based scintillators GS2037 (RÖHM) with different dimensions. The solid lines are calculations with an analytical method taking into account the various orders of reflection before reaching the phototube. The dashed curve is a MC-simulation (s. ch. 3.2.3). With a given reflectivity of the walls and light absorption in the scintilla-
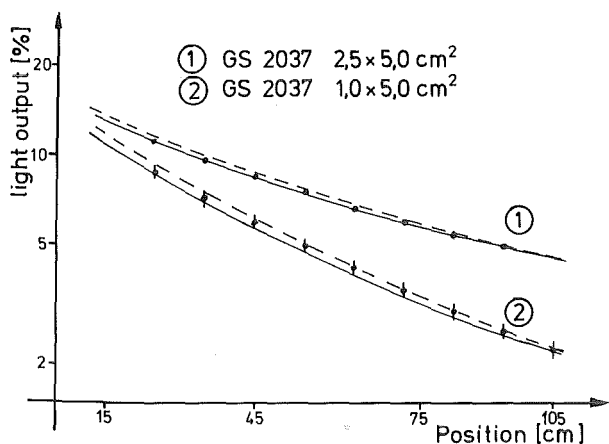
Fig. 3:

Position dependent light output for acrylic scintillator bars (GS2037); solid line: analytical order of reflection calculation, dashed line: Monte Carlo simulation.
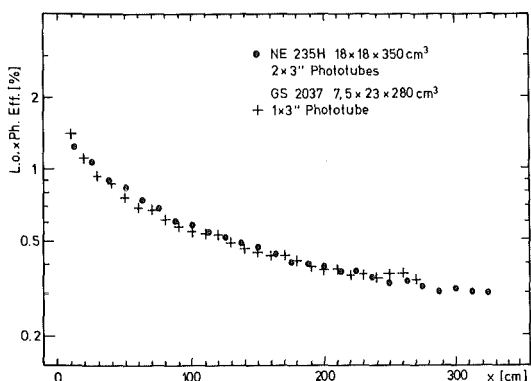
Fig. 4:

Monte Carlo calculation for position dependent light output a) liquid scintillator (NE235H). B) solid scintillator (GS2037).

tor both methods allow to calculate position dependent light output curves for any geometry.

Fig. 4 shows the MC calculations for a mineral oil based scintillator NE 235H (Nuclear Enterprise) and the GS2037 scintillator (RÖHM) both for realistic dimensions. No significant difference in the performance is to be seen.

The decision to use a mineral oil based scintillator was finally based on cost arguments. In addition GS2037 contains 15% oxygen which causes additional background reactions and decreases the number of ^{12}C and ^{1}H atoms. All other suitable polystyrene or polyvinyltoluene based solid scintillators like NE110 (Nuclear Enterprise), BC412 (BICRON) or SCSN20 (KYOWA) could not be taken into account as they are much too expensive.

MONTE CARLO CALCULATIONS

The energy resolution mainly determined by the number of photoelectrons in the phototubes has been investigated with detailed Monte Carlo calculations and cross checked with experimental results from prototype measurements. The crucial parameters which besides the actual geometry enter into these calculations are the specific light output, the emission and absorption spectra of the scintillator, reflectivity of the scintillator walls, fractional scintillator area covered by the phototubes, photo ef-

ficiency spectrum and photoelectron collection efficiency. A critical point is the reflecitivity which has to be as good as possible as it enters exponentially into the light collection with an average of about 30 reflections before reaching the phototube. Due to the fabrication procedure of the totally internal reflecting sheets there are always some small blind areas along the corners of each bar which has to be taken into account. In addition it was necessary to consider the spectral response of emission and absorption of the scintillator light as well as the spectral photo cathode efficiency to understand the results from prototype measurements. Fig. 5 shows the MC results of the light output along a 350 cm long liquid scintillator (NE 235H) with totally reflecting walls with cross sections 15×15 cm^2 viewed by a 2" phototube. The deviation from a pure exponential decrease of light output with distance from the phototube is not a geometry effect but stems from wavelength dependent light absorption which has been measured in a separate experimental setup. Agreement of the MC calculations with experimental data from triggered cosmics measured with the prototype detector is fairly good so that the properties of such a scintillator module are now quite well understood.

Fig. 5:

Position dependent light output for liquid scintillator (NE235H) ($15 \times 15 \times 350$) cm^3 viewed by a 2" phototube; solid line: Monte Carlo calculation.

PHOTOTUBES

To achieve optimum energy resolution due to photoelectron statistics one would like to cover as much of the scintillator surface as possible with photosensitive material. For the face area of a scintillator bar of 18×18 cm^2 cross section this would mean to use a phototube with a large area photocathode. Unfortunately the collection efficiency of a 5" phototube is only half as good as that of a 2" or 3" tube. Thus we decided to look at each face of a scintillator bar with two 3" phototubes with common HV supply and signal output. A complicated and expensive light guide could only provi-

de a light collection improvement by a factor of 1.2 and is therefore omitted. For a dynamic range of 500 for the detector signal a gain of 10^6 and a linearity up to 100 mA is required for the phototubes. For a time resolution of about 1 nsec the rise time of the phototube should not be worse than 3 nsec. Various tubes of different manufactorors are under test now.

OPTICAL SEGMENTATION

For optimum energy resolution any dead volume which could absorb the small amount of energy available has to be avoided. Therefore the optical boundaries of the 512 scintillator bars have to be as thin as possible. On the other hand they have to provide optimum reflectivity. 1 mm lucite sheets and even thinner plastic foils have been considered to use for totally internal reflecting double layers. Besides the lucite sheets only a Hostafan foil showed satisfactory reflectivity. The sealing at the edges of the double layer has to be minimized for optical reasons. On the other hand it is very delicate to handle as any small even invisable crack in the sealing causes the reflectors to be filled with liquid thus being demaged. Reliable sealing techniques as well as to find out easy and cheap fabrication procedures are under investigation.

ELECTRONICS AND DATA HANDLING

Design of the electronics for the scintillation detector has been worked out and first modules are being built and tested. Due to the characteristic signature of true events within a fairly high background the detector as a whole has to provide:

i   precise measurement of the total energy absorbed
ii   absolute event time with respect to the proton spill
iii relative timing of the individual bars contributing to an event
iv   ability to detect a time coincidence within one bar with minimum delay and complete energy and time information (delayed coincidence signature).

Fig. 6 shows a block diagram of the electronics. High voltage for the phototubes is provided by a computer controlled HV system for 1024 individual channels (LeCroy 1440). For each of the 512 scintillator modules the analogue signal of the phototubes (energy), the time difference between the two ends of the module (Δt), and the relative time with respect to the first fired bar (t) is stored within an event time of 70 nsec. Digitizing is ini-

tialized by a software controlled trigger processor after 300 nsec into fast ADC's with buffer memories. A multihit TDC initialized as well by the trigger processor measures the absolute event time. A second event following a first one even in the same scintillator module may be detected after a minimum deadtime of 3 μsec. Readout of the ADC- and TDC-buffer registers via "intelligent" CAMAC control takes place after 16 msec i.e. 4 msec before the next proton spill of the SNS. The "valid event" decision in the trigger processor is based on a "sum energy (ΣE)/multiplicity (M)" matrix mask set by RAM's. In addition a neutrino induced event has to show up in the first 9 μsec due to the neutrino time spectra. Having detected such an event the trigger processor is switched to a "watch dog" mode for the second part of a delayed coincidence event and will reject any other event which concerning the ΣE/M-matrix do not promise to be a valid one. For single events the trigger processor applies reasonable scale down suppression factors. The purpose is to measure the background explicitely but to minimize the background related deadtime.

Detector control will be provided by a light pulser system with fiber optics fed by a UV N_2-laser. Logic control will be done by a software controlled event pattern pulser system.

Data acquisition and experiment control will be performed via CAMAC by a LSI 11/23 microcomputer. A DMA interface connects the Q-Bus of the LSI 11/23 with the UNIBUS of the VAX 11/750. The VAX will be used for one line data handling and programme executing. 2 MByte memory and 2 ×80 MByte mass storage allows to store large data arrays and programs. The system is already operating and programme development has started.
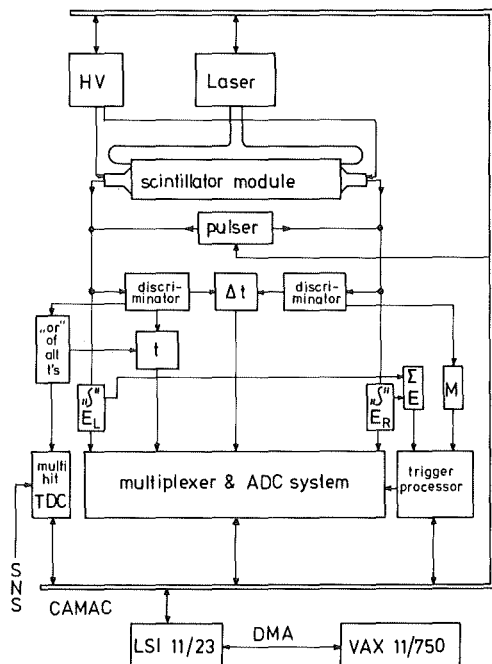
Fig. 6:
Blockdiagram of the electronics for one out of 512 scintillator modules.

3.1.3 PROTOTYPE RESULTS

Two prototype liquid scintillator detectors have been built using totally internal inflecting sheets for optical segmentation. One is a 350 m long module with 15×15 cm^2 cross section viewed by a phototube at each end. The other is a 1000 ℓ detector with 9 modules of 17×17 cm^2 cross section and 175 cm length each (Fig. 7). This detector is triggered by large area multiwire proportional chambers on top and bottom of the scintillator tank.
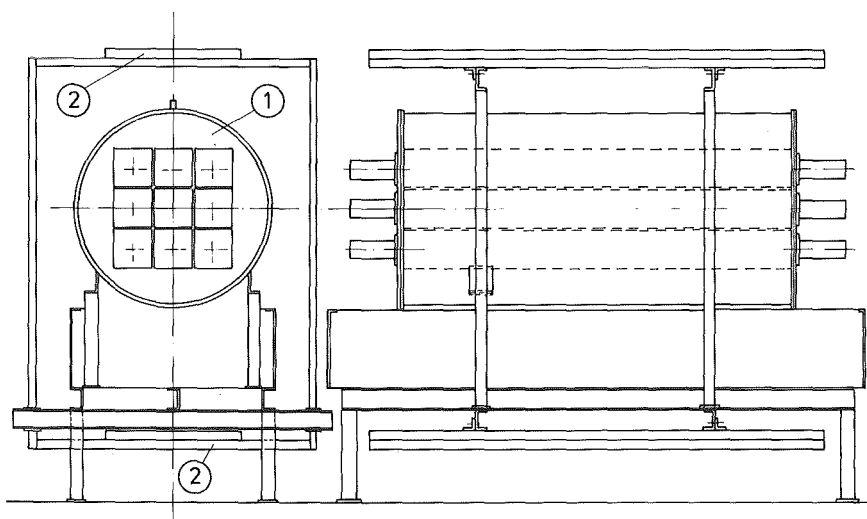
Fig. 7: 1000 ℓ liquid scintillator detector (NE235H)
   1. scintillator tank with 9 optically isolated modules
   2. large area proportional counters (cosmic trigger)

With this detector cosmic runs are planned to study in detail the exact position dependence of energy, time and spatial resolution as well as the correlation between neighbouring modules.

These informations will serve as a basis for the actual "detector Monte Carlo" programme. The prototype II detector which has gone under operation in August 83 will also be used to test the electronics and data handling system.

Measurements with prototype I have been performed with 2" phototubes. The position dependent light output for triggered cosmics has already been shown in Fig. 5.

Fig. 8 shows the pulse height spectrum for minimum ionizing particles
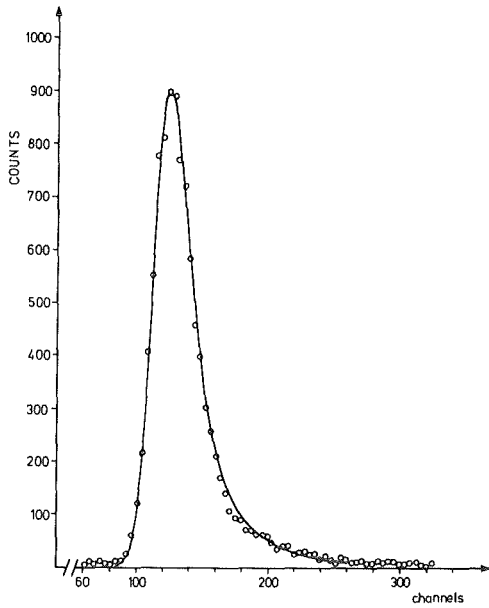
Fig. 8:

Pulse height spectrum of m.i. particles passing a (15×15) cm^2 liquid scintillator module at 175 cm from a 2" phototube. Solid line: χ^2 fit with Landau energy loss distribution and Gaussian resolution curve with $\sigma = 8\%$.

with energy loss of $\Delta E = 25$ MeV seen by a 2" phototube at a distance of 175 cm from the position of energy absorption. The solid line represents a χ^2-fit where the appropriate Landau distribution has been folded with a Gaussian resolution curve of 18% FWHM. Extrapolation to the 50 ton detector with two 3" phototubes at each end of a scintillator module approaches roughly the design goal of $\sigma = 10\%/\sqrt{E(\text{MeV})}$. The time resolution between the two phototubes at each end which has been corrected for amplitude walk was 1.5 nsec FWHM. Fig. 9 shows the measured time difference versus the position
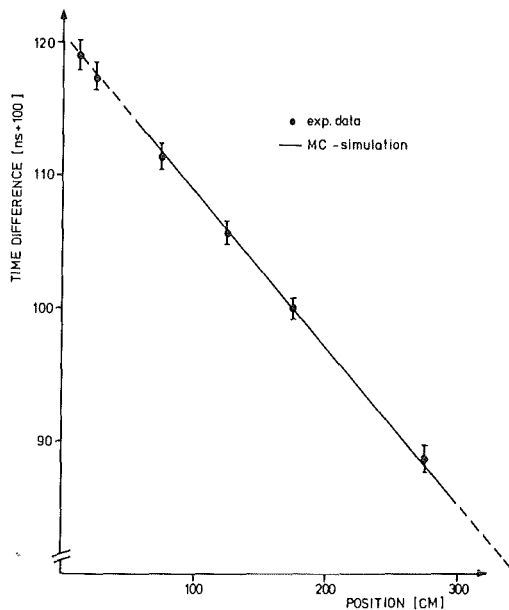
Fig. 9:

Time difference between phototubes at a 350 cm long scintillator module versus position of energy absorption.

Solid line: Theoretical distribution from Monte Carlo simulation.

of energy absorption together with the results for the average light path from a Monte Carlo calculation.

Further experiments with prototype I are going on to test improvements of the optical segmentaticn as well as different phototubes.

3.1.4 THE LIQUID ARGON TEST DETECTOR

A 50 ton liquid argon time projection chamber is planned to measure the differential cross section of the neutrino electron scattering.

In a small test device described in the annual report of 1982 signals from α particles of an ^{241}Am source could be observed. In a drift chamber configuration with a grid in front of the anode the electron spectrum of a ^{207}Bi conversion source has been measured. Further developments to increase the drift gap up to > 10 cm and to test different electrode configurations for time projection techniques are going on.

(1)   R. Maschuw, B. Zeitnitz, Neutrino Physics at the Pulsed Spallation Neutron Source SNS, KfK 3362 (Jun. 1982) and Addendum (Nov. 1982)

3.2 INELASTIC SCATTERING OF NEUTRINOS FROM ARGON

S. Furui, Z. Phys. A308 (1982) 339

Institute for Theoretical Physics of the University of Tübingen

In the planned neutrino experiments with a liquid argon target only the electrons[1] are detected in the final state. Therefore, it's necessary to know the total and differential cross section for the reaction

$$\nu_e + {}^{40}Ar \rightarrow {}^{40}K + e^-.$$
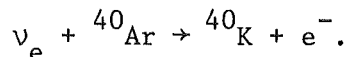
We used the statistical model[2] to calculate total cross sections for allowed and first forbidden transitions and found that the quenching of the Gamow-Teller giant resonance can't be neglected. In the case of the Fermi transition, the results of the statistical model and the microscopic model of Donnelly and Peccei[3] are almost identical. We calculated the differential cross sections for allowed transitions in the microscopic model and normalize the intensity to get the identical total cross sections in both models. Because of the Lorentz transformations, the differential cross section of neutrino-electron scattering has a pronounced forward peak in the lab system, in which respect it differs from the neutrino-nucleus reaction.

(1)   R. Maschuw and B. Zeitnitz, Neutrinophysics at the Pulsed Spallation
        Neutron Source SNS, KfK 3364 (1982)
(2)   N. Itoh, Y. Kohyama and Y. Fujii, Nucl. Phys. A287 (1974) 501
(3)   I.W. Donnelly and R.D. Peccei, Phys. Rep. 50C (1979) 1

3.3 STUDY OF AN HIGH ACCURACY HELICITY MEASUREMENT OF THE ELECTRON NEUTRINO

A. Draut, P. Blüm, L.M. Simons

The theory of weak interaction is based on the V-A hypothesis. Although the latter is generally accepted, some theorists have proposed a V+A part, whose amplitude is believed to be less than 10%.

A method to reduce this upper limit would be the measurement of the neutrino helicity

$$H = < \vec{\sigma} \cdot \vec{p} > / \sigma \cdot p$$

with an accuarcy better than 1%. The values of the helicity of the ν_e-, measured up to now, have an accuracy of about 20% (1).

Therefore we have studied the feasibility of an experiment using the $^7_4$Be decay:

$$^7_4Be + e^- \rightarrow {^7_3Li}^* + \nu$$
$$\hookrightarrow {^7_3Li} + \gamma$$
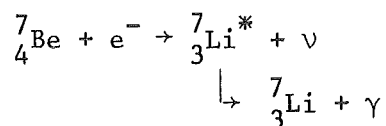
Because e^- capture is mainly a two body decay (competing processes are of the order of 10^{-4}) the neutrino's momentum is transferred to the $^7Li^*$ and it is polarized according to the spin of the neutrino. After the decay of Li^* the γ carries the information about the momentum as a Doppler shift of its energy and about the spin as a partial circular polarization.

The Be decay was analysed in order to extract the information about the momentum by means of nuclear resonance fluorescence (NRF) and of the circular polarization by scattering resonantly at a polarized Li target.

In order to achieve the NRF we need a high temperature of the source to increase the recoil velocity of Li^+.

Due to the long mean lifetime (10^{-13}s) of Li^*, large slowing down effects occur in solid and liquid sources. However we found good conditions in a gaseous source at low pressure. Because of the high temperature, the NRF cross section rises several orders of magnitude above the background.

In particular we investigated the use of the very volatile $BeCl_2$ in an Ar atmosphere within a closed quartz tube. The high temperatures can be reached by electrodeless high frequency excitation.

Detailed calculations gave all parameters needed to obtain the neutrino's helicity from counting the γ rays scattered resonantly from the Li target, polarized alternatively in or opposite to the γ direction.

Thus the desired accuracy can be reached by measuring only several days with a source of an activity of 1 Ci.

(1)   Goldhaber, Grodzins, and Sunyar, Phys. Rev. 109(1958)1015

4.   INTERMEDIATE ENERGY PHYSICS

4.1   LEPTONIC ATOMS

4.1.1 PERTURBED ANGULAR CORRELATIONS IN MUONIC ATOMS

L.M. Simons

The idea to use perturbed angular correlations to determine the ratio of the line width Γ and the hyperfine splitting energy $\Delta E_{F,F'}$ of two hyperfine levels characterized by the quantum numbers F and F' in muonic atoms was discussed several years ago by the author and was independently discovered by Batkin (2).

One makes use of the fact, that the time integrated attenuation coefficient G_{kk} for the hyperfine interaction deviates from the hard core value in a rather simple way (3). Thus the effect to be measured is the deviation of the intensities in an angular correlation from the predicted fully disturbed values which is proportional to the interference term

$$\sum_{F \neq F'} \frac{(2F+1)(2F'+1)}{2J+1} \left\{ \begin{matrix} F & F' & \lambda \\ I & I & J \end{matrix} \right\}^2 \frac{1}{1 + \left(\dfrac{\Delta E_{FF'}}{\Gamma}\right)^2}$$

where I = quantum number of the nuclear spin, J = total quantum number of the muonic state without hyperfine interaction, and λ = degree of orientation.

Usually J = 3/2 (muonic $2p_{3/2}$ state) should be taken for an angular correlation 3d $\rightarrow$ $2p_{3/2}$ $\rightarrow$ 1_s where only intensities are observed (λ = 2). Ideally the 3d $\rightarrow$ $2p_{1/2}$ $\rightarrow$ 1_s transition chain may serve as a calibration transition because it will be isotropic and can be used to disentangle systematic errors.

A modern coincidence arrangement will use planar Ge-detectors measuring the 3d $\rightarrow$ 2p transitions in coincidence with the 2p $\rightarrow$ 1_s transitions detected by CsF detectors. In order to keep accidental coincidences small a muon channel in a momentum mode with negligible micro time structure has to be used. The method is useable at first sight only for the measurement of magnetic moments in the cases where quadrupole moments are small. Usually a "normally" large quadrupole moment will lead to a complete splitting with $\Delta E_{FF'} \gg \Gamma$.

Fortunately enough for all nuclei with I = 3/2 the quadrupole splitting of the F = 1, F' = 3 levels is zero in first order approximation. Therefore muonic atoms with these nuclei are ideally suited to measure magnetic moments (Bohr-Weisskopf effect) or the influence of higher order terms of the quadrupole splitting.

(1)   L.M. Simons, The depolarization of negative muons in muonic atoms, Proceedings of the IKO study week on physics with low energy beams of pions and muons, I.K.O. Amsterdam, (1978)
(2)   I.S. Batkin, Sov. J. Nucl. Phys. 31(1980)3
(3)   R.M. Steffen and K. Alder, Chapter 13 in The electromagnetic interaction in nuclear spectroscopy, (North Holland, Amsterdam, 1973)

4.1.2   THE QUADRUPOLE MOMENT OF ^{97}Mo

W. Kunold, W. Oesterle, M. Schneider, L.M. Simons, R. Abela[+]

In order to increase the accuracy of an earlier experiment (1) of our group a measurement of the $2p_{3/2}$ hyperfine splitting of ^{97}Mo was performed at the μE1-channel at the Swiss Institute for Nuclear Research. Both the 3d → $2p_{3/2}$ and the 2s → $2p_{3/2}$ transitions have been observed with two high resolution intrinsic planar Ge-detectors. Special care was taken to avoid background events and neutron induced events. For the analysis muonic energies and relative intensities were computed by the programs MUON and RURP. One excited nuclear state had to be taken into account and no neutron induced background was found during the evaluation process in contrast to Ref. 1. The results are:

$2s_{1/2}$ → $2p_{3/2}$ transition: Q = .218 ± 008   barn

$3d_{5/2}$ → $2p_{3/2}$ transition: Q = .221 ± 012   barn

The weigthed average is Q = .219 ± 007   barn.

(1)   P. Heitlinger, Präzisionsmessung des Kernquadrupolmoments von $_{42}$Mo^{97} mit Hilfe der Methode myonischer Atome, Dissertation Universität Karlsruhe (1980)

+   Institut für Physik, Universität Basel

4.1.3 LASER-INDUCED ELECTRON-ION CAPTURE AND ANTIHYDROGEN FORMATION

R. Neumann[+], H. Poth, A. Winnacker[+], A. Wolf, (1)

The influence of intense light on the recombination of electrons and ions during electron cooling has been considered in this work. It appeared that, under realistic conditions at LEAR, an enhancement of the proton-electron recombination rate by a factor of 10^2 can be expected during a laser pulse sent along the common trajectory of electrons and protons. This enhancement is due to induced radiative electron capture which can be understood considering a proton within the electron gas as an atomic system in which only continuum states are occupied and which, hence, is strongly inverted.

As opposed to the spontaneous recombination already observed in earlier electron cooling experiments, the initial kinetic energies of the electrons involved, and the final levels of the atoms formed, are well defined in induced recombination by the energy of the photons sent in. The induced recombination rate, as a function of the laser frequency, significantly depends on the shape of the electron velocity distribution; therefore, its measurement appears very useful for the diagnostics of electron cooling.

Further, induced recombination might find an application in producing a pulsed beam of antihydrogen atoms in well defined atomic states provided a high quality positron beam would be available in a set-up similar to that used in electron cooling. An estimation, under realistic conditions at LEAR, considering positron sources available, reveals an antihydrogen intensity of a few atoms per second.

An experiment investigating electron-proton recombination with the LEAR electron cooler, in collaboration with a laser physics group from Heidelberg, is being prepared. The dye laser system to be constructed for this purpose shall, in addition, be used for a Thomson scattering experiment with the LEAR electron cooler, before its installation at LEAR. As has been discussed in a separate report (2), the spectral analysis of photons scattered by the electron beam would allow to determine the space-charge related energy profile of the beam at a count rate of ~ 0.4 photons/sec.

(1)   dto., CERN-EP/83-66, submitted to Z. Phys.
(2)   A. Wolf, unpublished report

+   Physikalisches Institut der Universität Heidelberg

4.2 HADRONIC ATOMS

4.2.1 ANTIPROTONIC X-RAYS AT LEAR

L. Adiels[+], G. Backenstoß[++], I. Bergström[+], P. Blüm, S. Charalambous[++++], S. Dedoussis[++++], K. Fransson[+], A. Hancock, J. Hauth, H. Koch, T. Köhler, A. Kreissl, A. Nilsson[+], P. Pavlopoulos[++], H. Poth, U. Raich, D. Rohmann, J. Repond[++], M. Suffert[+++], L. Tauscher[++], D. Tröster[++], K. Zioutas[++++].

The aim of the experiment PS 176 at LEAR is the measurement of the strong interaction between antiprotons and nuclei at kinetic energies near zero. Furthermore, it is intended to investigate the γ-spectra of the residual nuclei in order to get information on the break up of nuclei after p̄-absorption. The measurement of high energy γ-rays in the energy region up to several hundred MeV aims at the search for deeply bound p̄-nuclear systems of considerably long life times.

The experiment is realized in a collaboration with Basel, Stockholm, Strasbourg and Thessaloniki, and in cooperation with Munich. During the past year the set up - as already presented in the last Annual Report (4.2.1) - was built in the Karlsruhe workshops, tested and transported to CERN. The target ladder was added from Munich, and the telescope counters and moderators were supplied by Basel. An electronic scheme for simultaneous runs with six and more Si/Ge - diodes or NaI - detectors for promt and delayed coincidences was worked out. The data analysis system using a fast μ -processor at the front end and our PDP 11/34 at the rear end was finally tested. In the spring 1983, the electronic hut was installed and the analog and digital electronics for the de- tector system was set up. A series of careful test⁻ ᴻᶜ the diodes was performed resulting in an excellent timing behaviour for all energies of interest. In parallel the on- and off-line programs for the data acquisition system and the off-line evaluation were written.

For the first test run at LEAR with protons the complete system was set up. The few hours with protons were used to optimize the beam focus, to measure the range curve and to fix the relative timing between the counter telescope and the X-ray detectors.

In the first days of August antiprotons of 300 MeV/c momentum were available during a short period of about two hours in total. The system was tuned so well that not only range curves and beam dimensions could be deter-

mined but even first data on antiprotonic ^{16}O-X-rays could be measured. Six diodes were in operation covering an energy range between 3 keV and 6 MeV and a time range from 0-16 μs. In addition high energy γ-rays were measured with a 15x10" NaI provided by Strasbourg, and a neutron spectrum was obtained using a special counter delivered from Stockholm. The first spectrum of anti-protonic atoms seen at LEAR is shown in Fig. 1. The peak to background ratio was very good because of the excellent on-line timing conditions. The com-
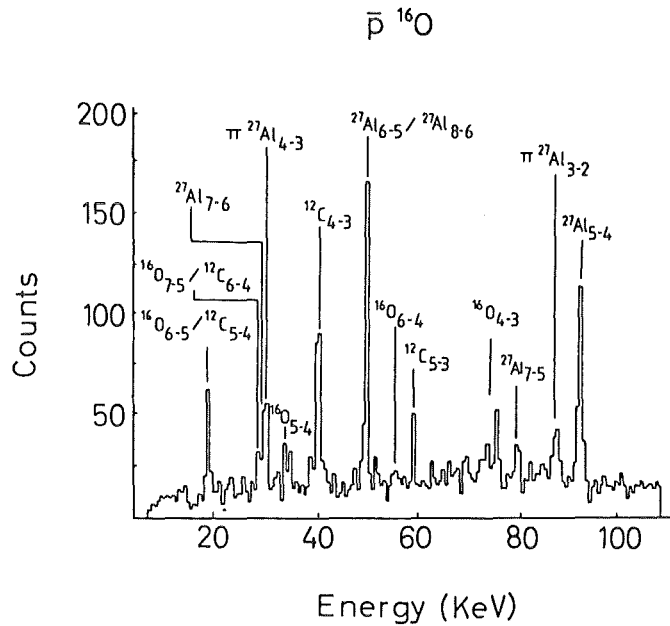
Fig. 1: $\bar{p}$-^{16}O spectrum measurde at LEAR. About 20 minutes measuring time, 5000 $\bar{p}$/s in average.

parison with the former data and the fact that the $\bar{p}$-rate delivered by LEAR was by more than a factor ten lower than the design value gives confidence for a successful and interesting measuring program of $\bar{p}$-X-rays in the future.

+   Research Institute for Physics, Stockholm, Sweden
++   Institute for Physics, University of Basle, Switzerland
+++   Centre de Recherches Nucléaires and Université Louis Pasteur, Strasbourg, France
++++   Department of Nuclear Physics, University of Thessaloniki, Greece

4.2.2 FEASIBILITY STUDIES FOR HIGH PRECISION MEASUREMENTS OF THE MASS AND THE MAGNETIC MOMENT OF THE ANTIPROTON

G. Büche, H. Koch, A. Kreissl

The LEAR facility at CERN will provide for high fluxes of antiprotons in the near future. This opens the way for a lot of experiments which can be tried for the first time or can be continued on a higher level of quality standards. To this second category can be attributed the intention for higher accuracies in the values of the mass and the magnetic moment of the antiproton. We have started to find criteria how to extend these accuracies in connection with the measurement of X-rays from antiprotonic atoms. On one hand, the discussion includes the energy resolution of the experimental equipment as well as the absolute and relative calibrations of photon energy, respectively, as far as the measurement is concerned. On the other hand, the evaluation of data with respect to the mass or the magnetic moment comprises a careful analysis of a whole series of electromagnetic corrections to the Dirac atomic energies as well as the influence of the strong interaction of antiprotons to the low lying levels. Until mid of 1983 several computer programs were made available at Karlsruhe which are suitable for calculations of the energies of atomic levels by integration of the quantum mechanical equations and of the intensities of X-ray components from a cascade model. A systematic study of antiprotonic X-ray transitions with respect to (Z,A) of the nucleus and to the size of the various corrections is in preparation in order to minimize the expected uncertainties in a determination of $m_{\bar{p}}$ and $\mu_{\bar{p}}$.

4.3 PION-NUCLEUS INTERACTION

4.3.1 MEASUREMENTS OF iT_{11} in $\pi-d_{pol}$ SCATTERING BETWEEN 140 AND 325 MeV

G.R. Smith, E.L. Mathie, E.T. Boschitz, M. Meyer[+], F. Vogler[+]

M. Daum[++], S. Mango[++], J.A. Konter[++]

Due to the importance of measurements of the vector analysing power iT_{11} in $\pi-d$ scattering for the investigation of dibaryon resonances we have drastically enhanced the data taking rate by employing a different measuring technique and an improved polarized deuteron target.

The experiment was performed at the $\pi M3$ area of the Swiss Institute for Nuclear Research. The polarized deuterium target was the same as for the earlier measurements of iT_{11} [1,2] except for the following improvements: The teflon cell containing the deuterated butanol target was replaced by a thin (100 μm) brass cell in order to reduce the background and energy loss of the outgoing (recoil) deuterons. The corresponding deterioration of the observed deuteron NMR signal was compensated for by employing a FET in an impedance matching circuit contained physically in the cryostat (at a magnetic field of 2.5 T and a temperature of $0.5^{\circ}K$). As usual the magnitude of the target polarization was determined from comparisons of the dynamic polarization NMR signal with the thermal equilibrium (natural polarization) NMR signal.

The particle detection system was quite different from that employed previously. In order to enhance the data taking rate we introduced a multiple detector time of flight "spectrometer". Pions were detected simultaneously at 6 angles in coincidence with their corresponding recoil deuterons. Scintillation counter telescopes were used for both pions and deuterons. The deuteron counters were followed by absorbers (whose thickness was adjusted for each setting to discriminate between recoil deuterons and the higher energy protons of background reactions) and a veto counter. In order to obtain optimum timing resolution, the pion and deuteron TOF scintillators were each viewed at both ends by phototubes. The pion solid angles in each arm was 30 msr, and the angular acceptance was $\Delta\Theta_\pi = 5^{\circ}$. Pions could be detected in the angular range 30° to 140° in 2.5° steps, with the deuteron arms being adjusted correspondingly. In this new $\pi-d$ coincidence set-up, the following conditions were imposed on a

$iT_{11}(\%)$

T$_\pi$=140 MeV

T$_r$=256 MeV

T$_\pi$=180 MeV

T$_\pi$=275 MeV

T$_\pi$=219 MeV

T$_\pi$=294 MeV

T$_\pi$=238 MeV

T$_\pi$=325 MeV

Θ_{cm} (degrees) Θ_{cm} (degrees)
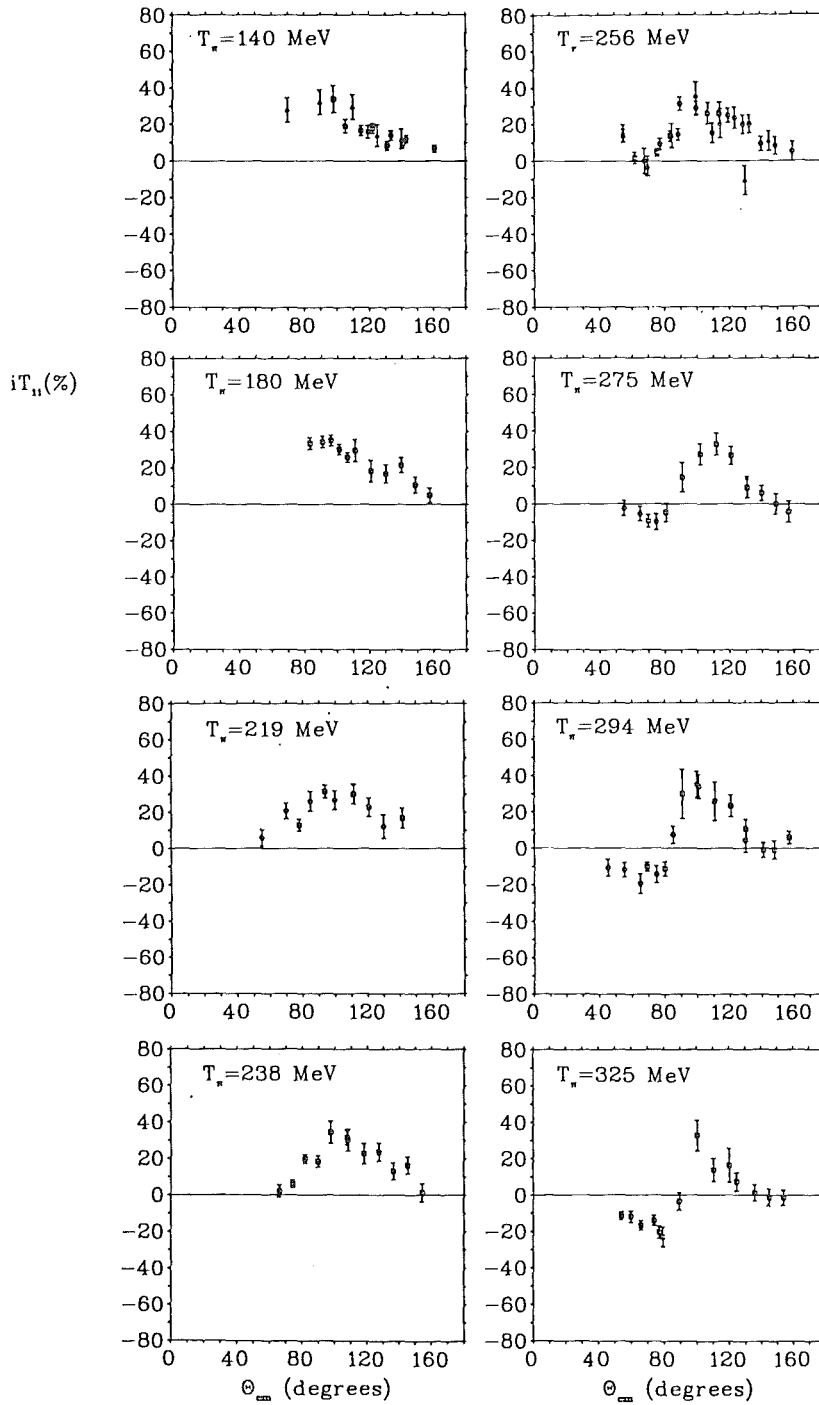
Fig. 1: The vector analysing power iT_{11} as a function of energy and c.m. angle.

π-d signature: pion energy loss, deuteron energy loss, deuteron range, and the time of flight difference (TOF) between signals in the pion arm and the deuteron arm.

The results are presented in Fig. 1. The data taken earlier with the pion spectrometer are well confirmed except for the datum at 130 degrees at 256 MeV. As one can see, there is a clear trend of the data from 140 to 325 MeV. For angles larger than 100 degrees iT_{11} changes little with

energy. Around 70 degrees however, a pronounced dip develops at the higher energies. This behaviour is not accounted for by predictions from Faddeev type calculations (4,5) or by Glauber respectively impulse approximation calculations.

(1)   B. Blankleider and I.R. Afnan, Phys.Rev. C24(1981)1572
(2)   W. Grein and M.P. Locher, J. Phys. G7(1981)1355
(3)   N. Giraud, Y. Avishai, C. Fayard, G.H. Lamot, Phys. Rev. C19(1979) 465
(4)   A.S. Rinat, E. Hammel, Y. Starkand, A.W. Thomas, Nucl. Phys. A329 (1979)285

+   Physikalisches Institut, Universität Erlangen-Nürnberg
++   Schweizerisches Institut für Nuklearforschung

4.3.2   SEARCH FOR RAPID   ANGULAR AND ENERGY DEPENDENCE OF $d\sigma/d\Omega$ AND iT_{11} IN LARGE ANGLE π-d SCATTERING

E.L. Mathie, G.R. Smith, E.T. Boschitz, M. Meyer[+], F. Vogler[+], M. Daum[++], S. Mango[++], J.A. Konter[++]

Recent measurements of the tensor polarisation t_{20} below the (3,3)-resonance have produced puzzling results. Two sets of conflicting data exist at a pion laboratory energy near 142 MeV and $\Theta_{cm} > 120^{o}$. One set shows a tensor polarisation which varies relatively slowly with angle and is always more negative than -0.3 in this angular region. The other set displays a smooth relatively flat distribution at T_{π} = 117 MeV. With increasing energy a double hump distribution develops, becomes largest at T_{π} = 134 MeV and reduces to a flat distribution at T_{π} = 151 MeV. Most of these data have positive values.

If the latter data set is correct a strong angular and energy dependence may also show up in the observables $\frac{d\sigma}{d\Omega}$ and iT_{11}. Therefore, we have made accurate measurements of the angular and energy dependence of iT_{11} and the differential cross section between T_{π} = 117 and 151 MeV. The main goal was to provide a broader, more restrictive data base for realistic phase shift analyses. It was further hoped that the energy and angular behaviour of iT_{11} in this region would help to indirectly confirm or rule out one of the conflicting t_{20} data sets. The experimental results are presented in Fig. 1 and Fig. 2.

Neither the differential cross-section nor the vector analysing
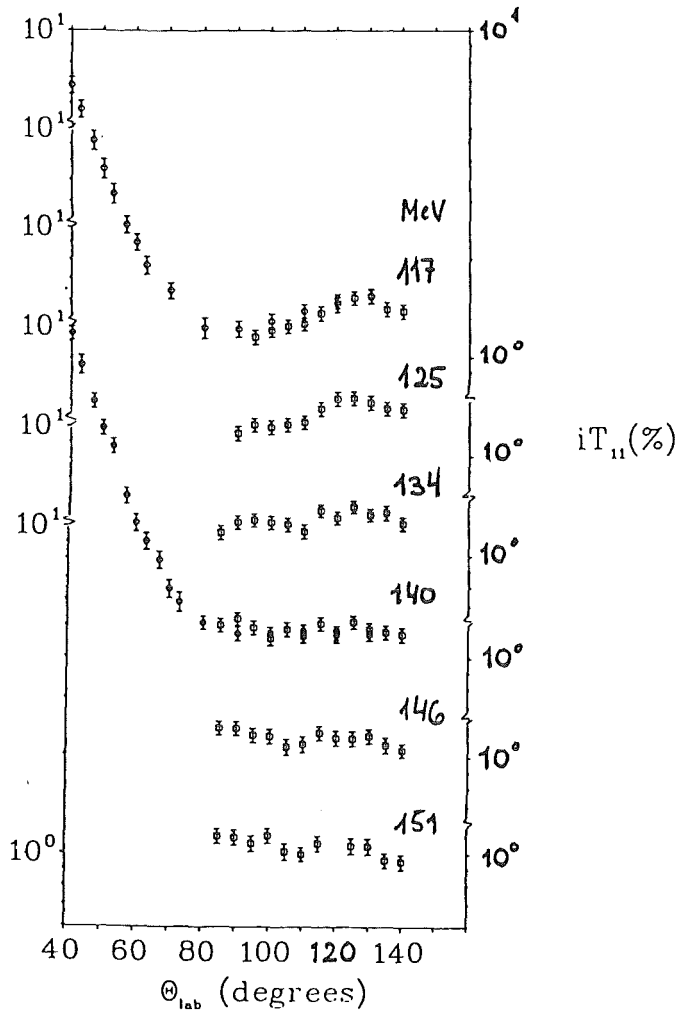
Fig. 1: Differential cross
sections for π-d elastic
scattering
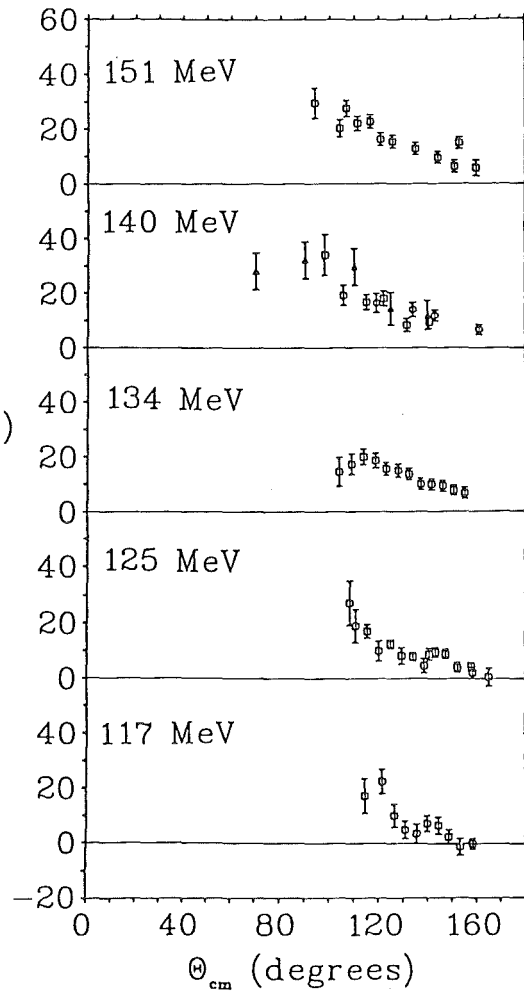
Fig. 2: Vector Analysing power
iT_{11} for π-d elastic
scattering

power show within the measured accuracy rapid changes as a function of angle and energy in the backward hemisphere.

Obviously, the question arises whether or not the smooth dependence of iT_{11} and $d\sigma/d\Omega$ together with the oscillating nature of the SIN t_{20} angular distribution can be reproduced by any set of reasonable phase shifts. The only published attempt of doing so (1) found numerous solutions and predicted oscillatory behaviour in iT_{11} which is not observed at 134 MeV. It remains to be seen if the extensive iT_{11} and $d\sigma/d\Omega$ presented here will help further reduce the number of solutions.

(1)   N. Niroshige, W. Watari, M. Yonezawa, Prog.Theor.Phys. 68(1982)327

+   Physikalisches Institut der Universität Erlangen-Nürnberg
++   Schweizerisches Institut für Nuklearforschung

4.3.3 POSITIVE PION ABSORPTION ON DEUTERIUM AT ENERGIES ABOVE THE 3,3 RESONANCE

E.L. Mathie, G.R. Smith, E. Boschitz, J. Hoftiezer, M. Meyer[+]

The experiment was performed at the πM3 pion channel at the Swiss Institute for Nuclear Research (SIN). A coincidence technique requiring the detection of the incident pion and both outgoing protons was used. The incident pions were detected with a plastic scintillation detector and one of the three elements of a hodoscope detector. A coincidence requirement with the cyclotron rf effectively eliminated the muon and electron contamination in the beam. The forward going (higher energy) proton was was detected by two scintillation detectors (F1 and F2). The F1 detector simply constrained the particle direction. The F2 detector both defined the solid angle, and through the use of two phototubes, constant fraction discriminators, and mean timing, enabled an excellent time of flight measurement for the forward going proton. The backward going proton was detected by two similar detectors (R1 and R2), the latter also arranged to give an optimum timing signal. The time of flight difference was then calculated for the forward and recoil particles in the F2 and R2 detectors respectively. This difference was found to have a 450 psec FWHM, and separation of the πd → 2p (free absorption with the quasifree absorption reaction part of the same peak), πp quasielastic, and πd quasielastic was good. In all cases the measurements were made with a CD_2 target and with a CH_2 target, to enable an explicit background subtraction.

The number of πd,2p events was determined for each case from the histogram of the time of flight difference for the outgoing protons,

Fig. 1: Center of mass system differential cross sections for πd → pp. The error bars shown are typical of all the data and the curves are the empirical fit to the data with a series of even order Legendre polynominals

$$\frac{d\sigma}{d\Omega^*} = \frac{1}{4\pi} \sum_{i=0}^{3} a_{2i} P_{2i} (\cos\Theta^*)$$
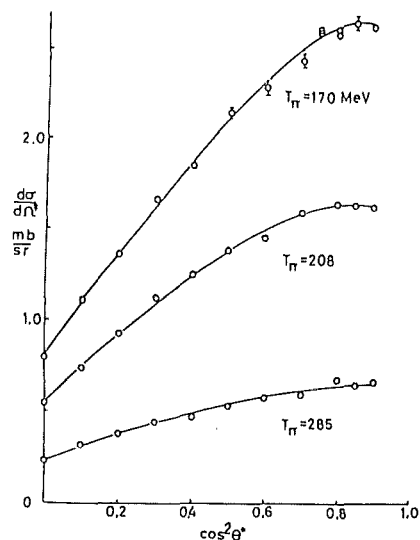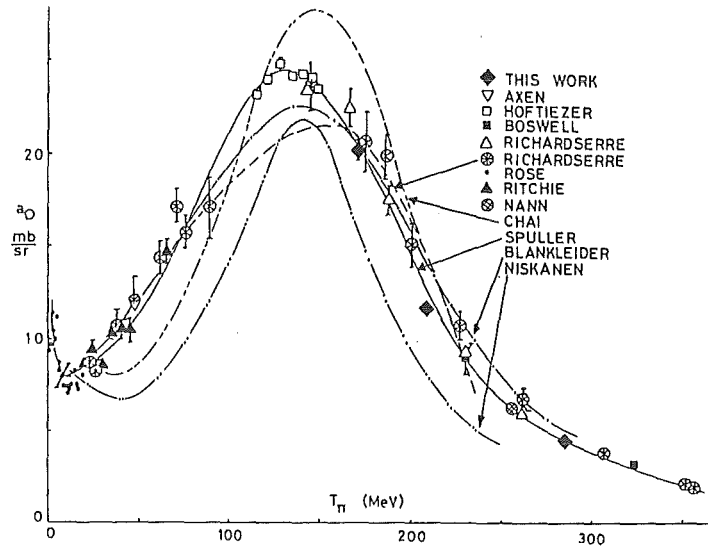
Fig. 2: The a_o fit parameter as a function of incident pion energy with data from other recent experiments; the empirical fits of Spuller and Richard-Serre; and various theoretical calculations. The calculations of Chai and Niskanen clearly do not describe the data. The most successful theory (Bankleider) does not adequately describe the data in the peak region.
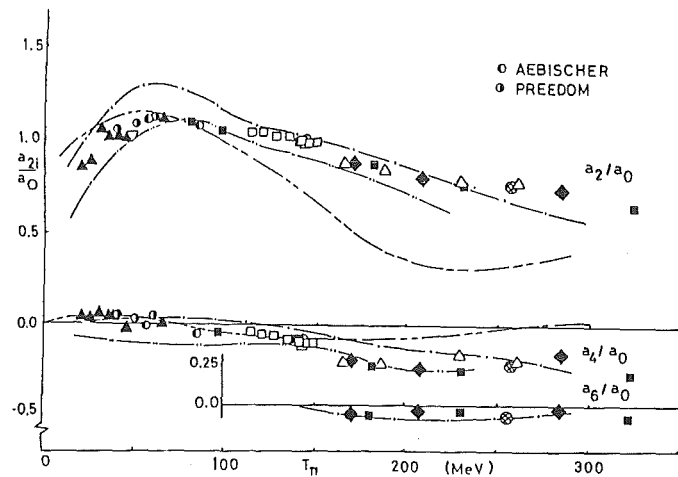
Fig. 3: The ratios a_{2i}/a_o as a function of incident pion energy. The meaning of the curves is the same as in Fig. 5. The failures of the most successful theory (Blankleider) are reflections of the underestimate of a_o in the energy region 80 - 180 MeV.

suitably corrected for quasifree events from the carbon in the CD_2 target (based on the background measurements). Taking into account various corrections due to detector efficiency, Coulomb multiple scattering, pion decay etc. the data presented in Fig. 1 were obtained. In Figs. 2

and 3 the fit parameter a_0 and the ratio a_2/a_0 are shown for our data in comparison to earlier data and theoretical predictions.

+   Physikalisches Institut der Universität Erlangen-Nürnberg

4.3.4 ABSORPTION OF π^+ AND π^- IN ^{3}He AT 120 MeV

S. Cierjacks, S. Ljungfelt, U. Mankin, G. Schmidt, H. Ullrich, G. Backenstoss[+], M. Izycki[+], M. Steinacker[+], P. Weber[+], H.J. Weyer[+], M. Furić[++], T. Petković[++]

Our understanding of pion absorption in nuclei is mainly based on the knowledge of the absorption process in deuterium. Kinematically complete experiments on ^{3}He give access to new observations: 1) Absorption on a T = 1 nucleon pair; 2) The influence of a third nucleon. Experimentally the two points can be well separated. Quasi-free absorption process (QFA) and those with final state interaction (FSI) take place under different kinematical conditions. Also, events where three nucleons share comparable amounts of energy show a special kinematical signature.

A surprisingly large value for the QFA ratio R = $(\pi^- np \to nn)/(\pi^- pp \to np)$ has been discovered for the first time in our previous experiment with stopped π^- (1). The representation of the data in the form of a Dalitz plot has also revealed pronounced FSI effects. Both observations urged a continuation of the measurements with pions in flight.

The measurements have been performed on the $\pi E1$-channel at SIN. Incoming pions with 220 MeV/c momentum have been identified by a conventional counter telescope. A liquid ^{3}He target has been used. Emitted neutrons, protons and deuterons have been detected in a large area (2 m x 0.5 m) position sensitive TOF counters capable of particle identification. Charged particles have also been detected in a large total absorption hodoscope consisting of a 4×3 array of plastic scintillators (17×1×30 cm^3 each) in connection with two MWP chambers for track identification.

The following results have been obtained:

a) As for stopped ions, a strong enhancement of the events appears on the perimeter of the Dalitz plot. Since the measurement did not yet cover the complete kinematically allowed region, the existence of more

events in the middle of the plot cannot strictly be excluded.

b) The number of events in the FSI-region is smaller than in our experiment with stopped pions and also smaller than in the preliminary TRIUMF-data at 65 MeV (2).

c) An important results is the value of $R' = (\pi^+ np \rightarrow pp)/(\pi^- pp \rightarrow np) = 32 \pm 11$. This quantity corresponds completely to R. Its observed value is much higher than 6.5 as expected from isospin considerations alone.

First theoretical calculations for QFA using the isobar model have been published recently by Lee et al. (37, Toki et al. (5), and Silbar et al. (5). All authors give explanations for the T = 0 enhancement over the T = 1 absorption but seem to overestimate the effect, at least at lower energies. A summary of the experimental and theoretical results on R is given in Fig. 1.
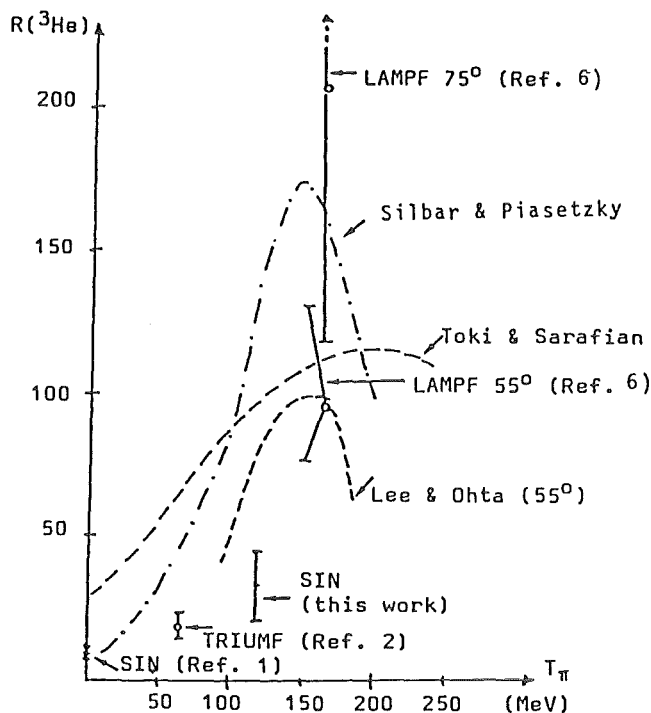
Fig. 1: The dependence of R on pion energy. Experimental points and theoretical curves are shown.

In conclusion we can say that we confirmed the dominant role of QFA in ^{3}He also for pion absorption in flight. The observed isospin dependence, however, is still not well understood.

(1)   D. Gotta, M. Dörr, W. Fetscher, G. Schmidt, H. Ullrich,
        G. Backenstoss, W. Kowald, J. Schwanner, H.J. Weyer, Phys. Lett.
        112B(1982)129

(2)   D. Ashery et al., Symposium on Delta-Nucleus Dynamics, Argonne,
        Illinois, 1983

(3)   T.-S.H. Lee and K. Ohta, Phys. Rev. Lett. 49(1982)1079

(4)   H. Toki and H. Sarafian, Phys. Lett. 119B(1982)285

(5)   R. Silbar and E. Pisaetzky, LAMPF Preprint (1983)

(6)   D. Ashery, R.J. Holt, J.R. Specht, K.E. Stephenson, R.E. Segel,
        P. Zupranski, Phys.Rev. Lett. 47(1981)895

+   Institut für Physik, Universität Basel
++   Faculty of Sciences, University of Zagreb

4.3.5   MEASUREMENT OF THE ^{12}C($\pi,\pi'\gamma$) ^{12}C(2^+, T=0; 4.44 MeV)
        ANGULAR CORRELATIONS: A TEST OF THE ISOBAR-HOLE MODEL

F. Vogler[+], R. Olszweski[+], M. Meyer[+], E.L. Mathie, G.R. Smith,
E. Boschitz, S. Chakravarti[++], D. Dehnhard[++], M. Thies[+++].

It has been shown that the effects of the nuclear medium on pion-
nucleon interactions in nuclei cannot be neglected in the analysis of
elastic and inelastic pion scattering from nuclei. At pion energies near
the (3,3)-resonance the pion-nucleus interaction is dominated by the for-
mation, propagation, and decay of intermediate Δ-hole states.

Recently, it was pointed out that the double-differential cross
sections for (π,π'p) quasi-elastic scattering from ^{16}O (to ^{15}N states in
the continuum) are fitted much better with the Δ-hole model than in the
standard closure approximation to the first order theory (static-model).
Here, we report on the first measurement, and the analysis of ($\pi,\pi'\gamma$)
angular correlation functions for the transition to a discrete state in
^{12}C(2^+, 4.44 MeV). The double-differential cross section $d^2\sigma/d\Omega_\pi d\Omega_\gamma$ for
($\pi,\pi'\gamma$) contains information on the magnetic substate populations (which
cannot be obtained from (π,π')) and is therefore expected for provide more
detailed information about the reaction mechanism than a single differential
cross-section.

The experimental results are shown in Fig. 1. The errors in
$d^2\sigma/d\Omega_\pi d\Omega_\gamma$ ($\sim \pm$ 27% were derived from the uncertainties in background
subtraction, dead time losses, γ-detector efficiency and statistics. The
horizontal "error bars" simply indicate the angular width of the γ-detector
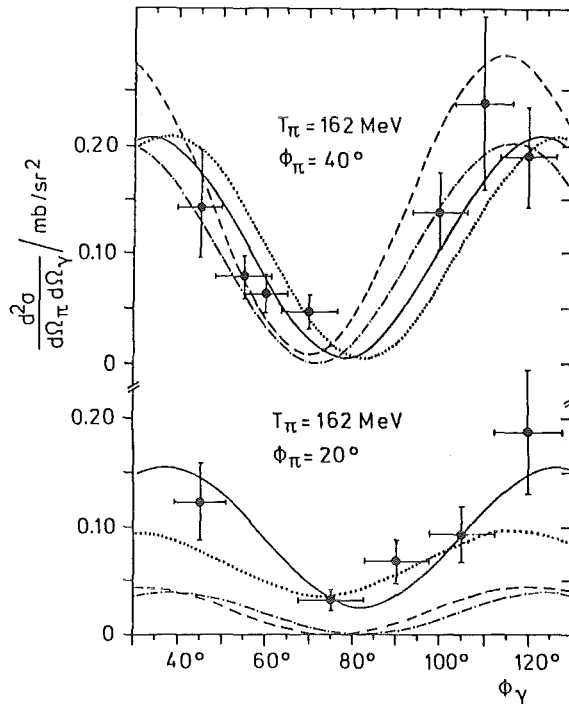
Fig. 1: Double differential cross sections at $\phi_\pi = 40^\circ$ (upper part) and $\phi_\pi = 20^\circ$ (lower part) for the $^{12}C(\pi^+,\pi^{+'}\gamma_{4.44})$ reaction at $T_\pi = 162$ MeV. Data points: this experiment. Solid lines: full Δ-hole model predictions (including L·S term) ; dotted lines: Δ-hole model predictions without ⁻   ⁻ ᵈᵃshed-dotted lines: static model 1; dashed lines: sta

($\Delta\phi_\gamma = \pm 5^\circ$) as determined by its aperture. The finite opening of the pion detector ($\Delta\phi_\pi \simeq \pm 5^\circ$) also resulted in an averaging of the double differential cross section over a range of ϕ_π. The theoretical results at $\phi_\pi = 20^\circ$ needed to be averaged over this range of angles since $d^2\sigma/d\Omega_\pi d\Omega\gamma$ changes very rapidly as a function of ϕ_π near 20°. At 40° $d^2\sigma/d\Omega_\pi d\Omega_\gamma$ is nearly constant across the size of the pion detector so that non-averaged and averaged predictions are almost the same.

Angular correlation functions were calculated with the Δ-hole code of Lenz et al.. The results from these calculations are shown in Fig. 1. We have also done calculations with the code ARPIN of T.-S.H. Lee (dashed lines, labelled static model (2) in which a different transition density was used.

As one can see from Fig. 1 the angular correlation at $\Theta_\pi = 20^\circ$ is more sensitive to the different theoretical predictions than at 40°. The data at $\Theta_\pi = 20^\circ$ clearly favour the predictions from the Δ-nucleus dynamics. More accurate data can certainly be obtained detecting the pions in the SUSI spectrometer (which has not been done in this first preliminary experiment). They will allow a more definite statement about the need of

a L·S term in the Δ-hole-model.

+   Physikalisches Institut der Universität Erlangen-Nürnberg
++   Physics Department, University of Minnesota, Minneapolis, USA
+++   Schweizerisches Institut für Nuklearforschung

4.4   NUCLEON-NUCLEON INTERACTION

4.4.1   THE DIFFERENTIAL CROSS SECTION OF THE REACTION pp→πd FOR PROTON ENERGIES BETWEEN 500 AND 600 MeV

J. Hoftiezer, Ch. Weddigen, P. Chatelain[+], B. Favier[+], F. Foroughi[+],
C. Nussbaum[+], J. Piffaretti[+], S. Jaccard[++], P. Walden[++,+++],

Nucl. Phys. A402(1983)429

The reaction pp → π^+d is of basic interest from several points of view. Its understanding is essential for the interpretation of pion interactions with nuclear matter as regards absorption and production. As to two particle reaction it is amenable to the investigation of detailed balance, time reversal and isospin symmetry by comparing with results from the inverse reaction and with np → π^0d, respectively. Inelastic channels in pp scattering, such as the pp→πd reaction may have considerable feedback to the elastic channel, in which peaked structures in spin correlated cross sections gave rise to speculations on the possible existence of dibaryon resonances. These 'resonances' are highly inelastic. Therefore - if real - they should show up as resonance structures in the production amplitudes describing in pp → πd reaction, in addition to the well-known NΔ resonant like production mechanism near 600 MeV.

An amplitude analysis calls for precise data. Therefore we measured the differential cross section $\sigma(\theta)$ of the pp→πd reaction for seven energies between 516 and 582 MeV with an overall absolute precision better than two percent. Pions and deuterons were detected in coincidence with scintillation detectors, using time-of-flight techniques for event identification. Special techniques for absolute energy calibration, normalization and measurement of relative distributions were used. Detailed corrections have been applied to the data for multiple scattering, pion decay, detection of decay muons, and for finite solid angle acceptance. The data have been fit with Legendre polynomials to obtain the expansion coefficients a_{2i}^{oo}. In Fig. 1 our results (solid symbols) are compared with those obtained by Boswell et al. (1) for the inverse reaction and with theoretical predictions. Blankleider et al. (2) reproduce a_0^{oo} and a_2^{oo} reasonably well, whereas for a_4^{oo} Niskanen (3) obtained better results.

Our corrected results show only small differences from preliminary data reported earlier (4). The effect of the applied corrections is that we can now
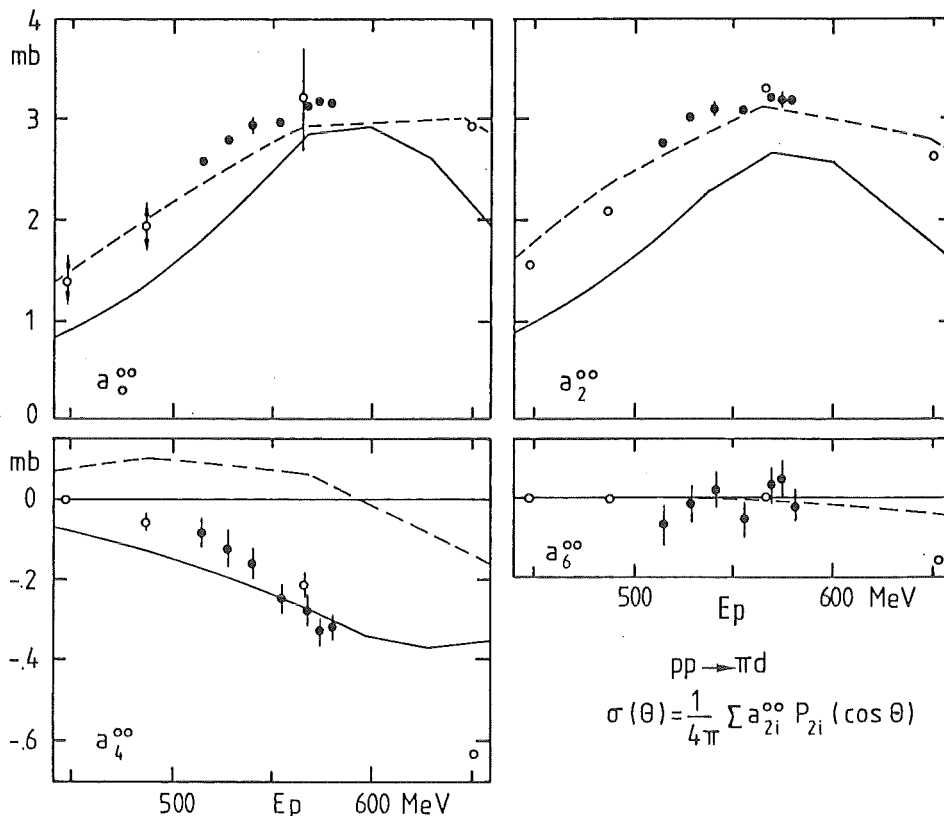
Fig. 1:Comparison of our results (full symbols) for Legendre polynomial
expansion coefficients with recent data from the reverse reaction
(Ref. 1, open symbols) and with theoretical predictions of Niskanen
(3) (solid lines) and Blankleider (2) (broken lines). For data with
arrows no uncertainties are given in Ref. 1.

exclude an a_6^{oo} contribution within the quoted precision of $\pm$ 50 μ b in the
energy range between E_p = 516 and 582 MeV. Thus the conclusions in Ref. 4
remain valid.

(1)   J. Boswell, R. Altemus, R. Minehart, L. Orphanos, H. J. Ziock, and
        E. A. Waldinger, Phys. Rev. C25(1982)2540
(2)   B. Blankleider and I. R. Afnan, Phys. Rev. C24(1981)1572 and
        B. Blankleider, private communication (1982)
(3)   J. A. Niskanen, Phys. Lett. 79B(1978)190
(4)   J. Hoftiezer, Ch. Weddigen, B. Favier, S. Jaccard, P. Walden,
        P. Chatelain, F. Foroughi, C. Nussbaum, and J. Piffaretti:
        Phys. Lett. 100B(1981)462

+   Institut de Physique, Université de Neuchâtel, Neuchâtel
++   Schweizerisches Institut für Nuklearforschung (SIN), Villigen
+++   On leave from TRIUMF, Vancouver

4.4.2 THE ANALYSING POWER A_{yo} OF THE REACTION pp → πd FOR PROTON ENERGIES BETWEEN 500 AND 600 MeV

J. Hoftiezer, Ch. Weddigen, P. Chatelain[+], B. Favier[+], F. Foroughi[+], J. Piffaretti[+], S. Jaccard[++], P. Walden[++,+++] (1)

The interpretation of inelastic pp-scattering at medium energies is still an unresolved problem. From a theoretical point of view a unified treatment taking the most important elastic and inelastic channels into account and including two and three particle unitarity promised to clarify the situation. However, for the channel pp → πd significant differences remain between theory and primary observables. This is a stimulating situation for experimentalists. By providing precise data on polarization observables and on the differential cross section it should be possible to determine the most important production amplitudes in a direct manner. Accordingly, our group (NESIKA) first performed precision measurements (2) on the differential cross section σ(θ) for the pp → πd reaction. Here, we report on our second series of experiments namely the measurement of the analyzing power A_{yo} for pion production via pp → πd in the same energy range. The availability of precise data on σ(θ) at identical energies is a unique advantage for the interpretation of our A_{yo} results.

The experiment was performed at the PM1 beam line of SIN. The apparatus and the data handling system were similar to those used for our σ(θ) measurements and are described in more detail in Ref. (2). Our results for A_{yo} are plotted in Fig. 1 as a function of the CM pion production angle θ. The indicated errors of A_{yo} rarely exceed one per cent.

The product

$$\sigma(\Theta)A_{yo} = \frac{1}{4\pi} \sum_{j} b_j^{yo} P_j^1(\cos\Theta) \qquad (1)$$

can be expanded using associate Legendre polynomials P_j^1. The expansion coefficients b_j^{yo} can be expressed as bilinear forms of production amplitudes (3). The curves shown in Fig. 1 are five-parameter fits to our results.

The expansion coefficients b_j^{yo} are plotted as a function of the proton energy in Fig. 2 and compared to theoretical predictions. These are the very first (4) based on a coupled channel formalism for the NΔ intermediate state and recent results (5) of a "unified" model calculation. This treats the elastic channels (pp and πd) together with the transition channel (pp↔πd) taking two- and three-particle unitarities into account. It can be seen that

Fig. 1: Results for the analysing power A_{yo} as a function of the CM pion production angle θ. The curves are Legendre polynomial fits according to Eq.(1).
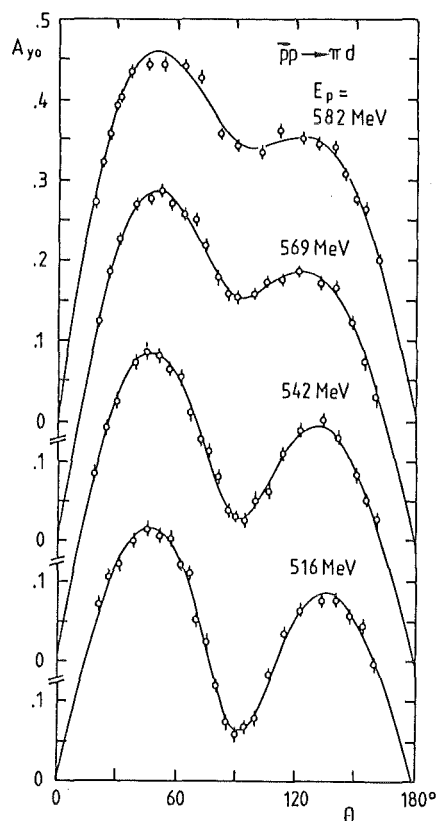
Fig. 2: Comparison of our results for Legendre polynomial expansion coefficients b_i^{yo} (Eq. (1)) with theoretical predictions of Niskanen (4) (———, Ni) and of Blankleider (5) (— —,Bi). Quantities concerning b_5^{yo} are magnified by 10.
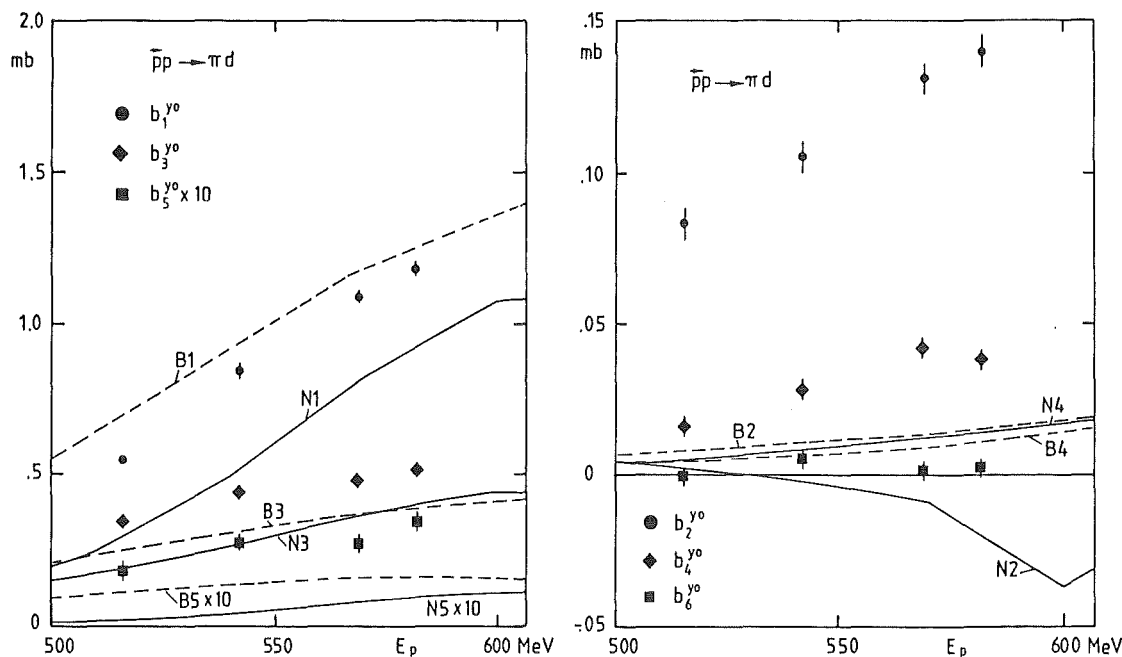
the large coefficients (j odd) describing interferences between initial-state triplet and the dominant singlet amplitudes are reasonably well reproduced, whereas the triplet-triplet interferences (j even) show discrepancies in sign and magnitude.

(1)   dto., Nucl. Phys. in press (June 1983)
(2)   J. Hoftiezer, Ch. Weddigen, P. Chatelain, B. Favier, F. Foroughi, C. Nussbaum, J. Piffaretti, S. Jaccard, and P. Walden, Nucl. Phys. A402(1983)429

(3)   see e.g. Ch. Weddigen, Nucl. Phys. A312(1978)330
(4)   J. A. Niskanen, Phys. Lett. 79B(1978)190
(5)   B. Blankleider, private communication (1982)

+   Institut de Physique, Université de Neuchâtel, Neuchâtel
++   Schweizerisches Institut für Nuklearforschung (SIN), Villigen
+++   On leave from TRIUMF, Vancouver.

4.4.3   THE SPIN CORRELATION COEFFICIENT A_{xz} OF THE REACTION pp $\rightarrow$ πd FOR PROTON
        ENERGIES BETWEEN 500 AND 600 MeV

J. Hoftiezer, G.S. Mutchler[+++], Ch. Weddigen, J.A. Konter[+], S. Mango[+],
A. Berdoz[++], B. Favier[++], F. Foroughi[++](1)

In the framework of the NESIKA collaboration a series of experiments
were performed at SIN on the reaction pp $\rightarrow$ πd at proton energies between 500
and 600 MeV to provide precise data for a possible partial wave analysis of
this reaction in the energy range from 500 to 600 MeV. In the first experiment
(2) the differential cross-section $\sigma(\theta)$ was measured at seven energies. The
result was that a three-term Legendre polynomial expansion was sufficient to
describe $\sigma(\theta)$ in our energy range. In the second experiment (3) the analysing
power $A_{yo}(\theta)$ was measured at four energies. An associate Legendre polynomial
fit to the product $\sigma(\theta)A_{yo}$ yielded significant expansion coefficients b_ℓ^{yo} up
to the fifth order.

Here, we describe an experiment on the spin correlation coefficient
$A_{xz}(\theta)$ which was performed at 516, 542, and 582 MeV. A_{xz} is complementary to
A_{yo} in the sense that the complex quantity

$$\sigma(\theta)(A_{xz}+iA_{yo}) = \frac{1}{4\pi} \sum_k \underset{\sim}{b}_k P_k^1(\cos\theta) \tag{1}$$

can be expanded using associate Legendre polynomials P_k^1, where the complex
expansion coefficients $\underset{\sim}{b}_k = b_k^{xz}+ib_k^{yo}$ can be expressed as bilinear forms of
reaction amplitudes. A kinematical limit is given by

$$A_{xz}^2 + A_{yo}^2 \leq 1.$$

Our measurements were performed at the PM1 beam of SIN. Since the
available beam time with the polarized target was short, all of our A_{xz} re-
sults had to be obtained within a total of twelve days of target operation.

Fig. 1 shows the experimental set-up. The polarized target is viewed
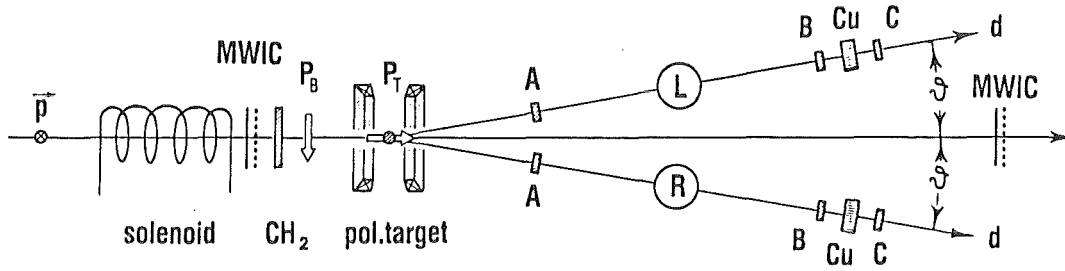
Fig. 1:Experimental set-up for the measurement of the spin correlation coeffi-
cient A_{xz} of the pp $\rightarrow$ πd reaction (not to scale). The target polariza-
tion P_T is inverted by changing the HF-frequency, while the beam pola-
rization P_B remained constant. A, B, and C are scintillation detectors.
The CH_2 target upstream of the target is viewed by two scintillation
telescopes (not shown) and serves for the relative normalization of
different runs. MWIC = multiwire proportional ionization chamber.

by two time-of-flight telescopes, the detectors B and A producing start and
stop signals, respectively. The copper Cu absorbers isotachic protons which
do not reach the coincident detectors C. The CM production angel θ of the un-
detected pions is deduced from the lab. angle δ and at the Jacobian cusp
(δ_{max} = 12°) from the deuteron TOF and the energy deposite in the C detectors.
A specially designed dummy target with equivalent amounts of carbon and ^{3}He
was used to measure background deuterons.

Fig. 2:Angular distributions of the spin
correlation coefficient A_{xz} with
a five-parameter fit according to
Eq.(1). The scales for the 582
and 516 MeV data are given on the
left, while the scale for the
542 MeV data is given on the right.
Broken curves are taken from recent
predictions of partial wave analy-
ses (4) with a dominant D (dash-
dotted) and dominant S (dashed)
production partial wave at 500, 550,
and 600 MeV, respectively. The pa-
rity-forbidden coefficient A_{yz} at
582 MeV and 97° was measured as a
trial. θ = pion CM production angle.
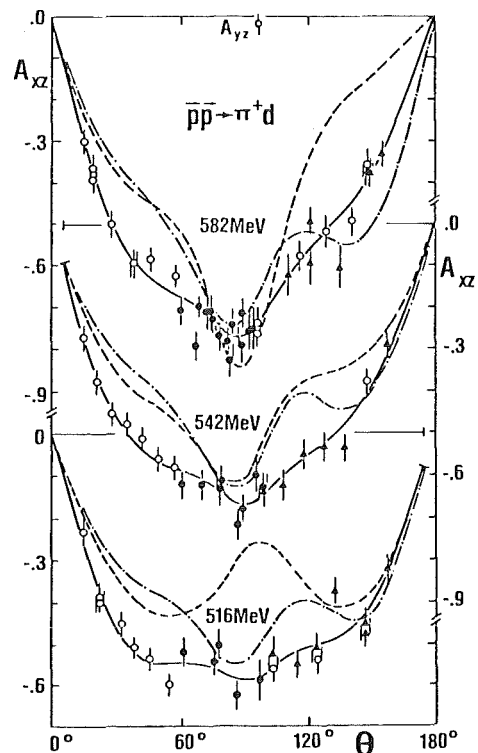
In Fig. 2 our results are compared with predictions of a recent phase-shift analysis (4). Our data do not definitively favour the S- or the D- dominant solution. However, it can be expected that our results will help eliminate ambiguities in such analyses, which are a powerful tool to search for possible hidden anomalies of inelastic pp-scattering at medium energies.

(1)   dto., submitted to Nucl. Phys. (April 1983)
(2)   J. Hoftiezer, Ch. Weddigen, P. Chatelain, B. Favier, F. Foroughi,
        C. Nussbaum, J. Piffaretti, S. Jacard, and P. Walden,
        Nucl. Phys. A402(1983)429
(3)   J. Hoftiezer, Ch. Weddigen, P. Chatelain, B. Favier, B. Foroughi,
        J. Piffaretti, S. Jaccard, and P. Walden, Nucl.Phys. in press
        (June 1983)
(4)   N. Hiroshige, W. Watari, and M. Yonezawa, Prog. Theor. Phys.
        68(1982)2074, and W. Watari, Progress Report of Partial Wave Ana-
        lysis, University of Osaka (February 1983)

+   Schweizerisches Institut für Nuklearforschung (SIN), Villigen
++   Institut de Physique, Université de Neuchâtel, Neuchâtel
+++   On sabbatical leave from Rice University, Houston TX.

4.4.4   PRECISION MEASUREMENT OF THE ANALYZING POWER A_{yo} FOR PROTON - PROTON
        ELASTIC SCATTERING AT 582 MeV

A. Berdoz[+], B. Favier[+], F. Foroughi[+], Ch Weddigen

The analyzing power is a frequently used input observable for N-N phase shift analysis (PSA) the results of which serve for different purposes such as comparison with results of interaction models, calculation of final-state interactions, or search for anomalies in the energy dependence of special partial waves ('dibaryons'). Existing data (1) near 580 MeV had a mean precision of only 1.9% and discrete differences up to 6.4% between PSA predictions and experiment occurred.

After the measurement of the absolute differential cross section (2) at a CM angel $\Theta = 90°$ and of relative angular distributions (3) for the p-p elastic scattering we measured the analyzing power A_{yo} at 582 ± 1 MeV under 13 angels between $\Theta = 20$ and $80°$. The experiment was performed in June '83 at the PM1 beam line of SIN. The experimental technique was essentially the same as for the A_{yo} measurement (4) for inelastic pp scattering.

Fig. 1 shows preliminary experimental results for A_{yo} together with a PSA prediction for 578 MeV taken from Ref. 1. The mean statistical error

Fig.1: Preliminary results for the analyzing power A_{yo} of elastic p-p scattering as a function of CM scattering angel Θ. The statistical errors ($\simeq$ .24%) are smaller than the dots. The PSA prediction for 578 MeV is taken from Ref.1.
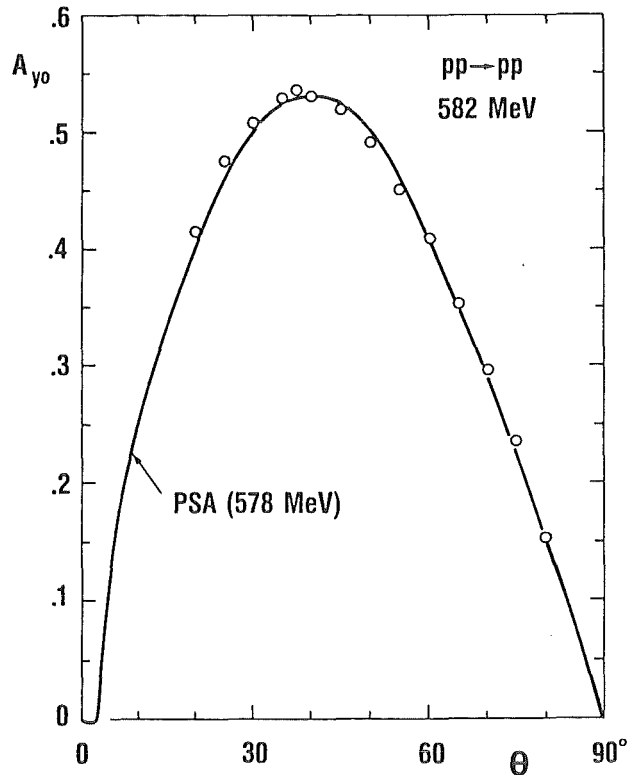
(.24%) is smaller than the experimental points. The angular distribution of A_{yo} is found to be smooth without discrete deviations from the PSA prediction.

(1)   D. Besset, Q.H. Do, B. Favier, R. Hausermann, E. Heer, R. Hess, C. Lechanoine-Leluc, W.R. Leo, D. Rapin, D.W. Werren, Ch. Weddigen, J.M. Cameron, S. Jaccard, and S. Mango, Nucl. Phys. A345(1980)435
(2)   P. Chatelain, B. Favier, F. Foroughi, J. Hoftiezer, S. Jaccard, J. Piffaretti, P. Walden, and Ch. Weddigen, J. Phys. G8(1982)643
(3)   A. Berdoz, B. Favier, F. Foroughi, J. Hoftiezer, G.S. Mutchler, and Ch. Weddigen, J. Phys. G8(1982)1363
(4)   J. Hoftiezer, Ch. Weddigen, P. Chatelain, B. Favier, F. Foroughi, J. Piffaretti, S. Jaccard, and P. Walden, SIN Preprint PR-82-18 and Nucl. Phys. in press

+   Institut de Physique, Université de Neuchâtel, CH-2000 Neuchâtel

4.5   NUCLEON-NUCLEUS AND -ANTINUCLEON INTERACTIONS

4.5.1   NEUTRON AND CHARGED-PARTICLE PRODUCTION CROSS SECTIONS
        FOR 590 MeV PROTONS ON THIN METAL TARGETS WITH $12 \leq A \leq 238$

S. Cierjacks, Y. Hino, F. Raupp, L. Buth[+]

Differential production cross sections for neutrons and charged particles from 590 MeV proton bombardment of various thin metal targets have been measured at the SIN cyclotron. Analyses of the experimental results have presently provided absolute neutron production cross sections for C, Al, Fe, Nb, In, Ta, Pb and U at laboratory angles of 23°, 30°, 90° and 150°. The analysis of the charged particle data (which is in a final stage and whose completion is expected by the end of 1983) will provide, in addition, differential production cross sections for secondary protons, deuterons, tritons and pions ($\pi^+ + \pi^-$) for the same target materials and laboratory angles of 23°, 45°, 90°, 135° and 157°. The systematic investigations of this type were primarily performed for testing the accuracy of cross sections predicted by modern intranuclear cascade-evaporation models and used in several high-energy nucleon-meson transport codes, e.g. the HETC Monte Carlo Code (1). While measured integral neutron yields from thick heavy metal targets are presently well described by these models, similar comparisions of differential yields and production cross sections have revealed significant discrepancies, particularly in cascade energy region.

Differential cross section measurements were performed by the time-of-flight technique employing the microstructure pulses from the SIN cyclotron (~ 200 ps pulse width at a pulse repetition frequency of 16.84 MHz). The principal detector was an NE 213 liquid scintillator used for its pulse shape discrimination (PSD) properties. Particle identification in terms of neutrons and charged particles was accomplished by a thin plastic scintillator placed in fromt of the main detector. While neutron events were accumulated by operating both detectors in anti-coindence, charged-particle data were collected in coincidence measurements.

A typical result obtained from these experiments is shown in Fig. 1. This figure displays the differential neutron production cross sections

for various elemental target materials at a laboratory angle of 30°. All invidual curves exhibit the well-known two-component shape resulting from evaporation reactions ($E_n \lesssim 15$ MeV) and cascade processes ($E_n \gtrsim 15$ MeV), respectively.

Fig. 1: Measured differential cross sections for neutrons from 590 MeV proton bombardment of various thin metal targets
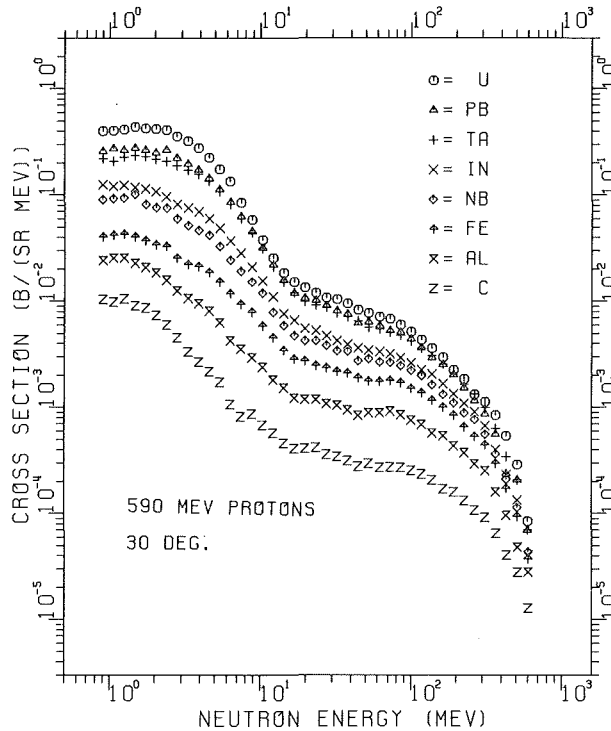
Fig. 2: Comparison of measured and calculated cross sections for tantalum. It can be seen that HETC-calculations provide reasonable predictions in the evaporation range ($E_n \lesssim 15$ MeV), but underpredict the data increasingly with energy in the cascade region ($E_n \gtrsim 15$ MeV).
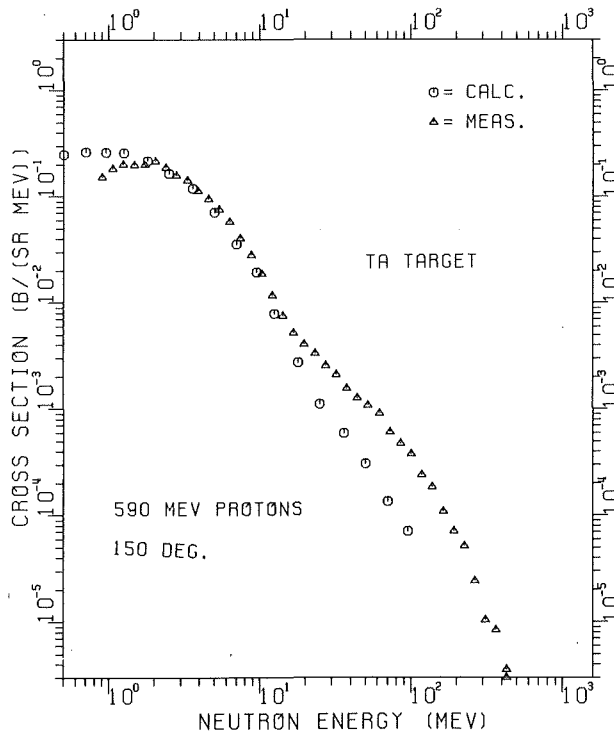
The experimentally determined cross sections are presently being used for extensive tests of model predictions provided by the High Energy

Nuclon-Meson Transport Code (HETC). The available data revealed that the neutron production cross sections in the evaporation region can sufficiently be predicted by this code. In the cascade region, however, large discrepancies continue to persist. A recent comparison of measured and calculated production cross sections is shown in Fig. 2. The results given for neutron production in tantalum illustrate the large existing discrepancies in the cascade region. At $E_n \simeq 100$ MeV the calculated data are almost by an order of magnitude smaller than the measured ones.

(1)   HETC, ORNL-4744, Oak Ridge Nat. Laboratory, 1972

+   Permanent member of the Institut für Neutronenphysik und
        Reaktortechnik, Kernforschungszentrum Karlsruhe

4.5.2   PROTON - ANTIPROTON ANNIHILATION AT REST INTO $\pi^0\omega$, $\pi^0\eta$, $\pi^0\gamma$, $\pi^0\pi^0$, AND $\pi^0\eta'$

G. Backenstoss[+], M. Hasinoff[+], P. Pavlopoulos[+], J. Repond[+],

L. Tauscher[+], D. Tröster[+], P. Blüm, R. Guigas, H. Koch, M. Meyer,

H. Poth, U. Raich, B. Richter, L. Adiels[++], I. Bergström[++],

K. Fransson[++], A. Kerek[++], M. Suffert[+++], K. Zioutas[++++], (1)

In an experiment on the inclusive γ-spectrum after $\bar{p}p$-annihilation at rest, we were able to extract branching ratios for so far unobserved neutral twobody annihilation channels like $\pi^0\omega$, $\pi^0\eta$, and the channel $\pi^0\gamma$. A new value for the $\pi^0\pi^0$ and an upper limit for the $\pi^0\eta'$ channel were deduced.

Owing to the fact that in a twobody reaction the particles are mono-energetic, the spectrum of the photons from the electromagnetic decay of a meson exhibits an uniform shape between the limits

$$E_{max/min} = \frac{1}{2} E \ (1 \pm \beta), \tag{1}$$

where E is the total energy of the decaying particle and β is its velocity. The edges of these distributions are sharp if the particles involved have narrow widths, and thus show up in the inclusive γ-spectrum from $\bar{p}p$-annihilation at rest. The lower the background and the better the resolution, the higher are the chances of observing these edges. Thus at the high-energy end of the spectrum such edges could be observed. In order to analyse these con-
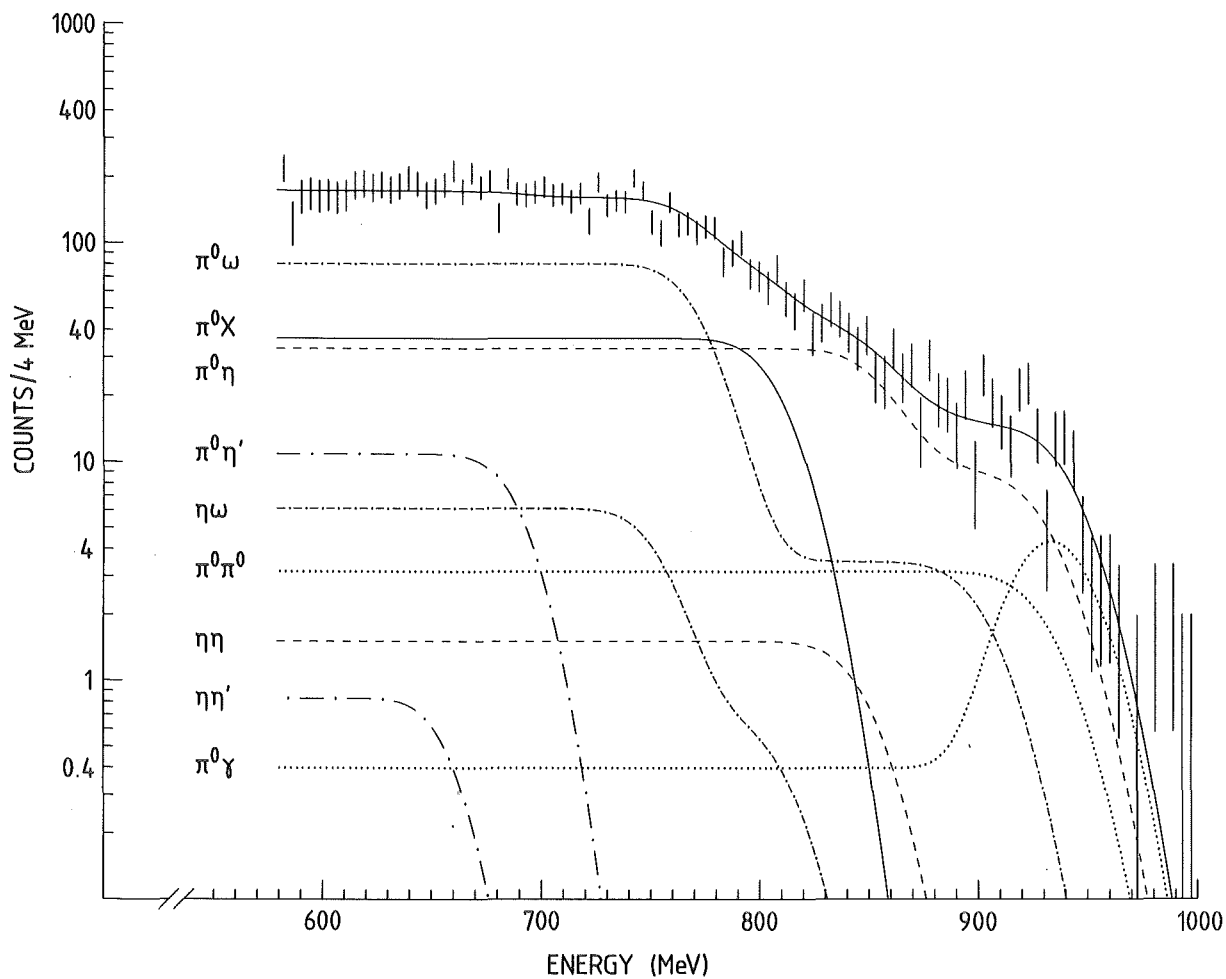
Fig.1: Experimental spectrum after subtraction of the continuous background. The solid line shows the final fit. The contributing distributions are indicated.

Table 1:Branching ratios of twobody annihilation channels in $\bar{p}p$-annihilation at rest

Channel	Yield	Error (stat.)	Error (syst.)
$\pi^0\eta'$	0.30	± 0.53	$+0.58$
			-0.30
$\pi^0\omega$	2.38	± 0.27	$+0.32$
			-0.52
$\pi^0\eta$	0.82	± 0.07	± 0.06
$\pi^0 X$	1.19	± 0.25	± 0.44
$\pi^0\gamma$	0.015	± 0.004	± 0.003
$\pi^0\pi^0$	0.06	± 0.03	± 0.01

tributions we subtracted a proper continuous background, which comes from annihilations into more than two particles. We defined a shape function by means of a Monte Carlo simulation (2) and subtracted the background after appropriate normalization. Fig. 1 shows the resulting experimental spectrum, which was analysed. The single distributions used to describe the spectrum and the final fit are shown as well. The results for the branching ratios are summarized in Table 1.

(1)   dto., submitted to Nuclear Physics B
(2)   Th. Köhler Diplomarbeit, Universität Karlsruhe (1980),unpublished

+   Institut for Physics, University of Basle, Switzerland
++   Research Institute for Physics, Stockholm, Sweden
+++   Centre de recherches nucléaires, Strasbourg, France
++++   Department of Nuclear Physics, University of Thessaloniki, Greece

5.   HIGH ENERGY PHYSICS

CELLO Collaboration

O. Achterberg, G. D'Agostini, W.-D. Apel, J. Engler, G. Flügge,
B. Forstbauer, D.C. Fries, W. Fues, K. Gamerdinger, Th. Henkes,
G. Hopp, J. Knapp, M. Krüger, H. Küster, M. Makowsky, H. Müller,
H. Randoll, K.H. Ranitzsch, G. Schmidt, H. Schneider
KfK and Universität Karlsruhe

H.-J. Behrend, H. Fenner, M.-J. Schachter, V. Schröder, H. Sindt
Deutsches Elektronen-Synchrotron, DESY, Hamburg

W. de Boer, G. Buschhorn, G. Grindhammer, P. Grosse-Wiesmann,
B. Gunderson, C. Kiesling, R. Kotthaus, U. Kruse, H. Lierl,
D. Lüers, H. Oberlack, P. Schacht
Max-Planck-Institut für Physik und Astrophysik, München

G. Bonneau, P. Colas, A. Cordier, M. Davier, D. Fournier,
J.F. Grivaz, H. Haissinski, V. Journé, F. Laplanche, F. Le Diberder,
U. Mallik, E. Ros, J.-J. Veillet
Laboratoire de L'Accélérateur Linéaire, Orsay, France

J.H. Field, R. George, M. Goldberg, B. Grossetête, O. Hamon,
F. Kapusta, F. Kovacs, G. London, R. Pain, L. Poggioli, M. Rivoal
Laboratoire de la Physique Nucléaire et Hautes Energies,
Université de Paris, France

R. Aleksan, J. Bouchez, G. Carnesecchi, G. Cozzika, Y. Ducros,
A. Gaidot, P. Jarry, Y. Lavagne, J. Pamela, J.P. Pansart, F. Pierre
Centre d'Etudes Nucléaires, Saclay, France

The main research activity of the High Energy Physics group of the
IK I has been the exploitation of the large spectrometer facility CELLO at
PETRA. Since June 1982 G. Flügge is spokesman of the CELLO collaboration.
The CELLO detector was built by a collaboration of the three German and
three french institutions listed above. Following a major upgrading in 1982
the detector was moved back into the beam in August 1982. After a running
in phase, during which various difficulties caused by the new components
and the increased background had to be solved, the detector is successfully
taking data since the beginning of 1983.

In autumn 1982 five groups of the former PLUTO collaboration, the
DESY groups F14 and F33 and the Universities of Glasgow, Hamburg, and Tel
Aviv joined the CELLO collaboration. Together with these groups a major up-

grading of the CELLO detector was proposed and accepted by the PRC and Directorate of DESY. In particular, a new inner detector is under construction.

The main activities of the Karlsruhe group were to

a)   improve and maintain the LAr electronics and cryogenics and participate to the planing for the new central detector

b)   process and analyse the CELLO data using the KfK computer. Physics analysis concentrated on hadronic final states and test of QCD (in particular total cross sections, event shape, inclusive electrons and electroweak interference effects in τ pair production.

5.1   HARDWARE ACTIVITIES

5.1.1   CELLO OPERATION

Experience with the upgraded detector was obtained in a first run in 1982. A high background showed up in the experiment consisting, mainly of synchrotron radiation due to the high beam energies. Many attempts were undertaken to cope with this background. Among others, a new beam pipe was built and additional triggers were installed using the information from the LAr calorimeters. These triggers are not sensitive to the synchrotron radiation as the track triggers from the inner chambers are. On the other hand, the calorimeter trigger suffers from pick-up noise in the sensitive amplifier system (10^4 channels). Special efforts was undertaken to reduce all sort of noise. As a result, a trigger reacting on a single photon in only one modul of the calorimeter could be installed which has a threshold of approximately 2.5 GeV.

During the running period 1983 the calorimeter, CELLO's trigger- and cryogenic system operated without any problems. For the future perspectives of the CELLO detector, the group participates in the design and construction of a new inner detector (1), the "Stereo Wire Chamber". The institute contributes to the mechanical and electronic construction.

(1)   DESY-CELLO-83-01, Proposal to Upgrade the CELLO Detector.

5.1.2   DEVELOPMENT IN THE INSTITUTE

For the calorimeter a new trigger system has been built using flash

ADC's and RAM's. With this unit a fast decision is taken already on the trigger level. Using the shower propagation within the calorimeter, the trigger discriminates between pattern of real shower and background like cosmic ray shower or pick-up signals.

For future applications we investigate the possibility to use the scintillation light in liquid argon, mainly for fast trigger proposes. The emitted light is in the far ultraviolett region at 125 nm, which makes it difficult to guide the light in large detector systems. Among others, it could be demonstrated that the light can be shifted to 175 nm by a small amount of Xenon (see Fig. 1). This shift circumvents the problem, since in this wavelength region aluminium is a reasonably good mirror.

In another line of development we try to replace the cryogenic liquid argon in the ionisation chamber by a medium which is liquid at room temperature. Good results with tetramethylsilane (TMS) could be obtained in a small test chamber representing a typical submodul (tower) of a calorimeter. The pulse height corresponds to 30% of that in liquid argon.
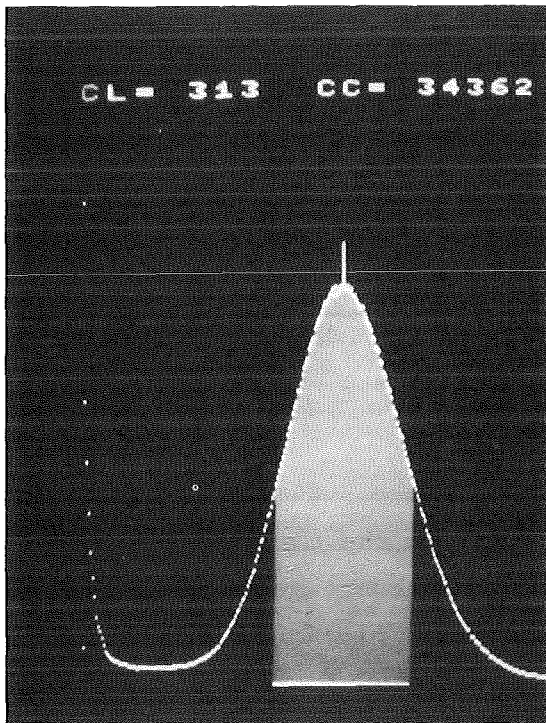
Fig. 1:
Scintillation Light from Liquid Argon excited by Am^{241} α's shifted with 460 ppm added Xenon to 1750 Å and reflected at the inner side of an aluminium tube.

5.2 TEST OF QCD AND HADRONIC FINAL STATES

5.2.1 THE INFLUENCE OF FRAGMENTATION MODELS ON THE DETERMINATION OF THE STRONG COUPLING CONSTANT IN e^+e^- ANNIHILATION INTO HADRONS *

Hadronic events obtained with the CELLO detector at PETRA were compared with first order QCD predictions using two different models for the fragmentation of quarks and gluons, the Hoyer model and the Lund model. Both models are in reasonable agreement with the data, although they do not completely reproduce the details of many distributions. Several methods have been applied to determine the strong coupling constant α_s. Although within one model the value α_s varies by 20% among the different methods, the values determined using the Lund model are larger by 30% or more (depending on the method used) than the values determined with the Hoyer model. Our results using the Hoyer model are in agreement with previous results based on this approach.

TABLE 1   Values of α_s obtained at $\sqrt{s}$ = 34 GeV with the Lund Model (LM) and the Hoyer Model (HM). (First order in QCD).
The error in the determination of α_s is statistical only (including statistical Monte Carlo error).

METHOD	LUND MODEL	HOYER MODEL	$\dfrac{\alpha_s(LM)}{\alpha_s(HM)}$
S $\geq$ 0.25 A $\leq$ 0.1	0.280 ± 0.045	0.190 ± 0.030	1.47
O $\geq$ 0.20	0.260 ± 0.040	0.190 ± 0.020	1.37
O $\geq$ 0.30	0.255 ± 0.050	0.200 ± 0.035	1.28
# of 3 clusters	0.235 ± 0.025	0.145 ± 0.020	1.62
Cluster Thrust	0.235 ± 0.025	0.155 ± 0.015	1.52
E.W.A.C *	0.250 ± 0.040	0.150 ± 0.020	1.67

* Energy Weighted Angular Correlation

5.2.2 INCLUSIVE PRODUCTION OF ELECTRONS AND MUONS IN MULTIHADRONIC EVENTS AT PETRA *

The e^+e^- annihilation into hadrons at PETRA energies is well described by assuming the pair production of u,d,s,c, and b quarks and gluon bremsstrahlung. Since weak decays of the hadrons containing light quarks (u,d,s) have guided the understanding of electroweak interactions, it is of great interest to explore the weak decays of hadrons containing heavy quarks (c,b). Assuming standard mixing angles, in the Kobayashi-Maskawa model (1) bottom is expected to decay predominantly into charm, and charm to strangeness.

The leptons resulting from the semileptonic decay of bottom hadrons are expected to dominate the region of transverse momentum larger than 1.0 GeV/c with respect to the jet axis. This feature combined with a more spherical event shape is used in the selection of hadronic $b\bar{b}(g)$ events.

The search for inclusive leptons in hadronic events provides therefore an indirect study of heavy quark production. From the inclusive lepton yield we obtain the fraction of "prompt" leptons, which result only from semileptonic b- or c-decays, including the cascade decay $b \rightarrow c \rightarrow l\nu X$ by subtracting all trivial lepton sources as π/K-decay, γ-conversion etc. The prompt lepton signals yield then with suitable additional cuts a measurement of the semileptonic branching ratios of heavy quarks.

A selection of events containing mostly $b\bar{b}(g)$ allows a measurement of the charge angular asymmetry predicted in the Weinberg-Salam model (2).

The final state hadrons result from the fragmentation of the original quarks. This fragmentation process is poorly known, and models with several free parameters are used to describe it. The measurement of the rate and spectra of inclusive leptons could thus help to understand better the fragmentation functions of heavy quarks. The model dependence of the determination of the semileptonic branching ratios has carefully been studied by comparing the data with the Hoyer et al. (3) and Lund (4) MC event generators.

The data were taken with the CELLO detector (5) at PETRA at average c.m. energies of W = 14, 22, and 34 GeV. The corresponding integrated luminosities are 1.1 pb^{-1}, 2.5 pb^{-1}, and 7.9 pb^{-1}.

To identify electrons all tracks measured in the inner detector have been extrapolated to the liquid argon calorimeter. The study of MC events

yields the electron efficiency in multihadronic events of typically 60% and the pion misidentification probability is about 3×10^{-3}. For the generation of multihadronic annihilation events we employed the Hoyer Model (3) using Feynman-Field fragmentation (6). The various prompt b- or c-decays and background contributions to the elctron candidates with $p_\perp > 0.5$ GeV at $W = 14$ GeV and with $p_\perp > 1$ GeV/c at $W = 22$ and 34 GeV are shown in Table 1.

TABLE 1

Source of electrons	W = 14 GeV	W = 22 GeV	W = 34 GeV
Light quarks (u,d,s)			
Misidentified π's	5.9%	5.5%	7.6%
Converted photons, π/K decay	11.8%	2.8%	11.8%
IC	0.0%	0.2%	1.4%
DIS	1.3%	2.8%	3.5%
Heavy quarks (c,b)			
Misidentified π's	4.2%	4.2%	8.0%
Converted photons, π/K decay	3.8%	4.4%	10.9%
Prompt electrons (all)	73.0%	80.1%	56.8%
b → e only	36.6%	60.0%	34.2%
Number of electron candidates	6	8	20
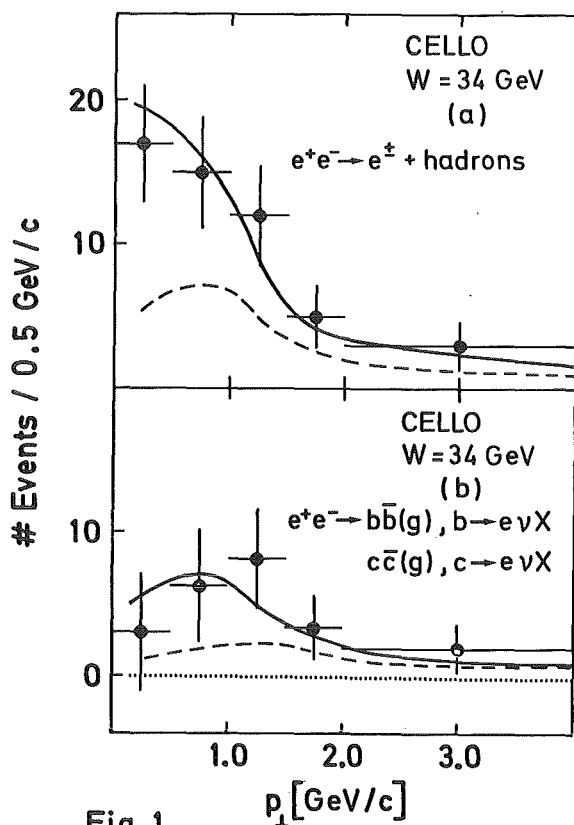
Fig.1

Fig. 1:

Distribution of the transverse momentum $p_\perp$ for electrons compared to MC siumlation

a) All electron candidates.

—— MC expected yield

—— prompt electrons as expected from MC events

b) Prompt electrons.

—— prompt electrons as expected from MC events

—— prompt electrons from the semileptonic decay b →eνX as expected from the MC

Fig. 1 shows the comparison between the data and the MC prediction for the
$p_\perp$-spectrum of the electrons at the highest c.m. energy. The sample of elec-
tron candidates is displayed in Fig. 1a together with the total MC expected
yield (solid line) and the MC expected prompt lepton yield (dashed line). A
good agreement between data and MC is observed. The $p_\perp$-distribution of
prompt electrons obtained after background subtraction is shown in Fig. 1b
and compared to the MC expected prompt electron yield (solid line). The
dashed line gives the contribution of the semileptonic b-decay only.

Inclusive muon candidates are selected using the information provi-
ded by the muon detector. To identify muons, space points reconstructed in
the muon chambers are associated with the charged particles recorded by the
central detector and extrapolated to the chambers. The contributions to the
muon yield for muons with $p > 1.6$ GeV/c and $p_\perp > 0.5$ GeV/c at 14 GeV and
$p_\perp > 1.0$ GeV/c at W = 22 GeV and W = 34 GeV is given in Table 2.

TABLE 2

Source of muons	W = 14 GeV	W = 22 GeV	W = 34 GeV
π/K-decay	10%	9%	9%
hadron - punch through	18%	22%	22%
Random associations	3%	5%	14%
Prompt muons (all)	69%	64%	55%
b → μ only	47%	40%	44%
Number of muon candidates	25	14	22

Fig. 2a shows the transverse momentum of the muon candidates with re-
spect to the thrust axis for the data at W = 34 GeV and MC genereated event
events (solid line). The dashed line shows the fraction of prompt muons ex-
pected from MC events. The corresponding distribution for the prompt muons
as obtained after background subtraction is shown in Fig. 2b and compared
to the MC expected yield (solid line). The dashed line gives the correspon-
ding fraction of muons expected from the semileptonic b-decay.

The influence of fragmentation models to semileptonic branching ra-
tios is studied with the Hoyer MC by changing the decay matrix element of
heavy quarks to V-A, by introducing the mass dependent QCD matrix element
and by variing the strong coupling constant α_s. Secondly fragmentation para-
meters as σ_q, the quark ratios u:d:s and the $p_\perp$ distribution of the primordi-
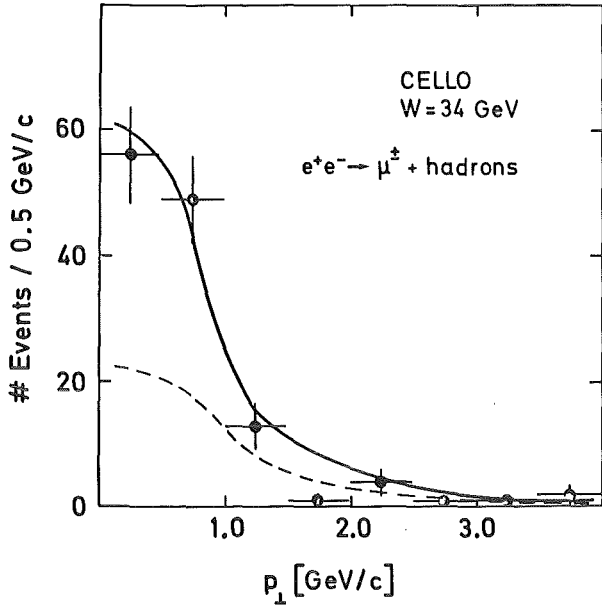
Fig. 2a
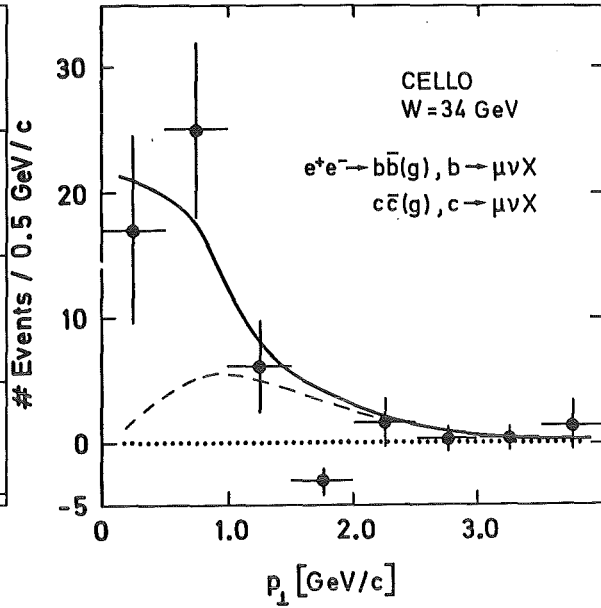
Fig. 2b

Fig. 2: Distribution of the transverse momentum $p_\perp$ for muons compared to MC simulation

    a) All muon candidates

        — MC expected yield

        -- prompt muons as expected from MC events.

    b) Prompt muons.

        — prompt muons as expected from MC events

        -- prompt muons from the semileptonic decay $b \to \mu\nu X$ as expected from the MC.

al 1st rank meson were changed. Thirdly the differences between the Hoyer and Lund generators were investigated. All together the overall systematic error is og the order of 18% for the c-decay and 5% for the b-decay. The variations of the not well known fragmentation of heavy quarks leads to an additional systematic error of about 15% of the semileptonic c-decay and 5% of the b-decay.

We derive from the prompt leptons the branching ratios of the semileptonic decay of the c- and b-quark by comparing the $p_\perp$ spectra of the data with the MC prediction of fixed branching ratios.

As discussed previously the leptons from b-decays are expected to have high transverse momenta. To enrich the b-sample we therefore take events with $p_\perp > 0.5$ GeV/c at W = 14 and with $p_\perp > 1.0$ GeV/c at W = 22 and W = 34 GeV. Table 3 shows the derived branching ratios:

TABLE 3

W (GeV)	Branching ratios		
	b → eνX	b → μνX	c → μνX
14	4.0±11.0±4.3%	26.0±8.2±3.9%	20.5±7.2±4.9%
22	21.3±10.5±2.1%	3.8±6.2±3.7%	15.0±4.9±3.4%
34	15.5± 9.0±2.8%	6.3±4.8±3.5%	8.1±4.3±3.9%
Average	14.1± 5.8±3.0%	8.8±3.4±3.5%	12.3±2.9±3.9%

The systematic errors include those discussed in the lepton identification and background subtraction and those due to the fragmentation and methods specific to the MC event generation. They were added in quadrature. We find an average branching ratio of 14.1 ±5.8 (stat.) ± 3.0 (syst.) % for b → eνX and of 8.8 ± 3.4% (stat.) ± 3.5 (syst.) % for b → μνX, in good agreement with previous results (7).

To extract the branching ratios for the semileptonic decay of c-quarks we use cuts in the thrust distribution of T > 0.88, 0.88, and 0.94 at the three c.m. energies (W = 14, 22, and 34 GeV). Due to large contributions from background processes to the elctron signal we are only able to determine the muonic branching ratio. Column 3 in Table 3 contains the c → μνX branching ratios with an average of 12.3 ± 2.9 (stat.) ± 3.9 (syst.) % again in agreement with previous measurements (8).

Using the sample of enriched b$\bar{b}$-events, we determined the asymmetry due to the electro-weak interference. We use the thrust axis as an approximate measurement of the quark direction of flight and the sign of the lepton to tag the charge of the parent quark. After background subtraction we fit the angular distribution of the asymmetry. For b$\bar{b}$-pair production an asymmetry of -27.3% is predicted. Due to the various background contributions we expect a reduced asymmetry of -5.8% for electrons and -8.0% for muons at W = 34 GeV with an uncertainty of 2.2% for electrons and 3.2% for muons respectively. This error on the predicted value includes all systematic uncertainties discussed above: lepton identification, model dependence and branching ratios. Even though we cannot really test in a definitive way these predictions with our limited statistics, our measurements of -38% ± 21% for electrons and of -43% ± 31% for muons are compatible with the expected values.

(1)   M. Kobayashi and T. Maskawa, Prog.Theor.Phys. $\underline{49}$ (1973) 652
(2)   J. Jersak et al., Phys.Lett. $\underline{98B}$ (1981) 363
        M.J. Puhala et al., Phys.Rev. $\underline{D23}$ (1981) 89
(3)   Hoyer et al., Nucl.Phys. $\underline{B161}$ (1979) 349
(4)   B. Anderson et al., Phys.Lett. $\underline{94B}$ (1980) 211
(5)   CELLO Collab., H.-J. Behrend et al., Phys.Scr. $\underline{23}$ (1981) 610
(6)   R.D. Field and R.P. Feynman, Phys.Rev. $\underline{D15}$ (1977) 2590;
        Nucl.Phys. $\underline{B136}$ (1978) 1
(7)   For a recent review: G. Kalmus, Rapporteur's talk at the XXI Intern.
        Conf. on High Energy Physics, Paris, July 1982, RL-82-090 (1982)
        CLEO Collab., C. Bebek et al., Phys.Rev.Lett. $\underline{46}$ (1981) 84
        CLEO Collab., K. Chadwick et al., Phys.Rev.Lett. $\underline{46}$ (1981) 88
        CUSB Collab., L.J. Spencer et al., Phys.Rev.Lett. $\underline{47}$ (1981) 771
        MARK-J-Collb., B. Adeva et al., DESY Report 83-029 (1983)
(8)   For a recent review: G.H. Trilling, Phys.Rep. $\underline{75}$ (1981) 57
        W. Bacino et al., Phys.Rev.Lett. $\underline{40}$ (1978) 671
                          Phys.Rev.Lett. $\underline{43}$ (1979) 1073 and
                          Phys.Rev.Lett. $\underline{45}$ (1980) 329
        J.M. Feller et al., Phys.Rev.Lett. $\underline{40}$ (1978) 274
        R.H. Schindler et al., Phys.Rev. $\underline{D24}$ (1981) 78

5.3 TWO-PHOTON PHYSICS

5.3.1 LEPTON PAIR PRODUCTION IN DEEP INELASTIC e-γ SCATTERING *

At PETRA we have measured the process $e + \gamma \to e + \ell^+ + \ell^-$, where ℓ is either an electron or muon, at an average Q^2 of 9.5 GeV^2/c^2. The total number of collected events is 240. We find that our data agree with QED predictions based either on exact Feynman graph calculations or on the photon structure function expressions.

5.3.2 EXPERIMENTAL STUDY OF THE HADRONIC PHOTON STRUCTURE FUNCTION **

We have measured at PETRA the process $e\gamma \to e + $ hadrons at an average Q^2 value of 9 GeV^2/c^2. The total number of observed events attributed to this process is 215. Our data are compared to calculations based on the estimation of the photon structure function F_2 in the quark parton model and in QCD.

5.4 QED PROCESSES AND ELECTRO-WEAK INTERFERENCE

5.4.1 INVESTIGATION OF TWO PHOTON FINAL STATES IN e^+e^- ANNIHILATION AT $(\sqrt{s}) = 34.2$ GeV *

Two photon final states in e^+e^- annihilation have been analyzed at CM energies around 34 GeV. Good agreement with QED is observed. Lower limits for the QED cutoff parameters of $\Lambda_+ > 59$ GeV and $\Lambda_- > 44$ GeV are determined. A search for two photons with missing energy yields an upper limit for the production of neutral particles which decay into a photon and a non-interacting particle. Constraints on the mass and the coupling strength of super-symmetry photinos are discussed.
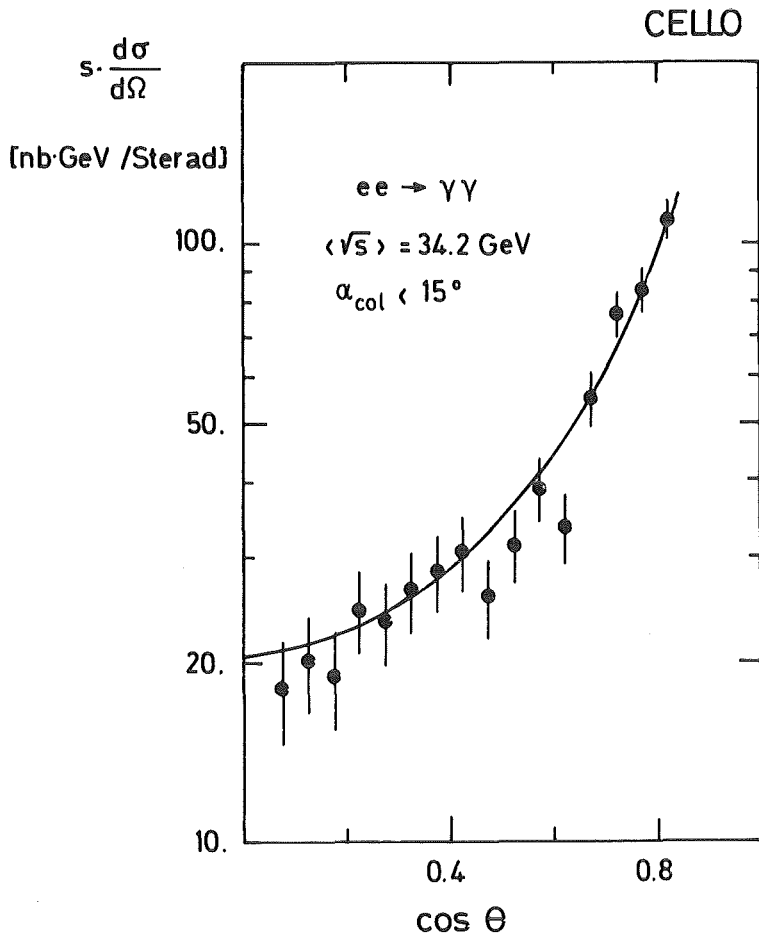
Fig. 1:
The differential cross section s dσ/dΩ for the reaction ee → γγ at $(\sqrt{s}) = 34.2$ GeV. The curve is the QED expectation normalized to the Bhabha scattering process.

5.4.2 MEASUREMENT OF THE τ LIFETIME **

Using 3 prong-decays of τ-leptons from the reaction $e^+e^- \to \tau^+\tau^-$ at 34.2 GeV and 22 GeV the τ lifetime has been determined by a maximum likeli-

* Phys.Lett. 123B (1983) 127
** Nucl.Phys. B211 (1983) 369

hood fit to the decay length distribution. The result

$$\tau_\tau = 4.7 \, {+ \, 3.9 \atop - \, 2.9} \times 10^{-13} \, s$$

agrees well with the lifetime of $(2.8\pm0.25)\times10^{-13}$s expected from $\mu-\tau$ universality and the known branching ratio for $\tau \to e\nu\bar{\nu}$.

5.4.3 τ BRANCHING RATIOS AND POLARIZATION LIMITS IN e^+e^- INTERACTIONS AT $\sqrt{s}$ = 34 GeV *

Considerable knowledge on the τ lepton has been obtained in low energy e^+e^- interactions both at SPEAR and DORIS (1). At center of mass energies far above the production threshold as provided by PEP/PETRA however, the signature of $\tau^+\tau^-$ events with respect to background is much cleaner, offering the possibility to extracts a virtually background-free sample of τ pairs without restriction to specific decay topologies. Our trigger logic incorporated a two-charged particle trigger with a momentum cutoff at 250 MeV/c and various calorimetric triggers. The results are based on 526 $\tau^+\tau^-$ events corresponding to an integrated luminosity of 11.2 (pb^{-1}) at a center of mass energy of 34 GeV. All $\tau^+\tau^-$ decay topologies are recorded by the detector. We report here on measurements of the decay channels $\tau \to \rho\nu$, $\pi\nu$, $e\nu\nu$, $\mu\nu\nu$.

$\tau \to \rho\nu$. ρ candidates were selected from 1 prong decays with one or two additional photons in the same hemisphere. Due to the large momenta of the decay particles, the two photons from the π^0 merge into one shower in about 60% of the decays. Thus in addition to the 1 charged + 2 photon final state also the 1 charged + 1 photon topology was considered. A minimal opening angle of 6° between the charged particle and any photon is required to reduce background due to shower fluctuations from hadronic interactions of the charged particle in the calorimeter.

Whenever two photons were accepted (about 40% the $\rho \to \pi \, \pi^0$ decays) a kinematical fit to the π^0 mass was performed in order to improve the ρ mass resolution. The spectrum of the effective $\gamma\gamma$ mass prior to the fit is shown in Fig. 1a together with the prediction from our Monte-Carlo calculation. The effective mass for the charged particle (assuming a π mass) and the photon (or the 2 photons after the kinematic fit) is shown in Fig. 1b. A clear ρ signal is observed. The following background contributions have been con-

$\tau \rightarrow \rho \nu$, $\rho \rightarrow \pi^{\pm} \pi^{o}$ CELLO $\sqrt{s} = 34$ GeV

a)

b)

#Events/.02 GeV/c²

#Events/.05 GeV/c²

10

8

6

4

2

20

15

10

5

0.0   .12   .24   .36

M(γγ) [GeV/c²]

0.0   .4   .8   1.2   1.4

M(π±π°) [GeV/c²]
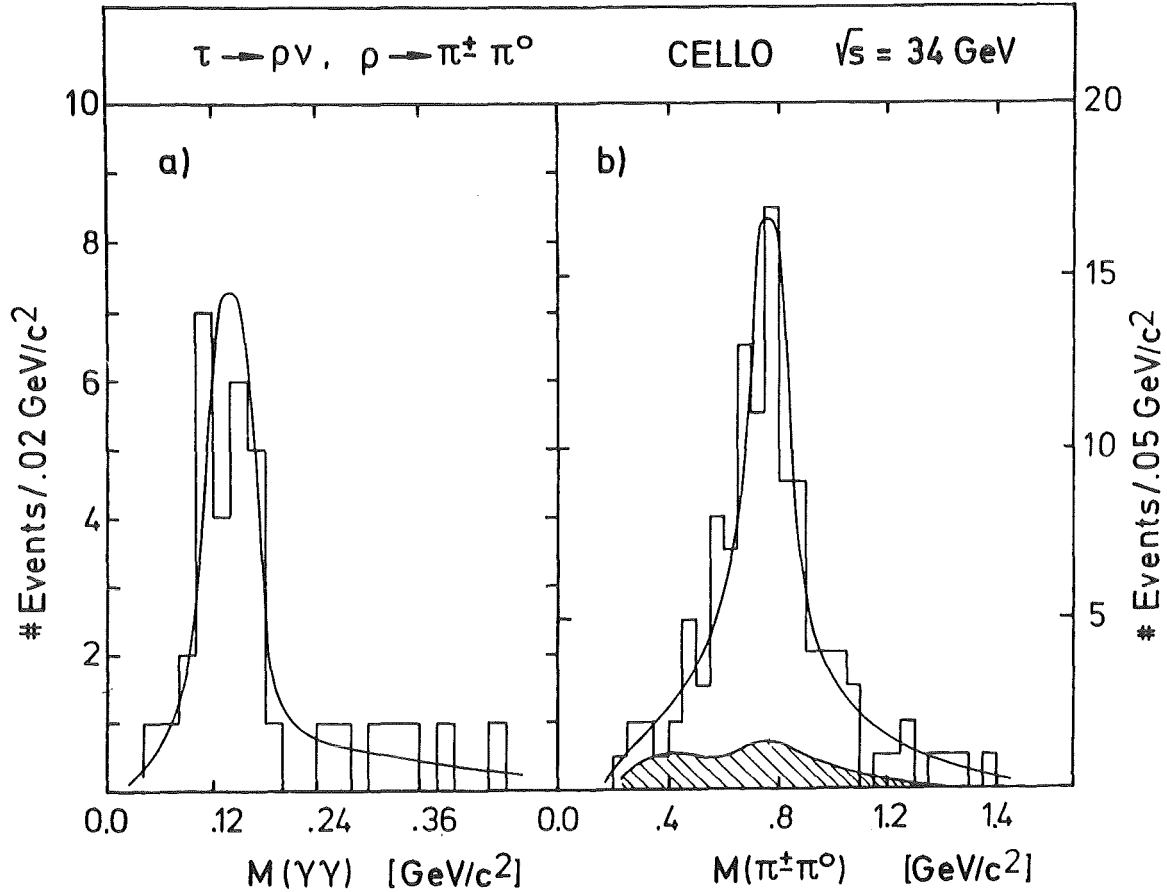
Fig. 1: a) Distribution of the invariant two photon mass for ρ candidates
where 2 showers were reconstructed (histogram) and the MC predic-
tion (curve).

b) $(\pi\pi^{0})$ invariant mass spectrum (histogram), the MC prediction is
superposed (curve). Also shown in the background contribution
(shaded area).

sidered (see Fig. 1b):

- τ decaying to $(\pi\pi^{0})\nu + \geq 1 \pi^{0}$ which are not detected, e.g. from
$\tau \rightarrow A_{1}\nu$.

- $\tau \rightarrow K^{*}\nu$. Since we do not distinguish experimentally K's from π's,
$K^{*}(890)$ decays also feed into our ρ sample.

Background due to other processes, such as electrons, muons, or pions
together with a radiative photon yielding an invariant mass within the ρ
band, is found to be negligible.

$\tau \rightarrow \mu\nu\nu$. Muons were identified in the calorimeter as minimum ionizing
particles and by their ability to penetrate the iron filter. A minimal par-
ticle momentum of 2 GeV/c and an associated hit in the muon chambers were
required. The pion punch through has been determined by Monte-Carlo simula-

tion.

$\tau \to e\nu\nu$, $\pi\nu$. Electrons and pions were separated with the help of their characteristic shower pattern in the calorimeter. Both energy-momentum matching and shower development in depth were employed. A considerable background from $\tau \to \rho\nu \to \pi\pi^0\nu$, due to undetected photons from π^0 decay, is expected. In order to reject ρ's in our pion sample we consider the showers within a cone of 45° half opening angle around the charged particle. The pion efficiency and the remaining ρ background have been determined by Monte-Carlo techniques.

Branching ratios have been obtained by normalizing to the corrected total number of τ events, i.e. to the measured total cross section for $e^+e^- \to \tau^+\tau^-$ at $\sqrt{s}$ = 34 GeV. We obtain the following values:

$$BR\ (\tau \to \rho\nu\ )\ =\ .228 \pm .025 \pm .021$$
$$BR\ (\tau \to \pi\nu\ )\ =\ .099 \pm .017 \pm .013$$
$$BR\ (\tau \to e\nu\nu)\ =\ .183 \pm .024 \pm .019$$
$$BR\ (\tau \to \pi\nu\nu)\ =\ .176 \pm .026 \pm .021$$

where the first error is statistical and the second one is systematic. Table 1 summarizes the four τ decay samples, selection efficiencies, and background contamination with their systematic errors.

TABLE 1   Summary of the four decay samples and their resp. efficiencies and background contributions

	ρ	π	e	μ
No. of events	101	34	60	47
Efficiency	.45± .04	.48± .04	.73± .04	.70± .06
Contamination from μ	0	1.4 ±1.4	0	–
e	0	0.5 ±0.5	–	0
π	0	–	0.7 ±1.2	2.0 ±1.0
$\pi\pi^0\pi^0$	15.4 ±8.4	0	0	0
K,K*	2.3 ±1.1	3.6 ±1.4	0	0

Our results for $\tau \to \pi\nu$, $e\nu\nu$, $\mu\nu\nu$ are in good agreement with determinations at lower energies (1,2). The branching ratio for $\tau \to \rho\nu$ has somewhat improved in the overall error as compared to previous publications (3) based

on larger $\tau^+\tau^-$ samples. We attribute this fact to our large selection effi-
ciency for ρ's and to the low background in the $\tau^+\tau^-$ sample (see Table 1).

Polarization. In the case of polarized τ's the angular decay asymme-
try in the τ rest frame (4) leads to a characteristic distortion of the la-
boratory momentum spectra of the decay particles. The spectra of ρ, π, e and
μ were determined by repeating the above described background subtraction
and efficiency correction bin by bin in the respective raw momentum distri-
butions. In Fig. 2 the corrected laboratory momentum spectra are displayed.
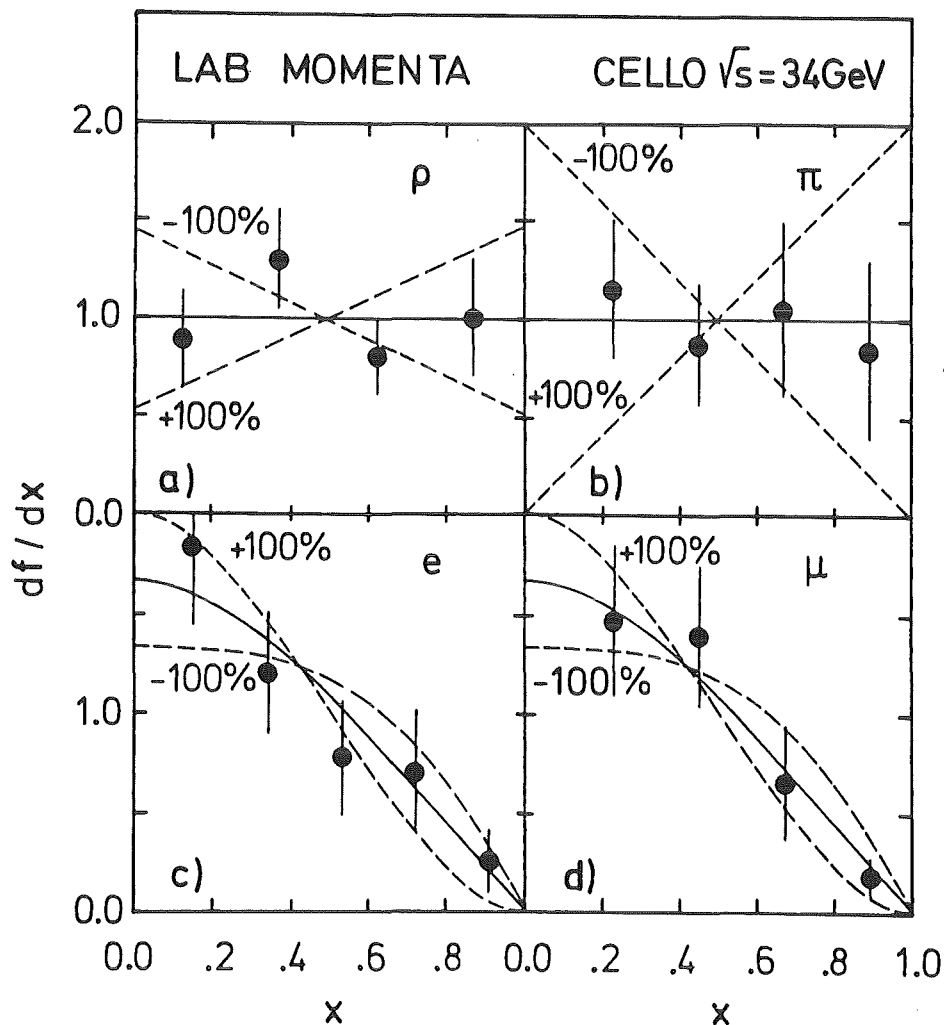
Fig. 2: Corrected laboratory momentum spectra for ρ, π, e, and μ, integra-
ted over the scattering angle. The errors shown include both the
statistical (dominant) and the systematic uncertainty. Also shown
is the expectation for no polarization (full lines) and for ± 100%
polarization (dashed lines), assuming a standard V-A charged cur-
rent decay for the τ.

For the two body decays $\tau \rightarrow \rho\nu$, $\pi\nu$ an unpolarized τ will produce flat laboratory momentum spectra, whereas a non-zero polarization results in a non-zero slope (see Fig. 2a,b). For the leptonic decays $\tau \rightarrow e\nu\nu$, $\mu\nu\nu$ the effects is less pronounced but still useful in deriving polarization limits (see Fig. 2c,d).

For the subsequent analysis of electroweak contributions, the laboratory momentum spectra have been determined in the forward (FW) and backward (BW) hemisphere separately, leading to a measurement of the average polarization in each hemisphere.

A fit combining the eight laboratory momentum spectra (FW and BW) derived for the four decay channels yields a polarization asymmetry defined as $A(P) = (<P_{FW}> - <P_{BW}>)/2$ of

$$A(P) = (+1 \pm 22) \%$$

corresponding to the 95% C.L. limit of $A(P) < 44\%$.

In the standard V, A ansatz for the weak neutral current (5) the final state polarization for the τ^- is a function of the laboratory scattering angle:

$$P(\theta) = -g(s) \cdot (v_e a_\tau + v_\tau a_e) \frac{2\cos\theta}{1+\cos^2\theta} \qquad (1)$$

with $g(s) = (G_F/\sqrt{2}\, 4\pi\alpha)) \cdot (sM_Z^2/(s-M_Z^2))$. G_F is the Fermi coupling constant, α the fine structure constant, s the square of the center of mass energy and M_Z the mass of the weak neutral boson assumed to be 89 GeV/c^2. The first term, independent of $\cos\theta$, contains the product of v_e and a_τ which are known from νe scattering, Bhabha scattering, and the $\tau^+\tau^-$ charge asymmetry. The term propoertional to $\cos\theta$ contains a_e, measured by νe scattering in combination with the Bhabha results, and the unknown quantity v_τ.

According to equ. (1) our result translates into a vector coupling constant of the τ to the neutral weak current of $v_\tau = -0.1 \pm 2.8$. The error is dominated by statistics*. Comparing to the value for $v_e = -0.04 \pm 0.06$ (6), our result is certainly consistent with the assumption of universality of the weak leptonic couplings. Due to the larger error on v_τ, however, no stronger conclusions can be drawn. Still, our measurement constitutes the first attempt to determine v_τ.

---

*It should be noted here that the 1 σ limit for v_τ derived from $e^+e^- \rightarrow \tau^+\tau^-$ total cross section measurements (2) is as large as ± 6.5, mainly due to the systematic errors ($\sim 8\%$) involved.

Assuming universality ($v_e = v_\tau = v$, $a_e = a_\tau = a$) one can try to test a general property of the weak Lagrangian (6) which supposedly factorizes into two currents coupled to a single neutral weak boson. With the universality condition, $P(\theta)$ assumes the form

$$P(\theta) = -g(s)\, 4h_{VA}\, \frac{(1+\cos\theta)^2}{1+\cos^2\theta} \tag{2}$$

Factorization (single Z^o) then implies $4h_{VA} = v \cdot a$. Fits incorporating the universality constraint yield $4h_{VA} = +1.0 \pm 1.4$, which can be compared to the 95% C.L. limit $v \cdot a < 0.14$ from ve and e^+e^- data (7).

(1)   C.A. Blocker et al., Phys.Rev.Lett. 109B (1982) 119
        W. Bacino et al., Phys.Rev.Lett. 42 (1979) 6
        G. Alexander et al., Phys.Lett. 78B (1978) 162
        G. Kalmus, Proceedings of the 21st International Conference on High Energy Physics, Paris (1982), p. C3-431, for further references
(2)   Particle Data Group, Phys.Lett. 111B (1982) 1
(3)   G.S. Abrams, Phys.Rev.Lett. 43 (1979) 1555
(4)   J.E. Augustin, Proceedings of the LEP Summer Study, CERN 79-01 (1979) p. 499
(5)   P.O. Hung, J.J. Sakurai, Nucl.Phys. B143 (1978) 81
(6)   Y.S. Tsai, Phys.Rev. D4 (1971) 2821
(7)   H.-J. Behrend et al., DESY 82-063
        D.P. Barber et al., Phys.Lett. 95B (1980) 149
        W. Bartel et al., Phys.Lett. 99B (1981) 281
        R. Brandelik et al., Phys.Lett. 117B (1982) 365
        For a review see e.g. M. Davier, Proceedings of the 21st International Conference on High Energy Physics, Paris (1982), p. C3-471

6.   DEVELOPEMENT AND APPLICATIONS

6.1   DETECTORS

6.1.1   CALCULATED EFFICIENCY OF A 4π DETECTOR OF BGO OR BaF_2 FOR MONOENER-GETIC GAMMA-RAYS AND GAMMA CASCADES FOLLOWING NEUTRON CAPTURE

K. Wisshak, F. Käppeler, G. Schatz, KfK-report 3580 (1983) and
Nucl. Instr. Meth. (submitted)

The applicability of a spherical shell of BGO or BaF_2 as a 4π detec-tor for high precision measurements of neutron capture cross sections was investigated. First the efficiency of both scintillator materials for mono-energetic gamma-rays was calculated in the energy range from 0.5 to 10 MeV. Configurations with different thicknesses and inner radii were considered. Second, neutron capture cascades were calculated for several isotopes with widely different capture gamma-ray spectra according to the statistical model. Both informations together allowed to determine the efficiency of an actual detector for neutron capture events in dependence of the threshold energy. A thickness of 10 cm BGO or 17.5 cm BaF_2 proved to be sufficient to registrate more than 95 % of all capture events above a threshold energy of 3 MeV. This reduces the systematic uncertainty due to the detector effi-
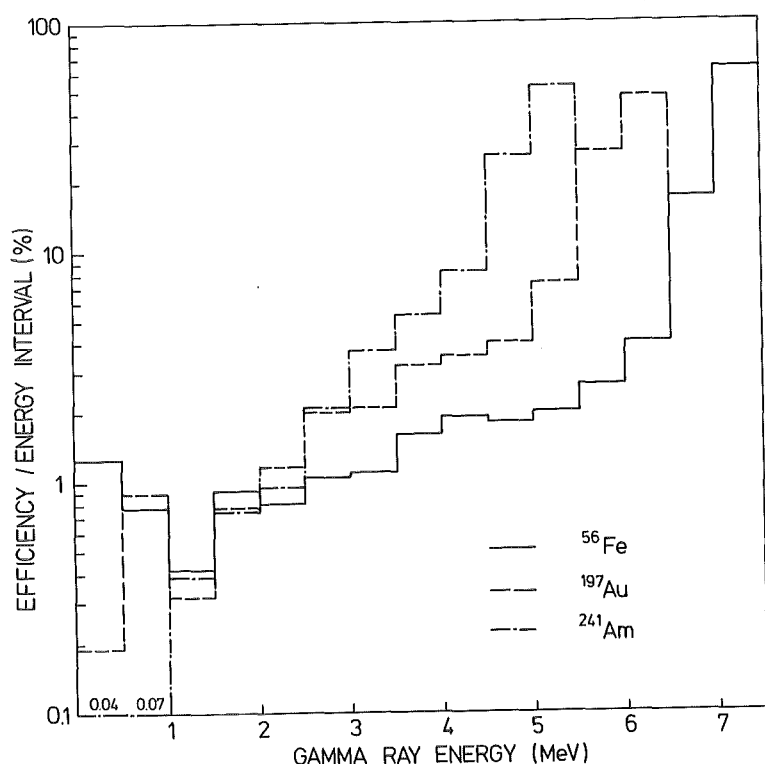
Fig. 1
Calculated efficiency of a spherical shell of BGO (R_i = 10 cm, R_o = 20 cm) for gamma-ray cascades following neutron capture in ^{56}Fe, ^{197}Au and ^{241}Am.

ciency in an absolute cross section measurement to less than 1 % and in a re-
lative measurement using a gold standard to less than 0.5 %.

6.1.2 SENSITIVITY OF A 4π DETECTOR OF BGO OR BaF_2 TO SCATTERED NEUTRONS

K. Wisshak, F. Käppeler

The most important source of background, using a BGO or BaF_2 detec-
tor in neutron capture cross section measurements, is due to capture of
sample scattered neutrons in the scintillator material. This was investi-
gated quantitatively by means of a Monte Carlo simulation. Each interaction
in the detector was randomly assigned to capture or scattering according to
the respective cross sections. Scattering by up to three isotopes is treated
separately in order to consider different angular distributions and energy
losses. The free path length between two interactions is randomly selected
from an exponential distribution. The code follows the neutron in time
and energy until it leaves the detector or is captured.

The calculations were performed under the following assumptions:

1.) The primary neutron spectrum is produced using a Van de Graaff acce-
lerator and the $^7Li(p,n)$ reaction
2.) The maximum neutron energy is 70 keV corresponding to a proton energy
10 keV above the reaction threshold.
3.) The flight path is 50 cm in case of a BaF_2 detector and 1 m for the
BGO detector. As the time resolution of BaF_2 is about a factor of
ten better compared to BGO, the energy resolution is still better for
BaF_2.
4.) The scattering cross section of the hypothetical sample material is
a factor of ten larger than the capture cross section. This is a
typical value for the samples of interest to nuclear astrophysics.

Fig. 1 shows the result for two configurations with compatible gamma-
ray efficiency. The solid line is the time-of-flight (TOF) distribution of
the primary capture events, while the dashed line is the background due to
capture of scattered neutrons. These curves represent a conservative limit
for the expected signal-to-background ratio. In an actual measurement there
are various possibilities to reduce the background. For instance, the shape
of the cross section will be determined by selecting pulse height channels
around the binding energy of the measured isotope. If this binding energy is

different from that of ^{135}Ba (9.1 MeV) a much better signal to background ratio is obtained. The absolute normalization of the cross section is performed in the energy range from 70 to 30 keV. This region is undisturbed by scattering events and thus all pulse height channels above a certain threshold energy can be used in the evaluation.

From the calculations the following conclusions can be drawn:

1.) For the two configurations shown in Fig. 1 the neutron sensitivity is about the same. In the energy range from 10 to 80 keV 90 - 95 % of the scattered neutrons leave the crystal, while 5-10 % are captured.

2.) The capture events are strongly delayed in time. Only $\sim$ 1 % the neutrons are captured in the first 100 nsec after leaving the sample.

3.) A much better signal to background ratio is obtained using the BaF_2 configuration. This is mainly due to the shorter flight path which causes the same number of primary capture events to be registered in a much shorter TOF interval.

4.) For the BaF_2 configuration there is an energy interval from 70 to 30 keV which is undisturbed by capture of scattered neutrons.

In summary, we find that BaF_2 is superior to BGO as far as neutron sensitivity is concerned, especially if one keeps in mind that the better time resolution allows for a shorter flight path (resulting in a fourfold neutron flux at the sample position) and for a better energy resolution at the same time.
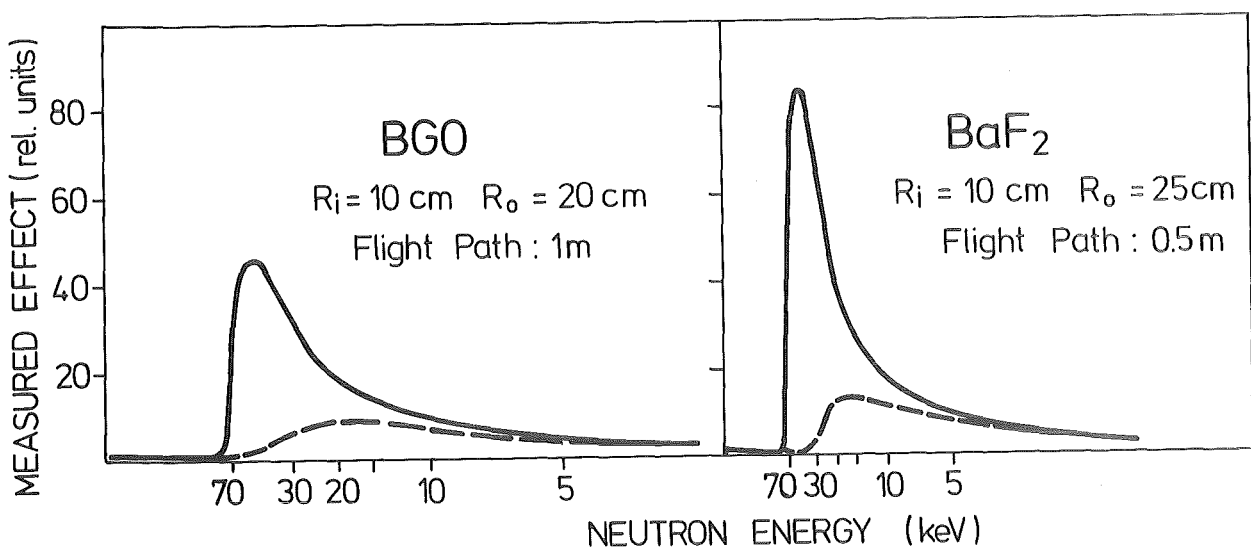
Fig. 1 Calculated TOF spectrum of capture events (solid line) and background due to the capture of scattered neutrons (dashed line) for a 4π detector of BGO and BaF_2.

6.1.3 PEAK-TO-BACKGROUND IMPROVEMENT OF SEMICONDUCTOR
X-RAY DETECTORS AT 10 keV

D. Gotta, M. Schneider, L.M. Simons

To study the strong interaction effects in antiprotonic atoms formed with hydrogen isotopes with the 'cyclotron trap' (1), the energies (about 10 keV) and the small intensities of the $n \to 1$ and $n \to 2$ transitions (of the order of $10^{-2} - 10^{-3} \to ?$) should be measured with high accuracy. Especially important therefore is a good peak-to-background ratio of the detectors to be used.

The most important sources of background in the interesting energy region (about 10 keV) are: i) Compton-scattered electrons with an energy around 10 keV or depositing an equivalent energy before leaving the crystal, ii) Compton gammas of higher energies produced in regions of poor charge collection, iii) backscattered electrons or gammas from the vicinity of the detector producing events in the low energy region, iv) spurious pulses from poor charge collection zones.

The largest background contributing factor (i) can be reduced by the following method: The interaction of a low energy X-ray takes place in the first 'μm' of the crystal (mean penetration depth of a 10 keV X-ray in Ge: ~ 50 μm), while the gammas interact uniformly over the whole detector (thickness several mm). This leads to different collection times of the deposited charge and therefore to different pulse-shapes. The gamma events have a much shorter risetime than the pulses from X-ray interactions. This makes pulse-shape investigations to improve the peak-to-background ratio feasible.

In the first tests we used an intrinsic planar Ge-detektor (IGP 87) of 7 mm thickness and an area of 80 mm. With different sources (e.g. ^{207}Bi with X-rays and gammas or ^{60}Co only with gammas) and different combinations of integration and differentation times two-dimensional spectra (energy vs. pulse-shape) are obtained. In Fig. 1 such a spectrum from ^{207}Bi is shown, where two pulse-shape groups with different risetimes are shown. In the second group (slower risetime) the Pb L X-rays (10.551 and 12.614 keV) and in the first group the events from Compton-scattered gammas are visible.

Taking a pulse-shape window from the second group a drastic reduction of the low energy background is achievable in the energy spectrum. Below 10 keV the reduction attaines 70% compared to the ungated spectrum, while the reduction of the Pb L X-ray is only 5%.

Fig. 1: Two-dimensional spectrum from ^{207}Bi (vertical: energy, horizontal: risetime) with two pulse-shape groups

Energy

Risetime
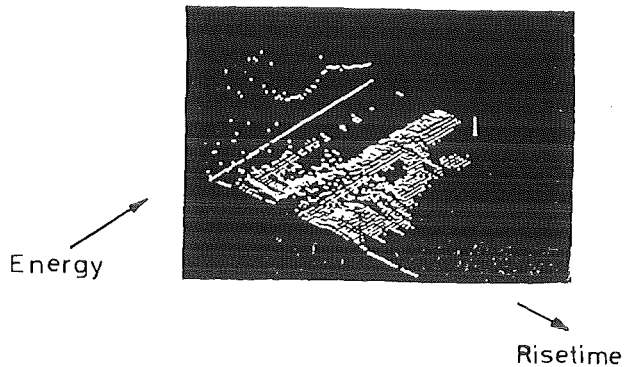
Fig. 2: Cut through the guard-ring reject detector crystal with inner (i) and outer (0) detector. The dashed line indicates the electronically reduced inner detector volume (all measure in mm)
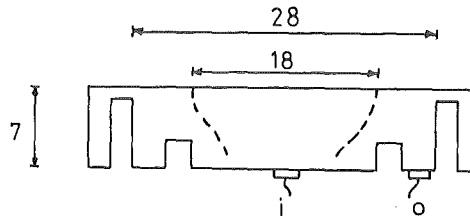
To reduce the background contributions from ii), iii) and iv) a guardring reject detector has to be used. Its consists of an inner and outer detector operated in anticoincidence (Fig. 2). With such a detector similar pulse-shape tests are made. It turned out that with the pulse-shape technique the inner detector delivers the same results in background reduction as the inner detector in anticoincidence with the outer one. This is understood through the electronic reduction of the volume of the inner detector through the veto of the outer one. In Fig. 2 the resulting inner volume is outlined, while in Fig. 3 the strong suppression of the low energy background through the guard-ring reject configuration is shown with the ^{207}Bi source.

These excellent reduction strongly supports the validity of our assumptions made for the pulse-shape technique, because both methods are equally sensitive to the penetration depth.

(1)   P. Blüm, E. Borie, D. Gotta, R. Guigas, H. Koch, W. Kunold,
       M. Schneider, L.M. Simons, SIN-proposal R-81-02.1, and
       P. Blüm, D. Gotta, R. Guigas, H. Koch, W. Kunold, M. Schneider,
       L.M. Simons, CERN-proposal PS 175/1980

Fig. 3: Spectra of the ^{207}Bi source.

a) Inner detector only (the
additional peak results from the
reset-pulse of the outer detector
through cross-talk). b) Inner
detector with anticoincidence of
the outer one.
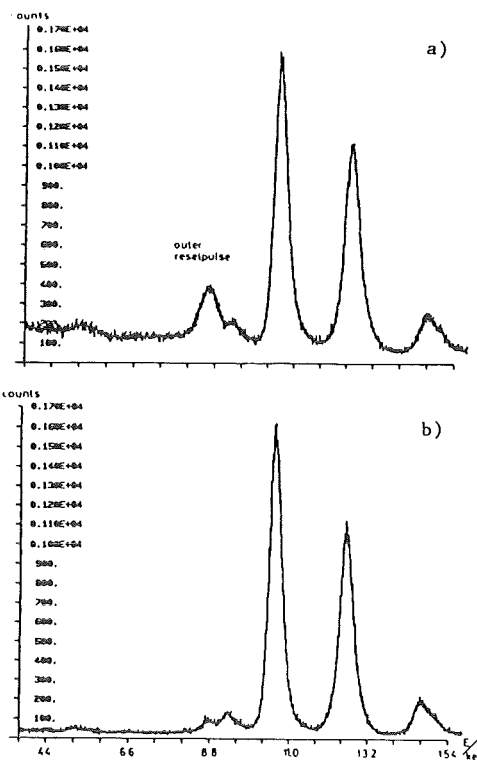
6.1.4 AN X-ray ABSORPTION FLUORESCENCE DETECTOR

D. Gotta, M. Schneider, L.M. Simons

One of the planned experiments with the so called 'cyclotron trap'
(1) aims to study the muonic 2s → 1s transitions in gases, especially in
Neon. This M1 X-ray transition should show a remarkable forward/backward
asymmetry as an effect of parity violating neutral currents.

The problem in observing the M1 2s → 1s X-ray line in muonic Neon
(207.79 keV) is its proximity to the 2p → 1s transitions (about 207.4 keV)
and the extremely low yield of about 10^{-4}. To separate the 2s → 1s from
the 2p → 1s transitions we considered a triggering scheme via a
coincidence measurement with the 3 → 2 transitions. It turned out that
there exists a possibility to separate the 3d → 2p (39.0 keV) and the
3p → 2s (38.6 keV) lines with an absorption K-edge. Thus with the
coincidence between 3p → 2s and 2s → 1s one could reach a good separation
and also a significant background reduction. For muonic Neon a 400 μm La
foil with a K-edge at 38.925 keV can separate the 3d → 2p and the 3p → 2s
transitions. While the 3p → 2s line should be attenuated by a factor of
about 2.5, the 3d → 2p line should be drastically reduced by a factor of
about 200.

Fig. 1: Schematic view of the 'absorption
filter' with different foils, a
Mo grid and the BaF_2-detector
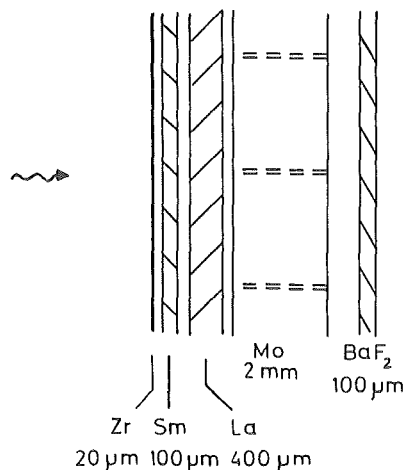
In Fig. 1 a possible configuation of such an 'absorption filter' is shown. The Zr foil in front of the La foil is used to attenuate the muonic Ne (n → 3)-transitions, while the Sm foil attenuated the (n ≥ 5 → 2)-lines. In the La foil fluorescence X-rays are produced isotropically. These X-rays should be attenuated in the following Mo grid of about 2 mm length, with 1 x 1 mm spaces and a wire-thickness of 100 µm.

For the Ne X-rays coming from a much greater distance the grid has a much higher transparency than the fluorescence X-rays, which should be strongly attenuated. Finally the muonic Ne X-rays should reach a BaF_2-detector (with a K-edge at 37.441 keV). Thus the LaK_a X-rays will not be detected.

To demonstrate the feasibility of this method we used an arrangement which simulates this behaviour. We used a Ce source with X-rays at 33.034, 33.44, 37.8, and 38.7 keV. As the absorber material Iodine was chosen, because its K-edge (33.170 keV) lies exactly between the $K_{\alpha 1}$ and $K_{\alpha 2}$ energies. In the tests an Iodine solution in ethanol was taken and in Fig. 2 the effect of the K-edge absorption is demonstrated. The $K_{\alpha 2}$-line is attenuated by a factor of 3.15, while the $K_{\alpha 1}$-line is suppressed by a factor ≳ 400. The effective Iodine thickness is about 300 µm. The reduction of the Iodine fluorescence X-rays (about 60%). through a Mo grid with a thickness of 2 mm is shown in Fig. 3.

(1)   P. Blüm, E. Borie, D. Gotta, R. Guigas, H. Koch, W. Kunold,
        M. Schneider, L.M. Simons, SIN-proposal R-81-02.1, and
        P. Blüm, D. Gotta, R. Guigas, H. Koch, W. Kunold, M. Schneider,
        L.M. Simons, CERN- proposal PS 175/1980

Fig. 2: La-K X-rays without (a) and
with (b) Iodine absorption
material
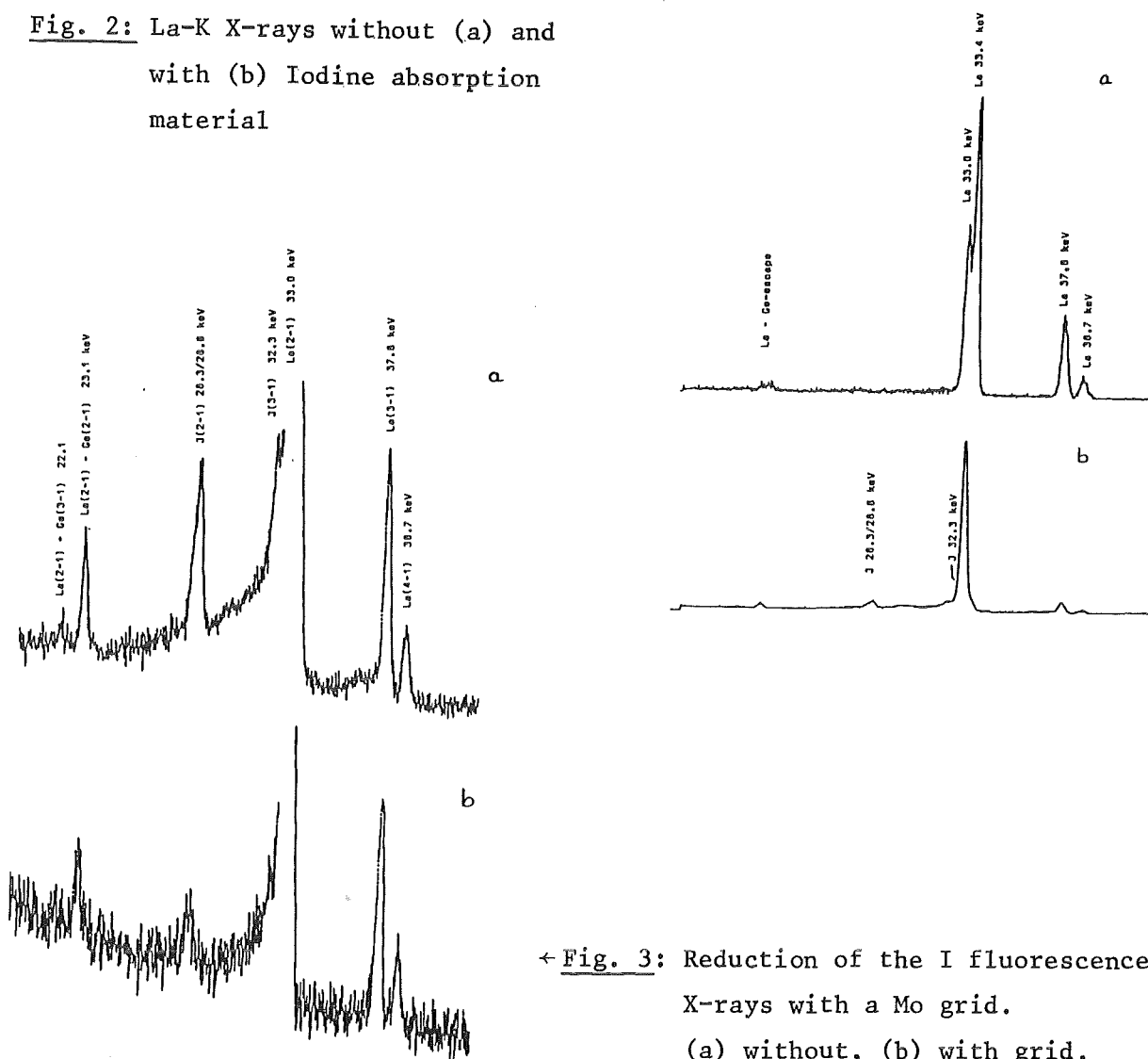
← Fig. 3: Reduction of the I fluorescence
X-rays with a Mo grid.
(a) without, (b) with grid.

6.1.5 PERFORMANCE OF A HIGH-RESOLUTION MODULAR NaI-DETECTOR

P. Blüm, R. Guigas, H. Koch, M. Meyer, H. Poth, U. Raich, B. Richter,
G. Backenstoss[+], M. Hasinoff[+], P. Pavlopoulos[+], J. Repond[+], L. Tauscher[+],
T. Tröster[+], L. Adiels[++], I. Bergström[++], K. Fransson[++], A. Kerek[++],
M. Suffert[+++], K. Zioutas[++++]

A NaJ-detector with a big volume (1/12 of the total solid angle) and
modular structure was used for the measurement of high energy γ-quanta, in
order to search for Baryonium states (1) and rare neutral annihilation channels
(2) in the p̄p-system. Its properties and performance were described in a recent
publication (3).

It turned out that the energy resolution as well as the separation of particles of different kinds was superior as compared to a conventional 12 x 10" monocrystalline NaI (4). In order to achieve a good energy resolution in the energy range between 20 and 1000 MeV a careful intercalibration of the 54 modules had to be done. At low energies, where the electromagnetic shower does not escape from one single module, the intercalibration was done with radioactive sources giving a zero approximation calibration for all energies by linear extrapolation. For the final intercalibration the reaction π^-_{stop} p → nγ was used yielding a 129 MeV monoenergetic γ-line. Events were selected, where more than 60% of the full energy was concentrated in one module. The addition of the low energy parts of the shower in the surrounding modules (calibrated with sources) must give a total energy of 129 MeV and served thus as a first order calibration of the central module. It turned out that only three iterations of this kind were necessary in order to get the excellent energy resolution of $\Delta E/E = 3.3\% \times (E/GeV)^{-1/4}$ ($\Delta E/E = 5.5\%$ at 129 MeV), a value which was never reached by the big brother of our detector, the Stanford crystal ball.

The running times for the search for Baryonium states lasted for several months in a row, and a careful stabilization of the detector and the electronics was necessary. This was achieved by a light pulser system consisting of a Xe-flash-tube the light of which was randomized and sent to all 54 photomultipliers. The light bulb itself was stabilized via the light output of a 2 x 2" NaI which was illuminated by a radioactive source. All elements of the system could be optimized such that a stability of better than 1% over a period of several months was reached.

In order to get a backgroundless γ-spectrum, particularly at energies below 100 MeV, the topology of events of different kinds was studied, and the results were used for a good particle separation. Finally, all charged particles and multiple hits could be eliminated, and it was possible, to get a low energy γ-spectrum free of neutron-background, which facilitated the identification of small structures in this energy domain.

(1)   B. Richter, L. Adiels, G. Backenstoß, I. Bergström, P. Blüm,
       K. Fransson, M. Glöckner, R. Guigas, M. Hasinoff, A. Kerek, H. Koch,
       T. Köhler, M. Meyer, P. Pavlopoulos, H. Poth, U. Raich, J. Repond,
       M. Suffert, L. Tauscher, D. Tröster, K. Zioutas, P.L. 126B(1983)284
(2)   G. Backenstoß, M. Hasinoff, P. Pavlopoulos, J. Repond, L. Tauscher,
       D. Tröster, P. Blüm, R. Guigas, H. Koch, M. Meyer, H. Poth, U. Raich,
       B. Richter, L. Adiels, I. Bergström, K. Fransson, A. Kerek, M. Suffert,
       K. Zioutas, CERN-EP/83-58, submitted to Nucl. Phys. B

(3)   P. Blüm, R. Guigas, H. Koch, M. Meyer, H. Poth, U. Raich, B. Richter,
       G. Backenstoß, M. Hasinoff, P. Pavlopoulos, J. Repond, L. Tauscher,
       D. Tröster, L. Adiels, I. Bergström, K. Fransson, A. Kerek, M. Suffert,
       K. Zioutas, CERN EP 183-37, to be published in NIM
(4)   M. Suffert, P. Pavlopoulos, K. Zioutas, A. Hegerath, CERN EP/83-22,
       to be published in NIM

+   Institute for Physics, University of Basle, Switzerland
++   Research Institute for Physics, Stockholm, Sweden
+++   Centre de Recherches Nucléaires and Université Louis Pasteur, Strasbourg,
       France
++++   Department of Nuclear Physics, University of Thessaloniki, Greece

6.1.6 A LARGE-AREA POSITION-SENSITIVE TIME-OF-FLIGHT COUNTER FOR

NEUTRONS AND CHARGED PARTICLES

S. Cierjacks, S. Ljungfelt, T. Petkovic[+], H. Ullrich

A large position-sensitive time-of-flight counter for subnanosecond
timing has been designed for pion absorption studies in few-nucleon
systems. The new counter has been extensively tested and successfully used
in a recent experiment on π^+/π^- absorption in ^{3}He at 170, 220 and 270 MeV/c
performed at the SIN cyclotron. Kinematically complete experiments of this
type require the coincidence measurement of either a neutron and a charged
particle or of two charged particles, respectively, depending on the
charge of the incident pion. Therefore, the time-of-flight counter was
designed to serve both purposes, i.e. to detect high-energy neutrons as
well as energetic charged particles.

The new counter consists primarily of thirty NE 102A plastic scintil-
lator rods, each 200 cm long, 10 cm high, and 5 cm thick. Each rod is
viewed from both ends by a Valvo XP 2230 photomultiplier. This provides
the event position in the rod from time differences in the two timing
signals, and individual flight times of the projectiles (from the target
to the detector) by the corresponding mean times. The thirty rods are
arranged in a 10 x 3 rod matrix to give a total counter size of 200 x
132 x 15 cm^3 with an effective counter area of 200 x 100 cm^2 facing the
incident particle beam. The total set of rods is grouped into five
vertically separated modules consisting of six rods each with two layers
in height and three layers in depth. While the optically separated rods
are packed as closely as possible in each module, the different modules
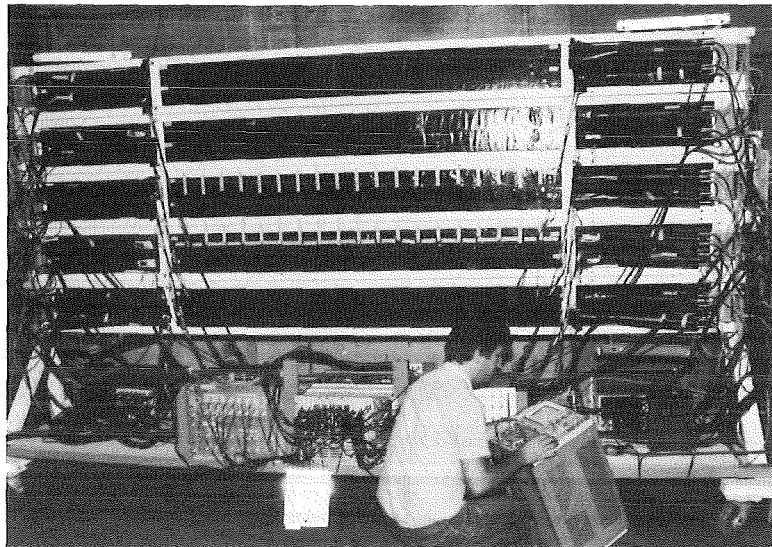
Fig. 1: Reverse side view of the new position-sensitive time-of-flight
counter for neutrons and charged particles.
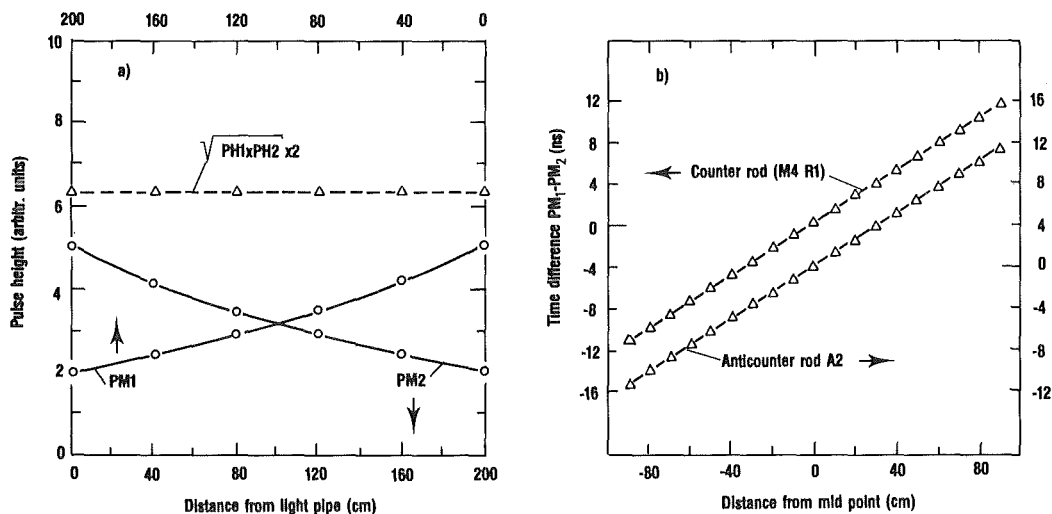
Fig. 2: Light attenuation and propagation characteristics:
a) Measured light attenuation over 200 cm of a main counter rod.
The mean pulse heights, $\sqrt{PH1 \times PH2} \times 2$, were calculated off-line.
b) Measured effective propagation time differences for a 200 cm
long, 10×5 cm^2, counter rod and a 200 cm long, 25×0.4 cm^2,
"anticounter" bar.

are separated by 8 cm in height, in order to facilitate their mounting in
a common counter rack. For testing and monitoring purposes light emission
diodes (LED's) were installed in the light pipes on both ends of each rod.
Particle identification in terms of neutrons or charged particles is
accomplished by five additional NE 102A "anticounter" scintillators,
200 cm long, 25 cm high and 4 mm thick, placed in front of each of the
five counter modules. These anticounters are also viewed from both ends
by XP 2230 photomultipliers to provide the necessary timing informations.
A photograph showing the whole counter arrangement from the reverse side is
shown in Fig. 1.

Pulse height TOF-Counter (Channels)
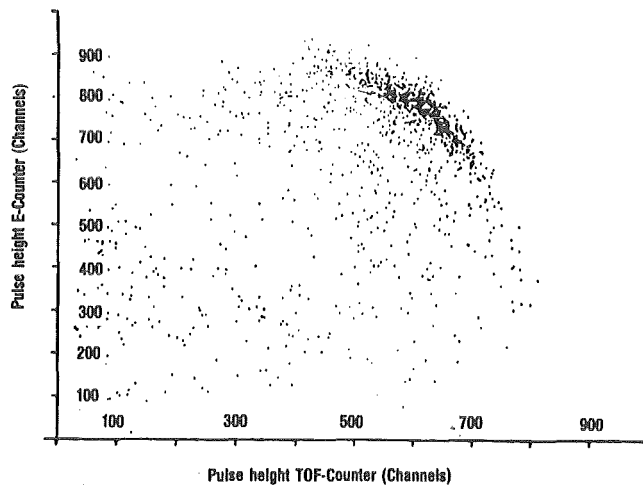
Fig. 3: Dalitz-like plot for protons from the π^+ ^{3}He $\rightarrow$ ppp reaction
investigated in a recent experiment at SIN employing the new
time-of-flight counter.

The specifications of the counter determined from test measurements
with a ^{60}Co and an Am-Be source are as follows: The light attenuation over
the whole rod length of 200 cm amounts to a factor of 2.5. But, if the
geometrical mean of the analog signals from both photomultipliers is
calculated off-line, the pulse height variation as a function of the
incoming radiation vanishes (see Fig. 2a). For the anticounters the light
attenuation factor over the whole length was determined as 8.2. The
effective propagation time difference for light initiated by radiation at
the near or the far end of the rod was determined as 24 ns. This effective
time difference is expectedly the same for the main counter rods and the
anticounter bars. The time differences from both photomultipliers versus

the distance from the middle of a rod are shown in Fig. 2b. The time resolution of the position-sensitive counter was determined both with uncollimated and collimated irradiation from a ^{60}Co source against a small fast NE 102 scintillator with a threshold corresponding to 500 keV. This gave a resolution of 850 ps (FWHM) for an uncollimated and of 700 ps for a collimated beam. Using the Monte Carlo Code of Cecil et al. (1) the detection efficiency for neutrons was calculated for a threshold of 5 MeV$_{ee}$. For neutron energies between 60 and 180 MeV the efficiency decreases smoothly from ~ 21% to ~15%. Valuable additional checks of the above stated counter specifications are expected from evaluations of the recent data taken at SIN involving monoenergetic neutrons from the π^- ^{3}He → dn reaction.

The good overall performance of the new time-of-flight counter is certainly best illustrated by some first results obtained from the recent pion absorption experiments. Fig. 3 shows a Dalitz-like plot of protons from the π^+ ^{3}He → ppp reaction measured in kinematically related elements of the TOF counter and an additional total-absorption scintillation counter. It can be seen that the region outside the kinematically-allowed range is extremely backgroundfree, and that the events from quasifree absorption (covering the region of high event density in the upper part of the figure) are contained in a very narrow band.

(1)   R.A. Cecil, B.D. Anderson and R. Madey, Nucl. Instr. and Meth. 161(1979)439

+   On leave from Zagreb University, Zagreb, Yugoslavia

6.1.7   INVESTIGATION OF A VERTICAL DRIFT CHAMBER

J. Jaki, H. Matthäy, A. Höhne, K. Kärcher, W. Kluge, U. Klein

The systematic investigation of the properties of a vertical drift chamber (VDC) (1) to be used as a focal plane detector for LEPS (Low Energy Pion Spectrometer, being presently installed at SIN) has been completed. Fig. 1 shows a cross-sectional view of the VDC perpendicular to the direction in which the 20 μm thick sense wires alternating with 45 μm shielding wires are stretched. The distances between a sense wire and the adjacent shielding wires is 2 mm. The gap width L, i.e. the distance between the read-out plane and the high voltage planes is 10 mm. The chamber was operated with a 50% argon, 50% isobutane mixture at a high voltage of -8 kV.
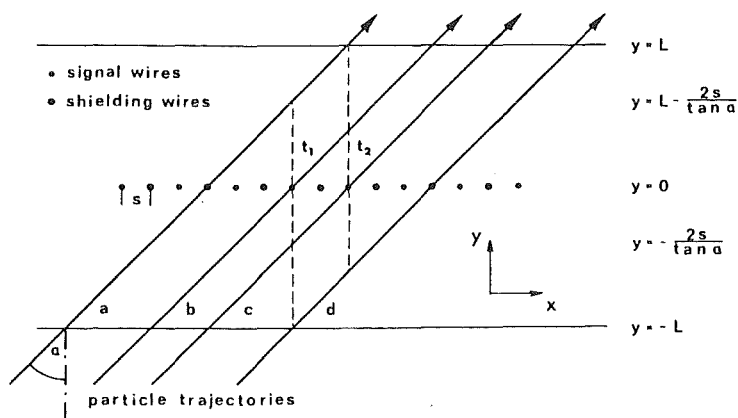
Fig.1: Geometry of the vertical drift chamber. The letters a - d denote particle trajectories which correspond to four points in Fig. 3.

As can directly be seen from Fig. 1 the main difference of the VDC as compared with a standard drift chamber consists in the mode of operation: the particle trajectories have to cross the chamber at angles of incidence α which typically range from 30 to 60°. This angular interval coincides with the angular range of particle trajectories crossing the LEPS focal plane which is tilted by 43° with respect to the central trajectory. The simultaneous measurement of e.g. N = 3-4 or N = 8-10 drift times (corresponding to α = 30° or α = 60°, respectively) allows a precise reconstruction of the trajectories' projection onto the x-y plane.

The redundant time information obtained from the VDC also makes it possible to measure directly its spatial resolution as a function of α. This is achieved by comparing the distance in y-direction between the trajectory and the sense wire measured in one drift cell with the same number determined from a least square fit to the y-values measured in all adjacent cells hit by the particle.

Fig. 2 shows experimental results of the variation σ_y (mm) versus y(mm) obtained with a parallel pion beam of 300 MeV/c from the πM3 channel of SIN and an angle of incidence α = 60°. In addition, the various contributions to the finite spatial resolution of one drift cell are plotted as dashed curves. The curves a) to c) represent the contributions due to the primary ionisation statistics calculated by a Monte Carlo method, due to the diffusion of electrons and the electronic time resolution, respectively. The three curves were added quadratically resulting in the full curve, which is found to be in good agreement with the experimental values. The variation σ_y for one cell was typically $\pm$ 100 μm. The spatial resolution based on drift time

measurements for N sense wires is given approximately by $\sigma_x \simeq \sigma_y \, tg\alpha/\sqrt{N}$, which represents the resolution within the wire plane and equals $\pm 60 \, \mu m$, almost independent of angle.
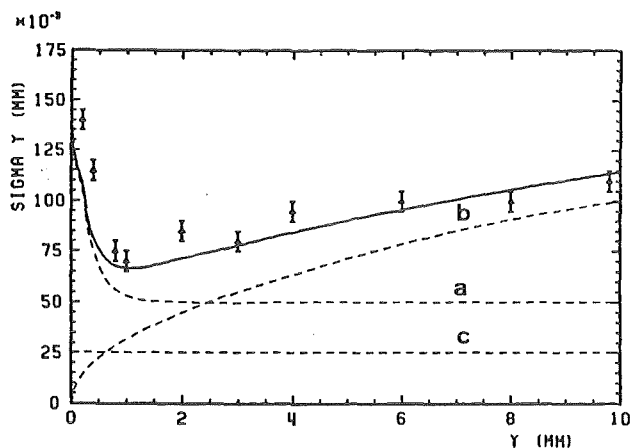
Fig.2: The variation of the spatial resolution σ_y in mm versus the spatial resolution y in mm for one drift cell as obtained in an experiment with a parallel pion beam of 300 MeV/c from the πM3 channel of SIN (α=60°). The dashed curves a - c represent various contributions to the finite spatial resolution as explained in the text. The full curve is the quadratic sum of the three curves a - c and agrees very well with the experimental points.

Fig.3: Correlation of the lengths $t_1 \times v_D$ and $t_2 \times v_D$ along the drift paths in two adjacent drift cells (v_D=drift velocity). The points a-d correspond to particle trajec ries indicated in Fig. 1.
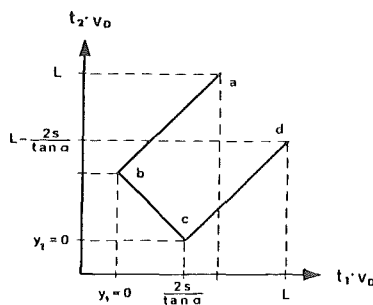
Fig.4: Experimental results for the correlation of the drift times t_1 and t_2 of two neighbouring cells measured with electrons of a ^{90}Sr source. The shadow of the 45 μm shielding wire between two sense wires is observed at t_1=t_2 revealing the excellent spatial resolution of the drift chamber.
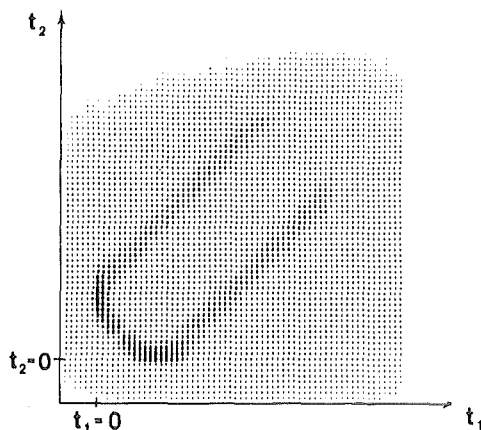
The excellent spatial resolution of the chamber is also clearly re-
vealed by the time correlation spectra of adjacent sense wires. The drift
times of neighbouring cells should be located on a u-shaped curve as shown
in Fig. 3 (see Fig. 1 for the explanation of numbers). Experimentally elec-
trons from a ^{90}Sr source were detected and the drift time correlation of two
adjacent wires relative to a scintillation counter was registered by a two-
dimensional multichannel analyser. The result is shown in Fig. 4 for $\alpha\approx45°$.
For $t_1=t_2$ the number of events on the U-shaped curve is drastically reduced
due to electrons, which are scattered by the shielding wire between the two
sense wires. Hence, Fig. 4 demonstrates clearly that the spatial resolution
is good enough to display the "shadow" of a 45 μm thick shielding wire.

(1)   Annual Report on Nuclear Physics Activities 1981/82
        KfK 3427 (1982) 210

6.1.8 DEVELOPMENT AND TEST OF MWPC's FOR NEUTRON INDUCED REACTIONS

A. Bischoff, F.P. Brady, P. Doll, H.O. Klages, H. Krupp

In continuation of our work to investigate the operation of multiwire
proportional chambers for detecting charged particles produced by fast neu-
trons the MWPC described last year was tested in the neutron beam. The colli-
mated neutron beam from POLKA exhibits a bell-shaped energy distribution ex-
tending up to a twobody reaction peak. It turned out that under normal opera-
tion conditions (- 2500 V on the Cathode foils, about 74% Argon, 1% Freon
(13B1) and 25% Isobuthane at normal pressure) signals on the anode wire planes
did range from 1-10 mV on 50 Ω load.(With the geometry chosen for this pro-
totype chamber a gas multiplication factor A ~ 10^4 is garantied.)They result
from charged particles like protons and α-particles and photons produced by
the neutron beam in the 1 mm CH_2 window of the chamber. Tests with an ^{55}Fe
source exhibited similar signal heights. However, the energy resolution was
poor, as a test run in combination with a charged particle $\Delta E/E$ telescope
showed. Several cathode foil materials where investigated, to improve the per-
formance of the chamber. The risetime of the signals on the anode wire plane
were about 2 - 5 ns and similar fast on the cathode planes.

Fig.1 shows the time-of-flight distribution between the cyclotron and the charged particle event detected in the MWPC. The time signal and the energy signal was deduced from the cathode foils. While the time-of-flight coordinate covers the bell-shaped flux distribution from the neutron beam nearly twice, the charged particle energy spectra are rather continuous. There is a weak indication of a pulse height separation of highly ionizing α-particles and less ionizing protons.

Fig.2 shows the spacial flux distribution of the narrow collimated neutron beam (20 mm $\emptyset$) after 5 m flight path behind the collimator. This distribution is measured by means of the two crossed anode wire planes, which cover an area of 100 x 100 mm^2. The multiplied signal on an anode wire propagates into both directions of a well matched delay line, where the time difference between both ends is a measure of the charge coordinate. The longtime behaviour of the chamber in the neutron beam was studied. With charged particle countrates of about 100 Hz, corresponding to a detection efficiency close to one (estimated from an integral conversion rate of neutrons into charged particles), the MWPC worked fine as monitor, however, deteriorated after several days, building up discharge tracks (Malter-effect), due to the lack of methylal in the gas mixture.

For future n,p experiments at the cyclotron a large area MWPC is presently constructed (Fig.3). It will be operated at normal pressure of either "magic" gas (1) or a argon-CO_2 mixture.

Fig.1

Fig.2

XY- MULTIWIRE - CHAMBER
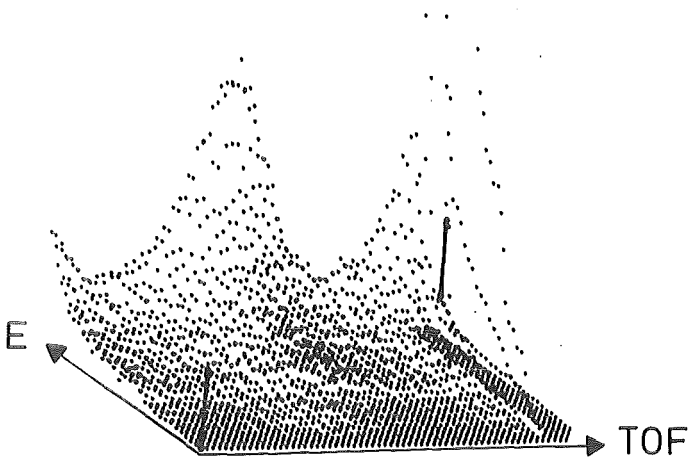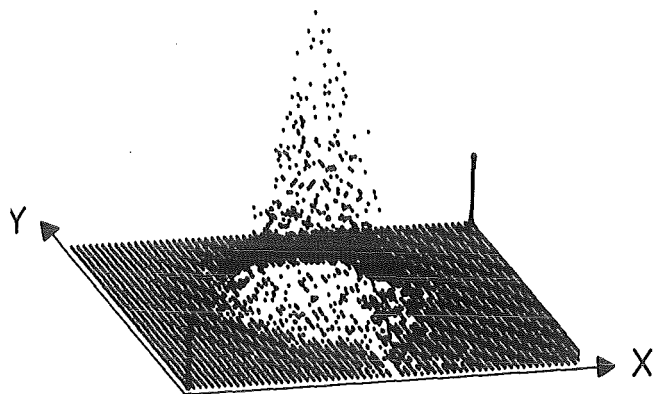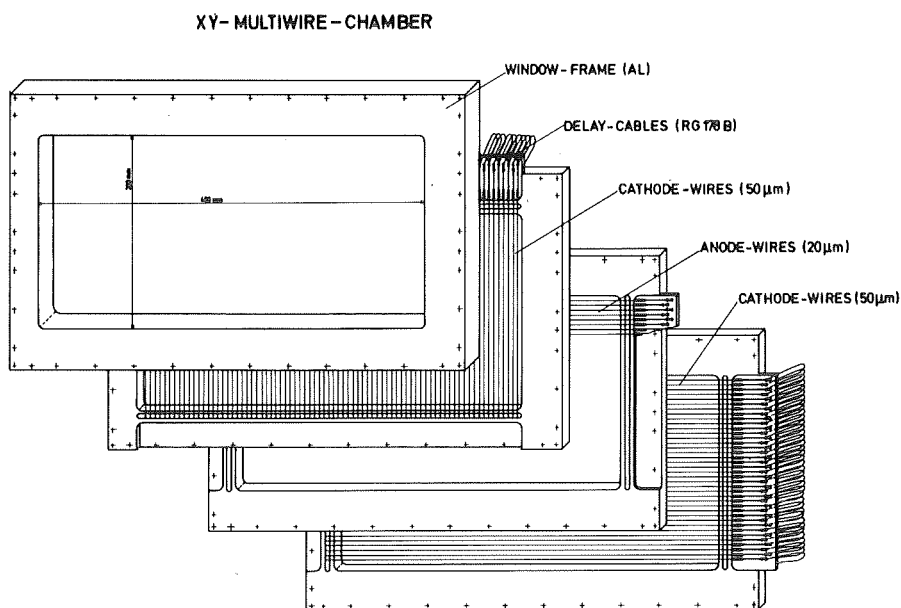
Fig.3

This new chamber typ, however, will use the influenced charge on two perpendicular oriented cathode wire planes to determine the position of the charge produced on the thin anode wires.

(1)   G. Charpak, H.G. Fischer, C.R. Cruhn, A. Minten, F. Sauli, G. Ploch and G. Flügge, NIM 99 (1972) 279

6.1.9   PROPERTIES OF A ΔE/E TELESCOPE FOR NEUTRON FLUX DETERMINATION

F.P. Brady, P. Doll, E. Finckh, H.O. Klages, J. Wilczynski

At POLKA most of the neutron flux is in the broad lower energy continuum due to deuteron breakup. The full energy peak at 50 MeV contains only about 5% of the total flux. (However such a continuum beam allows simultaneous measurements at neutron energies from 17 to 50 MeV.) To build a monitor which would be very stable and essentially threshold independent it was decided to use DE·E plastic scintillator telescopes[1]. These were mounted near the exit of the neutron collimator with the polyethylene CH_2 target at ~ 3.4 m from the neutron source and two symmetrical ΔE·E telescopes at small angles ($\pm$ 14° and later $\pm$ 20°) to the neutron beam as shown in Fig.1. These telescopes also provided accurate measurements of A_y for n-p at large scattering angles.
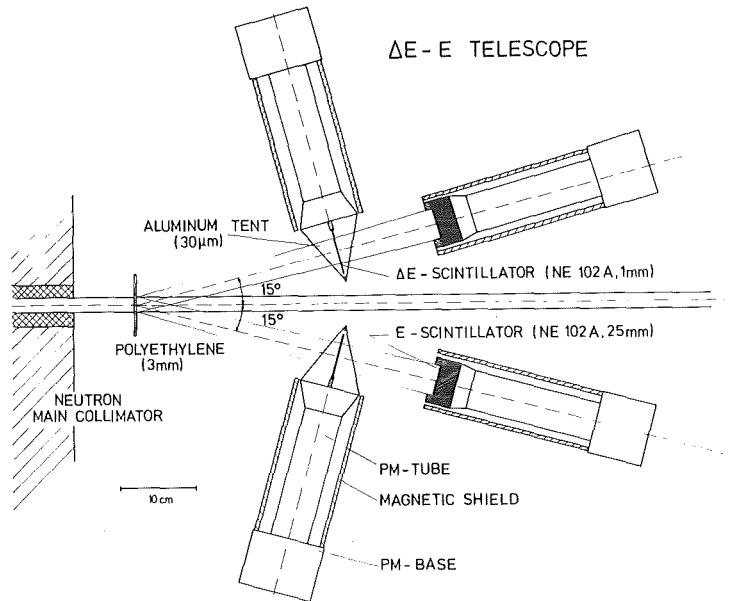
Fig.1: Horizontal schematic view of the $\Delta E \cdot E$ telescopes

The E plastics are coupled to the PMT via lucite light pipes as shown. Brass collimators 5 mm thick with 40 mm opening diameter are directly in front of the E plastics which are wrapped in 3 µ Al foil and taped on the sides to be light tight.

The ΔE plastics were mounted on two lucite "peg-legs" (2-3 mm diameter) so that the spacing between the top of the conical light pipe and the bottom of the scintillator is 11 mm. Clear epoxy is used on the joints, top and bottom of the pegs. This stand-off distance and the use of highly reflective Al foil on the inside of the tent surrounding the scintillator gives good uniformity in light collection from different parts of the scintillator. The uniformity of response of the ΔE detectors was checked by scanning them with a collimated ß-source. A uniformity of response to within 2-3% is observed.

The $\Delta E \cdot E$ coincidence gates the E and ΔE signals and provides the start TOF signal which, relative to the phase of the cyclotron RF, gives a measure of the incident neutron beam energy. The ΔE, E, and TOF parameter along with the telescope addresses are stored on magnetic tape for later off-line analysis. Gain changes are accounted for in ΔE and E, and time shifts in the TOF so that all runs have the same spectrum in three parameter space. This allows the same time and/or energy bin selection to be made for each run. After chosing an equivalent TOF flight window for the left and right telescope the integrated energy spectra provide an accurate monitor for the neutron flux. In A_y measurements, e.g. in $\vec{n}$-p, the flux cancels out when symmetric left-right pairs are used. However in measurements of A_{yy}, where the

target spin cannot (in the case of brute-force polarization) be quickly tur-
ned over, or in cross section measurements, a stable flux monitor is impor-
tant.
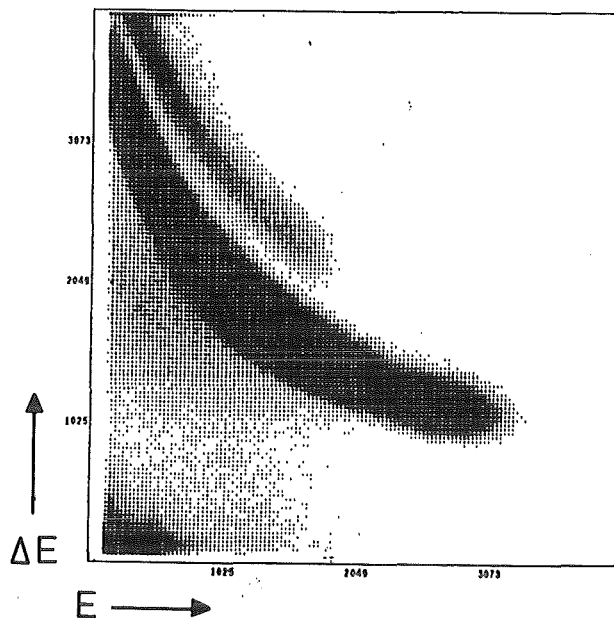
Fig.2: ΔE vs. E matrix of the "left" telescope for one run of 6000 s

For typical polarized deuteron beam currents (25 nA) and geometries
($\Omega_n = 10^{-4}$ sr, $\Omega_p \sim 10^{-3}$ sr) and 3 mm CH_2 target, the count rate in each
telescope is $\sim$ 3 cps. Combined, the two telescopes give a statistical un-
certainty of $\sim$ 0.5% for each run of 6000 secs. The spin "up-down" flux ratio
can be monitored to better than 1%.

(1)   T.S. Subramanian, J.L. Romero and F.P. Brady, NIM 174 (1980) 475

6.1.10 DETERMINATION OF ^{3}He-DETECTOR PROPERTIES USING A ^{252}Cf NEUTRON SOURCE

A. Chalupka[*], P. Doll, B. Haesner, H.O. Klages

With the availability of a low-mass ^{252}Cf neutron source, embedded in
a small ionization chamber (1) it was challenging to attempt to calibrate
neutron detectors. The fission chamber was exploited to calibrate a liquid

^{3}He-scintillator detector (2). Because the flux distribution of the fission neutrons from the ^{252}Cf source is assumed to be known fairly well (3), the absolute cross section for a specific reaction in the ^{3}He-scintillator: ^{3}He(n,p)^{3}T, can be measured. However, this measurement requires besides a careful knowledge of all background and attenuation effects from surrounding materials, a detailed understanding of the pulse height spectrum produced in the liquid scintillator. For a more quantitative understanding of pulse height variations in liquid ^{3}He, a standard Monte-Carlo code (4) was modified to calculate multiple scattering effects in a ^{3}He-scintillator of 7.2 cm diameter and 7 cm height exposed vertically to a neutron field of 6.4 cm diameter like in the real experiment. Cross sections and angular distributions for elastic scattering and all reaction channels were taken from the literature. For neutron energies between 0.3 and 4 MeV the knowledge of the total, elastic and the partial (n,p) cross section is poor (5). This statement holds even more for the differential cross sections. For higher energies, cross sections were taken from ref.6 and 7. Hardly anything is known about the light output of low energy charged particles in liquid ^{3}He. For scattering processes below 3 MeV the calculated pulse height spectra are very sensitive to the angular distributions and the light output for ^{3}He particles, protons and tritons. (Further investigations should be carried out in these energy range.) Fig.1 shows typical pulse height spectra at 2.1 and 4.2 MeV incident neutron energy. While the description of the measured spectra is satisfactory at 4.2 MeV, the above mentioned problems are evident at 2.1 MeV. The low pulse height spectrum is dominated by elastic scattering processes.The structure with the highest pulse height is due to the combined light output for the proton and triton from the ^{3}He(n,p)^{3}T reaction. The steep fall-off (short dashed line) indicates the boundary for events which experienced in the 1. scattering elastic scattering from ^{3}He only. Consequently, the pulse-height range between elastic and p + t scattering events seems to be contaminated by multiple scattering processes. By improving the description of the spectra, we will be able to correct the experimentally evaluated count rates in the ^{3}He(n,p)^{3}T reaction peak taking into account the finite energy resolution. This will allow us to determine the absolute cross section for this monitor reaction.

(1)   A. Chalupka, NIM 164 (1979) 105
(2)   R. van Staa, J. Reher, B. Zeitnitz, NIM 136 (1976) 241
(3)   J.A. Grundl and C.U. Eisenhauer, Symp. on Neutron Standards and Applic. Gaithersburg 28-31, 1977, NBS 493
(4)   G. Kanisch, Diplomarbeit, University Hamburg (1976)
(5)   R. Batchelor and K. Parkor, AWRE-Report 0-78/64
(6)   B. Haesner, Ph.D. thesis, University Karlsruhe (1982)
(7)   M. Drosg, Los Alamos LA-7268-MS 1978 UC-34C

*   Institut für Radiumforschung Wien
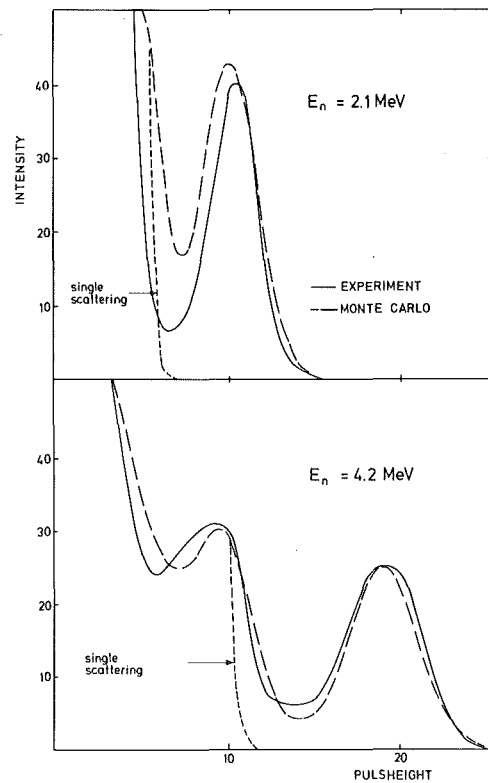
Fig.1: Pulse height distributions in a liquid ^{3}He scintillator detector

6.1.11 SHIELDING OF PMs IN STRONG MAGNETIC FIELDS

F.P. Brady*, P. Doll, H.O. Klages, P. Jany

Here we discuss the specific problems of shielding the ΔE - E teles-copes and the neutron detectors from the magnetic field of the polarized pro-ton target.

The magnetic field variation in the median plane (at 9 Tesla central field) is shown in the figure below. The detector arrangement for the $\vec{n}$-$\vec{p}$ A_{yy} measurement was the following: The E-detectores from the telescope were 125 cm from the target center (70 Gauss), the ΔE-detectors were 140 cm from the target (55 Gauss); a pair of small neutron detectors were at 55 cm (900 Gauss) and at 75 cm (338 Gauss) and a pair of large neutron detectors were at 125 cm (70 Gauss) from the target center.
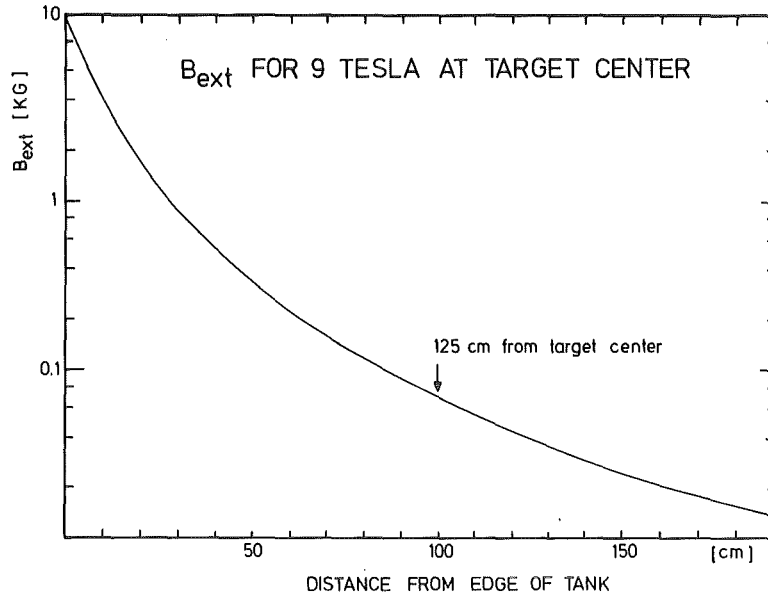
Fig.1: Radial dependence of the external field of the polarized proton target

The magnetic field inside the detector should be $\lesssim$ 0.5 gauss for a gain shift of $\lesssim$ 10% in XP 2020 and 2040 tubes. (0.1 G gives $\lesssim$ 1% gain shift.) The main contributions to B_i, the field inside the shields, from the external field, B_{ext}, come from through field, B_i^t, and both end fields, B_i^e (1). These contributions for single shields of inside diameter D, wall thickness, d, length, L, and (high) permeability, μ, have the form

$$B_i^t \simeq B_{ext} \cdot D/\mu d$$

$$B_i^e(x) \simeq B_{op} \, e^{-2k \cdot x/D}$$

x is the acial distance from the opening, B_{op} is the field on axis at the opening. These depend on whether B_{ext} is parallel or perpendicular to the cylinder axis, and are respectively (static field):

$$B_{op} \simeq 1.3 \sqrt{L/D} \, B_{ext} \qquad k = 2.25 \qquad \text{parallel}$$

$$B_{op} = 0.33 \cdot B_{ext} \qquad k = 3.5 \qquad \text{perpendicular}$$

Quenching factors $Q \equiv B_i/B_{ext}$ or shielding factors, $S = Q^{-1}$, are defined in this way. Because of the smaller k-parallel it was determined for the case of B_{ext} parallel to the axis of the cylindrical shield that it was not possible to shield the ΔE detectors adequately in this geometry. So the scintillators were rotated to have B_{ext} perpendicular to the cylinder axis.

Due to saturation effects it was necessary to use (at least) two shields, the outer one of iron which saturates around 20 kG (in the iron).

In the case of a μ-metal and a Fe shield the total shielding factor S_{tot} is somewhat less than $S_\mu \cdot S_{Fe}$. In the case of through fields, S_{tot} is further reducted by approximately $4\Delta/D$ (Fe) where Δ is the air gap between the μ and Fe shields.

Similarly for end fields the shielding factor for double shields is taken to be

$$B_i^{(e)}(x) = B_i^{(e)}(x_o) \cdot e^{-2kx/D}$$

where $B_i^{(e)}(x_o)$ is the end field for the inner cylinder which is x_o inside the outer cylinder.

For the ΔE and E detectors it was necessary to shield the anodes with μ metal shields (D = 60, L = 110 mm) which fitted tightly around the bottom of the tube. A second μ shield D ≈ 76 mm was used to shield the photocathodes. This overlapped the anode shield and enclosed the scintillator and light pipe of the E and went nearly to the top of the light pipe in the ΔE detector. Iron shields of 3 mm wall enclosed the E from base to the end of the colli-mator, and the ΔE from base to the bottom of the scintillator. These arrange-ments gave shielding factors of 10^3 for both "end" and "through" fields in the ΔE and E detectors.

For the small neutron detectors, two separate μ shields were neces-sary. The outer Fe shield was 5 mm thick and ran from base to the end of the scintillator (50 mm long on a 50 mm long light pipe) except for a slot at the end for the expansion tip. It was estimated that the field in the Fe cy-linder's wall was on the verge of saturating. In tests with the magnetic field it was shown that the extra layer of μ (d = 1 mm) was necessary to avoid a large gain decrease in the field.

The large neutron detectors had one large μ metal shield (d = 1 mm) and outside that a soft iron shield also of d = 1 mm. The field in the Fe wall is close to saturation. A thickness of 2 → 3 mm would be safer. (But this makes the detectors heavier.) Assuming the field in the walls is < 10 kG (as will be the case for most of the length then μ_{Fe} at 1 to 10 kG is ~ 2000. For μ metal assume μ = 50 K. Then through field quenching is Q_{tot} ~ 0.003. In the actual experimental arrangement the gain changes for the telescope detectors due to B field off and on were reasonably small, of the order of 10%. While for the neutron detectors at the largest distance no changes where observed the closest detectors exhibited changes of the same order of magni-tude.

(1)   Wirbelströme und Schirmung in der Nachrichtentechnik, H. Kadem, Springer-Verlag (1959)

*   Dept. of Physics, U.C. Davis, CA 95616

6.2   INSTRUMENTATION

6.2.1   POLARIZATION OF PROTONS IN TiH_2 SAMPLES

R. Aures, W. Heeringa, R. Maschuw, F.K. Schmidt

A brute-force polarized proton target has been developed for scattering experiments with fast polarized neutrons. The target material is pressed TiH_2 powder which has been pressed into copper cylinders. A method to determine the proton polarization is described here, in which the heat capacity of the proton spins in the polarizing magnetic field is measured.

THe schematic set-up is shown in Fig.1. The sample employed here has a length of 3.7 cm and a diameter of 2.5 cm. It has in its center a small copper rod on which a cobalt crystal (with a small amount of ^{60}Co) and a

MIXING CHAMBER

THERMAL SWITCH

COPPER ROD

COMPENSATION COIL

MAIN COIL

TiH_2 SAMPLE

MAIN COIL

HEATER   COPPER ^{60}Co SOURCE
              ROD
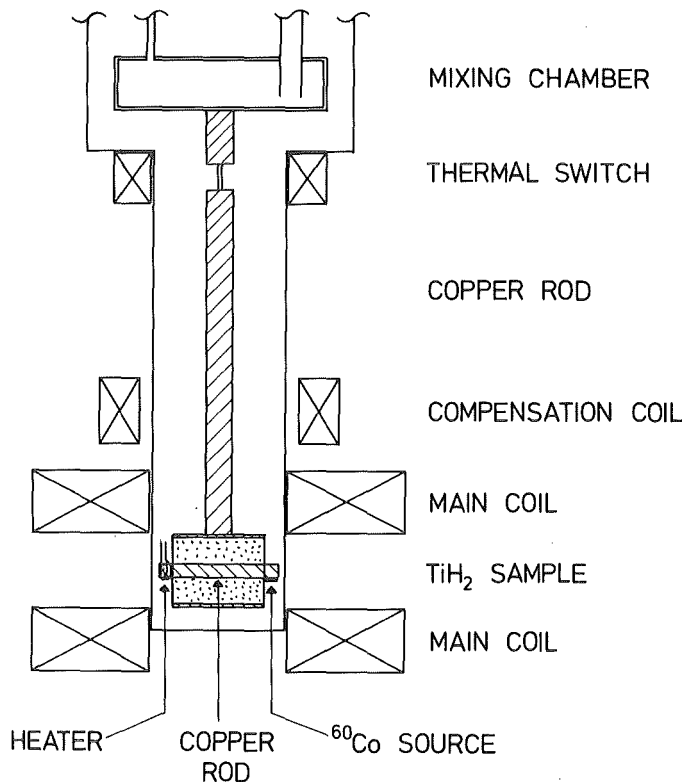
Fig.1: Schematic view of the set-up inside the cryostat

small heating coil are mounted. The anisotropy of the ^{60}Co γ-radiation is used for the temperature determination. With the heating coil accurate amounts of heat can be supplied to the sample. A second copper rod connects the sample

to the mixing chamber of a ^{3}He-^{4}He dilution refrigerator. Shortly below the mixing chamber this copper rod has been interrupted to insert a thermal switch. This is a piece of high-purity tin, which can be made superconducting or normally conducting by changing the magnetic field of a small coil around it. In the superconducting state the thermal conductivity is very low (switch open), in the normal state it is very high (switch closed).

The measurements were carried out as follows. First, the sample was polarized in a field of 4.2 T with the switch closed. It lasted about 30 h to reach 10 mK. Then the switch was opened to isolate the sample. Small amounts of heat were given to the target until it had reached about 30 mK. After each heat input we waited 0.5 - 1 h for the temperature to stabilize at its new higher value. These warming-up measurements were carried out 4 times with a TiH$_2$ sample and 2 times with a Ti dummy sample with the same dimensions and the same amount of Ti as the TiH$_2$ sample.

The dummy measurements are necessary to determine the heat capacity, which is not due to the protons. This background heat capacity is mainly caused by the copper nuclei in the cylinder and in the rods, which polarize to some extent. The background heat was determined to be about 30% of that of the protons. This agrees with the calculations.
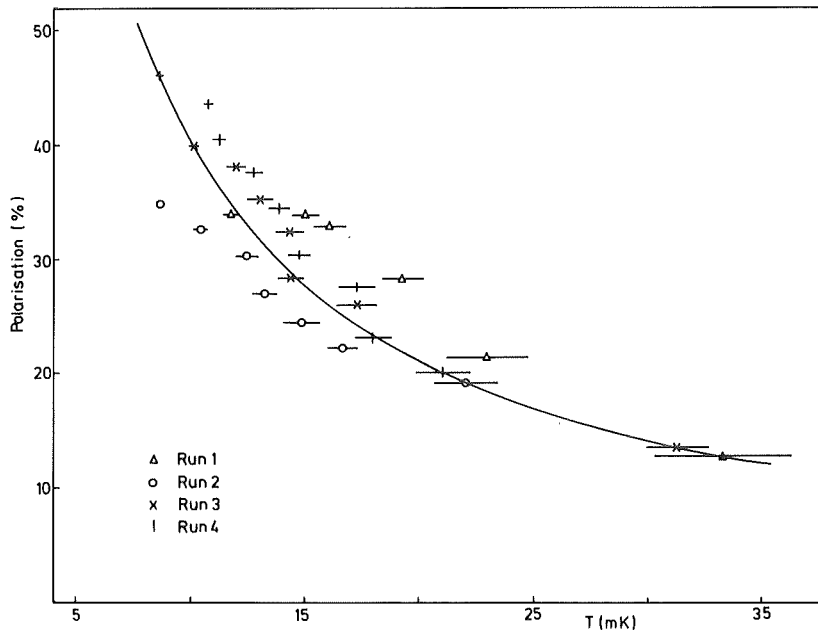
Fig.2: The theoretical polarization of protons in a field of 4.2 T (full line) compared with the experimental results

The amount of heat ΔQ, that a number of N protons in a magnetic field B can absorb is equal to $\Delta Q = N\mu B \, \Delta p$, where Δp is the change in polarization. With this relation the amount of heat ΔQ that was supplied to heat the sample over a certain temperature interval can be converted into a polarization decrease Δp over that interval. These polarization steps are shown in Fig.2. The warming-up could not be followed until zero polarization because the temperature measurements with ^{60}Co is too inaccurate above 30 mK.

Thus from these measurements an absolute value for the polarization is not obtained, but they allow to verify whether the theoretical curve is followed property between 10 and 30 mK. The data of the 4 runs were normalized to the theoretical curve at the highest temperature, where deviations are supposed to be smallest. Although there are large differences between the results of the different runs, the data follow the theoretical curve quite well on the average. The data indicate that the polarization at 10 mK has been at least 35%. It may be expected that in a larger field larger polarizations are achievable.

6.2.2 DEMAGNETIZATION OF PROTONS IN TiH_2 SAMPLES

R. Aures, W. Heeringa, R. Maschuw, F.K. Schmidt

Samples of pressed titanium hydride powder have been prepared to be used as polarized proton targets in scattering experiments with fast polarized neutrons. The protons are polarized with the brute-force method. Results of polarization measurements are given elsewhere in this report.

A sample of polarized protons is a potential nuclear refrigerant: it is a cooling medium, with which it should be possible to reach very low temperatures by adiabatic demagnetization. In fact titanium hydride shows some favourable properties compared to other nuclear refrigerants. It has a high nuclear density and the magnetic moment of the proton is large. Hence a large entropy reduction per unit of volume can be obtained. This property is expressed in a high value of the molar Curie constant λ divided by the molar volume V. In Table 1 the values of λ/V are compared for several possible materials for nuclear refrigeration. Another advantage of TiH_2 is that it does not become superconducting. For superconductors it is not possible to continue the demagnetization to below the critical field B_c. We report here on the

first adiabatic demagnetization experiments carried out with protons.

Material	λ/V (μK)	B_c (mT)
Nb	1.99	250
V	1.91	13
TiH_2	1.62	-
In	1.11	30
Al	0.87	10
Cu	0.57	-
Tl	0.21	20

Table 1:

Molar Curie constant λ divided by the molar volume V for some materials. The critical field B_c is also listed

The set-up was basically the same as that shown in the previous contribution. The titanium hydride is contained in a copper cylinder, which is connected to the mixing chamber of the dilution refrigerator by a copper rod. Because the Cu-atoms in the sample also polarize and demagnetize, we have made a dummy sample with the same dimensions containing pressed titanium powder instead of pressed titanium hydride powder. The results of two demagnetization runs are shown in Fig.1. The samples were magnetized at 4.2 T and precooled to somewhat below 10 mK. The demagnetization was performed in 3 h to a final field of B_f = 0.22 T. Ideally the temperature of the TiH_2 sample should have followed the lower straight line ending at 0.55 mK. The measured temperature
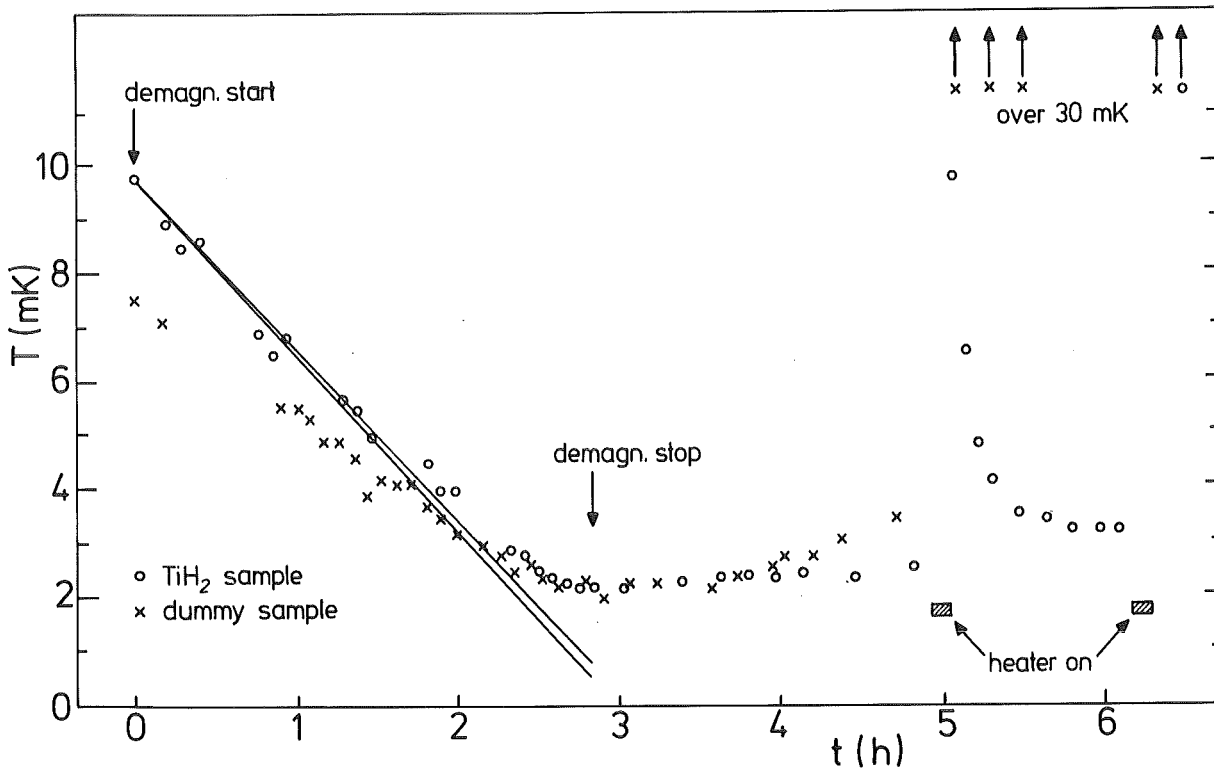
Fig.1: Results of the demagnetization experiments

did however not fall below 2.0 mK. This difference can not be explained by eddy currents, because a calculation allowing for very large eddy currents still comes down to 0.75 mK (upper straight line). We suppose that our thermometer (^{60}Co γ-anisotropy)was not reliable below about 3 mK and that the actual temperature has come below 2 mK. This is confirmed by the following observation. After 5 h we heated the samples with an amount of 0.64 mJ. The nuclei in the dummy sample could not absorb this amount, hence its temperature remained high, whereas the TiH$_2$ sample came back to 3.2 mK after having been heated from 2.6 mK. Theoretically the TiH$_2$ sample could only absorb 0.11 mJ between 2.6 and 3.2 mK. If we suppose that the 3.2 mK are correct, than the starting temperature should have been 1.3 mK instead of 2.6 mK to absorb 0.64 mJ.

We conclude that demagnetized protons in TiH$_2$ can effectively be used as a heat sink at least down to 2 mK. More precise measurements, falling outside the scope of our research program, are necessary to establish the properties at lower temperatures.

6.2.3   INJECTION STUDIES WITH A CYCLOTRON TRAP

P. Blüm, D. Gotta, W. Kunold, M. Schneider, L.M. Simons

The cyclotron trap (1) is a device designed to achieve high stopping densities of exotic atoms in dilute gases with pressures even lower than 1 Torr. The first problem is to inject the charged particle beam into the Trap in a way, that experiments can be done under best conditions. The whole injection process, which is similar to the injection of particles into a storage ring, is divided into two parts: 1) the transport of the beam through an entrance moderator into the focusing region of the Trap, 2) keeping the injected beam inside the Trap and avoiding that the beam hits the entrance moderator again after one or more revolutions.

To inject a beam, whose initial momentum is larger than the 'acceptance momentum' (about 110 MeV/c), at a desired radius, requires a moderator block with a given thickness to slow down the particles of the beam. The injection radius must be less than 140 mm, because of the radial focusing properties of the field. For radii less than 140 mm the field index n is less than 1, which means that particles whose momenta are essentially equal to the equilibrium momentum are focused to a therefore

given equilibrium radius, which must be smaller than the injection radius.
The difference between injection radius and equilibrium radius should not
be too large, to keep the betatron amplitudes small. From injection studies
with the computer code PATRAC (2) and first experimental injection studies
in air as well as studies with alpha-particles im Helium, it turned out,
that the injection radius has to be about 125 mm, whereas the equilibrium
radius is then about 115 mm.

In order to keep the geometrical extension of the beam passing
through the entrance moderator as small as possible, and therefore the
amount of accepted particles of the beam as high as possible, it is
necessary to overlap the acceptance of the Trap and the emittance of the
initial beam. A maximum overlap of the acceptance of the Trap and the
emittance of the beam requires essentially, that an injected beam has to
have a given phase space ellipse. In addition the acceptance of the Trap
as well as the emittance of the beam depend on the plane, where the beam
'sees' the magnetic field. To realise a suitable overlap of acceptance
and emittance in the experiment, it is necessary to shield the incoming
beam with an iron tube from the magnetic field up to a certain plane,
which should be tangential to the rotationally symmetric field to avoid
an azimuthal disturbance of the field. The measured small radial
disturbance was incorporated into PATRAC, allowing more realistic
conditions for the calculations of the now slighly different acceptance
of the Trap.

Fig. 1 shows the calculated vertical acceptance of the Trap with
the actual configuration of the iron shielding compared with the p̄-beam at
LEAR with a distance between the Trap and the last quadrupole of about
3.5 m. To keep the once accepted particles inside the radial focusing
region of the Trap, the beam coming out of the entrance moderator (in-
jection point) must be restricted to a limited range of radial and axial
momenta. At the injection point the beam starts with betatron oscillations,
corresponding to the radial and momentum mismatch and the radial momentum
itself.

Because the energy loss, and therefore the decreasing of the
equilibrium radius, for muons and pions is too small in a gaseous medium,
the beam would hit again the entrance moderator after one of the following
revolutions (Poincaré's Theorem). To avoid this, an inner soft moderator
system (polyethylene foils, some hundred microns thick) was installed. To
achieve then a well concentrated stopping distribution, the absolute value
of the radial momentum must be kept as low as possible. With a suitable
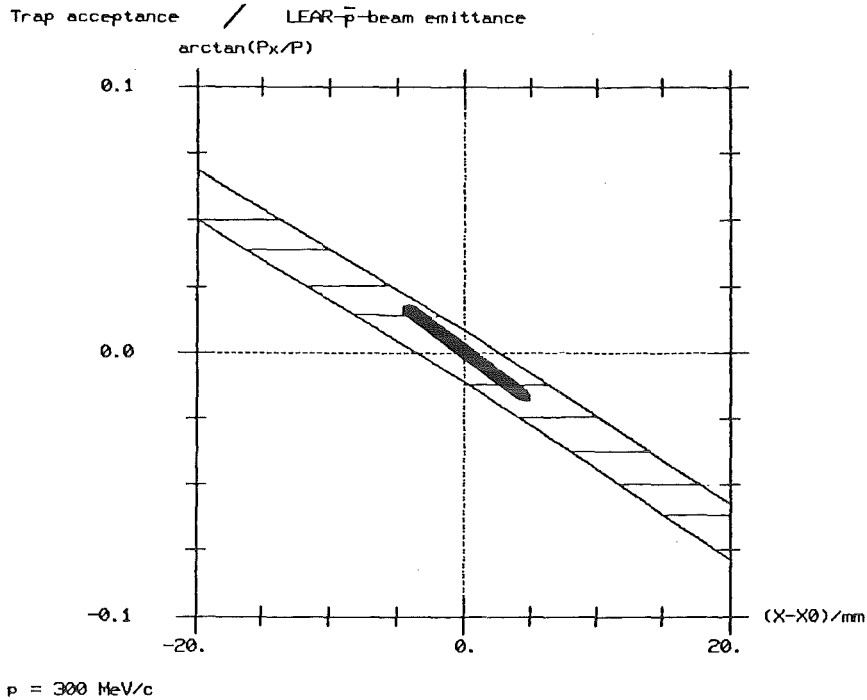
Fig. 1: Vertical acceptance of the cyclotron trap for 300 MeV/c anti-
protons, compared with vertical emittance of the p̄-beam at LEAR
at a distance of about 3.5 m from the window

arrangement of the foils this objective can be reached, thus ensuring that
the absolute value of the radial momentum at the injection point is not
exceeded during the whole slowing down process. Values from about -5 MeV/c
to about -10 MeV/c in combination with the foil are sufficient for the
particles to pass the entrance moderator, and to get a concentrated
stopping distribution.

(1)   P. Blüm, E. Borie, D. Gotta, H. Koch, W. Kunold, M. Schneider,
        L.M. Simons, SIN proposal R8-02.1, and
        P. Blüm, D. Gotta, R. Guigas, H. Koch, W. Kunold, M. Schneider,
        L.M. Simons, CERN proposal PS 175/1980
(2)   W. Kunold, Annual Report on Nuclear Physics Activities 1981/82,
        KfK 3427 (1982)

6.2.4   SLOWING DOWN OF α-PARTICLES IN A CYCLOTRON TRAP

P. Blüm, D. Gotta, W. Kunold, K. Meissner, M. Schneider, L.M. Simons

To slow down particles in a "cyclotron trap" (1) the beam must be
injected into the region of field index n between 0 and 1, where the

focusing properties of the magnetic field force the particles to perform betatron oscillations around equilibrium orbits in the symmetry plane. In a first measurement the incoming particle beam has been replaced by a (collimated) ^{241}Am α-source with an angular distribution of 150 mrad FWHM and p_α = 184 MeV/c momentum. The momentum p_α corresponds to 92 MeV/c momentum for single charged particles and an equilibrium orbit of 11.6 cm for a 3.7 T field in the central region. The α-particles were detected by a cylindrical plastic scintillator rod of 5 mm diameter and 80 mm extension perpendicular to the symmetry plane. The α-source and the detector were mounted opposite in a vacuum chamber. The radial positions of source and detector could be varied countinously from outside in the range of r = 0 to 18 cm (Fig. 1).

Fig. 1: Experimental set-up
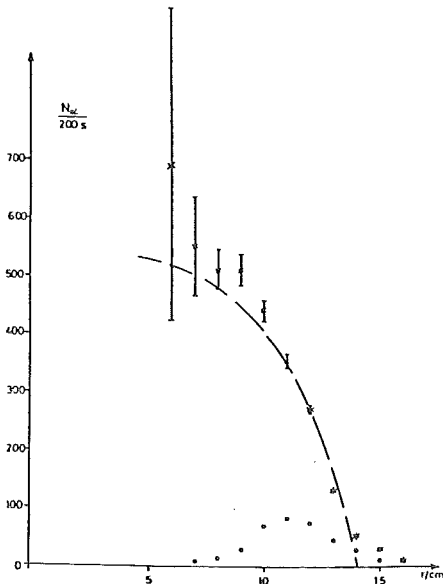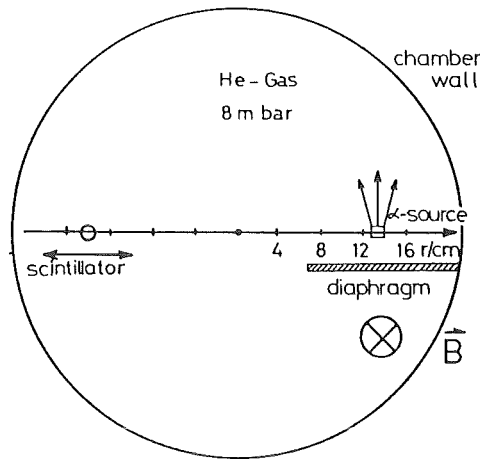
Fig. 2: Radial distribution of the α-particles
⟵   in the center of the He-gas chamber.
o: image of the α-source after 1/2
revolution (with diaphragm), ∗: radial
distribution corrected for detector
efficiency (without diaphragm).
Statistical errors only,
− − : Prediction by the scaling factor
$\sqrt{1-n}$

First the image of the α-source after 1/2 revolution in vacuum was recorded (diaphragm behind the source from r = 7 to 18 cm). Second the motion in a He atmosphere of different pressures was examined. Due to energy loss the particles spiral toward the center. A minimum pressure of 8 mbar is required to protect the α-particles from hitting the back of the source.

Fig. 3: Comparison between predicted and
measured radial distribution of
the α-particles. ⋇ : measurement
(statistical errors only), ● :
simulation without decharging of
the α-particles, o : simulation
decharging taken into account
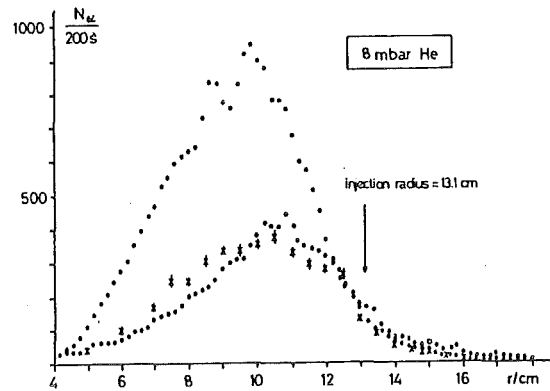
The maximum rate was achieved by injecting 12% outside of the equilibrium orbit (r = 13,1 cm) and the minimum pressure (8 mbar). The intensity increases by the predicted factor $\sqrt{1-n}$ (Fig. 2). The rates are corrected for the detection efficiency of the detector.

The results were compared to a computer simulation. The measured radial distribution at 8 mbar and the simulation with and without decharging of the α-particles taken into account is shown in Fig. 3.

(1)   P. Blüm, E. Borie, D. Gotta, R. Guigas, H. Koch, W. Kunold,
M. Schneider, L.M. Simons, SIN proposal R-81-02.1, and
P. Blüm, D. Gotta, R. Guigas, H. Koch, W. Kunold, M. Schneider,
L.M. Simons, CERN proposal PS 175/1980

6.2.5   FIRST EXPERIENCE WITH THE MAGNETIC SPECTROGRAPH "LITTLE JOHN"

H.J. Gils, J. Buschmann, M. Heinz, J. Krisch, H. Rebel, S. Zagromski,
H. Schlösser[+]

First test measurements have been performed with the magnetic spectrograph "Little John" partly using provisional equipment since some parts of the vacuum system (pumps, acceptance slits, target sluice) and of the control system (1) have not been completed. The main purposes of the tests were to study vacuum properties, reproducibility and constancy of magnetic fields and to obtain rough estimates of the ion optical properties of the spectrograph. The results of these tests are summarized in the following:

- Magnets: The settings of the magnets were found to be close to the design values and the reproducibility was sufficient within the so-far reduced requirements of the tests. No instabilities have been observed. The computer

controlled operation (software not yet realized) is necessarily needed in particular for calibration purposes during the experiments.

- Vacuum system: The design goal of the vacuum system of a pressure of 10^{-6} mbar anticipating a leakage rate of less than 10^{-5} mbar l/sec has been reached only when the focal plane detector was not mounted. The leakage rate of the detector foil (25 µm thickness, 50 x 6 cm² area) separating the vacuum system from the gas volume of the detector was found to be of the order of 10^{-3} mbar l/sec making the installation of an additional pump unit (already considered in the control system (1)) just in front of it necessary in order to reach the vacuum design goal under realistic conditions.
  The use of a cryotrap (2) between beam-line and target chamber was successful in bridging the difference in pressure of more than one order of magnitude between these parts.

- Ion optical properties: The ion optical properties have roughly been studied for one focal plane position FP8 (3). The preliminary values found are for the energy range $E_{min}/E_{max} = 0.8$ and for the momentum resolution (beam spot ⌀ 1 mm, position resolution $\Delta x = 0.8$ mm) $\Delta p/p = 8 \times 10^{-4}$.

These values indicate that already in the present status the design values (3) are closely approached.

(1)   J. Buschmann, F. Deutsch, H.J. Gils, G. Ludwig, D. Manger, H. Rebel,
       K.J. Rist, W. Seith, T. Thouw, O. Walz, contr. 6.2.3
(2)   J. Buschmann, G. Ludwig, unpublished results, Kernforschungszentrum
       Karlsruhe (1981)
(3)   H.J. Gils, KfK 2972 (1980)
       H.J. Gils, J. Buschmann, H. Rebel, S. Zagromski, unpublished results
       (1980)
+   Tandem Labor der Universität Erlangen

6.2.6   CHARACTERISTIC FEATURES OF THE DETECTION SYSTEM OF THE MAGNETIC SPECTROGRAPH "LITTLE JOHN"

S. Zagromski, M. Heinz

The focal plane (FP) detector (1) and its periphery were mounted and tested including operation in the spectrograph. The gas supply (argon/methan, 90/10 %, p = 970 ± 0.2 mbar) and the high voltage were optimized for best resolution of the two position sensitive (PS) detectors and the energy loss (ΔE) detector, respectively. Up to now a position resolution of 0.8 mm (FWHM)

was achieved with an alpha source (^{241}Am, ^{244}Cm, ^{239}Pu, 0.1 µCi) and a collimator of 0.2 x 10 mm² in front of it. The energy resolution of the ΔE-detector was determined with the same source to be 67 keV.

The window foils (25 µm hostaphan) of the FP-detectors burst two times in the spectrograph since they were stretched by gas pressure in the opposite direction than in laboratory tests by air pressure. This can be avoided when taking care that the foils are stretched only in one direction.

Preliminary data acquisition programs were developed which include charge division, display of spectra, particle track projections from the PS detectors and two-dimensional displays for the ΔE- and the scintillation (E) detector. A position spectrum of the first PS detector on the focal plane obtained from alpha particles (mixed Am, Cm, Pu source) is shown in Fig. 1.

In addition to the FP-detector the spectrograph is equipped with an acceptance detector (2) placed between the target chamber and the mechanical acceptance slit. The detector and its supply have been collected and tested in the laboratory with an α-source. Optimal values for gas pressure (isobutane) and anode voltage were found to be 16 mbar and 650 V, respectively. The position resolution was deduced to be 0,6 mm (FWHM), which should be improved furtheron. The efficiency of the detector does not yet fulfill the requirements. Changes of the geometry of the anode and cathode are promising ways to reach the planned detector specifications (2).
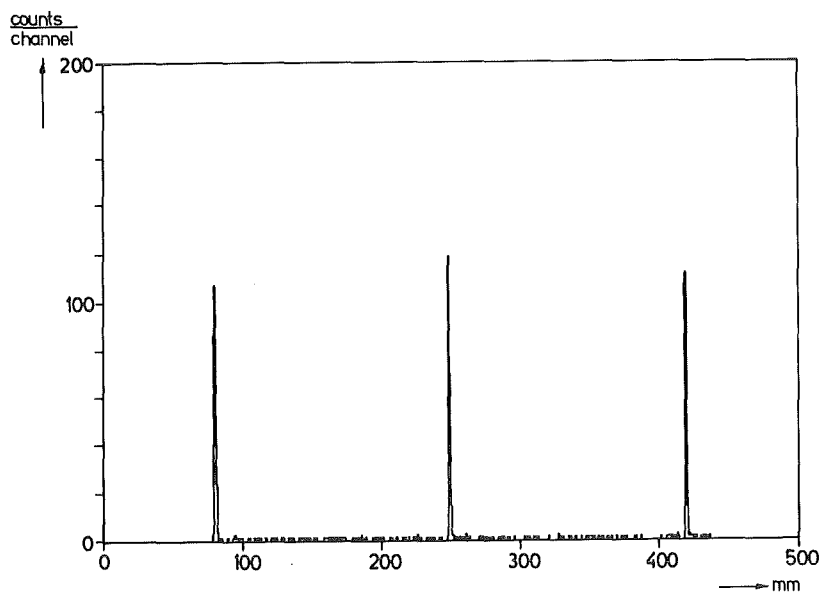
Fig.1   Position spectrum from the first position sensitive detector obtained with an alpha source (^{241}Am, ^{244}Cm, ^{239}Pu, 0,1 µCi) collimated with a slit of 0.2 mm width just in front of the detector at three positions of 170 mm distance.

(1)   S. Zagromski, unpublished results (1980)
       S. Zagromski, H.J. Gils, H. Rebel, KfK 3068 (1980) p. 111
(2)   M. Heinz, H.J. Gils, H. Rebel, KfK 3427 (1982) p. 170
       M. Heinz, Diplomarbeit Universität Karlsruhe (1983)

6.2.7   THE CONTROL OF THE MAGNETIC SPECTROGRAPH "LITTLE JOHN"

J. Buschmann, F. Deutsch, H.J. Gils, G. Ludwig, D. Manger, H. Rebel,
K.J. Rist, W. Seith, T. Thouw, O. Walz

The computer control of the magnetic spectrograph performs the following functions:

1.   Setting and control of the magnetic fields
2.   Setting of the acceptance slits
3.   Setting of the target position and angle
4.   Setting of the detector support
5.   Control of the vacuum system.

Most of the control and driving functions can be done either manually or computer controlled according to the choice of the experimenter. The tentative inclusion of a computer offers useful possibilities like automatic control or documentation of relevant experimental parameters.

The computer control is provided by a CAMAC system connected to a NOVA 2 computer (Fig.1) which is available exclusively for this purpose. The choice between manual and computer control is done by key switches on the control boards.

The magnetic field control and regulating units are the same as for the beam transport magnets of the Karlsruhe isochronous cyclotron (1).

For the mechanical setting of the acceptance slits, the target position, the target angle and the detector support angle the control concepts are similar: The desired positions will be given either by manually operated multi-switches or by the computer via CAMAC. The actual positions will be read by 36 turns absolute angular digitizers with 100 digits per turn. When the difference between the preselected and the actual position values is non-zero, the stepping motors are engaged in the required sense, otherwise they are stopped. In case of manual control, a start signal is needed to activate the comparator.

Experimental hall | 20m Electronic room | 100m Computer room
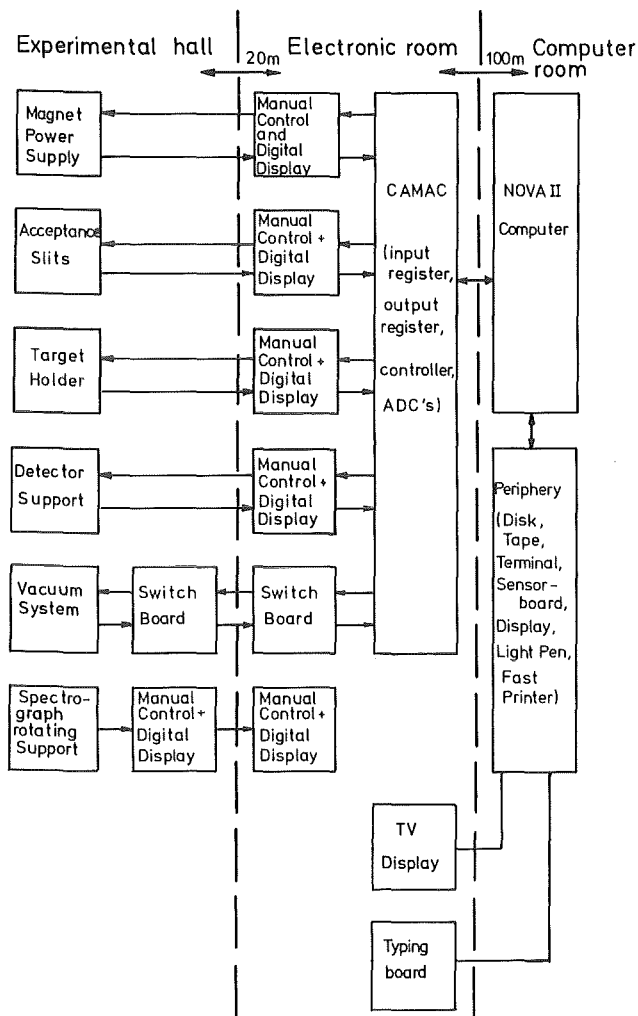
Fig. 1

Block diagram of the computer control system of the magnetic spectrograph

Magnet Power Supply — **Manual Control and Digital Display**

Acceptance Slits — **Manual Control + Digital Display**

Target Holder — **Manual Control + Digital Display**

Detector Support — **Manual Control + Digital Display**

Vacuum System — **Switch Board** — **Switch Board**

Spectrograph rotating Support — **Manual Control + Digital Display** — **Manual Control + Digital Display**

CAMAC (input register, output register, controller, ADC's)

NOVA II Computer

Periphery (Disk, Tape, Terminal, Sensor-board, Display, Light Pen, Fast Printer)

TV Display

Typing board

For the control of the vacuum system, two 19" switch boards are provided, one of which is installed in the experimental hall and the other in the electronic room for remote operation. It allows for simultaneous control of all important functions and to indicate the success of an action. In case of manual control, each manipulation on the push buttons directly drives the corresponding aggregates. In the computer control mode, manipulations of the vacuum system still have to be carried out manually via the switch boards. The corresponding switching signals are generated by CAMAC only if the control program (at present under development, (2)) accepts them to be allowed. In addition, in case of unforeseen events (vacuum leak etc.) the computer response protects the vacuum system against consequential damages.

(1)   W. Kneis, KfK-report 2835 (1979)
(2)   D. Manger, Diplomarbeit 1982

6.2.8 STATUS OF THE LOW ENERGY PION SPECTROMETER PROJECT

H. Matthäy, A. Höhne, K. Kärcher, W. Kluge

The mechanical design and the construction of the magnetic spectro-
meter LEPS (Low Energy Pion Spectrometer) have been completed during the
period of the present report.

A cross-sectional median plane view of LEPS is shown in Fig. 1. The
design parameters have been given elsewhere (1,2). Fig. 1 displays the spec-
trometer in the so called HHH-mode of operation which will be used for test
runs at the πM3 channel (HHH stands for Horizontal dispersion, Horizontal
scattering, Horizontal analysis). Finally LEPS will be operated in the VHV-
mode for which it is optimised (V for Vertical).

The main components of LEPS are a quadrupole triplet Q_1, Q_2, Q_3 and
two dipoles D_1 and D_2, the latter being mounted in a splitpole assembly. The
quadrupoles refocus the target spot onto an intermediate image detector (ac-
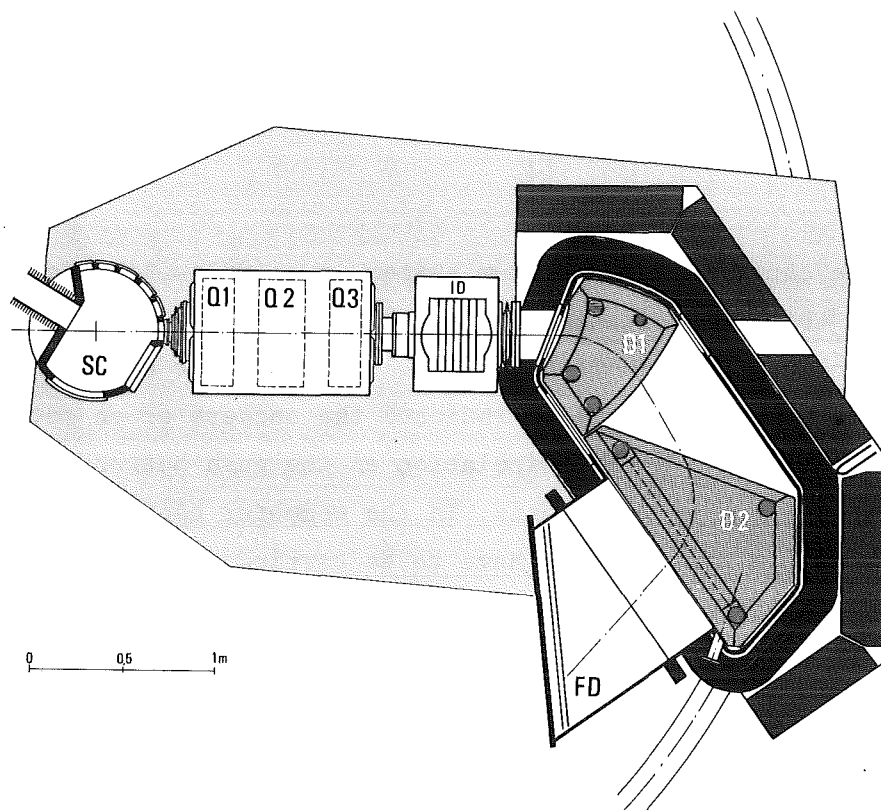
Fig.1: Sketch of the Low Energy Pion Spectrometer LEPS. SC = Scattering
Chamber, Q1-Q3 = Quadrupoles, ID = Intermediate image detector,
D1, D2 = Dipoles of the Splitpole assembly, FD = Focal plane de-
tector. The dashed-dotted curve corresponds to the unphysical
lay-out ray of the code RAYTRACE of H. Enge and S. Kowalski.

tually two multiwire proportional chambers) determining the primary momentum of the incoming pions. The momentum of the scattered pions is analysed by the splitpole using the focal plane detector (a vertical drift chamber (3)) and the intermediate image detector which both measure coordinates and angles of the particle trajectories. This allows detailed software corrections indispensable for a broad range ($\Delta p/p$ = -15,+20%) and large acceptance ($\Delta\Omega \approx 20$ msr) spectrometer.

So far all parts except for the vacuum chamber around the dipoles have been delivered. The pole plates of the two dipoles, as delivered by the manufacturer, had, however, intolerable mechanical deviations from the specifications and had to be remachined.

After the reassembly of the splitpole detailed measurements of field maps will be started. Higher multipole field components of the quadrupoles have proved to be sufficiently low after some shimming.

In the meantime considerable efforts have been paid, together with the SIN beam line group, to the design of the magnetic pion channel for LEPS. The basic requirements to be met by this channel in order to match the design parameters of the spectrometer are as follows:

energy range	30 - 100 MeV
vertical dispersion	$D \approx 5$ cm/(% in $\Delta p/p$)
momentum bite	$\Delta p/p$ = $\pm 1\%$
momentum resolution	$\lesssim 10^{-3}$ [+)]
flux	$\approx 5 \cdot 10^{6}$ π^{+}/s [+),++)]

[+)]   for the full solid angle,

[++)]   at 50 MeV for a proton current I_p = 100 μA and full momentum bite.

After thorough studies of numerous possible variants for pion beams the most promising solution was found for the existing πE3 channel by adding a 90° bending magnet, four quadrupoles and one sextupole. Before finally freezing the beam parameters careful raytrace calculations including both the beam and the spectrometer have still to be carried out.

(1)   H. Matthäy, W. Kluge, H.A. Thiessen
       Annual Report on Nuclear Physics Activities
       KfK 3427(1982)208
(2)   W. Kluge, H. Matthäy
       SIN Jahresbericht 1982, p. JB23
(3)   J. Jaki, H. Matthäy, A. Höhne, K. Kärcher, U. Klein, W. Kluge
       Contribution to the present Annual Report on Nuclear Physics Activities
       1982/83, p. 149

6.2.9 A FAST µP-CONTROLLED DATA ACQUISITION FOR SPECTROSCOPY EXPERIMENTS

T. Köhler, U. Raich[+], J. Hauth

In experiment PS-176 at the Low Energy Antiproton Ring (LEAR) at CERN we had to face new problems in the readout of the experimental data due to extremely high event rates (10^4) and due to the unusual beam structure of LEAR (15 min beam - 3 min pause). 6 semiconductor detectors are used to look for atomic X-rays from antiprotonic atoms. Each of these gives energy and time information. Since no other detectors are needed by the experiment, aside from scintillation counters used for trigger purposes, the complete information of an event may be stored in 2 dimensional spectra as long as one does not consider coincidence events. This sort of data structure is typical for spectroscopy experiments which are usually read out with multichannel analysers (MCAs). Since we are using 6 detectors covering different energy ranges, 6 MCAs including magnetic tape stations would be required. Such a set-up seems unreasonable because of the high cost. MCAs are also not able to cope with coincidence events.

The data acquisition system developed in our group uses a micro-computer system acting like a collection of 6 MCAs. The microprocessor system consists of a VME crate containing 2 Mbytes of memory and a CPU card with a MC 68000 microprocessor. The VME bus has been developed and standardized by several big microcomputer companies (Motorola, Mostek, Philips etc.). The large memory is necessary to allow the generation of 2 dimensional spectra with much higher precision than could be obtained with MCAs. The microprocessor program simulating the MCAs is a rather short assembler language program wich runs extremely fast. The readout speed obtained is comparable to MCAs (40 µs/event). One big advantage of the system is the capability of taking coincidence events by simply storing them into a memory region reserved for that purpose. The coincidence events may then later be evaluated offline.

The interfacing of the VME system to the experiment is done through CAMAC. CAMPORT, a CAMAC module developed in our group, allows the micro-processor to act as an auxiliary crate controller when used in conjunction with an A2 crate controller. This means that the MC 68000 may read the energy information stored in CAMAC ADCS and the time information stored in

CAMAC TDCs. It may also execute any other CAMAC funtion desired. On the
other hand CAMPORT may be used as a normal CAMAC station executing CAMAC
commands issued by a minicomputer (a PDP-11 in our case). The CAMAC
commands implemented in CAMPORT allow the PDP-11 to read and write VME
memory and to interrupt the MC 68000. Since there are no pripherals
connected to the VME system the spectra accumulated must be transferred
to the PDP-11 before they can be visualized and saved onto magtape. This
transfer is done during the beam pause using CAMPORT. Once the data are
on the PDP-11 disk (they fill one complete RK05J disk!) the microprocessor
may continue to readout the experiment while at the same time the PDP-11
processes the spectra accumulated during the spill before.

Fig. 1: Photograph of the data acquisition
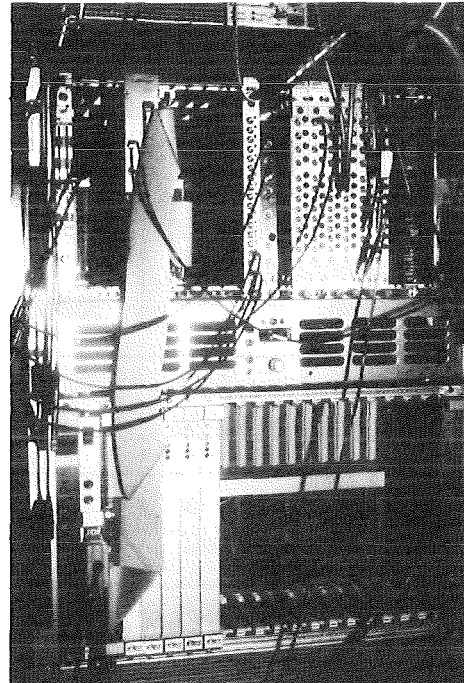
system

During this year the system has been debugged and extensivly
tested. It has taken it's first antiproton data in August 1983. Fig. 1
shows a photograph of the system.

+   CERN, Geneva

6.3 ACCELERATORS

6.3.1 OPERATION OF THE ISOCHRONOUS CYCLOTRON

F. Schulz, H. Schweickert

During the period of this report the machine has been in full operation (see Tables I,II). Even with a large total of available beam time of 7667 h for experiments we could not fulfill all the beam time requirements of our users. At the moment the machine is overbooked by more than 20 %. Table II displays the user statistics and the share of beam time between various activities.

Cyclotron Operational	With internal Ion Sources		With external Ion Sources		Total	
For Experiments	4759 h	85.6 %	2407 h *	80.8 %	7166 h	83.9 %
Beam Development						
Testing new Components						
Developments for Isotope						
Production	339 h	6.1 %	162 h	5.4 %	501 h	5.9 %
Total Time of Operation with the Beam on Targets	5098 h	91.7 %	2569 h	86.2 %	7667 h	89.8 %
Scheduled shut-down for maintenance, Repair and Installation	131 h	2.4 %	87 h	2.9 %	218 h	3.1 %
Unscheduled shut-down	329 h	5.9 %	324 h	10.9 %	653 h	7.6 %
Total Shift Time	5558 h	100.0 %	2980 h	100.0 %	8538 h **	100.0 %

* Polarized Deuteron 1440 h; ^{6}Li^{3+}-Ion (156 MeV) 967 h

** The real time of 8760 h is achieved by adding a total of 9 days shut down 24.12.82 - 2.1.83

Table I   Statistics of the cyclotron from July 1982 to June 1983

The machine operation in the preceding year was rather strenuous because of the increased demand for beam time to produce medical isotopes and the high interest in injected particles (^{6}Li^{3+}, d↑). To combine both activities, the machine has to be adjusted for high currents from Monday to Thursday, whereas over the weekends the axial injection system has to be implemented. These boundary conditions not only impose a lot of time critical work on the operating group, but sometimes also lead to ineffective beam times for

MATERIAL RESEARCH 1,2%

NUCLEAR CHEMISTRY 2,2%

NUCLEAR MEDICINE 8,9%

ENGINEERING 8,8%

NEUTRON PHYSICS 20,0%

NUCLEAR SPECTROSCOPY 1,3%

SOLID STATE PHYSICS 31,6%

NUCLEAR REACTIONS 25,9%
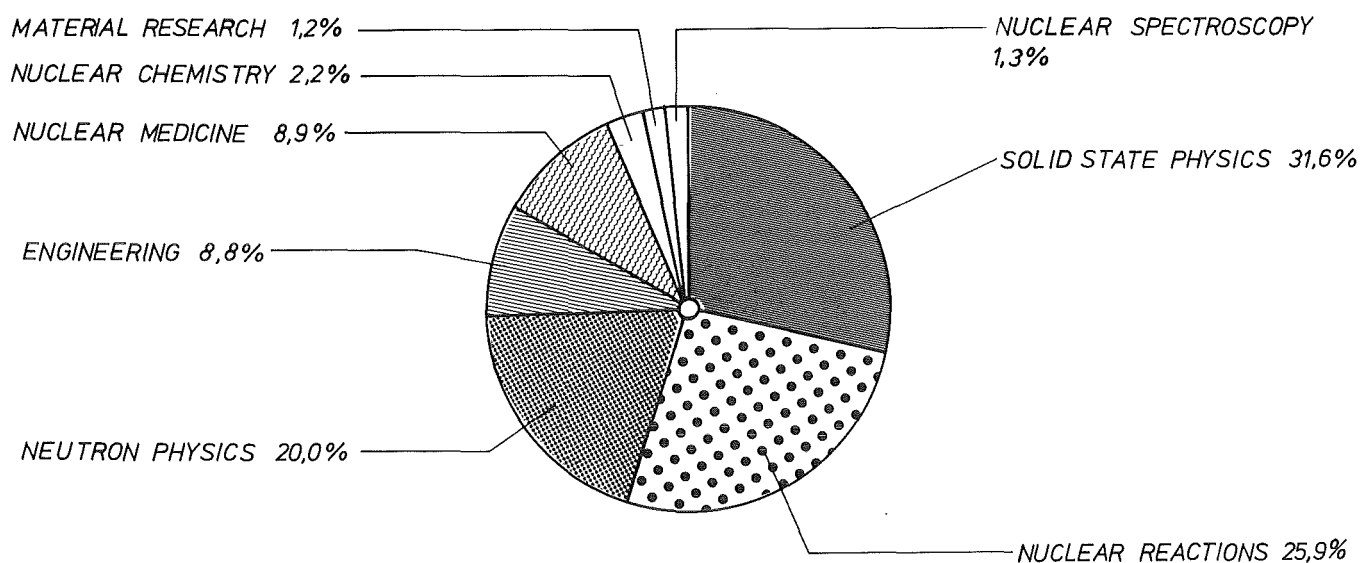
KfK-Karlsruhe Users

Institut für Kernphysik I	1436 h	20.1 %
Institut für Kernphysik III	768 h	10.8 %
Institut für Nukleare Festkörper-Physik	520 h	7.2 %
Institut für Radiochemie	81 h	1.1 %
Labor für Isotopentechnik	72 h	1.0 %
Institut für Heiße Chemie	47 h	0.6 %
Technologie Transfer	36 h	0.5 %
	2960 h	41.3 %

External Users

Freie Universität Berlin	849 h	11.7 %
Technische Universität München	665 h	9.2 %
Max Planck Institut für Kernphysik Heidelberg	589 h	8.2 %
Universität Erlangen	435 h	6.3 %
Universität Bonn	117 h	1.5 %
Universität Ulm	83 h	1.1 %
GSI Darmstadt	82 h	1.1 %
IRC Ispra	71 h	1.0 %
Universität Konstanz	71 h	1.0 %
Universität Mainz	36 h	0.5 %
Medizinische Hochschule Hannover	31 h	0.5 %
Universität des Saarlandes	8 h	0.1 %
Universität Hamburg	6 h	0.1 %
Transurane Karlsruhe	3 h	0.1 %
Universität Münster	3 h	0.1 %
	3049 h	42.5 %
Aktivierung von Maschinenteilen	571 h	8.0 %
Commercial Iodine-123-Production	392 h	5.5 %
Commercial Rb-81-Production	194 h	2.7 %
	7166 h	100.0 %

the nuclear physics group because of the short available times for the ma-
chine optimization (beam quality and current). The situation will improve at
the end of 1983, when the new compact cyclotron takes over the isotope pro-
duction.

At the end of 1982 it was decided to replace the existing self-excited
rf-system by a modern driven amplifier system. A 100 kW amplifier for a fre-
quency range of 20-40 MHz was ordered from ZARAT (Warsaw) and will be de-
livered in late 1983. The amplifier will be connected to the cyclotron by
a 30 m long 50 Ω transmission line.

6.3.2   STATUS OF THE KARLSRUHE CP-42H⁻ CYCLOTRON (KAZ)

J. Möllenbeck, H. Schweickert

The cyclotron was delivered with a delay of 3 months in August 1982
to Karlsruhe. In the beginning the installation by the TCC-group was very
effective but at the end of 1982 it had fizzled out, as TCC found itself in
financial problems and could not finish the project. In April 1983 we de-
cided, after a hard battle with the bonding company, to complete the cyclo-
tron installation by ourselves. All hard- and software are now operating
rather well and since the end of July the beam can be extracted in an energy
range from 30 to 42 MeV on the D-side. In this energy range the beam is
slightly bent downward in the fringing field, resulting in an angle of
0.37° with respect to the axis of the beam guiding system. This small angle
has been corrected by introducing a 50 cm long electrostatic deflector (10 kV/
cm) inside the cyclotron vacuum chamber. Figs. 1 to 6 illustrate the activi-
ties at the compact cyclotron during the period of report.

Fig.1   Rolling in the cyclotron
magnet into the vault (August 1982)
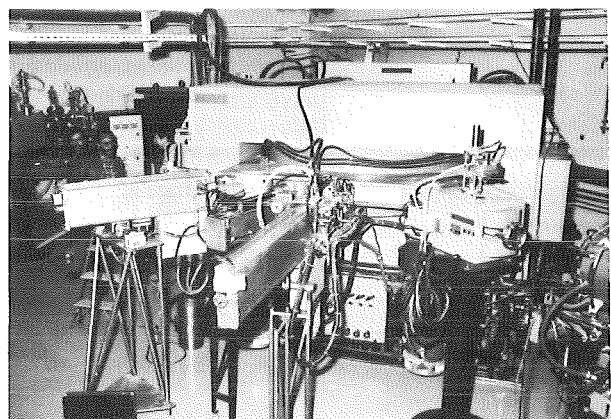
Fig.2   View of the CP-42H from the
side of the ion source
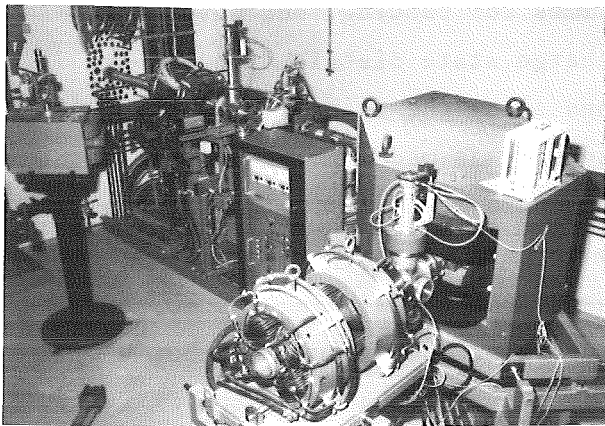
Fig.3 First part of the beam guiding system manufactured by Bruker
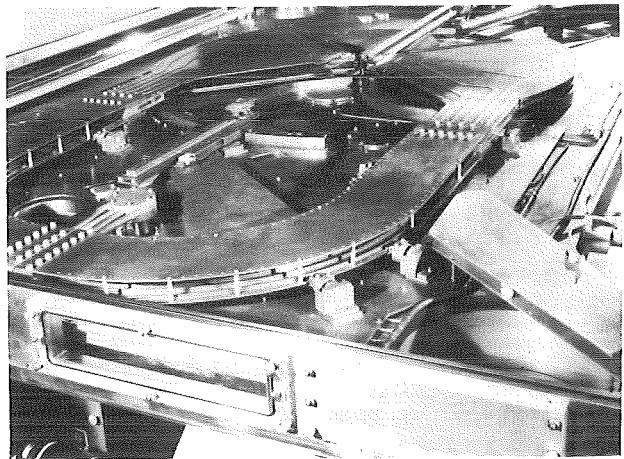
Fig.4 View into the vacuum chamber on the D-side, showing part of the D-system, stripping foil mechanism, and electrostatic corrector.
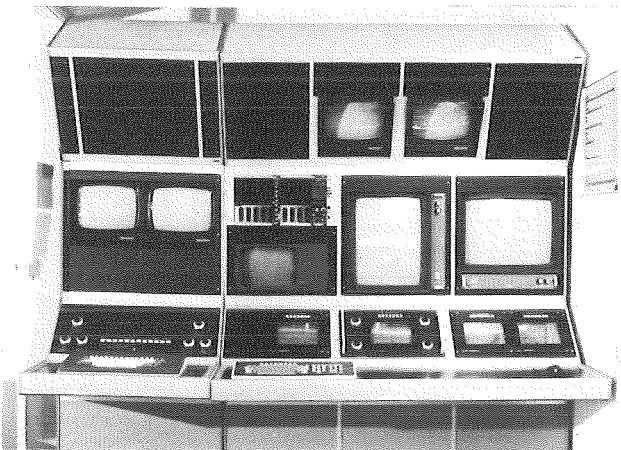
Fig.5 The main operator's console for the CP42H cyclotron and the beam guiding system
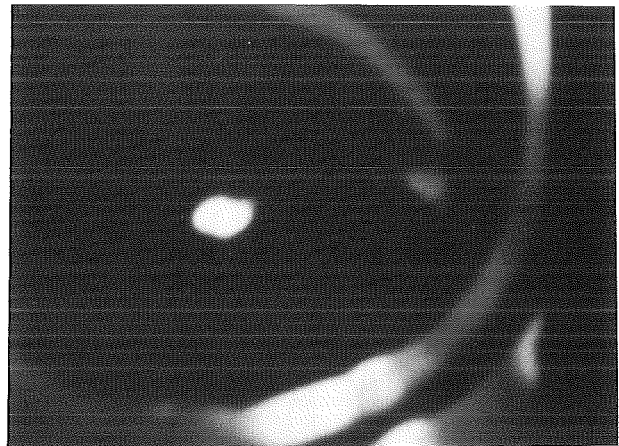
Fig.6 Beam at the position of the iodine production target.

6.3.3 ION SOURCE DEVELOPMENTS

V. Bechtold, L. Friedrich, H.P. Ehret, J. Kaltenbaek, L. Wiss, P. Ziegler

Three external ion sources are operated at the Karlsruhe cyclotron. The Penning source for Li^{3+} ions and the Lambshift source are extensively used, delivering some tens of nA of 26 MeV/A particles for nuclear physics experiments. The ECR-source HISKA is designed to deliver highly charged light ions, although at present only fully stripped light ions can be accelerated

by the cyclotron. A sudden rise of the liquid He evaporation rate of the superconducting coils allowed only short times for testing, but nevertheless progress was made concerning quality and charge state distributions of the extracted beam. In order to extract the ions along the axis of the longitudi - nal magnetic mirror field the extraction system was made movable in the ra- dial direction and adjusted observing the electron flow coming from the plas- ma. In the new construction, more care was taken over the pumping speed in the extraction region as well as in the charge state analysing system, for which a new Wien filter with permanent magnets inside a vacuum chamber was built. This resulted in a remarkable rise of the mean charge of the extracted N-ions from 2.8 to 3.8. Charge state spectra (Fig.1) show that now most of the extracted ions have only two electrons.
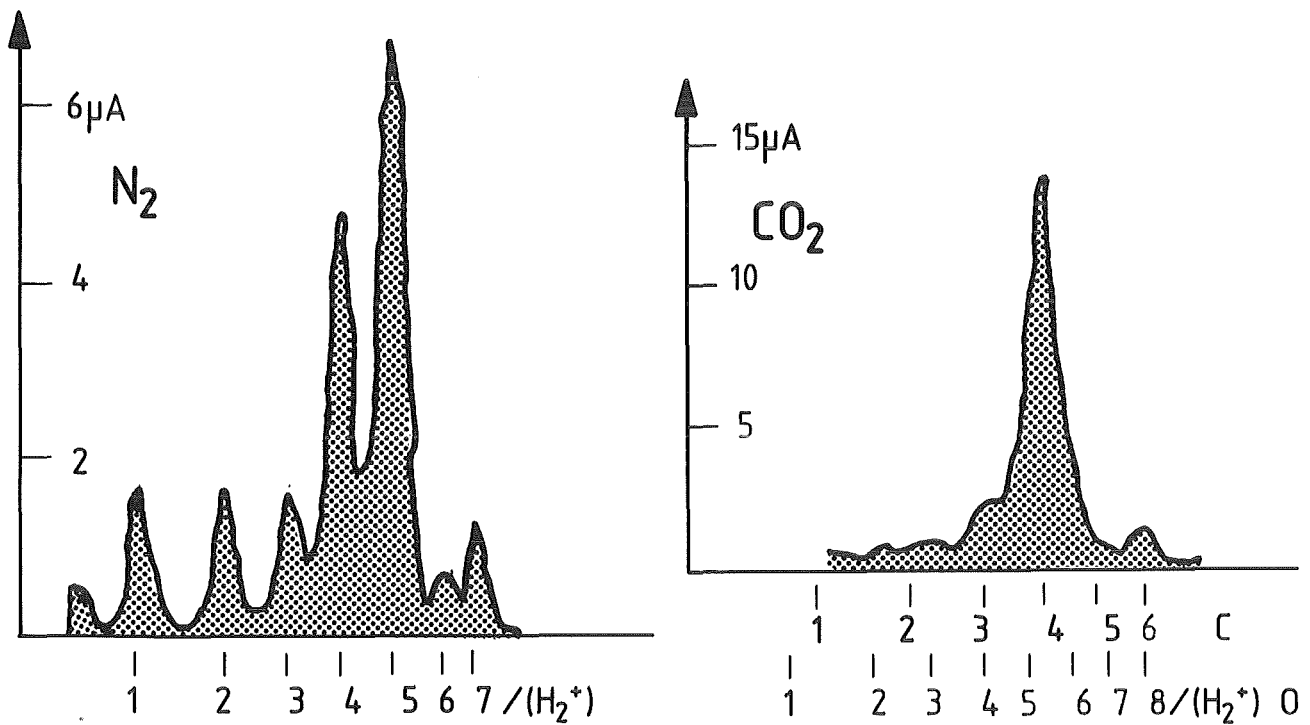
Fig.1   Charge state spectra of the extracted beam from HISKA operated
with N_2 and CO_2

The ECR-technique delivers high plasma density with low neutral back- ground. This allows the extraction of low velocity deuteron beams of about 10 mm diameter. This and the magnetic field might be favourable to overcome the space charge problems in the Lambshift source. First experiments in this field led one to expect a substantial gain of intensity, but it is not be- lieved that one can reach the intensity of the atomic beam source. So it was decided to replace the Lambshift source by an atomic beam source.

Experiments with Li-vapour in the ECR source p-HISKA demonstrated that at least 10 % of the extracted Li-ions were in the 3+ state. A special ECR-

source for Li-ions has been constructed and will be assembled in the near future.
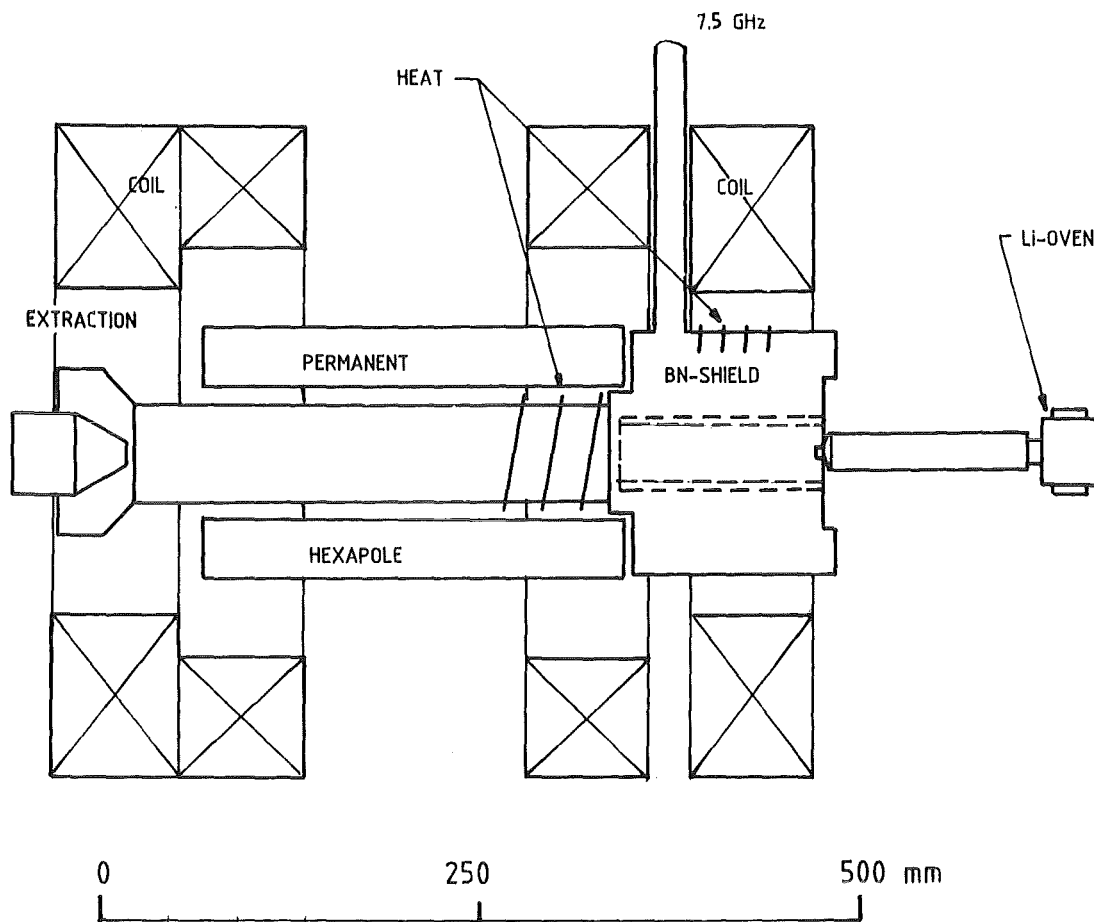
Fig.2   LISKA, the ECR source for Li^{3+} ions uses an external hexapole to enable heating of the walls to achieve the right vapour pressure of Li. At least 30 μA of Li^{3+} are expected.

6.3.4   ON THE POSSIBILITY TO CONVERT THE KARLSRUHE ISOCHRONOUS CYCLOTRON TO AN ENERGY VARIABLE MACHINE

J. Schwabe, H. Schweickert

In context with the discussions of the future use of the Karlsruhe Isochronous Cyclotron for nuclear physics it turned out, that for any post-accelerator project (1,2) a better flexibility of the injector is desirable. The actual machine is a simple FFAG-cyclotron for Z/A = 1/2 particles with a

Modified Cyclotron:

K=40 – 84 (Protons)   K=50 – 130 (Z/A=0.45 – 0.66)

Particle	Energy in MeV/Nucleon	
p, p†	40 – 84	h = 2
p, d†, Z/A = 1/2	18 – 35	h = 3
$^3H^+$	10 – 15	h = 3
$^3He^{2+}$	32 – 60	h = 2 or 3
$^6Li^{2+}$	11 – 15	h = 4
$^{12}C^{5+}$	18 – 24	h = 3
$^{14}N^{6+}$	18 – 24	h = 3
$^{16}O^{7+}$	19 – 26	h = 3
$^{20}Ne^{9+}$	19 – 28	h = 3

Particle	I [µA] extracted	Ion Source
p, d $\alpha, ^3He^{2+}$	80 – 100 30 – 50	Internal PIG
Z/A = 1/2 Z/A = <1/2	0,01 – 3 0,2 – 2	External HISKA
d†, p†	1 – 5	Atomic Beam (ordered)
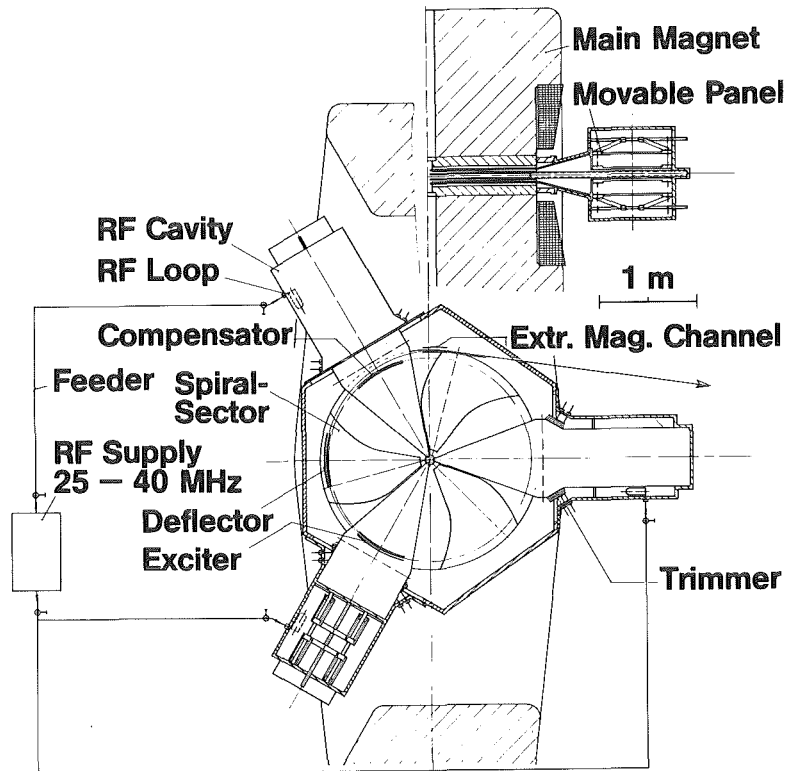
Fig. 1: Schematic diagram of the planned modification of the cyclotron, showing the new pole- tips and the resonators. All other components can be taken over from the "old" machine.

maximum energy of 26 MeV/Nucleon. The main design goals for the modified machine are:

1. Acceleration of protons up to an energy of ≥ 70 MeV.

2. Possibility for the acceleration of only partly stripped light ions, giving us at least one order of magnitude larger extracted currents for Lithium up to Neon ions.

3. Energy variability of a factor of two.

In the last months the theoretical basis for such a modification has been worked out. It could be shown, that by only exchanging the pole tips and the rf-system the above mentioned goals can be fulfilled.

The original straight Thomas sectors have to be replaced by spiraled ones. The spiral starts at 50 cm and is increased slowly, according to the beam dynamics calculations, up to 32°. The three-fold symmetry is maintained.

The rf-system has to be changed from the self-excited configuration, using a vertical transformation line to couple the 3 dees in the center, to a configuration where each dee is separately coupled with a special feeder to a common rf-amplifier. The maximum power level is 90 kW for 3 dees including the feeders and the coupling system for a D-voltage of 50 kV. For the second harmonic operation the second dee gets a phase shift of 180°. The frequency range of 25 - 40 MHz is adjusted by two vertical trimmer plates with a maximum lift of 15 cm.

(1)   E. Poth, this Annual Report, p.192
(2)   H. Schweickert, Ninth international conference on cyclotrons and their applications, Caen University, France, 1981

6.3.5 ISOTOPE PRODUCTION FOR MEDICAL APPLICATIONS

P. Kernert, J. Peters, H. Schweickert

Since the isotope production at the new compact cyclotron (KAZ) will start in autumn 1983, the installation of the isotope production targets at this facility were started while continuing the routine production with the Isochronous Cyclotron. The status of the various activities is as follows:

^{123}I The demand for ^{123}I again increased during the period of this report. In total, 846 batches were produced with a total activity of 38 Ci. They were sent to 10 hospitals and to 3 pharmaceutical firms where the labelling of more complex radiopharmaceuticals like hippuran, amphetamine, fatty acids etc. is carried out.

An irradiation facility for ^{123}I has been built at the KAZ. The target holder and the transportation system are fully compatible with the existing system. So, the already existing hot cell for dry-distillation and distribution needs no modification.
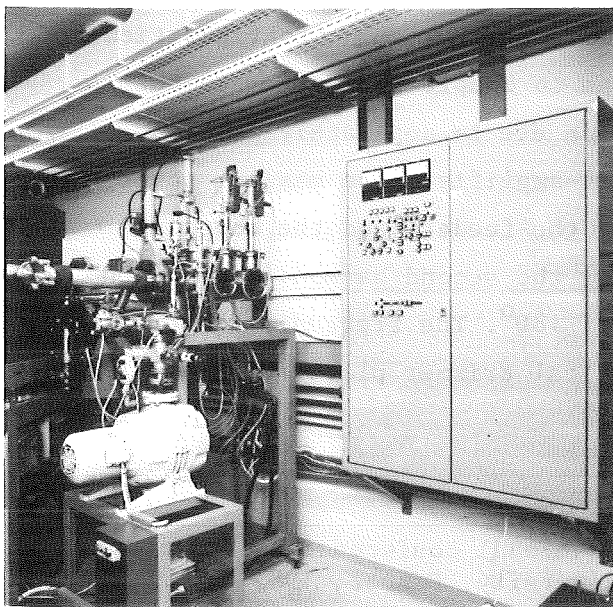
Fig.1 ^{123}I irradiation facility at the compact cyclotron

$^{81}Rb/^{81m}Kr$-Generator $^{81}Rb/^{81m}Kr$-generators are being produced two times per weak since November 1982. In total, 216 generators ($\cong$ 6.5 Ci ^{81}Rb) have been delivered for medical use. Additionally, 4 generators were produced for technical tracer experiments in nuclear reactor safety studies, each of them containing about 150 mCi of ^{81}Rb.

Some changes in the cooling and target handling system improved the stability of the entrance foil. The target assembly for the compact cyclotron

is completed and installation will start in August 1983.

^{201}Tl   To improve the chemical processing and to assure the radiochemical purity 12 Tl targets were irradiated and sent to Hoechst. One of these was irradiated at the JULIC-cyclotron of the KfA Jülich. Furthermore, seven batches were produced to develop an independent chemical process at the cyclotron laboratory in order not to sell the ^{201}Pb but the final product ^{201}Tl. Thus, only the pharmaceutical control, the distribution and the marketing is done by the industrial partner.

The production target system is being installed at the KAZ facility. In order to ensure the reliability, two identical targets can be connected to the beam-line by remote control.
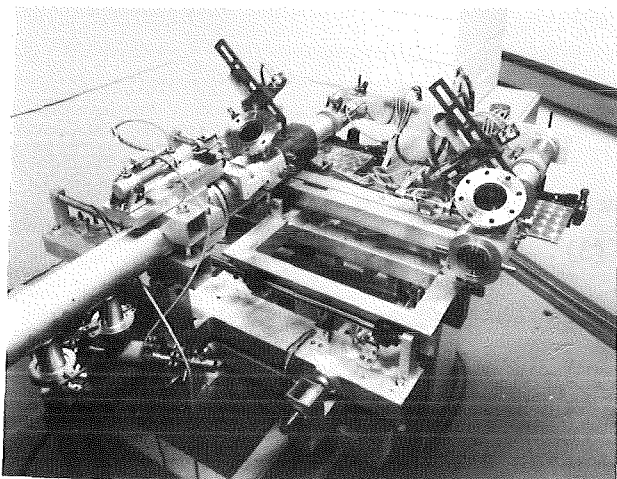
Fig.2

^{201}Pb production target and standby target

6.3.6   STATUS OF THE ELECTRON COOLING DEVICE FOR LEAR

L. Hütten, H. Poth, A. Wolf, H. Haseroth[+], C.E. Hill[+], (1)

The construction of the LEAR electron cooler has advanced considerably in the past year. A description of the system has been given in the last annual report.

The present set-up is shown in Fig. 1. The high voltage platform is installed next to the cooler magnet. A subassembly of the vacuum system has been set-up for the determination of the achievable vacuum conditions with cold and hot electron gun and for the study of the performance of a

1 Electron gun
2 NEG - pump chamber
3 Pick-up station
4 Torold chamber
  with pump and diagnostic ports
5 Central drift tube

6 Collector drift tube
7 Collector
8 Pumping group
9 Solenoid
10 Torold

1m
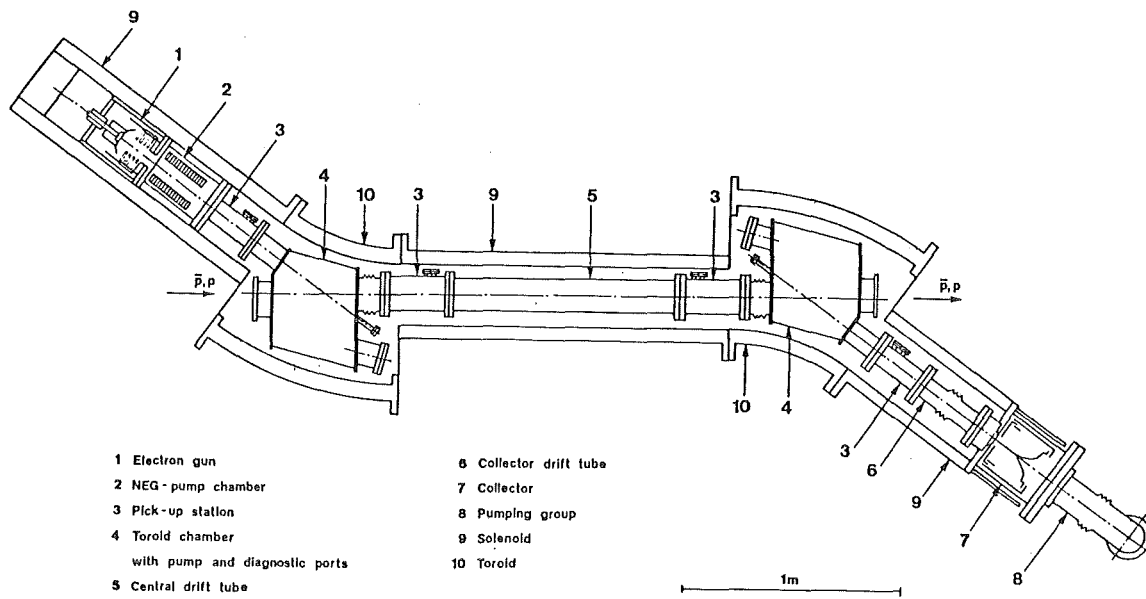
Fig. 1   LEAR electron cooler

new type of NEG-pumps (2). The measurements of the main magnet field
properties are completed and evaluated (3).

The LEAR electron cooler will be completely controled by an LSI 11
computer, CAMAC data acquisition and Fiber optics transmission between the
high voltage platform and the ground level. This system is to be completed
in the near future. During the next months an electron beam will be
generated and its properties will be studied using the subassembly. The
full system will be assembled by the end of 1983.

(1)   contributed paper to the 12th Int. Conf. on High-Energy Accelerators
       Fermilab (1983)
(2)   This Annual Report, p.191
(3)   This Annual Report, p.189

+   CERN, PS Division

6.3.7 THE MAGNETIC FIELD PROPERTIES OF THE LEAR ELECTRON COOLER

L. Hütten, H. Poth, A. Wolf

The field of the magnet assembly to be used for electron cooling at LEAR (solenoids and toroids from Initial Cooling Experiment ICE) has been investigated by careful field mapping. The properties of the longitudinal field guiding the electron beam deserve attention under the following aspects:

- transverse electron temperature: electron motion through an in-homogenous field excites cyclotron rotation in the transverse degrees of freedom;

- electron-proton alignment: the benefit that in practice can be gained from the strong magnetic cooling force depends on the straightness of the field lines in the cooling region; minimal rms variation of the field angle along the common trajectory of electrons and protons is crucial.

The guiding field was measured in a volume with a cross section of 3 x 3 cm^2 around the electron beam axis which is 4.5 m long and bent twice, in the toroids. A Hall plate field scanner designed for the mapping of dipole magnets at the CERN EP division (1) was slightly modified and used to obtain separate field maps of all cartesian components, in ten rectangular boxes covering the forementioned measuring region. In total, the field components were measured at appr. 26000 points. For merging these maps into a consistent overall field table, a special procedure has been developed in this work that includes careful survey and the correction of errors inherent to Hall-probe measurements (2).

Fig. 1 shows the field components longitudinal (a) and transverse (b,c) to the electron beam along the beam axis, and on trajectories displaced from the beam axis diagonally by appr. 3 cm in the transverse plane. The shaded areas in Fig. 1 illustrate the non-uniform transverse field shape due to variations of the longitudinal field strength. It demonstrates the improvement we achieved by mounting additional coils at both ends of the cooling solenoid where, otherwise, a field shape more similar to that measured at points 2 and 3 would appear.

Next steps in employing the results of the magnetic measurements are:
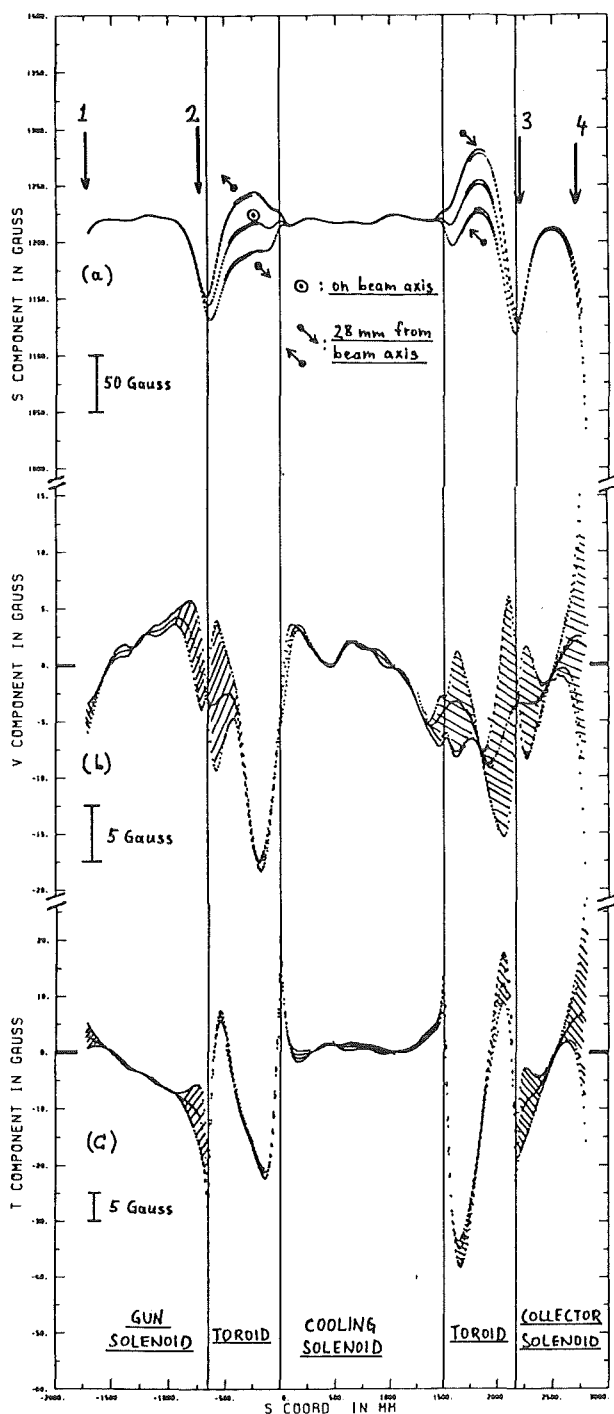
Fig. 1: Magnetic field components along the electron beam. S = path length along the beam.

- design of correction coils removing uniform transverse components in the cooling solenoid,

- calculation of electron trajectories for a drift motion in the measured field.

(1)   O. Runolfsson: Magnet Measurement in High-Energy Physics Experiments, Inivited paper, 6th Int. Conf. on Magnet Technology, Bratislava (29.8.-2.9.1977)

(2)   L. Hütten, H. Poth, A. Wolf, The magnetic field properties of the LEAR Electron Cooler, KfK report (in preparation)

6.3.8 ULTRA HIGH VACUUM TEST MEASUREMENTS ON THE LEAR ELECTRON COOLER

L. Hütten, H. Poth, A. Wolf

As the $\bar{e}$-cooler will be a highly gas producing device special effort has to be made in order to meet the extraordinary vacuum conditions of the LEAR, that is an average pressure of about 3×10^{-12} mbar in the beam area. This and the fact that there will be no access for a vacuum pipe into the $\bar{e}$-gun part where the greatest part of the gas produced by the cathode has to be trapped focussed the vacuum-pumping on the application of getters. A special device was made with some 5 1/sec getter pump units of the same Al-Zr getter material that is to be used in LEP (non evaporable getter NEG). The NEG getter traps the gas molecules of the ultra high vacuum selectively on its surface until saturation which stops the pumping process;that means increase of the partial pressure of the gas. The surface has to be activated again by heat treatment which provokes the diffusion of the gas molecule into the bulk or releases it into the space depending on the sort of gas trapped. Thus the physics of gettering implies that getters have to be activated and regenerated from time to time in a strictly observed process that has to be optimized by experience.

The construction of the experimental set up is shown in Fig. 1. The other pumping facilities are a 100 1/sec Varian ion getter pump and a 400 1/sec turbomolecular pump that was separated from the recipient by a UHV-valve after preevacuation and bake-out cleaning.

The first part of the measurements was to provide the fundamental data for the calculation of the conductance and effective pumping speed in various points as well as the degas-rates of the cathode. They were made without NEG integrated. The degas-rate of the cathode at $1060^{\circ}C$ was found to be about 2×10^{-6} mbar 1/sec, the greatest part of it being CO. In the second part of the measurements NEG was integrated to study its influence upon the vacuum.

After activation a final pressure of 6×10^{-12} mbar was reached with ion pump in operation and cold cathode. A long term run with cathode heated was made with various pumping conditions. The results for the final pressure are:

- with cold cathode, NEG, and ion pump 6×10^{-12} mbar
- with hot cathode, NEG, and ion pump $2,6 \times 10^{-10}$ mbar
- with hot cathode and NEG 2×10^{-9} mbar

Mass spectra were taken to measure the components of the degas-flow and the saturation behaviour of the NEG. Further measurements with e⁻ beam under final operation conditions are being prepared and will concern the optimal NEG operation as well as final vacuum equipment to match LEAR.
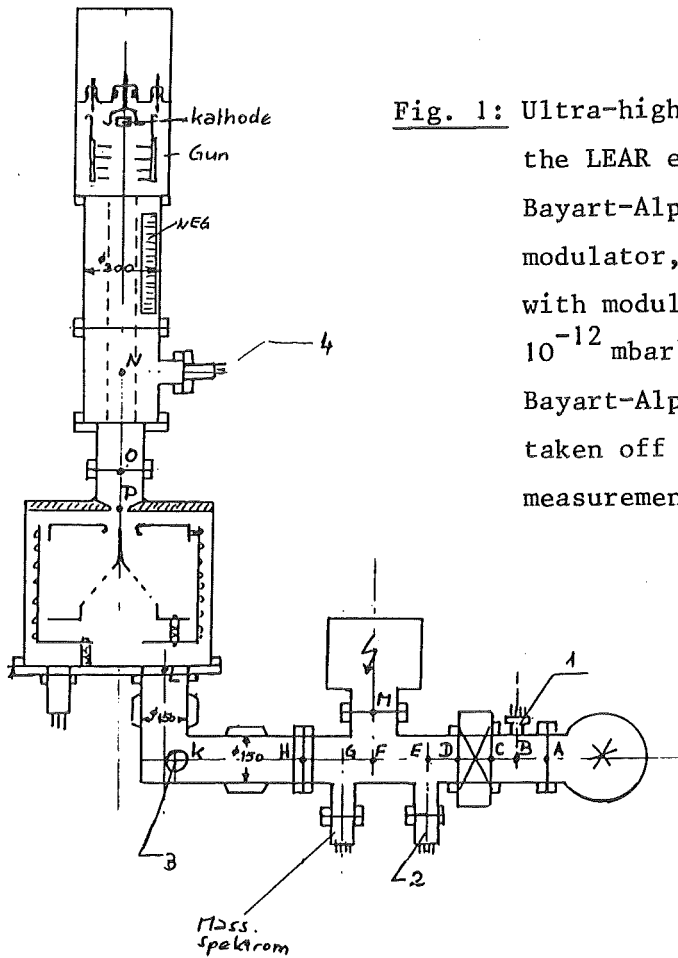
Fig. 1: Ultra-high vacuum measurements on the LEAR electron cooler. 1 = Bayart-Alpert gauge without modulator, 2 = Bayart-Alpert gauge with modulator (range down to 10^{-12} mbar), 3 = UHV-Penning, 4 = Bayart-Alpert gauge as 2 (was taken off for hot-cathode-measurements).

6.3.9 CONSIDERATIONS ABOUT AN ELECTRON COOLED STORAGE RING FOR MEDIUM ENERGY (POLARIZED) PROTONS AND LIGHT IONS

H. Poth

The recent progress in accelerator technology (particularly in beam cooling and the application of internal cluster beam targets), the evidence for dibaryon resonances and the need for high precision experiments in medium energy and nuclear physics initiated a first study on a cooler and storage ring for polarized protons, deuterons and for light ions. We consider the basis for such a project at the KfK very favourable for the

following reasons:

- The KfK-cyclotron could be used after slight modifications as an injector. The developments of different types of ion sources of the cyclotron group are recognized. Applying this experience high flux beams of polarized protons, deuterons and light ions could be anticipated. Moreover there exists a profound knowledge in accelerator physics at the KfK.

- We have collaborated with CERN during the ICE-electron cooling experiments. The gained experience was deepened during the development of LEAR at CERN. Presently we construct in collaboration with CERN the electron cooler for LEAR. The technical and physical boundaries in ICE and LEAR are very similar to those arising from the scheme discussed here.

- The cluster beam technology was pioneered in IKVT at KfK and served as a model for many internal cluster beam targets applied in various accelerators today. A configuration of an internal target for LEAR on the basis of such a cluster beam was worked out. The implications of the operation of this internal target were studied in detail in close collaboration with CERN. A similar target could be used in the machine discussed here. It would have to operate under similar but less restrictive conditions as in LEAR.

- There is a large community of present cyclotron users from the KfK and outside institutes interested in such a facility. There exists a strong activity in nuclear and medium energy physics at the KfK.

Such a machine would open the door to a wide field of high precision physics and would enable unique experiments.

The concept for a cooler and storage ring had previously been discussed under the hypothesis that the ICE-ring could be used (1) and recently in the context of a more general ring configuration (2). The basic features of the scheme are summarized in the following.

The ring has the task to collect (polarized) protons, deuterons or light ions at the cyclotron end-energy (80 MeV for protons, 35 MeV/N for $q/M = 1/2$ ions). During collection the circulating beam is cooled continuously by electrons allowing to reach the space charge limit. Thereafter the beam is accelerated to the desired working energy, the internal targets are activated and the experimental phase is started. The beam is continuously cooled. From physics arguments an upper operation energy of 1.3 GeV would be desirable. The experimental phase would range from a fraction of a minute to a few hours depending on stored projectile and the thickness of the internal targets. At the end the magnetic field will

be decreased and the filling is restarted. The collection and acceleration phase would last only a few seconds.

As projectiles (polarized) protons, deuterons and light ions could be collected, accelerated and stored. A high degree of vertical polarization for protons could be expected. An external neutron beam emerging tangentially out of the ring from an internal target could be set-up. The (polarized) neutrons would be produced through (p,n) and (d,n) reactions. By detection of the reaction partner they could be tagged.

Molecular clusters, (polarized) atomic and jet beams would be used as internal targets yielding a target density in the range between a few 1 $\mu g/cm^2$ and 5 pg/cm^2 or less. A tentative ring parameter list is given in Table 1. Similar concepts are presently realized at the Indiana cyclotron in Bloomington and in Uppsala and had been discussed in the KfK, Jülich. Some of the most important virtues of the scheme discussed here are again summarized in the following:

- The use of electron cooling in combination with accumulation would allow to built up dense stored particle beams even for low current cyclotron beams (e.g. $p_\uparrow$, $d_\uparrow$, t, light ions).

- The combination of electron cooling and internal target operation would allow for the most efficient use of the accumulated beam and enable high resolution experiments with high luminosity. The beam target interaction volume could be made very small.

- The application of thin internal targets would allow the detection of heavy and slow reaction products and would render target windows unnecessary. Secondary interactions would not occur.

- A high degree of beam and target polarization could be achieved, with the possibility of a rapid change of the target polarization direction and a change of beam polarization from cycle to cycle.

- A high energy neutron beam could be set-up. Through polarization transfer reaction the neutrons could be polarized. By detecting the reaction product the neutron could be tagged.

- Rare isotopes could be used as internal targets since only little material is needed for atomic beams.

Table 1: Tentative parameters of an electron cooled storage ring

possible projectiles	$p_{(\uparrow)}$, $d_{(\uparrow)}$, (t), ^{3}He, α, ^{6}Li ...
energy range	20 - 1300 MeV for protons
max. circul. current	0.6 A for protons, 0.3 A for other projectiles
mom. bite of cooled beam	$10^{-5} \div 10^{-3}$ *)
cooled beam diameter	$0.1 \div 5$ mm *)
average ring diameter	25 m
number of internal targets	$3 \div 5$
electron cooling length	4 m
electron cooling time	1 sec
average ring vacuum	$< 10^{-10}$ Torr
internal targets	(polarized) atomic beam, cluster beam, jets
density of internal targets	5 pg/cm$^{-2} \div 1$ µg/cm^2
maximum luminosity for	
pol. p-beam and pol. p-target	$\sim 10^{31}$ cm^{-2} s^{-1}
pol. p-beam and cluster target	$\sim 10^{34}$ cm^{-2} s^{-1}
unpol. beam and thick target	$\sim 10^{36}$ cm^{-2} s^{-1}

*) depending on beam intensity, projectile and target

(1) A. Citron, J. Gspann, W. Kluge, H. Poth, G. Rebel, G. Schatz, H. Schweickert, Ch. Weddigen, unpublished notes (1981/83)
(2) KfK-Cyclotron users meeting, Karlsruhe (June 1983)

6.4   APPLICATIONS

6.4.1 ELEMENTAL ANALYSIS OF SINGLE CELLS OF ORGANIC MATTER BY PROTON
       INDUCED X-RAYS

Trace element analyses in single cells of organic matter may be per-
formed with ion microbeams. The method uses proton induced X-ray emission,
the principles of which are presented; the Karlsruhe micro beam setup is
described. The requirements for sample preparation are discussed in detail.
The mass of the irradiated sample volume is determined by Rutherford back-
scattering. The calibration of the elemental concentrations is performed by
comparison with a reference standard of known composition. The efficiency of
the described method is demonstrated at the example of erythrocytes (red
blood cells).

6.4.2 ELEMENTAL ANALYSES PERFORMED WITH THE KARLSRUHE NUCLEAR MICROPROBE

Proton induced X-rays have been used in the Karlsruhe nuclear micro-
probe to determine the content of some trace elements in normal and cancer-
ously degenerated human stomach mucousa tissue. A 3 MeV proton beam produced
in a single stage Van de Graaff accelerator is focussed down to 3 µm at
600 pA and swept across the specimen in a meandrous pattern. The local mass
density of the specimens is determined by the yield of elastically scattered
protons, wich are registered in a surface barrier detector. Erythrocytes
served as test objects to demonstrate the feasibility of the procedure.
Specimens of stomach mucousa were prepared by two different methods of fixa-
tion. After irradiation the specimens were stained to identify the histolo-
gical structure. All specimens show rather low structure in elemental concen-
trations except for iron. No significant shifts in the trace element contents
between normal and concerous stomach mucousa could be observed.

+   Jagellonian University, Institute of Physics, Cracow, Poland

6.4.3 DOSE DISTRIBUTION AND ENERGY DEPOSITION SPECTRA OF π^-MESON BEAMS FOR BIOMEDICAL APPLICATIONS

G. Büche

Distributions of absorbed dose in depth and in lineal energy have been worked out using our Monte Carlo program named PIONDOSE. This computer code is based on a large set of experimentally approved input data and uses only a few model approximations. It has been the aim to get results which cannot be obtained from conventional dosimetry or even microdosimetry and which are essential for therapy planning procedures.

Fig. 1 shows a series of depth dose curves for a pencil beam in a water phantom. The absorbed dose as a function of depth has been integrated over $\pm$ 10 g cm^{-2} in both directions perpendicular to the beam axis. In particular, the contributions of pions, (secondary) protons and ^{4}He-ions from reactions in flight as well as from nuclear absorption of stopped pions are given. According to their short ranges the peak of He-ions is equivalent to the distribution of stopped pions and shows a shift existing between the maxima of absorbed doses from pions and from densely ionizing secondaries.

Fig. 2 shows energy deposition spectra calculated for various depths along the beam axis. Shortly behind the phantom surface (2.5 cm) the spectrum shows a sharp peak which is generated from fast pions crossing the sensitive volume (2 μm in diameter) of the spectrometer and a shoulder from δ-electrons. Above 10 keV μm^{-1} the contributions from pion reaction products are maximum. With increasing depth (up to 16.5 cm) the peak from pions is shifted to the right and the contributions from δ-electrons as well as from secondaries decrease. The following pictures of Fig. 2 cover the stopping region of pions. The Bragg peak is at 19.5 cm; the spectra at 18.3 and 20.9 cm result for ±1/2 FWHM and the positions 16.5 and 22.5 cm are related to 1/10 of the maximum value of the stopping distribution. This sequence of y-spectra shows clearly the variation of ionization density over the Bragg peak which is correlated with a variation of radiobiological effectiveness (RBE) of absorbed dose. Together with the decomposition into contributions from various secondaries (p,d,t,^{3}He, ...,n, recoils; not shown in this context) a series of spectra like this one is the physical part of the estimate of radiation quality in therapy planning in the case of negatively charged pions.

A third aspect of the calculations can be read from Table 1. The total absorbed dose and the part from the kinetic energy of the pions is given as a function of the phantom material integrated over the stopping region of

Table 1: The absorbed dose from secondaries related to the dose from pions in the Bragg peak for various phantom materials

Phantom material (i=0, H,TE,C)	H_2O	pig muscle	TE-plastic	$(CH_2)_n$
Number of transported π^-	10^4	$2 \cdot 10^3$	$2 \cdot 10^3$	10^4
Chemical composition H : C : O : N	2 : 0 : 1 : 0	34,24 : 3,97 : 12,94 : 1	39,23 : 24,62 : 1,42 : 1	2 : 1 : 0 : 0
Capture ratio O : (C+N)	1 : 0	0,836 : 0,164	0,080 : 0,920	0 : 1
Total dose D_{tot} integrated over stopping region	$27,571 \frac{MeV}{cm}$	$29,398 \frac{MeV}{cm}$	$32,590 \frac{MeV}{cm}$	$31,394 \frac{MeV}{cm}$
Pion dose D_π	$11,267 \frac{MeV}{cm}$	$11,915 \frac{MeV}{cm}$	$11,724 \frac{MeV}{cm}$	$11,076 \frac{MeV}{cm}$
$(D_{tot}-D_\pi)/D_\pi = D_{sek}/D_\pi = D_i$	1,447	1,467	1,780	1,834
overestimation of absorbed dose $\frac{1 + D_{TE}}{1 + D_M}$ =	0,992	1	1,127	1,149
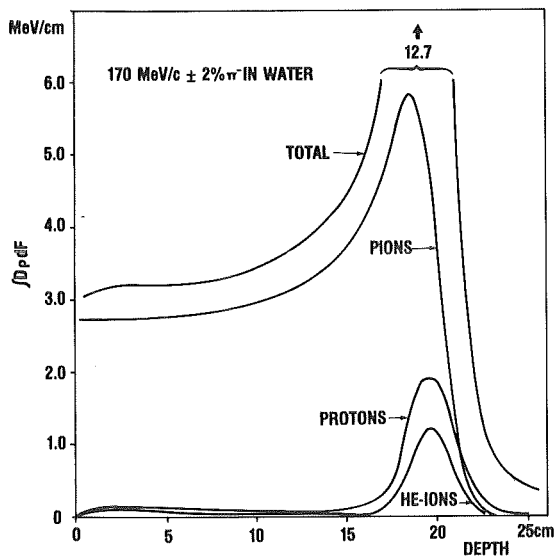
Fig. 1: Distribution of absorbed dose in depth for a pencil beam of π^- in a water phantom. The contributions from the kinematic energy of pions and from two secondaries (p, ^{4}He) are given separately.
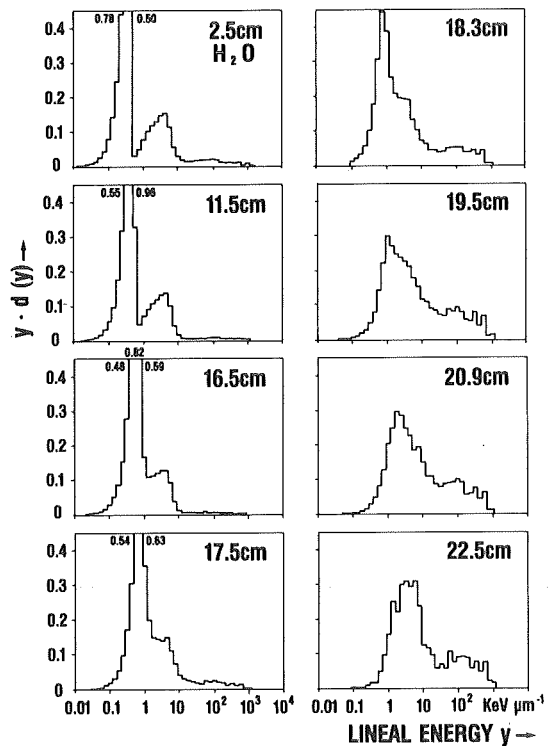
Fig. 2: Distributions of absorbed dose in lineal energy for various positions along the axis of a pencil beam of negatively charged pions.

pions. It is clearly revealed that the absorbed dose from heavy secondaries $D_{sek}/D_{\pi} = (D_{tot} - D_{\pi})/D_{\pi}$ increases with increasing carbon content of the phantom material. In cases of application an absorbed dose that is expected within e.g. muscle tissue is measured using a dosimeter which is made usually out of tissue equivalent (TE) plastic material. According to our calculation the absorbed dose in pig muscle tissue is overestimated by about 13%. A correction factor like this for differing target and dosimeter materials can not be obtained by other methods than a calculation.

7. LIST OF PUBLICATIONS

7.1 PUBLICATIONS AND REPORTS

Abela, R., Backenstoss, G., Kunold, W., W., Simons, L.M., Metzner, R.
Measurements of the polarization of the 2p and 1s states in muonic atoms and the helicity of the muon in pion decay
Nucl. Phys. A 395 (1983) 413-34

Adiels, L., Alberis, G., Backenstoss, G., Blüm, P., Bergström, I., Fransson, K., Guigas, R., Hasinoff, M., Koch, H., Kerek, A., Meyer, M., Pavlopoulos, P., Poth, H., Raich, U., Richter, B., Repond, J., Suffert, M., Tauscher, L., Tröster, D., Zioutas, K.
π^0 and η spectra from pp-annihilations at rest
CERN-EP 83-91 (1983)

Almeida, J., Bao, Z.Y., Beer, H., Erbe, D., Fabbri, F., Hong, L.D.
Käppeler, F., Macklin, R.L., Reffo, G., Rupp, G., Walter, G., Ward, R.A., Wisshak, K.
Prog. Rep. on Nuclear Data Research in the Institut für Angewandte Kernphysik II, Kernforschungszentrum Karlsruhe, for the Period April 1, 1981 to March 31, 1982, NEANDC (E)-232U, Vol. V., FIZ-KA-4, December 1982

Almeida, J., Käppeler, F.
Isotopic neon cross sections for a study of neutron balance and temperature during s-process nucleosynthesis
Astrophysical Journal, 265 (1983) 417-28

Andl, A., Bekk, K., Göring, S., Hanser, A., Nowicki, G., Rebel, H., Schatz, G., Thompson, R.C.
Isotope shifts and hyperfine structure of the $4s^2\ ^1S_0-4s4p\ ^1P_1$ transition in calcium isotopes.
Phys. Rev. C26 (1982) 2194-2202

Apel, W.D., Augenstein, K.H., Bertolucci, E., Donskov, S.V., Inyakin, A.V., Kachanov, V.A., Krasnokutsky, R.N., Krüger, M., Leder, G., Lednev, A.A., Mannelli, I., Mikhailov, Yu.V., Müller, H., Pierazzini, G.M., Prokoshkin, Yu.D., Quaglia, M., Schneider, H., Scribano, A., Siergiampietri, F., Shuvalov, R.S., Sigurdsson, G., Vincelli, M.L.
Measurement of $\pi^- p \to \pi^0\pi^0 n$ a t 25 GeV/c
Nucl. Phys. B 201 (1982) 197-204

Backenstoss, G., Dörr, M., Gotta, D., Kowald, W., Reich, J., Schmidt, G., Ullrich, H., Weyer, H.J.
Pion absorption in the lithium isotopes
SIN Newsletter No. 15 (January 1983) 31

Backenstoß, G., Gotta, D., Furic, M., Izycki, M., Ljungfelt, S., Mankin, U., Petkovich, T., Schmidt, G., Ullrich, H., Weyer, H.J., Weymarn, K.v.
Absorption of positive and negative pions in ^{3}He at 121 MeV
SIN Newsletter No. 15 (Jan. 1983) 39

Backenstoss, G., Hasinoff, M., Pavlopoulos, P., Repond, J., Tauscher, L., Tröster D.; Blüm, P.; Guigas, R.; Koch, H.; Meyer, M.; Poth, H., Raich, U., Richter, B., Adiels L., Bergström, I., Fransson, K., Kerek, A., Suffert, M., Zioutas, K.
Proton Antiproton Annihilations at Rest into $\pi\omega$, $\pi\eta$, $\pi\gamma$, $\pi\pi$ and $\pi\eta$
CERN-EP-58 (1983)

Beck, R., Dickmann, F.
On calculating matrix elements of slater determinant wave functions in the cluster model
II. Clusters with intrinsic orbital angular momentum
KfK-3402 (September 1982)

Beck, R., Dickmann, F., Oehlschlaeger, J.
Application of the algebraic programming system REDUCE2 to calculations in the nuclear cluster model
KfK-3539 (May 1983)

Beer, H., Macklin, R.L.
$(^{178,179,180})$Hf and ^{180}Ta(n,γ) cross sections and their contribution to stellar nucleosynthesis
Phys. Rev. C26 (1982) 1404-16

Beer, H.
^{176}Lu: cosmic clock and stellar thermometer
Astrophysical Journal 262 (1982) 739-41

Beer, H.
s-process chronometers
KfK-3451 (January 1983)

Berdoz, A., Favier, B., Foroughi, F., Hoftiezer, J., Mutchler, G.S., Weddigen Ch.
The relative cross section for elastic proton-proton scattering
J. Phys. G8 (1982) 1363

Blüm, P., Guigas, R., Koch, H., Meyer, M., Poth, H., Raich, U., Richter, B., Backenstoss, G., Hasinoff, M., Pavlopoulos, P., Repond, J., Tauscher, L., Adiels, L., Bergström, I., Fransson, K., Kerek, A., Suffert, M., Zioutas, K.
A modular NaI(TL) detector for 20 - 1000 MeV photons
Nucl. Instr. Meth. 213 (1983) 251

Borie, E.
Vacuum polarization corrections and spin-orbit splitting in antiprotonic atoms
Phys. Rev. A28 (1983) 555

Büche G.
Energy deposition spectra of π^- calculated from pion nulceus interaction data
Radiat. Environ. Biophys. 20 (1982) 255-262

Buth, L., Cierjacks, S., Hino, Y., Howe, S.D., Rainbow, M.T., Raupp, F., Swinhoe, M.T.
Nuclear data research in the Institut für Kernphysik, Kernforschungszentrum Karlsruhe,
Progr. Rep. on Nuclear Data Research in the Federal Republic of Germany for the Period April 1, 1981 to March 31, 1982
NEANDC(E)-232V, Vol. V, FIZ-KA-4, Dec. 1982

CELLO-Collaboration
Measurement of the reaction $e^+e^- \to \mu^+\mu^-$ for $14 < \sqrt{s} < 36.4$ GeV
DESY-82-019
Z. Phys. C14 (1982) 283-88

CELLO-Collaboration
Measurement of inclusive γ and π^0 spectra and a comparison of the neutral and charged components in hadronic events in e^+e^- annihilation at 34 GeV
Z. Phys. C14 (1982) 189-95

CELLO-Collaboration
Topology of hadronic e^+e^- annihilation events at 22 and 34 GeV cm energy
Phys. Lett. B110 (1982) 329-34

CELLO-Collaboration
Investigation of two photon final states in e^+e^- annihilation at $\sqrt{s} = 34.2$ GeV
DESY-82-080 (December 1982)

CELLO-Collaboration
Coupling strengths of weak neutral currents from leptonic final states at
22 and 34 GeV
Z. Phys. C16 (1983) 301-05
DESY-82-063 (1982)

CELLO-Collaboration
Observation of topologically isolated energetic electrons in e^+e^- inter-
actions
Phys. Lett. B118 (1982) 211-16
DESY-82-055 (August 1982)

CELLO-Collaboration
The influence of fragmentation models on the determination of the strong
coupling constant in e^+e^- annihilation into hadrons
Nucl. Phys. B218 (1983) 269-88
DESY-82-061 (September 1982)

CELLO-Collaboration
Lepton pair production in deep inelastic e-γ scattering
DESY-83-17 (March 1983)
Phys. Lett. B126 (1983) 384-90

Cierjacks, S.
Accelerator-based pulsed white neutron sources
in Neutron Physics and Nuclear Data in Science and Technology , Vol. 2:
Neutron Sources for Basic Research and Applications (Pergamon Press, Oxford,
December 1982) p. 81ff

Cierjacks, S.
Instrumental developments in high-resolution neutron measurements in
Physics and Applications, Vol. 10: Neutron Induced Reactions
(Inst. of Physics, Bratislava, August 1982) p. 423-44

Cierjacks, S. (editor)
Neutron Physics and Nuclear Data in Science and Technology, Vol. 2:
Neutron Sources for Basic Research and Applications (Pergamon Press, Oxford,
December 1982) 370 pages

Cierjacks, S., Behrens, H. (editors)
Progr. Report on Nuclear Data Research in the Federal Republic of Germany
for the Period April 1, 1981 to March 31, 1982
NEANDC(E)-232V, Vol. V, FIZ-KA--4, Dec. 1982

Cook, J., Gils, H.J., Rebel, H., Majka, Z., Klewe-Nebenius, H.
Optical model studies of ^{6}Li eleastic scattering at 156 MeV
Nucl. Phys. A388 (1982) 173-86

Corcalciuc, V., Rebel, H., Pesl, R., Gils, H.J.
Isoscalar octupole transition rates in ^{50}Ti, ^{52}Cr and ^{208}Pb from model
independent analyses of 104 MeV α-particle scattering
KfK-3377 (July 82)
J. Phys. G9 (1983) 177-84

Degitz, H.
Elastische Streuung von Pionen an ^{12}C im Bereich der Coulomb-Kern-Interferenz
unterhalb der Δ-Resonanz
KfK 3559 (1983)

Degitz, H., Klein, U., Kluge, W., Markus, R., Mattäy, H., Wiedner, U.
Coulomb-nuclear interference in the scattering of pions on ^{12}C at 76 MeV
SIN Newsletter Nr. 15 (1983), p. NL 36

Dörr, M.
Pionabsorption an ^{6}Li
Doktorarbeit Univ. Karlsruhe 1982

Effenberger, B., Kunold, W., Oesterle, W., Schneider, M., Simons, L.M.
Abela, R., Wüest, J.
Determination of the spectroscopic quadrupole moments of $^{75}_{33}$As and $^{63}_{29}$Cu
Z. Phys. A 309 (1982) 77

Engler, J.
Atomic and nuclear properties of materials
KfK 3386B (Juli 82)

Faust, H.R., Klewe-Nebenius, H., Rebel, H., Wisshak, K.
Determination of the multipolarity of prompt electromagnetic transitions
Nucl. Instr. Meth. 213 (1983) 277

Gerl, J., Ronge, K., Venkata, Ramaniah, K., Hanser, A.
The quadrupole moment of ^{176}Lu
Z. Phys. A309 (1983) 275-76

Guigas, R., Blüm, P., Koch, H., Meyer, M., Poth, H., Raich, U., Richter, B.
Backenstoss, G., Pavlopoulos, P., Tauscher, L., Adiels, L., Fransson, K.,
Nilsson, A., Suffert, M., Zioutas, K.
Strong interaction effects in antiprotonic ^{6}Li/^{7}Li atoms
CERN-EP/83-93 1983

Haesner, B.
Experimente zur Bestimmung der Wirkungsquerschnitte für das n-^{3}He-System im
Energiebereich von 1 bis 40 MeV
KfK 3395 (1982), Dissertation, Univ. Karlsruhe 1982

Heck, D.
Elementanalyse in einzelnen Zellen organischer Proben mit protoneninduzier-
ter Röntgenstrahlung
KfK 3399 (September 1982)

Heck, D., Rokita, E.
Elemental analysis performed with the Karlsruhe nuclear microprobe
IEEE Transactions on Nuclear Science, NS-30 (1983) p. 1220-23

Heeringa, W., Postma, H.
Neutron-nucleus spin-spin interaction in the low MeV range
Phys. Rev. C27 (1983) 2012-18

Hoftiezer, J., Weddigen, Ch., Chatelain, P., Favier, B., Foroughi, F.,
Piffaretti, J., Jaccard, S., Walden P.
The analysing power of the reaction pp → πd for proton energies between 500
and 600 MeV
SIN Preprint PR-82-18 (1982)

Hoftiezer, J., Weddigen, Ch., Chatelain, P., Favier, B., Foroughi, F.,
Nussbaum, C., Piffaretti, J., Jaccard, S. Walden, P.
The differential cross section of the reaction pp → πd for proton energies
between 500 and 600 MeV
Nucl. Phys. A402 (1983) 429-44

Hoftiezer, J., Mutchler, G.S., Weddigen, Ch., Konter J.A., Mango, S.,
Berdoz, A., Favier, B., Foroughi, F.,
The spin correlation coefficient A_{xz} of the reaction pp → πd for proton
energies between 500 and 600 MeV
SIN Preprint PR-83-06 (1983)

Ingram, C.H.Q., Gram, P.A.M., Jansen, J., Mischke, R.E., Zichy, J., Bolger,
J., Boschitz, E., Pröbstle, G., Arvieux, J.
Quasielastic scattering of pions from ^{16}O at energies around the Δ(1232)
resonance
Phys. Rev. C27 (1983) 1578-1601

Jaki, J., Degitz, H., Klein, U., Kluge, W., Mattäy, H.
Design and test of a vertical drift chamber
SIN Newsletter No. 15 (1983), p. NL 37

Käppeler, F., Wisshak, K., Hong, L.D.
Neutron capture resonances in ^{56}Fe and ^{58}Fe in the energy range from 10 to 100 keV
KfK-3412 (November 1982)
Nuclear Science and Engineering, 84 (1983) 234-47

Käppeler, F., Schatz, G., Wisshak, K.
Vorschlag zum Bau eines Wismut-Germanat-Detektors für Präzisionsmessungen zur Elementsynthese im s-Prozeß
KfK-3472 (February 1983)

Kiefhaber, E., Fröhner, F.H., Käppeler, F.
Kerndaten und Neutronik-Rechenprogramme
KfK-Nachrichten, 15 (1983) 76-88

Kluge, W., Mattäy, H.
Das neue Magnetspektrometer für die Streuung niederenergetischer Pionen LEPS
SIN Jahresbericht 1982, p. JB 23

Krüger, Th., Appel, H., Thies, W.G., Behrens, H.
Spectrum shape studies of the β-transitions ^{34m}Cl$(3^+\to2^+)^{34}$S and ^{34}Cl$(0^+\to0^+)^{34}$S
Phys. Lett. 121B (1983) 303-06

Maier, T.
Nachweis von Neutronen aus pioninduzierten Kernreaktionen
Diplomarbeit, Universität Karlsruhe 1982

Markus, R.
Bau und Test einer zylindrischen Vieldraht-Proportionalkammer
Diplomarbeit, Universität Karlsruhe 1982

Mengoni, A.
Direct radiative capture: test of the Lane-Lynn model and development of a methodology for calculations
KfK-3452 (December 1982)

Münchmeyer, D., Amols, H.I., Büche, G., Kluge, W., Mattäy, H., Moline, A., Randoll, H.
Energy spectra of charged particles emitted following the absorption of negative pions stopped within oxygen containing organic compounds
Phys. Med. Biol. 27 (1982) 1131-1149

Neumann, R., Poth, H., Wolf, A., Winnacker, A.
Laser enhanced electron-ion recombination and antihydrogen formation
CERN-EP/83-66

Ottmar, H.
An advanced nondestructive assay system for reliable and timely nuclear materials accountancy in reprocessing
ESARDA Bulletin (1983) No. 4, p. 19-22

Patin, Y., Cocu, F., Lachkar, J., Sigaud, J., Haouat, G., Cierjacks, S.
Etude de la dissipation d'énergie dans la fission de ^{234}U a l'aide de la réaction ^{233}U(d,pf)
Nucl. Phys. A382 (1982) 31

Pesl, R., Gils, H.J., Rebel, H., Friedman, E., Buschmann, J., Klewe-Nebenius, H., Zagromski, S.
Optical potentials and isoscalar transition rates from 104 MeV alpha-particle scattering by the N=28 isotones ^{48}Ca, ^{50}Ti and ^{52}Cr
KfK-3378 (February 1983); Z. Physik A313 (1983) 111-122

Poth, H.
LEAR Workshop: Kalte und langsame Antiprotonen
Physikalische Blätter 38 (1982) 324-26

Poth, H.
Antiproton mass measurement using stored beams cooled by electrons
Nucl. Instr. Meth. 203 (1982) 597-99

Poth, H., Wolf, A.
A new tuneable and pulsed vacuum-ultraviolet and X-ray line
Phys. Lett. 94A (1983) 135-38

Randoll, H., Amols, H.I., Kluge, W., Matthäy,H., Moline, A., Münchmeyer, D.
Energy spectra of charged particles emitted following the absorption of
stopped negative pions in calcium
Nucl. Phys. A381 (1982) 317

Randoll, H.
Untersuchung hadronischer Ereignisse in hochenergetischen e^+e^- Annihilatio-
nen gemessen mit dem Detektor CELLO
KfK-3569 (July 1983)
Dissertation, Universität Karlsruhe 1983

Raupp, F.
Messung der orts- und winkelabhängigen Spektren schneller Neutronen und
geladener Sekundärteilchen aus Spallationsreaktionen von 590 MeV Protonen
in dicken Urantargets
KfK-3511B (April 1983)
Diplomarbeit, Universität Karlsruhe 1982

Reffo, G., Fabbri, F., Wisshak, K., Käppeler, F.
Calculated gamma-ray spectra for keV neutron capture in ^{240}Pu, ^{242}Pu, ^{238}U
Nuclear Science and Engineering 83 (1983) 401-407

Richter, B.
Suche nach gebundenen Baryoniumzuständen und seltenen Annihilationskanälen
mittels γ-Spektrometrie
KfK-3441 (February 1983)
Dissertation, Universität Karlsruhe 1983

Schatz, G.
Note on technetium in stars
Astronomy and Astrophysics 122 (1983) 327-29

Schwarz, P., Klages, H.O., Doll, P., Häsner, B., Wilczynski, J., Zeitnitz,
B., Kecskemeti, J.
Elastic neutron-deuteron scattering in the energy range from 2.5 to 30 MeV
Nucl. Phys. A398 (1983)1-18

Schwarz, P.
Messung des differentiellen Wirkungsquerschnittes der elastischen Neutron-
Deuteron-Streuung im Energiebereich 2.5 - 30 MeV
KfK-3396 (1982)
Dissertation, Universität Karlsruhe 1982

Thompson, R.C., Anselment, M., Bekk, K., Goering, S., Hanser, A., Meisel,
G., Rebel, H., Schatz, G., Brown, B.A.
High resolution measurements of isotope shifts and hyperfine structure in
stable and radioactive lead isotopes
KfK-3455 (December 1982)
J. Phys. G9 (1983) 443-58

Walter, G., Beer, H., Kurcewicz, W., Kirchner, R., Röckl, R., Schardt, D.
The ^{180}Lu β decay to the ^{180}Hf 8^- isomeric state and the r-process formation
of $^{180}Ta^m$
KfK-3417 (November 1982)

Wisshak, K., Wickenhauser, J., Käppeler, F., Reffo, G., Fabbri, F.
The isomeric ratio in thermal and fast neutron capture of Americium-241
Nuclear Science and Engineering 81 (1982) 396-417

Wisshak, K., Käppeler, F.
Neutron capture and fission cross section of Americium-243 in the
energy range from 5 to 250 keV
KfK-3503 (April 1983)

Wisshak, K., Walter, G., Käppeler, F.
Self-absorption of neutron capture gamma-rays in gold samples
KfK-3542 (June 1983)

7.2   CONFERENCE CONTRIBUTIONS

Workshop on ECR-Sources for the 88"-Cyclotron at LBL, Lawrence-Berkeley-Laboratory, Berkeley, (USA) August 16-20, 1982

Bechtold, V., Friedrich, L., Schweickert, H.
Operation of the Karlsruhe ECR-sources HISKA and p-HISKA

Brasov Int. Summer School 'Nuclear Collective Dynamics', Brasov, (Romania) August 26 - September 8, 1982

Rebel, H.
Studies of the spectator break-up component in inclusive charged particle spectra from 156 MeV-^{6}Li induced reactions.

Micek, S., Gils, H.J., Rebel, H., Majka, Z., Heinz. M.
Macroscopic and microscopic features of ^{6}Li-light nucleus scattering potentials at E_{Li} = 156 MeV

Int. Conf. on High Energy Spin Physics, Brookhaven, (USA) August, 1982

Hoftiezer, J.H., Weddigen, Ch., Jaccard, S., Walden, P., Chatelain, P., Favier, B., Foroughi, F., Piffaretti, J.
Measurement of the analyzing power in the $pp \rightarrow \pi^+ d$ reaction

Mathie, E.L.
Dibaryon search in the π-d-system

6. European Symposium on Nucleon-Antinucleon and Quark-Antiquark Interaction, Santiago, (Spain) August 30-September 4, 1982

Blüm, P.
$\bar{p}p$-annihilation at rest and two neutral mesons

Int. Conf. on Nuclear Structure, Amsterdam, (Netherlands) August 30 - September 3, 1982

Doll, P. Haesner, B. Hansmeyer, J., Hiebert, J., Klages, H.O., Schwarz, P. and Wilczynski, J.
Measurement of the neutron-proton analyzing power in the energy range from 17 MeV to 50 MeV

Int. Conf. on Nuclear Data for Science and Technology, Antwerp, (Belgium) September 6-10, 1982

Almeida, J., Käppeler, F.
Neutron capture cross sections of ^{20,21,22}Ne between 5 and 200 keV and the neutron balance in s-process nucleonsynthesis

Beer, H., Macklin, R.L.
The neutron capture cross sections of ^{178,179,180}Hf and the origin of nature's rarest stable isotope ^{180}Ta

Cierjacks, S., Hino, Y., Howe, S.D., Raupp, F., Buth, L.
Differential neutron production cross sections for 590 MeV protons

Mengoni, A., Reffo, G., Fabbri, F.
Valence neutron capture in Fe and Ni Isotopes

Wisshak, K., Käppeler, F.
Neutron capture cross section of ^{243}Am in the energy range from 10 to 250 keV.

Vortragstagung 'Kern-, Radio-, Strahlenchemie-Grundlagen und Anwendungen',
Karlsruhe, September 20-24, 1982

Penzhorn, R.D., Schuster, P., Beer, H., Käppeler, F., Walter, G.
Neutroneneinfang-Querschnitte von in Zeolith 5A immobilisierten Edelgasen
(Kr-84 und Kr-86) und ihre Bedeutung für die Nukleosynthese in Sternen

Tagung der Österreichischen Physikalischen Gesellschaft, Silberberg, (Austria)
September 20-21, 1982

Fries, D.C.
PETRA-Ergebnisse

DESY-Workshop, Hamburg, September 28-30, 1982

Flügge, G.
Search for new particles in e^+e^- annihilation

Int. Conf. on Nucleus-Nucleus Collisions, Michigan State University,
East Lansing, (USA) September 27 - October 1, 1982

Micek, S., Gils, H.J., Rebel, H., Majka, Z., Heinz, M.
Macroscopic and microscopic features of ^{6}Li-light nucleus scattering potentials
at E_{Li} = 156 MeV

Workshop über Fragen der nuklearen Astrophysik, Mainz, October 13-15, 1982

Beer, H.
s-Prozess Chronometer

Käppeler, F.
Neutronendichte und Temperatur beim s-Prozeß

Schatz, G.
Technetium im s-Prozeß

American Physical Society Meeting, Amherst, (USA) October 1982

Boschitz, E.T.
Evidence for dibaryon resonances in π-d$_{pol}$ scattering

Int. Symp. on Recent Advances in Nuclear Material Safeguards,
Vienna, (Austria), November 8-12, 1982

Ottmar, H., Eberle, H., Matussek, P. Michel-Piper, I.
Qualification of K-absorption edge densitometry for applications in
international safeguards

Conf. on the Application of Accelerators in Research and Industry,
Denton, (USA), November 8-10, 1982

Heck, D., Rokita, E.
Elemental analyses performed with the Karlsruhe nuclear microprobe

21th Internat. Nuclear Physics Winter Meeting, Bormio, January 24-29, 1983

Rebel, H.
Isotopic variation of nuclear charge radii in Pb from atomic beam laserspectroscopy

Wire Chamber Conf., Vienna, (Austria), February 15-18, 1983

Engler, J.
Electromagnetic calorimeters using wire chambers

Jaki, J., Matthäy, H. Degitz, H.,Kluge, W., Klein, U.
Vertical drift chambers for a low energy pion spectrometer

47. Physikertagung DPG, Regensburg, March 14-18, 1983

Dembczynski, J.
Effekte zweiter Ordnung in der Hyperfeinstruktur von PbI Übergängen

Poth, H., Wolf, A., Neumann, R, Winnacker, A.
Stimulierter Elektroneneinfang in der Elektronenkühlung

Poth, H., Wolf, A.
Eine neuartige VUV und Röntgenlinienquelle

Thompson, R.C., Anselment, M., Bekk, K., Goering, S., Hanser, A., Meisel, G., Rebel, H., Schatz, G.
Laserspektroskopische Untersuchungen an instabilen Bleiisotopen

Frühjahrstagung DPG, Kernphysik, Münster, March 21-25, 1983

Aures, R., Heeringa, W., Maschuw, R., Schmidt, F.K.
Polarized proton target

Aures, R., Heeringa, W., Maschuw, R., Schmidt, F.K.
Properties of the Karlsruhe polarized protontarget

Bechtold, V., Doran, A., Ehret, H.P.,Friedrich, L., Kaltenbaek, J., Schweickert, H. Sheikh, S., Wiss, L., Ziegler, P.
ECR ion source development at the Karlsruhe cyclotron

Beck, R., Dickmann, F.
Application of the algebraic programming system reduce 2 to calculations in the cluster model of light nuclei

Beck, R., Dickmann, F., Kruppa, A.
Eigen energies and electromagnetic properties of ^{6}Li in a generalized cluster model

Beer, H., Walter, G., Macklin, R.L., Patchett, P.I.
The neutron capture cross sections and solar abundances of ^{160}Dy, ^{176}Lu and ^{176}Hf and the age of chemical elements

Brady, P., Doll, P., Finckh, E., Hofmann, K., Klages, H.O., Nitz, W., Wilczynski, J.
Measurement of A_y for the elastic n-d scattering from 15 MeV to 50 MeV

Brady, P., Doll, P., Heeringa, W., Hofmann, K., Jany,P., Klages, H.O., Maier, Chr., Wilczynski, J.
Measurement of the analyzing power of the elastic n-^{3}He scattering

Brzychczyk, J., Freindl, L., Grotowski, K., Majka, Z., Micek, S., Planeta, R., Albinska, M., Klewe-Nebenius, H., Gils, H.J., Rebel, H., Zagromski, S.
Fusion and nonfusion phenomena in the ^{6}Li + ^{40}Ca reaction at 156 MeV

Doll, P. Haesner, B., Hansmeyer, J., Hiebert, J.,Klages, H.O., Krupp, H., Oexner, M., Plischke, P., Schwarz, P., Wilczynski, J.
Neutron-proton-scattering experiments and nucleon-nucleon phase shift analyses

Doll, P., Haesner, B., Hiebert, J., Klages, H.O., Krupp, H., Oexner, M., Plischke, P., Wilczynski, J., Zankel, H.
Analyzing power of ^{4}He($\vec{n}$,n)^{4}He elastic scattering in the energy range from 15 to 50 MeV

Doll, P., Hiebert, J.,Klages, H.O., Krupp, H., Oexner, M., Schmalz, G., Bechtold, V., Friedrich, L., Ziegler, P.
The Karlsruhe collimator POLKA for the production of fast polarized neutron beams

Eyrich, W., Fuchs, K., Hofmann, A., Rebel, H., Scheib, U.
Untersuchung des Neutronenzerfalls aus dem Riesenresonanzgebiet von ^{90}Zr

Gemmeke, H., Lassen, L., Luecking, W., Schreck, R.
Sequential emission of fast neutrons in 7.5 - 9 MeV/u ^{16}O + ^{64}Ni

Gils, H.J., Brown, B.A., Friedman, E., Rebel, H.
Odd-even-effects of nuclear matter densities in the $1F_{7/2}$ shell

Giorginis, G., Kiontke, S., Maschuw, R., Schulz, R., Wochele, J.
A He- MWPC neutron polarimeter

Mengoni, A., Mathews, G.J.
The role of direct radiative capture for the reaction rates of the r-process

Smith, G., Boschitz, E., Mathie, E.L., Daum, M., Frosch, R., Konter, J.A., Mango, S., Meyer, M., Vogler, F.
Messung der Vektoranalysierstärke der elastischen π^+d(pol)-Streuung im Bereich der Dibaryonresonanzen

Walter, G., Beer, H., Käppeler, F., Penzhorn, R.D.
The s-process branching at ^{85}Kr in the light of new cross sections

Winters, R.R., Käppeler, F., Wisshak, K., Reffo, G.,Mengoni, A.
^{148,150}Sm: A test for s-process nucleosynthesis

ECR-Workshop, Louvain-la-Neuve, (France), March 20-23, 1983

Bechtold, V., Friedrich, L., Schweickert, H.
Present status of the ECR sources at Karlsruhe

Frühjahrstagung DPG, Teilchenphysik, Wuppertal, March 28-30, 1983

CELLO-Collaboration,
Gamerdinger, K.,
Identifizierung von Elektronen in multihadronischen Ereignissen mit dem
Flüssigargon-Kalorimeter des Detektors CELLO

CELLO-Collaboration,
Kuester, H.
Tau-Verzweigungsverhältnisse und tau-Polarisationsgrenzen in e^+e^- -
Wechselwirkung bei $\sqrt{s}$ = 34 GeV

Forstbauer, B.
Szintillationslicht in Flüssig-Argon-Ionisationskammer

Poth, H., Wolf, A.
Elektronenkühlung von (Schwer-)Ionenstrahlen

International School on Heavy Ion Physics, Alushia, (USSR), April 1983

Gönnenwein, F., Oed, A., Perrin, P., Brissot, R., Geltenbort, P., Nifenecker, H.,
Aker, E., Engelhardt, D., Pannicke, J., Heeg, P., Hoffmann, K. F., Mutterer, M.,
Theobald, J. P., Weingärtner, K., Barreau, G., Leroux, B.
Fission studies with new instruments at I.L.L.

Symposium on Delta-Nucleus Dynamics, Argonne, (USA), May 2-4, 1983

Weyer, H.J., Backenstoss, G., Huck, A., Kowald, W., Weber, P., Weymann,
K. v., Gotta, D., Ljungfeld, S., Mankin, U., Schmidt, G., Ullrich, H.
Pion absorption in ^{3}He

2. BMFT-Präsentation Tribologie 1983, Koblenz, May 3-5, 1983

Fehsenfeld, P., Bollmann, E.
Radionuklidtechnik im Maschinenbau

Workshop on Intense Polarized Proton Ion Sources,Vancouver, (Canada),
May 23-29, 1983

Bechtold, V., Friedrich, L.
ECR-technique to intensify polarized hydrogen beam in the Karlsruhe
Lambshift Source LASKA

6th Internat. Balaton Meeting on High Energy Nuclear Physics, Balatonfuered,
(Hungary), June 6-11, 1983

Brady, P., Barasch, G., Castaneda, C., Christie, B., Romero, J., Tull, C.,
Bieser, F., Crawford, H.,Flores, M., Greiner, D., Lindstorm, P., Porter, J.,
Sann, H.
Using MUSIC to study relativistic nuclear collisions

Workshop on Nuclear Astrophysics, Ringberg Castle, Tegernsee, June 6-10, 1983

Käppeler, F.
The status of the σN - curve and the s-process neutron density

Schatz, G.
The ^{176}Lu-^{176}Hf s-process chronometer and planned projects with a 4πBGO
detector

8.   PERSONNEL

Head of the Institute IK I: Prof.Dr.Bernhard Zeitnitz

Scientific and Technical staff:

Achterberg, O., Dr.	Knapp, J.
D'Agostini, G., Dr.	Krüger, M., DP
Apel, W.-D., Dr.	Krupp, H., DP
Aures, R., DP	Küster, H., DP
Bischoff, A.	Lutz, R.
Cernohorsky, I.	Maier, Ch.
Deutsch, G.	Makowsky, M.
Dittmann, R.	Maschuw, R., Dr.
Doll, P., Dr.	Momayezi, M.
Drexlin, G.	Müller, H., Dr.
Engler, J., Dr.	Nitz, W.
Flügge, G., Prof.Dr.	Oexner, M.
Forstbauer, B.	Ottmann, K.H.
Fries, D.C., Dr.	Plischke, P., Dr.
Fues, W., Dr.	Randoll, H., DP
Gamerdinger, K.	Ranitzsch, K.H., Dr.
Gemmeke, H., Dr.	Raupp, F.
Giorginis, G., Dr.	Remane, E.
Grimm, A.	Reuscher, M.
Gumbsheimer R., DI(FH)	Schmalz, G., DI
Haesner, B., Dr.	Schmidt, F.K., Dr.
Hagert, H.	Schmidt, G., DP
Hansmeyer, J., DP	Schneider, H., Dr.
Henkes, Th.	Schulz, R.
Heeringa, W., Dr.	Schwarz, P., Dr.
Hofmann, K., DP	Skacel, H.
Hopp, G., DP	Spohrer, G.
Hucker, H.	Ullrich, G.
Husson, L., Ing.	Wilczynski, J., DP
Jany, P.	Wochele, J.
Keim, H.	Ziegler, P.
Kiontke, S., DP	
Klages, H.O., Dr.	Guest scientists:
	Brady, F.P., Prof.Dr., UC Davis, USA
	Finckh, E., Prof.Dr., U.of Erlangen

Head of the Institute IK II: Prof.Dr.Anselm Citron

Scientific and Technical staff:

Aker, E., DP

Blüm, P., Dr.

Borie, E., Dr.

Boschitz, E., Prof.Dr.

Büche, G., Dr.

Cierjacks, S., Dr.

Degitz, H., DP

Draut, A.

Dröge, M.

Engelhardt, D., Prof.Dr.

Gotta, D., Dr.

Hancock, A., Dr.

Hauth, J.

Hilgendorff, H.

Höhne, A.

Hoftiezer, J., Dr.

Hütten, L.

Jaki, J.

Kärcher, K.

Klein, U., DP

Kluge, W., Prof.Dr.

Koch, H., Prof.Dr.

Köhler, T., DP

Kreissl, A., DP

Kunold, W., DP

Ljungfelt, S., DP

Maier, Th.

Mankin, U.

Mathie, E., Dr.

Matthäy, H., Dr.

Meissner, K.

Metzler, M.

Poth, H.

Reich, J.

Richter, B., DP

Rohmann, D., Dr.

Sambale, K.

Schmidt, G., Dr.

Schneider, M., DP

Simons, L.M., Dr.

Smith, G.R., Dr.

Ullrich, H., Prof.Dr.

Vogel, R.

Weddigen, Ch., Prof.Dr.

Wiedner, U., DP

Wolf, A., DP

Guest scientists:

Furić, M., Prof.Dr., U.of Zagreb, YU

Hino,Y., Dr., Tohoku Univ., Japan

Mutchler, G.S., Prof.Dr., Rice Univ.

Petković, T., U. of Zagreb, YU

Head of the Institute IK III: Prof.Dr.Gerhard Schatz

Scientific and Technical staff: Guest scientists:

Scientific and Technical staff	Guest scientists
Anselment, M., DP	Albinska, M., Dr.
Beck, R., Dr.	Albinski, J., Dr.
Beer, H., Dr.	Dembczynski, J., Prof.Dr.
Bekk, K., Dr.	Kruppa, H., Dr.
Buschmann, J., Dr.	Mathews, G.J., Dr.
Dennerlein, H.-D.	Mengoni, A., Dr.
Dickmann, F., Dr.	Micek, St., Dr.
Dohrmann, H., Ing.	Mordechai, S., Prof.Dr.
Dürrschnabel, D.	Planeta, R., Dr.
Eberle, H., Ing.	Winters, R.R., Prof.Dr.
Feurer, B.	Yokoi, K., Dr.
Friederich, H.M.	
Gils, H.J., Dr.	
Göring, S., DP	
Hanser, A., Dr.	
Heck, D., Dr.	
Heinz, M.	
Hoeffgen, H., Dr.	
Käppeler, F., Dr.	
Kunigkeit, G., Ing.	
Liewehr, W., DP	
Lingenfelder, B.	
Manger, D.	
Matussek, P., DP	
Meisel, G., Dr.	
Michel-Piper, I., DI(FH)	
Oehlschläger, J., D.-Math.	
Ottmar, H., Dr.	
Rebel, H.G., Prof.Dr.	
Rupp, G.	
Schmidt, K.A., DP	
Walter, G., DP	
Wisshak, K., Dr.	
Zagromski, S., DI(FH)	

Head of the Cyclotron Laboratory: Dr.Hermann Schweickert

Scientific and Technical staff:

Acharya, H.	Mayl, R.
Assmus, K.H.	Möllenbeck, J., Ing.
Bauer, G.	Peters, J.-W., DP
Bechtold, V., Dr.	Pfeifer, R.
Bialy, J., DP	Rämer, Ch., Ing.
Biber, J.	Ripp, H.
Blank, R.	Roth, H.
Bollmann, E., DP	Sahm, U., Dr.
Dressen, R.	Schimpf, P.
Ehret, H.P.	Schüssler, B.
Erbe, D.	Schulz, F., Ing.
Ernst, R.	Seidel, H.
Fehsenfeld, P., Dr.	Seitz, J.
Fischböck, T.	Seufert, H.
Foßhag, E., Dr.	Sheikh, S.
Franz, J.	Stöbener, E., Ing.
Friedrich, L., Dr.	Thouw, T., Dr.
Gegenheimer, B.	Uchatius, R.
Günther, O.	Uhlemann, S.
Haßpacher, G.	Wiss, L.
Haushahn, G., DP	Ziegler, P.
Heidenreich, K.	Zimmermann, H.
Heinzmann, H., D.-Inf.	
Herlan, A.	
Herrmann, P.	Guest scientists:
Hirth, W.	
Holler, H.	Doran, A.
Kaltenbaek, J.	Schwabe, J., Dr.
Kappel, W.-R., Ing.	
Kauther, P.	
Kernert, N., DP	
Kessel, M.	
Kirste, E.	
Kleinrahm, A., Dr.	
Kögel, B.	
Maier, W.	
Mangold, D.	